MODELLING HIV DYNAMICS AND EVOLUTION: PROSPECTS FOR VIRAL CONTROL



Hannah Roberts

Pembroke College

Nuffield Department of Medicine

A thesis submitted for the degree of
Doctor of Philosophy

Michaelmas 2016

Abstract

Modelling HIV dynamics and evolution: prospects for viral control

Hannah Roberts
Pembroke College
Doctor of Philosophy, DPhil
Michaelmas 2016

The human immunodeficiency virus (HIV) epidemic is far from over. Antiretroviral therapy (ART) is effective at suppressing viral replication within a patient but it must be taken daily and is life-long. Therefore, the development of a therapy that could induce drug-free remission or constitute a functional cure is a key focus of HIV research. In this thesis I explore three mechanisms which could lead to more individuals being able to control their viraemia in the absence of ART: (1) T-cell immunity, (2) early initiation of ART, and (3) viral evolution. Firstly, a strong HIV-specific T-cell response has been linked to rare cases of spontaneous viral control, but the extent to which this arm of the immune response contributes to viral control is debated. Several types of data are used to answer this question, including the rate at which the virus evolves to escape the $CD8^+$ T-cell response. I study the frequency of incident immune escape in the largest cohort used for this purpose to date. Secondly, some patients, with characteristics dissimilar to spontaneous HIV controllers, are able to control the virus for years after the interruption of ART that was initiated early in infection. I use mathematical models to investigate a new hypothesis for the differing outcomes of early- and late- initiated ART. Thirdly, since HIV is a relatively new infection of humans it is still adapting to its new host. Recent studies suggest that the virus could be evolving towards decreased virulence at the population level. I study whether the widespread administration of ART has the potential to alter the course of virulence evolution and might result in a further attenuated virus. I conclude by discussing the implications of these results for viral control at the individual level and also for population level epidemic control.

Contents

1 Introduction **13**

1.1 Chapter summary 14

1.1.1 Questions addressed in Chapter 3 14

1.1.2 Questions addressed in Chapter 4 15

1.1.3 Questions addressed in Chapter 5 16

1.2 Contributions to this thesis 17

1.2.1 Chapter 3 17

1.2.2 Chapter 4 17

1.2.3 Chapter 5 18

2 Literature review **19**

2.1 The HIV pandemic 19

2.1.1 Population structure and molecular epidemiology 19

2.1.2 Global burden of disease 20

2.1.3 Controlling HIV epidemics 21

2.2 The natural course of an HIV infection 23

2.2.1 The HIV life-cycle 23

2.2.2 Natural history of an infection 24

2.2.3 An overview of the immune response to HIV 25

2.2.4 CTLs and viral control 27

2.3 The evolution of HIV 29

2.3.1 Within-host viral evolution 30

2.3.2 Immune escape in HIV 30

2.3.3 Between-host evolution 33

2.3.4 Virulence evolution 34
2.4 The course of a treated infection and post-treatment control 36
2.4.1 The action of drugs 36
2.4.2 The establishment of the HIV reservoir 36
2.4.3 Latent HIV infection in $CD4^+$ T cells 37
2.4.4 The measurement and characterisation of the reservoir in $CD4^+$ T cells 38
2.4.5 The persistence of the HIV reservoir 39
2.4.6 The dynamics of the reservoir in $CD4^+$ T-cells 41
2.4.7 Attempts to eradicate the reservoir 42
2.4.8 Viral rebound and post-treatment control 43
2.5 Mathematical modelling of HIV 45
2.5.1 Within-host models of HIV 47
2.5.2 Models of T-cell turnover 50
2.5.3 Between-host models of HIV 52

3 T-cell immunity **55**
3.1 Introduction 55
3.2 Results 56
3.2.1 Cohort characteristics 56
3.2.2 Escape prevalence at baseline and after 1 year 57
3.2.3 Incidence of escape during up to three years of observation 58
3.2.4 When does escape happen? 60
3.2.5 Having a protective HLA type is associated with earlier first escape 62
3.2.6 Waiting time to escape for a wild-type epitope 63
3.3 Discussion 64
3.4 Materials and Methods 68
3.4.1 Ethics Statement 68
3.4.2 Participants and Trial Design 69
3.4.3 Sequences 69
3.4.4 $CD8^+$ T cell ELISpot assays 70
3.4.5 HLA genotyping 70

3.4.6 Defining escape . . . 70
3.4.7 Identification of escape in the data . . . 71
3.4.8 Statistics . . . 72
3.5 Questions addressed in this chapter . . . 74

4 Early initiation of ART 77
4.1 Introduction . . . 77
4.1.1 Data review: factors contributing to post-treatment control . . . 78
4.1.2 Data motivating this chapter . . . 84
4.1.3 Questions addressed in this chapter . . . 84
4.2 Results . . . 85
4.2.1 Model development . . . 85
4.2.2 Accounting for replication incompetent provirus . . . 95
4.2.3 Is this mechanism compatible with the Brodin data? . . . 100
4.3 Discussion . . . 104
4.4 Questions addressed in this chapter . . . 109

5 Viral evolution 111
5.1 Introduction . . . 111
5.2 Modelling and results . . . 113
5.2.1 What are the observed patterns of changing HIV virulence? . . . 113
5.2.2 In the absence of treatment, how would we expect the virulence of a novel infection to change? . . . 115
5.2.3 Would we expect widespread ART to drive changes in HIV virulence evolution? . . . 121
5.2.4 Defining the infection-age dependent model . . . 122
5.2.5 When does ART favour less virulent viruses? . . . 124
5.2.6 What is the expected magnitude and direction of this ART effect? . . . 127
5.2.7 Can we find data to test these model predictions? . . . 129
5.3 Discussion . . . 130
5.4 Questions addressed in this chapter . . . 135

6 Conclusion 137

A Supplementary material relating to chapter 3 **181**

A.1 Supplementary methods . . . 181

A.1.1 Estimating the number of escape events before first time point . . . 181

A.1.2 Is escape associated with clinical failure and if so would this lead us to underestimate the rate of escape? . . . 182

A.1.3 Multivariate Cox models for time to escape . . . 183

A.1.4 Extending the definition of escape . . . 183

A.2 Tables . . . 184

A.3 Figures . . . 190

B Supplementary methods relating to chapter 4 **205**

B.1 Parameterising the force of infection . . . 205

B.2 Full solution to ODEs . . . 210

B.3 A homogeneous model does not suffice . . . 212

B.4 Effect of ART initiation time and duration . . . 213

B.5 Homeostatic proliferation . . . 215

C Supplementary methods relating to chapter 5 **217**

C.1 Supplementary methods relating to the original model . . . 217

C.1.1 ODE model equations . . . 217

C.1.2 PDE model definition and solution at epidemic equilibrium . . . 218

C.1.3 Relating the ODE and PDE models at equilibrium . . . 223

C.1.4 Equilibrium population size calculations for the ODE model . . . 224

C.2 Low heritability of SPVL . . . 227

C.2.1 Methods . . . 227

C.2.2 Results: Magnitude and direction of the ART effect . . . 228

C.3 Model with increased transmission in acute infection . . . 233

C.3.1 Methods . . . 233

C.3.2 Results: Magnitude and direction of the ART-effect . . . 235

C.4 Modelling increased transmission amongst a subsection of the population . 240

C.4.1 Methods . . . 240

C.4.2 Comparison of generalised and concentrated epidemics . . . 241

C.5 Treatment initiation in all patients as soon as possible 245
C.5.1 Methods 245
C.5.2 Results 245
C.6 Additional sensitivity analyses 248

Acknowledgements

I am indebted to my supervisors, Angela McLean and John Frater, for their role in shaping this work and for their patient support throughout. As a result of Angela's guidance my scientific thinking and writing skills have been much improved and I am very grateful for her investment in me as well as in this research. I have hugely valued being part of John's lab group, through whom I have picked up most of the biology that I know. Thank you to both Angela and John for reading this thesis from cover to cover, and in particular to Angela for tirelessly reviewing drafts before the assembly of the final version. I am grateful also to Rodney Phillips, for his critical eye over the CTL escape chapter, and to Jacob Hurst for his mentorship throughout that project.

Laurent Hocqueloux and Veronique Avettand-Fenoel are gratefully acknowledged for sharing the data on HIV DNA decay. I am also grateful to the Nuffield Department of Medicine and the Medical Research Council for jointly funding this work.

The community of researchers in the 'infectious diseases' corner of the Zoology department have provided a wonderfully supportive and stimulating working environment and an ever-present source of advice – thank you all. In particular, my long-running officemate, Duncan, was a sounding board for many ideas and questions relating to this work.

Thanks are also due to many other faithful supporters, encouragers and teachers. In particular, thank you to my wonderful housemates at number 39 for their love and wisdom and for providing a home of joy. Thank you Frances, Daniel, Nick, Iza, Emily and all on Roots table 3 for your weekly and even daily encouragement at points, and for regularly reminding me of Col. 3:23. Thank you, Summer, for our Wednesday afternoon writing sessions. Huge thanks to my parents for your steadfastness and for lovingly nurturing (and, more recently, feeding) me. Finally, I would like to echo the small words on the title page of this thesis: *Dominus illuminatio mea.* He is indeed.

1

Introduction

Human immunodeficiency virus (HIV) infects 37 million people worldwide. In 2015 there were approximately two million new infections and the number of people living with HIV is still increasing [1]. The virus infects and destroys cells called $CD4^+$ T-cells that are crucial to the function of the immune system, eventually causing acquired immune deficiency syndrome (AIDS) [2]. The World Health Organisation now recommends that all infected individuals are given anti-retroviral therapy (ART) upon diagnosis [3]. ART is effective at suppressing viral replication, raising $CD4^+$ T-cell counts and reducing the risk of transmission, but it is not a cure [4–6]. The drugs must be taken daily for the rest of a patient's life. Cessation of treatment usually results in the virus rebounding to close to pre-treatment levels and consequent eventual progression to AIDS [7, 8].

Whilst there is only one documented case of HIV 'cure' [9], some patients are able to control the virus in the absence of ART, so that it is below detectable levels in the blood plasma [10,11]. Such patients also have healthy $CD4^+$ T-cell counts and low risk of onward transmission [12, 13]. In this thesis I explore three mechanisms which might lead to more individuals being able to control their viraemia in the absence of ART.

Chapter 3 focusses on T-cell immunity. ART-naive 'elite controllers' are a rare subset of individuals who spontaneously control following acute infection. The over-representation of particular Human Leukocyte Antigen alleles amongst elite controllers suggests that their ability to control is partly related to the strength and specificity of their cytotoxic T-lymphocyte (CTL) response [14]. The virus can acquire mutations that allow it to escape from this arm of the adaptive, HIV-specific immune response, and such escape may contribute to loss of viral control [15–18]. In chapter 3, I study the prevalence, incidence

and determinants of CTL escape in the largest cohort used for this purpose to date.

Chapter 4 focusses on early initiation of ART. Whilst ART is successful at suppressing viral replication, it is not a cure because a replication-competent HIV reservoir remains. This reservoir includes quiescent, latently infected $CD4^+$ T-cells that persist through their longevity and clonal proliferation, and may also be replenished through ongoing replication in drug sanctuaries [19, 20]. The term 'post-treatment controller' is used to describe individuals who have interrupted ART and continued to suppress the virus (below detectable levels in blood plasma) for at least two years in the absence of treatment. To date, recorded cases of post-treatment control have been restricted to patients who started ART in primary infection (within 6 months of infection) [21]. The size of the persistent HIV reservoir in latently infected $CD4^+$ T-cells has received much attention as a key factor determining a patient's ability to control [11, 22, 23]. In chapter 4, I consider how particular qualities of the reservoir, in addition to its size, may be affected by the timing of ART initiation and may combine with size to influence post-treatment control.

Chapter 5 focusses on viral evolution. It is not unreasonable to speculate that population-level viral evolution could lead to HIV becoming less virulent, enabling increasing numbers of patients to control their infection without ART. HIV is a relatively new infection of humans and there is evidence that the virus is adapting to its new host at the population level [24–26]. Given the now widespread administration of ART [1], in chapter 5 I ask whether the routine administration of ART might drive the evolution of the virus towards lower virulence.

I summarise the questions asked in each of the chapters in further detail below.

1.1 Chapter summary

1.1.1 Questions addressed in Chapter 3

Many studies of CTL escape have been based upon small groups of patients (often fewer than 5, rarely more than 10) which are not necessarily representative of the HIV-infected population as a whole [27–31]. I use longitudinal data from a cohort of over 100 UK patients to address the following questions:

- What is the prevalence at the time of infection and incidence thereafter of CTL

escape in these patients?

- When during infection does CTL escape tend to occur?
- Is there evidence for a disproportionately high or low number of escape events in some patients?
- Are there any host immunity factors associated with a greater incidence of escape?
- Is there any evidence that CTL escape reduces a patient's ability to control the virus?

1.1.2 Questions addressed in Chapter 4

Measuring and characterising the HIV reservoir (infected cells that persist on ART and could be the source of rebounding viraemia post-ART) has proved challenging [32, 33]. In chapter 4 I seek to use mathematical modelling to uncover key properties of the HIV reservoir and their relationship to post-treatment control. I hypothesise that considering heterogeneity in activation rates of latently infected cells may enable us to explain several observations around the dynamics of the reservoir. I focus on two data sets containing particularly rich information. One consists of HIV DNA decay data (longitudinal measures of cell-associated HIV DNA, a large part of which is integrated provirus) which shows differing patterns of decay between patients treated early in infection compared with patients treated later in infection. The second data set comprises longitudinal viral sequence data from which the time of infection of latently infected cells is inferred. We use this to inform our understanding of the dynamics of latently infected cells prior to the initiation of ART. I address the following questions:

- Does a model with heterogeneity in activation rates fit the different patterns of HIV DNA decay seen in early vs late treated-patients?
- Does this mechanistic explanation for the data still hold when we account for a majority of the HIV DNA being replication incompetent, defective provirus?
- Is the model compatible with the estimate of pre-ART turnover of latently infected cells derived from viral sequence data?

1.1.3 Questions addressed in Chapter 5

It is often assumed that an emerging infection which is unadapted to its new host will either increase or decrease in virulence until it reaches an evolutionary optimum. The value of this optimum would depend upon the relationship between virulence and transmission potential, amongst other factors [34]. However, empirical data on the virulence evolution of HIV to date present a confusing picture with no clear trend [35]. Whatever the trend so far, the widespread use of ART has the potential to alter the optimum strategy and so change the course of virulence evolution. In chapter 5 I use a simple two-strain deterministic model of epidemic spread to address the following questions:

- What are the expected patterns of virulence change in the initial decades of an epidemic?
- Could administration of ART drive changes in virulence evolution?
- What is the potential size and direction of any ART-effect?
- How does the effect vary according to different possible treatment guidelines?
- Should these results alter how we treat?

In chapter 6 I summarise how addressing these questions has contributed to our understanding of the prospects for viral control at the individual level. I then conclude by putting this discussion within the context of wider efforts to tackle the HIV epidemic.

1.2 Contributions to this thesis

1.2.1 Chapter 3

This chapter was submitted as a manuscript with the following co-authors: Hannah E. Roberts, Jacob Hurst, Nicola Robinson, Helen Brown, Peter Flanagan, Laura Vass, Sarah Fidler, Jonathan Weber, Abdel Babiker, Rodney E. Phillips, Angela R. McLean, John Frater, SPARTAC trial investigators [36]. Jacob Hurst is co-first author on this paper in recognition of the large amount of work involved in pre-processing the sequence data (see below).

The chapter is a post-hoc analysis of data collected from participants in the SPARTAC clinical trial. Sarah Fidler, Jonathan Weber, John Frater and the SPARTAC trial investigators were involved in the design and implementation of the trial and in curating samples and data. Nicola Robinson, Helen Brown, Peter Flanagan and Laura Vass conducted the laboratory assays for the collection of immunological and viral sequence data from patient samples. Jacob Hurst curated the sequence data and pre-processed the relevant sequences into FASTA file format.

Angela McLean, John Frater and Rodney Phillips provided supervision throughout this project. I, along with my supervisors, had an active role in deciding which research questions should be asked and how they should be addressed, given the available data. I designed and conducted all the analyses presented in this chapter (both descriptive and statistical) and wrote the necessary R code. This included designing and writing the algorithm for the detection and assignment of HLA-matched and -mismatched escape mutations according to multiple definitions. Jacob Hurst and Abdel Babiker provided advice on statistical methodology. I wrote the original manuscript.

1.2.2 Chapter 4

This chapter is a mathematical modelling project. The model development, testing and analysis are wholly my own work, under the guidance of my supervisors. Previously published data was kindly provided upon request by Dr Laurent Hocqueloux and Dr Veronique Avettand-Fenoel, which I used to test modelling hypotheses.

1.2.3 Chapter 5

This chapter was submitted as a manuscript with the following co-authors: Hannah E. Roberts, Philip J. R. Goulder, Angela R. McLean [37]. The preliminary modelling that I conducted when starting out on this chapter also contributed to the supplementary analyses in Payne et al., 2014 (doi: 10.1073/pnas.1413339111).

The chapter is a mathematical modelling project. The initial research question was motivated by data collected by Philip Goulder, and formulated through discussions between Philip Goulder, Angela McLean and myself. The model development and analysis are wholly my own work, under the supervision of Angela McLean. I wrote the original manuscript.

2

Literature review

2.1 The HIV pandemic

Human immunodeficiency virus (HIV) was identified as the etiologic agent of acquired immune deficiency syndrome (AIDS) in the early 1980s [38]. By then the virus had been circulating in humans for several decades in West and Central Africa, having crossed over from non-human primates multiple times in the first half of the 20th century [24, 39]. The epidemic growth of HIV is thought to have been facilitated by the social climate in post-colonial Africa. In particular, increased rail links, changing healthcare practices involving the use of unsterilised injections, and changes in sexual behaviour have all been suggested as playing a significant role [24]. The virus is transmitted through exposure to infected blood or semen, with the main routes being sexual transmission, parenteral transmission (use of unsterilised needles or blood products) and perinatal transmission (from mother to child) [40]. Sexual transmission accounts for the vast majority of new infections worldwide [41].

2.1.1 Population structure and molecular epidemiology

Multiple independent zoonotic transmissions of simian immunodeficiency virus (SIV) into humans have given rise to several different HIV lineages: HIV type 1 (HIV-1) groups M–P and HIV type 2 (HIV-2) groups A-H [39]. HIV-2 is largely confined to West Africa and has lower infectivity and virulence than HIV-1 [42]. Of the HIV-1 groups only group M is pandemic, while groups N-P are limited to far smaller numbers of individuals (of the order of 10 to 100,000) and have not spread much beyond West-Central Africa [39].

Group M viruses are further classified into nine subtypes. The global distribution of subtypes partly reflects the structure of the pandemic into sub-epidemics amongst particular risk groups, but regional variation has also been influenced by founder effects, transport links and migration, amongst other factors [39, 43]. Subtype C has consistently had by far the highest global prevalence and is particularly dominant in Southern Africa, where the main route of transmission is heterosexual contact [41, 44–46]. However, much research attention has been directed towards subtype B, which accounts for around 70% of HIV incidence in Europe and is also prevalent in the Americas, North Africa and the Middle East [45, 47]. Subtype B initially spread rapidly amongst injecting drug users (IDUs) and men who have sex with men (MSM) and in the developed world it remains primarily associated with these risk groups [47–49]. Superinfection of HIV infected individuals has resulted in the emergence of circulating recombinant forms (CRFs, viruses that have resulted from the recombination of distinct subtypes). Many different CRFs exist, some, such as CRF02_AG, are globally dispersed and account for a up to 10% of all infections [45].

There is some evidence that infectivity and virulence vary between subtypes, but the importance of this in shaping epidemic growth is unclear since any subtype-specific effects are often confounded by host ethnicity, behavioural and socioeconomic factors [39, 46, 50].

2.1.2 Global burden of disease

Figure 2.1 shows global trends in HIV/AIDS from 1990 to 2015. While HIV incidence (the number of new infections per year) peaked between 1995 and 2000, the estimated number of people living with HIV is still increasing. It currently stands at an estimated 37 million. HIV/AIDS was the fifth highest cause of disability adjusted life years (DALYs, a measure of disease burden) worldwide in 2010. This represented a 351% increase on DALYs due to HIV/AIDS in 1990 and was in spite of large declines in AIDS-related mortality since 2005. In sub-Saharan Africa HIV/AIDS accounted for nearly 40% of all DALYs in 2010 [51]. The socioeconomic impact of the epidemic has included profound changes in population structure in the worst-affected countries and deepening poverty in households that have lost young adults due to AIDS [52]. There were 15 million orphans due to AIDS in sub-Saharan Africa in 2009 [53].

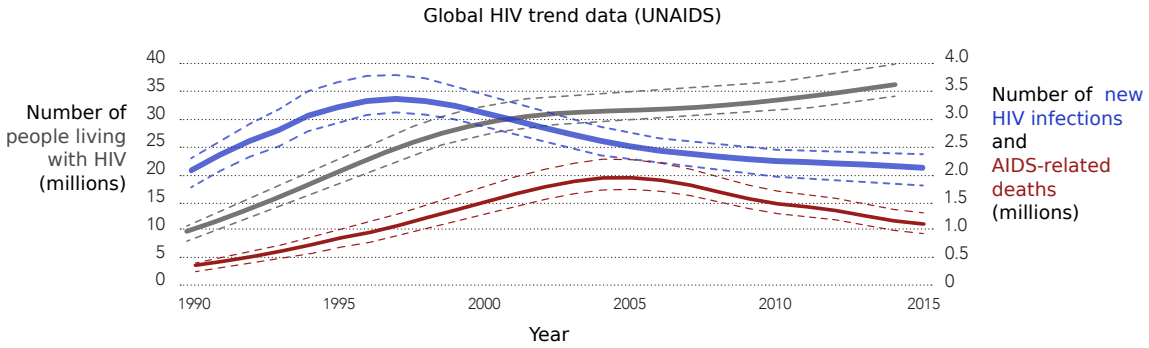


Figure 2.1: Global trends in the number of people living with HIV (grey, left hand axis), the number of new infections per year (blue, right hand axis) and the number of AIDS-related deaths per year (red, right hand axis). Solid lines show the UNAIDS modelled estimates from 2016 and dotted lines indicate the uncertainty bounds. Figure reproduced from data published in [54].

Heterogeneity in the burden of disease

Sub-Saharan Africa has been disproportionately affected by the HIV pandemic. The region was home to 70% of new HIV infections in 2012 and several countries in Southern Africa have a prevalence of >15%, compared to the <1% prevalence across the developed world [53, 55, 56]. There is also marked variation within countries; in 13 out of 33 countries in sub-Saharan Africa, HIV prevalence among adults is at least 5 times higher in some provinces than others [56]. Certain key populations, including sex workers, MSM, IDUs and transgender people, are particularly at risk of HIV infection. Outside of sub-Saharan Africa, the majority of new infections are among these key groups [57].

2.1.3 Controlling HIV epidemics

There is currently no vaccine or cure for HIV. Initial efforts to control the spread of the epidemic were focussed on preventing transmission through behaviour change interventions such as voluntary counselling and testing, sexual health education via mass media campaigns, promotion and provision of condoms, and interventions specifically targeted at high risk groups [58, 59]. Randomised controlled trials of several different interventions in various contexts have found little evidence for these interventions having an effect on HIV incidence, possibly because they do not result in a significant changes in behaviour, or because the trials are not powered to detect that change [58]. However, there are a handful of well-documented cases where behavioural prevention efforts are thought to

have contributed to declines in HIV prevalence. The number of people reporting multiple and casual partners in Uganda more than halved from 1989 to 1995, a change that has been attributed in part to a 1987 campaign to reduce multiple sexual partnerships [60–63]. There is evidence that similar behavioural change contributed to reductions in HIV prevalence in the heterosexual epidemics of Kenya and Zimbabwe and, somewhat transiently, to reductions in HIV incidence in MSM in San Francisco [64–68]. However inferring causality is challenging. HIV prevalence may be expected to decline as a result of the natural dynamics of the epidemic, but the exact patterns of growth and decline and their interaction with behaviour change will depend upon factors such as the distribution of the epidemic amongst different risk groups [69].

The development of an HIV vaccine that would be efficacious for preventing infection has been a major area of research for more than 25 years [70]. The first phase III trials (large studies in humans powered to detect low-level efficacy) aimed to elicit antibody-mediated protection but found no efficacy (having been powered to detect 30% efficacy) [70, 71]. Focus then shifted towards eliciting cell-mediated immune responses but several such trials were halted early after a subgroup of participants in the Step vaccine trial were found to have increased HIV incidence, believed to be related to the specific viral vector used [70, 71]. The RV144 trial, completed in 2009 in Thailand combined antibody and cell-mediated approaches and was the first trial to show significant efficacy [71]. A Bayesian statistical analysis concluded that there was a $\geq 22\%$ chance that the vaccine had 0% efficacy, depending on the assumed prior expectation of efficacy [71]. These results were too modest to support the licensing of the vaccine and further trials are needed to confirm the result.

In 1997, combination antiretroviral therapy (cART) became available, also referred to as highly active antiretroviral therapy (HAART). Current recommended HAART regimens have been shown to effectively suppress viral replication within a patient, halting progression to AIDS and reducing the rate of heterosexual transmission by more than 90% [72–74], with low risk of drug resistance developing. ART did not immediately become widely available in the developing world; in 2003, coverage still remained at less than 1% in sub-Saharan Africa [75]. However, globally, 17 million (of 37 million) people living with HIV are now on ART (as of 2015). The most recent WHO guidelines recommend

that ART should be initiated in anyone living with HIV, reflecting evidence that early ART initiation results in better clinical outcomes for the individual compared with later treatment [3, 57]. Additional support for this recommendation comes from several studies suggesting that initiating ART earlier could drive further declines in HIV incidence at the population level given sufficiently high uptake [76–78]. ART is also effective at preventing perinatal transmission and is now recommended for use by uninfected individuals at substantial risk of acquiring HIV (termed pre-exposure prophylaxis) [3].

HIV incidence has remained relatively stable since 2005 (see Figure 2.1). The 2015 Global Burden of Disease study concluded that 74 countries have actually seen an increase in incidence over the past decade, and UNAIDS estimates suggest 40% of infected individuals are unaware of their status [79]. Hence, achieving the end of the AIDS epidemic by 2030, as outlined in Sustainable Development Goal 3 [80], presents a huge challenge. There is a consensus that this will require a combination prevention approach, integrating biomedical interventions (including voluntary male circumcision, which has been found to reduce female-to-male transmission rates by approximately 50% [81], condom use, and the provision of ART to all recommended groups), structural interventions (such as combatting stigma, empowering young women and removing other barriers to accessing treatment and prevention), and behavioural interventions [79, 82]. Aside from the challenges of prevention there is also a need for a cure. Rising numbers of patients are facing life-long ART, which does not eliminate all the complications associated with chronic HIV infection, and will place a large burden on healthcare systems long into the future [83].

2.2 The natural course of an HIV infection

2.2.1 The HIV life-cycle

HIV is a retrovirus – an RNA virus which replicates via reverse transcription and subsequent integration of the viral DNA into the host cell's genome (see Figure 2.2 for the life-cycle). It infects cells expressing the CD4 surface receptor, including $CD4^+$ T lymphocytes and, to a lesser extent, monocytes and macrophages [84, 85].

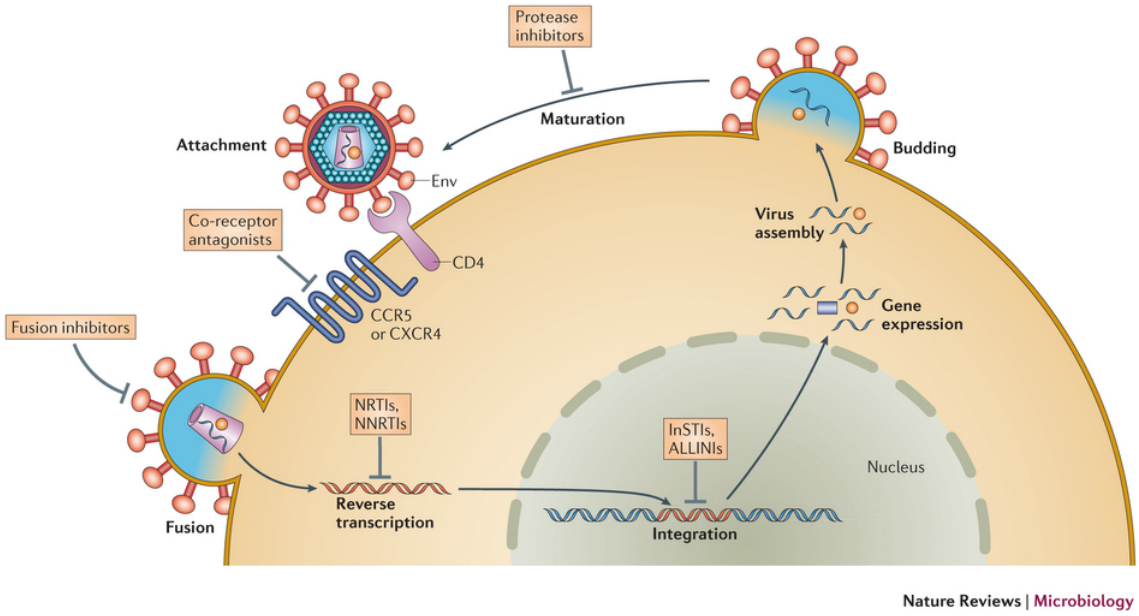


Figure 2.2: The life-cycle of HIV. HIV attaches to target cells through the binding of HIV Env with CD4 molecules. A CCR5 or CXCR4 co-receptor is also necessary to facilitate this process. After fusion of the virion with the cell membrane, viral RNA is released into the cytoplasm and reverse transcribed into DNA. This DNA is then integrated into the host cell's genome where the cell's machinery will make new viral proteins from it. New virions are assembled and bud from the cell to go on to infect new cells. Figure reused with permission from *A mechanistic theory to explain the efficacy of antiretroviral therapy*, Laskey & Siliciano, Nature Reviews Microbiology (2014) [86].

2.2.2 Natural history of an infection

Most HIV infections are transmitted by sexual contact and so virions or infected cells have to cross a mucosal barrier in order to gain access to the blood stream. The process by which this occurs has not been fully elucidated – transmission only occurs in a small fraction of exposures but it can be made easier by the presence of abrasions or tissue damage caused by other sexually transmitted infections [87]. After transmission, virus disseminates throughout the body reaching high levels of infection in $CD4^+$ T-cells within lymphoid tissue. Peak viraemia occurs 20-30 days following infection and the patients's CD4 count reaches a nadir around this point. The HIV-specific immune response kicks in around peak viraemia, causing high levels of immune activation, often resulting in feverish symptoms for the infected individual. Fiebig staging has been a useful clinical tool for stratifying patients diagnosed in acute infection [88]. The stages describe the points at which HIV antigens and antibodies sequentially become detectable by clinical assays. In

more detail, stage I is defined as the detection of viral RNA in the plasma by PCR, then stage II is marked by detectable levels of p24 antigen. Stage V is the last acute stage, starting approximately 20 days after stage I and corresponding to the detection of HIV-specific antibodies by western blot. This stage description is not without its limitations – it relies on being able to correct for different sensitivities of assays, and may better reflect the patterns seen following some modes of transmission than others. However, Fiebig staging was used to stratify acute infection cohorts until very recently, when it was super-seeded by 4th generation antigen-antibody combination enzyme immunoassays which are able to further stratify patients in Fiebig I [89].

Following seroconversion, viral load in the plasma declines to a set-point, the value of which is strongly negatively correlated with the length of asymptomatic infection, i.e. time until progression to AIDS [90, 91]. During asymptomatic infection, CD4 count gradually declines to a point where the immune system is no longer able to function adequately, viraemia rises again and the patient is vulnerable to opportunistic infections. Time between seroconversion and AIDS can vary from several months to more than 20 years [92, 93]. Correspondingly, set point viral load varies by several orders of magnitude and some rare patients ($< 1\%$) are able to durably control the levels of viral replication such that viral load is below the 50 copies/ml limit of detection for at least a year [93, 94].

The exact mechanism that leads to a gradual decline in CD4 count during chronic HIV infection is unclear. It was noted early on that direct killing by CTLs could not explain the effect since only a small fraction of $CD4^+$ T-cells are infected at any one time. Rather, it seems there is an increased death rate of uninfected 'bystander' $CD4^+$ T-cells. Possible explanations for this include an increase in apoptotic signals, a larger proportion of short-lived activated T-cells, and a direct cytotoxic effect of free viral proteins [95–97].

2.2.3 An overview of the immune response to HIV

The innate immune response represents the first barrier to the spread of infection. Dendritic cells ingest pathogens at the site of infection and transport them to the lymph nodes, and may consequently promote the dissemination of HIV more than they aid the host's defence [87]. Natural killer (NK) and natural killer T (NKT) cells produce cytokines and chemokines and are involved in the cytolysis of infected cells. In HIV infection, the in-

nate response results in a 'cytokine storm' which is detectable around the time of peak viraemia. These cytokines inhibit replication but may also help the virus come into contact with susceptible target cells through the recruitment, activation and proliferation of $CD4^+$ T-cells [87]. There are also intracellular mechanisms by which the host counters infection – APOBEC3G is known to be important in HIV infection. It is an antiviral protein which causes hypermutation in reverse transcribed HIV DNA and may have a particular role in disrupting HIV infection of resting $CD4^+$ T-cells [98]. HIV is able to mount a defence to this antiviral activity through the Vif protein, which enhances the degradation of APOBEC3G.

The cell-mediated adaptive immune response, in particular the action of cytotoxic $CD8^+$ T-cells (also known as cytotoxic T-lymphocytes, or CTLs), is key in the host defence against many intracellular pathogens such as viruses. Our understanding of the role of the cell-mediated response in HIV was greatly advanced and enabled by the elucidation, in the late 1980's, of the mechanism by which T-cells recognise foreign antigen. Viral (or other non-self) proteins are fragmented into peptides in the cytoplasm of infected cells, bound to major histocompatibility complex (MHC) proteins and transported to the cell surface where the peptide-MHC protein complex can interact with T-cell receptors [99–101]. $CD8^+$ T-cells recognise peptides of around 8-10 amino acids in length bound to MHC class I molecules [101] whereas $CD4^+$ T-cells recognise peptides of 13-17 amino acids in length bound to MHC class II [102]. CD8 recognition commonly leads directly to the death of the infected cell (amongst other functions). CD4 recognition leads to the production of cytokines, the activation and proliferation of CTLs and the regulation of the adaptive immune response. The first $CD8^+$ T-cell responses to HIV arise in Fiebig stage I or II. Both the frequency of HIV-specific CTLs and their capability to lyse infected cells *ex vivo* are remarkably high in acute infection but decline in advanced infection as CD4 count drops [87, 103–106]. HIV-specific CD4 responses are also present in early infection but decline during primary infection and become functionally impaired [107–109]. There is good evidence that the host CTL response accounts for some part of the variation in viral set point or time to AIDS progression [110, 111] (as discussed in detail below). The strength of the HIV-specific $CD4^+$ T-cell response is less well studied but has also been implicated in determining disease progression [108, 112].

Antibodies can block viral replication by binding to virus coat proteins and preventing the viruses from entering host cells. This particular action of antibodies is termed neutralisation and is important in immunity against influenza, for example, where neutralising antibodies against the hemagglutanin molecule also form the basis of current vaccines [113, 114] Antibodies against HIV largely target epitopes on the Env glycoprotein. HIV Env is highly variable between patients and evolves fast within a patient, which both presents a challenge to the immune response and hampers efforts to design an effective vaccine. The first Env-specific antibodies arise 2-3 weeks following infection but many of these early responses are unable to neutralise the autologous virus – neutralising antibodies (NAbs) may not arise until 13+ weeks after infection [87, 115, 116]. Only 20-25% of patients develop cross-reactive neutralising antibodies against HIV, and even fewer of these are classed as 'broadly neutralising' [116]. There is debate over the extent to which the antibody-mediated response contributes to viral control in HIV infection. Mathematical modelling studies have both concluded that it has little effect in acute infection, and suggested that antibody induction is key for viral control [117,118]. The fast rate at which HIV Env evolves to evade NAbs, and a case of B cell depletion leading to a rise in viral load, support a role for NAbs in the control of chronic infection [115, 119].

The interaction between HIV and the immune response is particularly complex given that the virus' host cells are $CD4^+$ T-cells. The depletion of $CD4^+$ T-cells as a result of HIV pathogenesis likely contributes to the dysfunction of the immune response in chronic infection. Insufficient numbers of HIV-specific $CD4^+$ T-cells (which are preferentially infected by HIV [120]) impairs the stimulation of HIV-specific CTLs and their transition to long-term memory cells and also results in reduced production of NAbs [109, 118].

2.2.4 CTLs and viral control

The temporal association between the expansion of the HIV-specific CTL response and the decline in viraemia during acute infection led to early suggestions that CTLs played a key role in controlling the replication of the virus. This was combined with observations, on small groups of patients, of an association between the strength of the CTL response and the efficiency of control of primary viraemia [104, 105]. The CTL response was soon after shown to be important in the SIV-macaque model, where the administration of anti-

CD8 antibodies led to loss of viral control [121]. However larger studies in humans found no correlation between $CD8^+$ T-cell responses (as measured by IFN-γ ELISpot assays) and HIV viral load [122]. It was suggested that the 'temporal association' observed may be coincidental since the depletion of susceptible target-cells, in the absence of a specific immune response, could cause the observed dynamics [123].

When examining this evidence, it should be noted that whilst the IFN-γ ELISpot assay has historically been the most widely used assay for assessing the quality of $CD8^+$ T-cell responses, there is now evidence that it reflects true *in vivo* CTL strength poorly compared to other assays. For example, one study found that assays for $CD8^+$ T-cell mediated inhibition of heterologous virus correlated significantly with $CD4^+$ T-cell decline in chronically infected patients, while gag-specific IFN-γ responses showed no correlation [124]. Additionally, qualitative, per-cell measures of the cytotoxic capacity of $CD8^+$ T-cells, such as lytic granule contents and HIV-specific perforin production, have been shown to differ between non-progressing or Elite Controller patients versus progressors, while IFN-γ production did not allow the same differentiation [125, 126]. IFN-γ ELISpot assays rely on the loading and recognition of exogenous peptides added at very high concentrations, which could explain a disconnect between the results of these assays and *in vivo* IFN-γ production of HIV-specific $CD8^+$ T-cells [124].

Recent evidence for the role of CTLs in viral control has come from longitudinal data showing that the extent to which the virus sequence is adapted to the host's HLA profile is predictive of viral load (greater adaptation leads to higher viral loads) [111]. Other studies have highlighted a significant relationship between the specificity of CTL targetting in primary infection and viraemia [127,128]. Studies of the host genetic effects on HIV disease progression have found the strongest associations are with HLA class I loci [110, 129]. This has led to the classification of HLA types and supertypes that are 'protective' for HIV. HLA-B*27 and HLA-B*57 are two of the alleles with the strongest protective effect amongst Caucasians; patients possessing one of these alleles have an approximately 2-fold lower hazard of progression to AIDS in survival analyses [130]. Protective HLA alleles have further been found to have a high capacity to elicit CTL responses [13, 131, 132].

Consequently, that CTLs have a role in viral control is no longer a point of debate. However the magnitude and mechanism of the effect is still contested. The strength of

CTL killing estimated in different modelling studies varies considerably, from 10-20% of productively infected $CD4^+$ T-cells per day across all responses to 15-35% per day for a single response [133,134]. One source of killing rate estimates is data documenting the rate at which wild-type virus is replaced by mutated strains that are able to escape the host's dominant CTL responses [133, 134]. Estimates from this data depend heavily upon the assumed fitness cost of escape mutations [133]. Since it is not clear whether *in vitro* fitness assays translate well into *in vivo* measures, the ideal method for determining fitness cost would be from the rate at which the mutated strain reverts to wild-type in the absence of a CTL response. There has been no comprehensive study of reversion rates that is able to take account of the effect of compensatory mutations and clonal interference [135, 136]. Hence, fitness costs remain unknown and absolute rates of CTL killing cannot be reliably determined from escape data [136]. A second source of data is viral load dynamics following the perturbation of the system by ART. It has been observed that neither (1) the rate of viral load decline on ART or (2) the rate of rebound following treatment interruption correlate with the strength of the CTL response [137,138]. Since the second of these studies relied on the IFN-γ ELISpot assay, it is unclear whether this is evidence for a weak effect of CTLs on viral control, or whether it is a consequence of the assay poorly quantifying true CTL strength. Or, in the case of viral load decay, whether the decay rate is not reflective of CTL killing strength – alternative models that are consistent with the data result in different interpretations of this viral load slope [136]. Note that the role of $CD8^+$ T-cells in viral control may also include non-lytic effects which are rarely considered in these modelling studies [139].

2.3 The evolution of HIV

The HIV genome is $\sim$9.7 kilobases in length [140]. In common with other retroviruses, it includes three major genes: *gag* (encoding proteins that make up the matrix, capsid and nucleocapsid), *pol* (encoding the enzymes protease, reverse transcriptase and integrase), *env* (encoding the glycoproteins that make up the envelope) [141]. HIV also encodes for the accessory proteins Vpu, Vpr, Vif anf Nef, and the regulatory proteins, Tat and Rev [140].

2.3.1 Within-host viral evolution

HIV evolves fast within host due to the high mutation rate of its reverse transcription, a short generation time of around 2.5 days, and strong selection pressure exerted by the host immune response [142–144]. Recombination, which results from coinfection of a single cell by more than one virus followed by template switching of reverse transcriptase, has also been found to significantly contribute to sequence diversity in HIV [145]. An estimated 80% of infections originate with a single transmitted/founder virus and diversity increases roughly linearly over the next few years [31, 146]. A recent study of nine patients found that divergence varied by ∼10 fold across the genome but was only ∼1.5 fold different between patients. Highest rates of evolution were consistently found in the variable loops in gp120 (the glycoprotein on the surface of the viral envelope), while regions coding for protease, reverse transcriptase and the rev response element (necessary for the transport of HIV mRNA from the nucleus to the cytoplasm) were much more conserved [146]. The action of APOBEC 3G has been found to contribute to HIV sequence diversity and aid adaptation both in *in vitro* models and in early infection *in vivo* [147, 148].

2.3.2 Immune escape in HIV

Immune escape occurs when selection pressure exerted by the host immune system results in the virus adapting so that it can 'escape' the host's defences. Escape in HIV takes the form of single or multiple mutations that prevent MHC-restricted recognition of HIV epitopes or prevent antibody binding, without completely disrupting the virus' ability to replicate.

Escape from CD4$^+$ T-cells and the innate response. The possibility of CD4 escape in chronic viral infection was demonstrated in Lymphocytic choriomeningitis virus (LCMV) in mice in 2001 [149]. Prior to this work, the existence of circulating viral variants eliciting diminished CD4 responses had been noted in patients with chronic HIV infection [150]. However the existence of these mutations was not sufficient evidence that they resulted in a selective advantage within host. Good evidence of this came from a recent study which identified HLA-II associated sequence polymorphisms within CD4 epitopes and confirmed that these conferred at least partial escape from CD4 recognition and that

CD4 targeting of the epitopes correlated with viral control [151]. Out of 99 patients in acute infection cohorts, 9 were observed to develop one of these escape mutations. There are few studies on HIV escape from the innate immune response. Sequence polymorphisms that could help the virus to evade the NK-cell-mediated response have also been identified, but this population-level analysis does not provide information on how frequently these mutations become fixed within host [152].

Escape from neutralising antibodies. Escape from NAbs has been documented as occurring as early as 3-6 months post seroconversion, with escape mutants taking of the order of weeks to become fixed in the population, possibly due to low initial NAb titres [153,154]. There are multiple different pathways to NAb escape, even for antibodies targeting the same epitope. These commonly involve one or both of direct within-epitope mutations and mutations outside the epitope that result in glycan shifts [154–156]. *In vitro* viral replication assays have found that NAb escape mutations seem to incur a low fitness cost [153, 157]

CTL escape. Viral escape from host CTL responses was first demonstrated in LCMV in mice [158]. The within-host evolution of an HIV mutant able to escape CTL recognition was described a year later in a HLA B8-restricted epitope in the *gag* gene [15]. In HIV infection, CTL escape occurs through the acquisition of mutations in or around CTL epitopes which either prevent the epitope binding to MHC class I molecules, or prevent recognition by $CD8^+$ T-cell receptors, or disrupt an earlier part of the antigen processing pathway [16, 17, 159, 160]. These mutations may carry a fitness cost [161, 162] and consequently can revert to wildtype in the absence of selection pressure from CTLs (most evidently in individuals lacking the restricting HLA type(s)) [163, 164]. Compensatory mutations, which appear to abrogate the fitness cost of escape mutants, have also been described [17, 165].

Early studies on CTL escape were limited to looking for variation within small numbers of well-defined epitopes [15,29,30,166,167]. More recently, techniques such as genome wide association studies to identify HLA-associated sites at the population level, whole-genome deep-sequencing of longitudinal plasma virus samples, and single genome amplification to deduce the transmitted/founder virus have greatly extended the number of epitopes and escape sites that can be studied [134, 144, 168]. This is combined with mapping $CD8^+$

T-cell responses to the full proteome using autologous overlapping peptides to give an unbiased assessment of the footprint of the CTL response on the viral population within a patient. Such methods have led to claims that the majority of non-*env* mutations fixed in the first years of infection are CTL-related [169].

Estimates of escape and reversion rates vary by orders of magnitude. It is worth clarifying the two possible uses of the term 'escape rate' before covering reasons for this variation in estimates. Firstly, there is the rate at which the mutant (escape strain) outgrows the wild-type. This rate is estimated from longitudinal data by fitting a model of infected cell dynamics to the outgrowth curve [133,170]. Secondly, 'rate' is also used to describe the time point during infection at which an escape in a particular epitope tends to arise. This estimate is often derived from cross-sectional data and will incorporate data from patients (with the restricting HLA type) who never drive the escape [171]. The two 'rates' are not equivalent measures since CTL pressure is not constant during the course of infection and there is likely to be some waiting time until the initial establishment of the mutant strain. They are, however, related quantities – both will depend on the fitness cost of an escape, for example.

The rate of outgrowth of escape mutants has been found to be faster the earlier in infection an escape occurs [133,170]. It has been hypothesised that this decrease in outgrowth rate could be a result of weaker CTL killing, increasing breadth of the CD8 response over time and/or a higher fitness cost of late escapes [133,170]. There is also significant inter-epitope variation in the average time until an escape occurs [171,172]. It has been shown that epitopes with lower Shannon entropy escape later in infection (low Shannon entropy is thought to be an indication of high fitness cost of mutation within that epitope) [27,160], and that immunodominance hierarchies of $CD8^+$ T-cell responses within a patient account for 39% of the variation in time to escape [160].

Several studies have demonstrated the existence of very early, rapid escape, occurring within the first 3 months of infection. The studies in [27, 28, 160, 173] collectively report on 25 patients and, in 23 cases, identify rapid ($<$ 3 months) replacement of the transmitted/founder virus within epitopes targeted by autologous CD8 responses. These studies may overestimate the incidence of very early escape since some of them intentionally report on cases previously known to exhibit early escape [28]. Other studies have

looked at the incidence of escape *within pre-defined epitopes* restricted by an individual's HLA type and found evidence of no escape within 3 months of infection [166, 174–176], while cross-sectional studies have found that few epitopes consistently escape early [171]. These studies may underestimate the incidence of early escape since they are restricted to previously known epitopes.

2.3.3 Between-host evolution

All RNA viruses have similarly high mutation rates, yet patterns of population-level evolution differ greatly between them depending on the epidemic behaviour and extent of cross-immunity. For example, seasonal influenza A virus, which has a short duration of infection and can relatively easily escape immunity shows high levels of adaptive evolution at the between-host scale. For measles, on the other hand, immune selection has little effect on the population-level phylogeny since individuals mount highly cross-reactive immune responses which are equally effective against all strains [177]. These differences have direct public health implications - vaccines for influenza A must be updated annually whereas measles vaccines need not.

In the case of HIV, while positive selection has a large effect on within-host evolution, between-host evolution seems to be more closely tied to spatiotemporal differences in epidemic dynamics. The dominance of subtype C globally is most likely due to its chance introduction into populations with continually high rates of partner change and transmission, rather than due to its higher fitness [46, 178]. Not only do between and within-host phylogenies for HIV have very different shapes, the rate of between-host evolution has been estimated as 2-6 times slower than within-host evolution [179]. Several factors could account for this. Firstly, a bottleneck at transmission (at least in sexual transmission) results in a single strain establishing a new infection in the majority of cases [31]. It has been suggested that strains that were prevalent early in infection could be preferentially transmitted, either because they are better adapted for transmission or because archived virus is more likely to be present in the genital tract. A mathematical modelling study found that this 'store and retrieve' hypothesis could make a major contribution to the slow rate of divergence at the population level [179]. Secondly, if within-host selective forces are stronger in chronic infection, yet a high proportion of transmissions occur in acute infection

(as discussed in [180,181]) then this would result in a mismatch in within and between-host evolution rates. However, current evidence would seem to suggest that, if anything, the selective pressure exerted by CTLs is higher earlier in infection [133]. Thirdly the exact nature of selective pressures differs between hosts, largely because restricted CTL epitopes differ between HLA types, and consequently reversion of escape mutations may contribute to the low rate of between-host evolution [163, 171].

However, despite these factors, there is evidence of HIV adapting to its host at the population level. In particular, adaptation to host HLA types has been observed in large studies which have seen the frequency of HLA-associated polymorphisms in individuals without the relevant HLA increase by $\sim$2 fold in 20 years of epidemic history [182], or documented a correlation between the frequency of an HLA allele in various populations and the frequency of an associated escape mutation [183].

2.3.4 Virulence evolution

If the virulence of a pathogen (i.e. its potential to cause harm to the host) is linked to its potential for onward transmission and is at least in part determined by pathogen genetics, then we would expect virulence to evolve as the pathogen adapts to its new host. One of the best documented cases of virulence evolution is the introduction of myxomatosis into rabbits in Australia in the 1950s. The virus evolved an attenuated virulence compared to the original strain, but infections still remained fatal in the majority of cases. The observed changes were in agreement with the trade-off hypothesis [184]; an intermediate virulence was reached that had a longer survival time while maintaining the high titres necessary for onward transmission by mosquitos [185]. In HIV, the term virulence is used to refer to the rate at which a patient progresses to AIDS. Here also, virulence is known to be linked to transmission potential; patients with high set point viral load (SPVL) progress quickly to AIDS [186], but high viral load is also associated with a high risk of transmission per exposure [187].

The empirical data on whether or not the virulence of HIV is changing present a confused picture. Several large cohort studies have been conducted, but these have returned a range of results, explainable to some extent by genetic and environmental differences between local sub-epidemics and cohort types (meta-analysis in [35]). The increasing use

of ART, changing measures used to assess virulence and various measurement and sampling biases all contribute to the difficulty of interpreting these results [35, 188]. A recent study (not included in the original meta-analysis), including measurements of SPVL in over 15,000 individuals pooled from seroconverter cohorts across Europe showed non-monotonic patterns of changing virulence. SPVL (often used as a proxy for virulence) increased from 1980-2002 but started to plateau and then decrease thereafter [189].

At the same time there has been uncertainty over what, if any, changes in virulence evolution we should expect. There was previously debate over the heritability of SPVL, in other words, the extent to which variation in SPVL can be explained by viral genetic factors as opposed to host factors (reviewed in [190]). A recent summary of estimates suggested that 20-46% of variation in SPVL can be attributed to the virus [190]. This non-zero estimate of heritability, combined with data suggesting that HIV is becoming better adapted to maximise its transmission potential, could be seen as evidence for selection for SPVL at the population level [190, 191]. Some have put forward an alternative hypothesis, contending that within-host evolution alone could give rise to the current observations and that we should expect the evolution of HIV to be short-sighted, which would result in increased population-level virulence in the long term [192, 193]. In support of the former hypothesis, it has been noted that population-level selection of SPVL could occur in spite of fast within host evolution via two possible mechanisms. First, the existence of heritable virulence factors under low selection pressure within host [194, 195] or second, the preferential transmission of viruses from early in infection combined with the genotype of early viruses having a particular influence on SPVL [196, 197]. It is not clear to what extent either of these mechanisms occurs. Which of between-host or within-host selection pressures is having the greater effect on virulence evolution will become evident as more data on long term virulence trends become available – further observations of decreasing SPVL (like those very recently reported in Uganda [191]) would favour the impact of population-level selection pressures over the short-sighted evolution hypothesis.

2.4 The course of a treated infection and post-treatment control

2.4.1 The action of drugs

Combination antiretroviral therapy (cART), developed in the 1990s, is effective at blocking the replication of HIV *in vivo*. In involves the daily administration of 3-5 drugs from at least two different classes, each of which acts at a particular stage of the virus life cycle (see Figure 2.2). The major classes of drugs used today are reverse transcriptase inhibitors (both nucleoside reverse transcriptase inhibitors, NRTIs, and non-nucleoside reverse transcriptase inhibitors, NNRTIs), protease inhibitors (PIs), and integrase inhibitors (INSTIs). Current WHO guidelines recommend that first-line ART for adults should consist of two NRTIs plus an NNRTI or INSTI. If treatment failure occurs, then two NRTIs and a ritonavir-boosted PI are recommended [198]. For many years, ART was initiated based on a patient's CD4 count. In 2003 the recommended treatment threshold was CD4 count below 200 cells/mm^3, but this had been raised to 500 cells/mm^3 by 2013. In 2015, following good evidence that early treatment initiation is clinically beneficial, the WHO updated this guidance so that now all infected patients should be given ART, regardless of CD4 count [3, 5].

2.4.2 The establishment of the HIV reservoir

Under successful antiretroviral therapy, virus becomes undetectable in the blood within a few weeks. However, early hopes that treatment would eliminate the virus from the body and eventually cure patients were countered by the discovery of a replication-competent persistent reservoir for HIV which either decayed very slowly or not at all during ART [6, 19, 199]. The term 'HIV reservoir' is now used to refer to cells harbouring replication-competent virus, which are kinetically stable (i.e. persist during cART) and could contribute to rebounding viraemia if the patient were to stop treatment [200, 201]. It is established very early in infection, as demonstrated by examples of patients who were treated within the first few days of infection but later experienced viral rebound [202, 203].

This reservoir was initially identified in latently infected, resting CD4$^+$ T-cells [19].

These continue to be the portion of the reservoir of primary concern, since they are believed to constitute the majority of the reservoir and have been demonstrated to be a source of rebounding viraemia [204–206]. Studies on the HIV reservoir often look at resting $CD4^+$ T-cells in the peripheral blood, due to ease of sample collection. However, only a small proportion of resting $CD4^+$ T-cells are circulating at any one time and so the lymph nodes, gut-associated lymphoid tissue and genital tract are likely to be key anatomical sites of the reservoir [207, 208]. These sites may additionally harbour drug sanctuaries in which ongoing replication occurs [20] (discussed later under 'persistence'). Macrophages and astrocytes in the central nervous system may also represent an important section of the HIV reservoir, but while brain tissue (which must be obtained from autopsies) is known to contain HIV DNA in cART-treated patients, studies have been unable to demonstrate whether these infected cells might be capable of producing infectious virus [209, 210].

2.4.3 Latent HIV infection in $CD4^+$ T cells

HIV latency has been defined as the reversible nonproductive state of infection of an individual cell [201]. Latently infected cells therefore contain an integrated provirus that is replication competent, while not expressing a full set of viral gene products, if any [211,212]. The direct infection of resting $CD4^+$ T-cells is known to be inefficient, though it may be facilitated by interaction with dendritic cells or chemokines [213–215]. An alternative, favoured hypothesis for the establishment of latent infection in resting $CD4^+$ T-cells is that activated $CD4^+$ T-cells become infected and survive long enough to revert to a resting state [213].

Molecular mechanisms for persistence of individual latent infections are multifactorial and incompletely understood. At the transcriptional level, it is known that HIV is usually integrated within genes that are actively transcribed in resting cells [216]. HIV could maintain transcriptional silence in spite of this through chromatin modifications, DNA methylation or transcriptional interference (which can occur when the provirus is integrated with the opposite polarity to the host gene, or with the same polarity but downstream of the host gene). Additionally, levels of the transcription factors NF-κB and NFAT are lower in the nucleus of resting cells, as are levels of cyclin T1 – all three of these are involved in promoting the transcriptional initiation and elongation of HIV [213, 217].

At the post-transcriptional level, there is evidence that viral RNA export may be impaired in resting cells through the lack of full-length polypyrimidine tract binding protein [211]. Certain microRNAs (non-coding RNA molecules), which are expressed in resting cells but down regulated upon T cell activation, may be involved in suppressing viral protein expression [218]. It is worth noting that the resting state is not necessary or sufficient for latency, but the two usually equate [211, 219].

2.4.4 The measurement and characterisation of the reservoir in $CD4^+$ T cells

There is currently no gold standard measure of the size of the HIV reservoir in an infected patient. The quantitative viral outgrowth assay (QVOA) is resource and labour intensive but is considered to more accurately reflect the size of the 'true reservoir' than PCR-based measures of cell-associated HIV DNA [32]. The latter are unable to distinguish between replication-competent and -incompetent proviruses, and consequently have been found to overestimate the size of the replication-competent fraction by nearly 100-fold in some cases [219, 220]. In comparison, the QVOA measures the number of infectious units per million resting $CD4^+$ T-cells – the frequency of cells that are able to produce infectious virus following stimulation with a global T-cell activation agent, phytohemagglutinin (PHA). This measure could underestimate the size of the reservoir by as much as 60-fold: A 2013 study found that the majority of cells ($> 90\%$) containing proviruses with replication competent genomes and normal long terminal repeat (LTR) function *do not* revert to productive infection upon stimulation with PHA. While it is not clear what fraction of these latently infected cells could be induced *in vivo*, approximately 25% of the intact, originally non-induced proviruses were able to be induced *in vitro* on a second round of activation [219].

Recent efforts to measure the size of the HIV reservoir more accurately include the tat/rev Induced Limiting Dilution Assay (TILDA). This measures the frequency of cells that produce multiply-spliced HIV RNA transcripts upon activation and results in measures of reservoir size that lie between those of PCR-based assays and the QVOA [221]. Some have suggested that either the avidity and concentration of HIV antibodies, or markers of immune activation could be more accurate, though indirect, measures of the size of

the HIV reservoir (since they may reflect levels of sporadic viral reactivation or ongoing viral protein production) [222, 223]. Ultimately, the most useful measure would be one that could accurately predict time to viral rebound post-ART, on which there is currently insufficient data.

While there has been much interest in estimating the size of the reservoir, others have been concerned with further characterising the latently infected $CD4^+$ T-cells in which the reservoir resides. Various sources of heterogeneity amongst $CD4^+$ T-cells could result in some subpopulations of cells being preferentially infected and/or more persistent than others on ART. Indeed there is evidence suggesting that HIV enters naive $CD4^+$ T-cells less efficiently than memory cells and, perhaps correspondingly, that naive and terminally differentiated cells only make a marginal contribution to the reservoir (constituting 2% of cells with integrated provirus in peripheral blood) [224, 225]. Cells with a memory stem cell phenotype (T_{SCM}s; a small memory T-cell population at an early developmental stage) and cells expressing immune exhaustion markers such as PD-1 have been reported to be enriched for HIV DNA in patients on ART [225–227]. Amongst PD-1^{Hi} cells, T follicular helper cells (which largely reside in immune privileged B-cell follicles) may constitute a major source (around 50%) of replication-competent HIV in cART-treated individuals [228]. It has also been reasoned that the antigen specificity of a cell or the integration site of the provirus might affect the expected length of time that a cell persists in the reservoir [229–231].

2.4.5 The persistence of the HIV reservoir

Central memory $CD4^+$ T-cells have an estimated inter-mitotic time of ∼48 days, compared to ∼1 year for naive cells and ∼15 days for effector memory cells [232] (though a recent assessment of the methods used in this calculation suggests it is likely to be an underestimate [233]). This estimate implies that persisting clonal memory T-cell populations divide several times a year on average. This persistence of individual clones occurs through the combined processes of homeostatic proliferation (cytokine-dependent) and clonal expansion (antigen-dependent). It might be expected that, in the case of latently infected cells with replication competent provirus, division would induce HIV production and hence induce viral toxicity [234]. Until recently, while it was known that homeostatic proliferation

and/or clonal expansion have a clear effect on the phylogeny of cell-associated HIV DNA in treated patients, it had not been conclusively shown that these proliferative processes contribute to the maintenance of the true, replication competent HIV reservoir [225, 235–237]. Data have now been presented that show a highly expanded clone containing replication-competent, infectious provirus which persisted in a patient on ART for many years [238]. Further to this, studies of IL-7 administration have given support to the model in which cytokine-mediated proliferation can occur without inducing HIV replication in latently infected cells, hence contributing to the persistence of the reservoir while maintaining the size of the T-cell pool [239–241]. A study of viral persistence in untreated HIV controllers found evidence that antigen-driven clonal expansion of cells with integrated provirus can also occur without resulting in cell death [242].

Additionally, ongoing replication may contribute to the persistence of the reservoir [243]. Support for this theory has come from data showing much lower drug concentrations in lymph nodes compared to the peripheral blood, suggesting the existence of drug 'sanctuaries' [244]. Studies have also shown an increase in 2-LTR circles (an unintegrated form of HIV DNA) following the addition of an integrase inhibitor to the treatment regime, consistent with new rounds of infection becoming blocked at the integration phase [245, 246]. However, such treatment intensification was not associated with a decrease in viral RNA or cell-associated DNA [246, 247]. Some have suggested that the residual vireamia in some treated patients may indicate the presence of ongoing replication, but it could also result from viral re-activation of latently infected cells without new rounds of infection [248]. Evidence of continued HIV evolution under ART is needed to conclusively demonstrate that ongoing replication fuels the reservoir. Little evidence of evolution on long timescales has been found [249, 250], but a recent study reported significant evolution in lymphoid tissue over the first 6 months of ART [20]. In the same study, mathematical modelling was used to demonstrate that ongoing replication in drug sanctuaries is possible without seeing the evolution of drug resistance [20]. However, this is still a controversial finding; it has been argued that the observed evolution could be a false signal resulting from the faster average decay rate of recently infected cells [250]. The issue remains unresolved. Either data will need to be presented showing that the decay of recently infected cells cannot account for the signal of short-term evolution, or evidence of longer term, forward

evolution will need to be found. In SIV-infected macaques, whole body *in vivo* imaging using a labelled env-specific antibody revealed low level replication occurring in tissues 5 weeks post ART (following viral suppression below 60 copies/ml at 3-4 weeks) [251].

The mechanisms underlying the persistence of the HIV reservoir could vary between different cell subsets, different anatomical sites, and at different points in time. For example, proliferation may occur at a higher rate in cells where HIV is integrated into cancer genes [252], ongoing replication may be more prevalent in T follicular helper cells located in immune privileged sites [228], and bursts of replication may occur at times of increased immune activation, such as following immunisation [253, 254].

2.4.6 The dynamics of the reservoir in CD4$^+$ T-cells

As previously mentioned, it is known from cases of patients treated very early in infection that the reservoir is established effectively immediately after infection [202, 203]. Studies in the SIV model have also found that the reservoir is seeded rapidly, within 3 days [255]. Longitudinal data on the dynamics of the reservoir establishment are difficult to obtain since it is now rare for patients to be followed while untreated (given ethical concerns), while in the pre-ART era it was not common to measure HIV DNA specifically in resting CD4$^+$ T-cells. However, cross-sectional studies in which patients were treated at different stages of infection provide indirect data on how quickly the reservoir builds up during the course of untreated infection. These show a clear difference between the levels of PCR-based measures of the reservoir in primary- vs chronic-treated patients, where 'primary' is often defined as the first 6 months of infection and the measures are taken after months or years of ART [221, 225, 256–259]. One study compared patients initiating ART in Fiebig stage I vs stage II or III and found lower levels of HIV DNA in the very early treated patients after 24 weeks of ART [260]. Another found a significant correlation between resting cell infection numbers and the area under the pre-treatment viral load curve [261]. These all suggest that there is significant accumulation of the reservoir during primary infection and into the start of chronic infection, though it is also possible that the decay rate of the reservoir (as measured by PCR) differs between primary- and chronic-treated patients [262]. Another study found indirect evidence that levels of integrated HIV DNA continue to accumulate during chronic infection, such that a 50% level is reached after

approximately 2 years of infection [263]. However, there is no other data that I am aware of that shows a significant difference in reservoir size between patients treated at different points in chronic infection.

Early estimates of the half-life of the HIV reservoir in treated patients were based both on measures of proviral HIV DNA and viral outgrowth assays and varied from 6 months to 44 months [264, 265]. Larger studies of patients on ART for up to a decade or more have since concluded that the decay rate of the reservoir is decelerating, and continues to decelerate beyond the first year or so of ART [262, 266–269]. Some have explained the pattern of decay by subdividing it into phases and associating each phase with a different subset of latently infected cells. It has been suggested that different transcriptional subclasses of latently infected cells or phenotypically distinct T-cell subsets with differing lifespans could account for the separate phases of decay [249, 267, 268, 270]. Others view the deceleration as more continuous and suggest that heterogeneity in activation rates of the cells, or decreasing levels of immune activation following therapy could account for decelerating decay [229, 267].

2.4.7 Attempts to eradicate the reservoir

Efforts to reduce the size of the latent reservoir have largely focussed around the 'kick and kill' approach (also termed 'shock and kill'; [271]). The 'kick' involves the administration of latency reversing agents (LRAs) in order to reactivate proviruses in the HIV reservoir, while the 'kill' requires the action of a strong immune response alongside continued ART to prevent new infections arising. LRAs must be able to promote the transcription of latent proviruses without inducing global T cell activation – histone deacetylase (HDAC) inhibitors are one such class of drugs [272]. *In vitro* studies and phase 1/2 clinical trials have demonstrated the ability of several different LRAs to disrupt latency [273–276]. However, these interventions have so far failed to cause a lasting reduction in the latent reservoir [272]. This could be due to ineffective killing of re-activated cells [277] or low potency of the 'kick' effect, which in some cases has declined on repeat administration of the drugs [278].

Other potential strategies and therapies currently in the early stages of research include the permanent silencing of the provirus, T-cell vaccines or monoclonal antibodies to en-

hance the clearance of infected cells, and gene therapies to either kill infected cells directly or disrupt integrated HIV genomes [230]. Additionally, a recent study in SIV-infected macaques showed that administration of an antibody known to disrupt CD4 trafficking to gastrointestinal tissue resulted in viral control for nine months post-ART in all eight animals [279]. The exact mechanism of this effect is currently unclear but it suggests that therapies that manipulate lymphocyte trafficking and limit damage to gastrointestinal tissues could hold promise.

2.4.8 Viral rebound and post-treatment control

Upon cessation of antiretroviral therapy, the reversion of latently infected cells to a productive state (or, additionally, ongoing viral replication in drug sanctuaries) has the potential to cause rebounding infection. The majority of patients experience viral rebound within weeks of interrupting ART [11, 23, 280]. Several studies have sought to describe the source of rebounding viraemia and there is disagreement over whether a single reactivated cell or multiple foci are likely to be responsible [249, 281, 282]. Sequencing has identified clonally expanded latently infected cells as a potential source, and also suggested that cells within the gut-associated lymphoid tissue are not responsible, but difficulties in sampling lymphoid tissue present a barrier to accurately identifying the source(s) of rebounding infection [206, 281, 283]. A necropsy of one macaque which had rebounded 10 days following 8-week ART suggested that the viral-protein-producing cells in this animal were mainly located in the follicles of lymph nodes [284].

Approximately 5-15% of acute-treated patients are able to control viraemia below the level of detection for more than 2 years following treatment interruption (TI) [21]. Examples of so-called post-treatment controllers (PTCs) are particularly striking when compared with the 'Boston patients', who experienced viral rebound within 8 months of TI despite receiving bone marrow transplants that sharply reduced the size of their latent reservoir [285]. The VISCONTI study describes a case series of 14 patients, constituting the best studied group of PTCs [11]. They all initiated ART in primary infection and received ART for 12-92 months before TI, after which they had low levels of cell-associated HIV DNA. In contrast to spontaneous HIV controllers, the PTCs were not found to have higher than average CD4 counts or lower than average viral loads pre-ART (when compared to the

larger primary infection cohort from which they originated), and also were not enriched for protective HLA alleles [11]. These observations suggest that ART was necessary to induce control in these patients, and are anecdotal evidence that the timing and duration of ART may additionally be important.

Many studies have sought to uncover the correlates of time to viral rebound post-TI, which may in turn aid our understanding of post-treatment control. The best supported marker at TI that correlates with time to rebound is the size of the HIV reservoir as measured (using PCR-based assays) from PBMCs [22,23,286–288]. In one study involving 164 patients, those that were able to maintain low viral load (< 500 copies/ml) for at least a year post-TI had $\sim 0.5 \log_{10}$ lower levels of HIV DNA on average (measured at TI) than patients who saw larger viral increases post-TI ($p = 0.03$) [286]. Several different assays have been used to measure HIV reservoir size, and there is not yet a consensus over which is the best predictor of time to viral rebound [22, 23].

Several other markers have been suggested as correlates of time to rebound whose effect may be mediated in part through their impact on the size of the HIV reservoir. For example, low pre-treatment viral load has been found to be significantly associated with longer times to rebound in two studies of over 150 patients [286, 289], and also with low measures of the viral reservoir during suppressive ART [261,290]. However, the VISCONTI PTCs did not have significantly lower viral loads than the patients in the larger cohort from which they were drawn [11], and in another study of patients who initiated ART in chronic infection, pre-ART viral load was not predictive of loss of control ($n = 95, p = 0.6$) [288]. Initiation of ART in primary (compared to chronic) infection is significantly predictive of longer times to rebound in a few studies [23, 280, 291], and is related to low levels of HIV DNA at treatment interruption in several more [225, 256–259, 262, 292]. A longer duration of ART was significantly associated with prolonged time to rebound in one large study [289] but not in others [286, 288]. The particular range of durations could account for the differing results - all patients in the former study were treated for less than a year, whilst in the latter studies treatment times ranged from 1-3 years and 4-6 years. Finally, there is some evidence that levels of immune activation or exhaustion correlate with time to rebound. In one study, $CD8^+$ T-cell activation measured during suppressive ART was found to be significantly lower in patients with greater control post-ART [286].

In another, studying a range of activation and exhaustion markers on both $CD4^+$ and $CD8^+$ T-cells but involving smaller numbers of patients, no marker measured at treatment interruption predicted time to rebound but low levels of immune exhaustion (in particular the surface marker PD-1) *measured at baseline* were significantly associated with longer times to rebound [293]. There was also a strong positive association between levels of the activation marker HLA-DR on $CD4^+$ T-cells at treatment interruption and levels of HIV-DNA at the same time point [293]. Immune activation may be both a cause and consequence of high HIV reservoir levels and so understanding this relationship requires further study.

It has been suggested that the strength of the HIV-specific immune response should have an effect on time to viral rebound that is independent of the size of the reservoir [294]. However, so far there is little evidence for this effect. In a study of 130 HLA-typed patients the frequency of HLA B57 and B27 alleles did not differ between 3 groups stratified by their extent of post-ART control [286]. Another study with 70 patients found a similar result [291], and there was also no indication that the VISCONTI patients were enriched for particular HLA-types [11]. The frequency of HIV-specific $CD8^+$ T-cells (as measured by IFN-γ production) was found to be lower in patients with greater post-treatment control at all time points (at baseline, on ART and post-ART) [286]. In 13 patients with multiple treatment interruptions there was no association between the frequency of HIV-specific $CD8^+$ T-cells and viral growth rate during treatment interruption [138]. However, a high CD4:CD8 ratios is associated with greater post-ART control [286].

2.5 Mathematical modelling of HIV

In this section I give an overview of the mathematical models that have been developed to aid HIV research, focussing on the areas which underly the work in chapters 2-4. I will largely restrict my attention to mechanistic models. The mechanistic vs. phenomenological modelling dichotomy roughly corresponds to the divide between mathematical vs. statistical models and is articulated well in Bolker's book on ecological models [295]:

> Phenomenological models concentrate on observed patterns in the data, using function and distributions that are the right shape and/or sufficiently flexible

to match them; mechanistic models are more concerned with the underlying processes, using functions or distributions based on theoretical expectations.

Mechanistic models have been successfully used to provide insight into the dynamics of a system, infer rates or parameters, and predict behaviour. An illustrative example corresponding to each of these three categories is given below.

Understanding dynamics. Pre-1980s, the conventional wisdom was that, in adapting to a new host, pathogens would be expected to evolve to eventual avirulence [296]. Yet this did not fit with observed data - there were several examples of 'old' infections that were still virulent [34]. The formulation of the trade-off hypothesis aided our understanding of how different patterns of virulence evolution could emerge. The trade-off arises from a simple model of epidemic spread, from which the value of R_0 (the average number of new infections caused by a single infected host in an entirely susceptible population) can be calculated and is found to be a function of the transmission rate vs the death rate plus the recovery rate of infected hosts [297]. Under certain assumptions, pathogens would be expected to evolve to maximise R_0. Hence, if we know how virulence and transmission and/or recovery rate are linked we can use this to understand whether virulence would be expected to evolve to an intermediate, high or low level. The model is not universally applicable - evolution at multiple levels, high prevalence of co-infection, and spatial structure can all complicate the picture [34]. However, it has proven useful, for example in understanding the patterns of virulence change of myxomatosis in rabbits.

Inferring rates. The first clinical trials of highly active antiretroviral drugs showed a sharp decline in plasma viral load during initial therapy [298, 299]. These data, along with earlier observations lead researchers to conclude that the rate of virus replication must be higher than might have been inferred from the slow rate of disease progression alone. In 1996 Perelson et al formulated a simple mechanistic model of viral dynamics (see Figure 2.3A) and fitted this to the decay curves of viral load on therapy [143]. This enabled them to estimate the rates of clearance of both free virus and infected cells, and to show that virus clearance was the faster of the two rates. These studies also improved our understanding of HIV pathogenesis by showing that the vast majority of plasma virus is produced by recently infected cells as opposed to cells that chronically produce virus or the reactivation of latently infected cells [143].

Predicting behaviour. Where sufficient data are available to parameterise models, prediction of future dynamics can be made and the effect of various interventions can be assessed. For example, many studies have sought to quantify the impact of universal initiation of ART at HIV diagnosis upon the future of the epidemic. Data such as the distribution of CD4 counts in healthy individuals, variation in infectiousness during the course of an infection, and distribution of survival times are required to feed into these models [300]. A meta analysis using 12 such models, which differ in their structure and parameterisation methods, found that they resulted in a broad range of long term projections [301]. However they all predicted substantial decreases in incidence in the short term as a result of ART scale-up [301] and hence were used to strengthen the case for early ART initiation and 'treatment as prevention'.

2.5.1 Within-host models of HIV

The modelling of within-host HIV infection dynamics started with a basic model describing the behaviour of uninfected target cells ($CD4^+$ T-cells, T), infected cells (I) and free virus (V) [143]. New infections of target cells occur at a rate that is proportional to the product of the virus population size and the number of target cells (βVT). There is a constant influx of new target cells from a conceptual 'source' and a constant death rate. Infected cells are cleared at rate δ and produce virus at rate p, which is often expressed as $p = N\delta$, the viral burst size multiplied by the infected cell clearance rate. Virus is cleared at rate c (a model diagram is shown in Figure 2.3A). This model is a much simplified representation of reality. For example, by including just one compartment of both uninfected and infected target cells, it assumes that the behaviour of all cells in each class can be described by average parameters. It also encompasses CTL-mediated killing, viral cytopathic effect, liver filtration, etc. in a single step and parameter (the clearance rate of infected cells). This simplicity was necessary – the model was initially developed to infer clearance parameters from viral load data, and it would not have been feasible to explicitly model the action of the immune response, for example, without data on the dynamics of $CD8^+$ T-cells. The simplicity is also intentional, because in capturing just the key processes, the model enables us to 'see the wood for the trees'.

This model, like many in the field of HIV research, was developed to analyse a specific

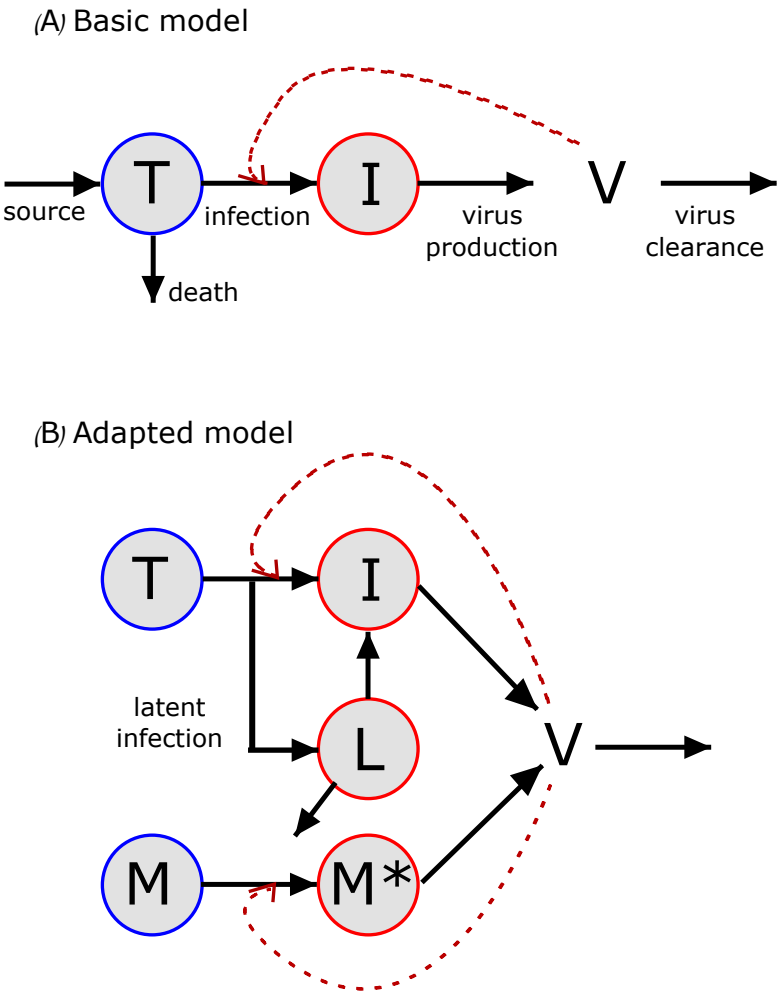


Figure 2.3: Viral dynamics models. (A) When target cells, T, become infected they transition to the infected class, I. Infected cells die and release virus, V which goes on to infect new cells. (B) The adapted models described are similar to (A) but with the addition of one or both of long-lived cells, M, and latently infected cells, L. Infected long-lived cells are denoted by M^*. Solid arrows represent the main transitions to or from classes and dotted arrows represent the dependency of infection rate on virus load, V.

process or period in the course of infection. It cannot aid our understanding of or explain AIDS progression, for example, because once the populations in the model reach their equilibrium values the solution remains, indefinitely, in that state. Even now, most known models that can explain the whole course of infection either include parameters that change through time or incorporate virus evolution [302]. Indeed, uncovering and modelling the mechanisms of HIV pathogenesis from acute infection through to AIDS is an active area of research [303–305].

Following the initial estimates of viral and infected cell clearance parameters, further

longitudinal data revealed a second, slower phase of viral load decay [306]. Various hypotheses were suggested to account for this: the decay of longer-lived infected cells such as macrophages, release of virions from follicular dendritic cells, and activation of latently infected cells. An adapted version of the basic model was developed to test each of these hypotheses (see Figure 2.3B) but the modelling analysis was not initially able to distinguish between them from fitting to the viral load data alone [306]. However, additional data from cell-associated infectivity assays and proviral DNA in PMBCs suggested that activation of latently infected cells did not make a substantial contribution to this second phase virus population.

The latently infected compartment formulated in [306] is incorporated into the model as follows. A fraction, f, of new infections result in latently (as opposed to productively) infected cells. Latently infected cells (L) move into the productively infected class (I) at a rate, a, corresponding to viral activation. They also die at rate d_L. This structure formed the basis of later attempts to model the decay of the latent reservoir under long-term ART. This later work has modelled the replenishment of the reservoir by homeostatic proliferation [307, 308], sporadic antigen-mediated expansion [309] or ongoing replication in drug sanctuaries [20] and shown all to be theoretically feasible mechanisms for long-term persistence. Population dynamic data alone (i.e. data that just tells us how the size of each modelled population changes over time) does not enable us to determine the relative contribution of each of these mechanisms though, particularly given that we know little about how the dynamics of anatomical compartments may differ and have an effect. When it comes to explaining the long-term dynamics of the latent reservoir, several models have been proposed. Accounting for heterogeneity in the activation rates of latently infected cells allows explanation of the decelerating decay of HIV DNA on ART [229], while a model considering several transcriptional subclasses of infected cells also fitted well to data on HIV dynamics during ART [270]. These are not mutually exclusive hypotheses for explaining patterns in the data, and which theoretical framework is most helpful will depend on the modelling question and available data. Other hypotheses may also result in good fits, but it seems likely that including some source of heterogeneity within the latently infected pool is necessary for capturing the dynamics of HIV DNA decay. Once again, rigorously testing these model hypotheses would require additional data on how the

composition of the latently infected pool (for example the distribution of activation rates or transcriptional subclasses) changes over time.

The majority of work undertaken to explain post-treatment control has involved correlative approaches. However there have been two mechanistic modelling studies of particular interest. Firstly, Conway et al [294] extended the model of latent dynamics in Figure 2.3B to include the action of 'effector cells' (CTLs). They showed that, within this framework, there was a range of CTL killing strength for which patients would not be able to spontaneously control the virus pre-ART but would be able to control post-ART if they had a sufficiently small HIV reservoir. The major prediction of this model is that CTL killing strength should differ between PTCs and non-PTCs that are matched for reservoir size at treatment interruption. Hence, testing whether this model reflects reality requires experimental data giving accurate information on *in vivo* CTL killing strength. Secondly, Hill et al [310] developed a stochastic model that simulates the reactivation of latently infected cells and possible viral rebound post treatment interruption. This model assumes no ongoing replication. It is unlikely to be useful for predicting time to viral rebound in a individual patient, since that would require precise measurement of the size of the latent HIV reservoir and average activation rate of the reservoir. However it can be applied to using measures of time to viral rebound to refine estimates of reservoir size at treatment interruption, and hence could be useful for estimating the reservoir-reduction caused by LRAs in clinical trials [311].

2.5.2 Models of T-cell turnover

The literature on T-cell turnover includes several modelling studies which seek to infer the rates of death, proliferation, activation etc. of CD4 and $CD8^+$ T-cells. These models and the parameter estimates resulting from them have been used to uncover the mechanisms of HIV-1 pathogenesis [96] and also contributed to our understanding of the persistence of the HIV reservoir. The experimental data that they are based on largely falls into one of three categories: chromosome damage data, stable isotope labelling data and proviral sequence data (for turnover of HIV infected cells). The studies differ in their design, normalisation procedures and underlying models.

Models applied to chromosome damage data gave rise to some of the first estimates of

T-cell lifespan in humans [312]. They confirmed that memory cells divide more frequently than naive cells, with naive cells dividing once every 3.5 years on average. However the estimates should be interpreted carefully given that the patients were likely in the process of replenishing their T lymphocyte pool.

Stable isotope labelling experiments have been extensively used to study T-cell turnover. Heavy glucose or heavy water can be used to label cells *in vivo*; upon division, D_2 is incorporated in place of H_2 into newly synthesised strands of DNA. Initial studies found that the death rate of labelled T-cells was much higher than their proliferation rate, yet the total size of the T-cell population was assumed to be constant [313]. This discrepancy is explained well by a model with kinetic heterogeneity; cells with faster kinetics will be over-represented amongst labelled cells and this gives rise to a higher death rate of labelled cells compared to the average death rate of the T-cell population as a whole [232,314–317]. It is possible that temporal heterogeneity (in which all cells behave in the same way but have an increased probability of death immediately after cell division, for example) would explain the data equally well [318]. A model with separate resting and activated T-cell compartments, similar to that used in [312], has also been used for the interpretation of labelling data [96].

The data and modelling from these stable isotope labelling experiments showed again that memory cells have proliferation and death rates that are an order of magnitude faster than naive cells [232,316,317]. Within memory cells, effector memory cells turnover faster than central memory cells [232]. Studies comparing HIV infected and uninfected patients found higher rates of death, proliferation and activation of T-cells in infected patients [96,313,315,319], with the turnover rate becoming lower again in patients on long-course ART [313]. Turnover estimates from isotope labelling studies were higher than those from chromosome damage studies. Kinetic heterogeneity amongst T-cells could contribute to this disparity; chromosome damage has the potential to affect all cells, whereas deuterium labelling only labels recently divided cells [314].

In the study by Strain et al. [320], proviral sequence data from patients who had been on changing drug regimens (as a result of resistance developing) were studied. By examining the dynamics of mutant and wild-type virus they were able to show that more recently infected $CD4^+$ T-cells decayed at a significantly faster rate than those that had

been infected a long time previously. These results are once again consistent with kinetic (or temporal) heterogeneity playing an important role in shaping the patterns seen in data of T-cell dynamics.

2.5.3 Between-host models of HIV

The theory of compartmental epidemiological models ('S–I–R' models) grew out of work done by Kermack and McKendrick in the early 20th century [321]. In their simplest form, the models stratify individuals into susceptible (S), infected (I) and, for some infections, recovered (R; not relevant for HIV) compartments. Further stratification may be added if it is necessary to distinguish between vaccinated/unvaccinated, treated/untreated, male/female etc. In these models, the force of infection, λ, describes the transition rate from the susceptible to the infected compartment, and its form varies depending on the mode of transmission. For sexually transmitted diseases, λ is generally assumed to have the form $\lambda = \beta cI/N$, where β and c are constant parameters; c is equal to the contact rate between individuals and β is the probability of transmission per contact. N is the total number of individuals. Hence the risk of a susceptible individual becoming infected depends upon the proportion of infected individuals within the population.

The prediction that widespread administration of ART might reduce the incidence of infection led to many modelling studies assessing the impact of ART on the HIV epidemic [301]. Granich et al used a compartmental epidemiological model to suggest that HIV might be 'eliminated' within 50 years if 90% of a population were to be tested annually and ART initiated immediately upon a positive diagnosis [300]. Several other compartmental models have been published since, which vary in their structure and assumptions. Particular model features have been shown to be important when making quantitative predictions: heterogeneous sexual mixing [322], behaviour change in response to a (perceived) reduced risk of infection, and varying transmission risk during the course of infection [301, 323]. The early modelling study by Granich et al was criticised for not including all of these features [323].

Accounting for heterogeneous assortative mixing (where high-risk individuals are disproportionately more likely to come into contact with other high risk individuals) leads to a lesser impact of universally targetted ART on HIV incidence compared with a ho-

mogeneous risk distribution or random mixing [322]. This is because high risk individuals make a large contribution to the spread of infection and are more likely to transmit early in infection, before ART initiation.

Accounting for varying transmission risk during the course of infection is important since ART will only prevent the later stage transmissions that occur after a patient is diagnosed and eligible for treatment. The risk of transmission is linked to viral load [187] and is consequently known to be highest in primary infection and during the final stages of infection when CD4 count is low. Empirical studies had estimated that up to 40% of transmissions occur in primary infection, but these estimates have since been revised downwards after accounting for sampling methods and heterogeneity in individual-level transmission risk [180, 181, 324]. An analysis of 12 different HIV epidemic models found that between 4-28% of transmissions occurred during early infection in these models, and 20-51% occurred once the CD4 count had dropped below 200 copies/ml. The same analysis found that differences in the proportion of transmissions occurring in each stage of infection was able to explain some of the variation in model predictions of reduction in HIV incidence by 2020 [301].

Most of the models used in the literature are deterministic, but some are individual-based stochastic models [301]. These track all or some of behaviour/risk group, infection status, viral load and age of individuals and then simulate transmission, death or other events stochastically.

In the field of HIV virulence evolution, simple deterministic compartmental models have been used to understand the different patterns of virulence change that might be expected, dependent on factors such as the natural history of an infection and the relationship between virulence and transmission [34,325]. However, more complex, mechanistic models are necessary for making quantitative predictions of virulence change. Individual-based models often capture this greater complexity and have been used for this purpose. In Herbeck et al.'s model, [188] individuals are linked via an underlying sexual contact network and are assigned SPVLs chosen randomly from a distribution. Transmission is dependent on VL (which changes during the course of each infection), and progression is dependent on SPVL. SPVL is heritable. The model is used to understand variation among empirical trends in virulence, which they conclude could be a result of sampling biases, initial SPVL

distributions varying between epidemics, or non-linear patters of adaptive viral evolution. van Dorp et al. [193] developed a different model in which within-host evolution (driven by the CTL response) was linked to population-level evolution of SPVL. Following suggestions that the intermediate virulence of HIV could evidence between-host viral adaptation to maximise transmission potential [25], this model was used to provide an alternative hypothesis for intermediate virulence, namely that it is the result of within-host selection in the context of host heterogeneity. It is likely that further data on recent patterns of virulence change will allow us to determine the impact that within-host evolution has on population-level evolution and hence refine these models and their resulting predictions (as discussed in section 2.3.4).

3

T-cell immunity

This work has been published in PLoS Genetics (as detailed in section 1.2: *Contributions to this thesis*) and is included here in its final form.

3.1 Introduction

The HIV-1-specific cytotoxic T-lymphocyte (CTL) response begins as early as 2 to 3 weeks after infection [87], and there is evidence to suggest it may play an important role in the early control of viraemia [127, 134]. The onset of the response coincides with the decline of viral load. Certain host HLA genotypes (and therefore certain specific responses) have been found to be significantly associated with delayed progression to AIDS [129, 326, 327]. In addition to this, some studies based on the depletion of $CD8^+$ T-cells in SIV-infected macaques have shown that the CTL response makes a crucial contribution to viral control in this animal model of AIDS [121]. However, others have questioned the role of CTL in controlling productive infection, both in the SIV-macaque model and in humans [137, 328].

Many studies have demonstrated the capability of the HIV-1-specific CTL response to select for viral variants that escape recognition by $CD8^+$ T-cells or prevent antigen presentation by HLA class I molecules and so evade the immune response [15–17, 133, 159]. Indeed, work done to quantify the effects of the various selective forces acting on HIV has found that 53% of non-*env* mutations that rise to fixation in the first few years represent viral adaptation to $CD8^+$ T-cell responses [169] whilst a detailed deep sequencing study of one patient found that the majority of early mutations were CTL related [144].

CTL escape has been observed to occur throughout the different stages of HIV-1 in-

fection, from soon after seroconversion [16, 28, 29, 160, 164] to many years into chronic infection [17, 166, 174]. Some epitopes consistently escape earlier and more frequently than others [171, 329–331] but time to escape also varies considerably between patients and is likely to be influenced by factors such as strength and quality of the $CD8^+$ T-cell response as well as pre-existence of compensatory mutations in sequences surrounding epitopes [17, 166, 332]. Escape pathways are complex; in many cases low frequency variants arise early, replacing the transmitted sequence, but it is not until some time later that one escape mutant, often containing multiple amino acid mutations, emerges and rises to fixation [134, 175, 176, 333]. In the absence of selective pressure from CTLs, reversion of escape mutations back to wild type has been documented [163, 164].

In this study we analysed the timing and extent of CTL escape in 125 patients across the HIV-1 *gag*, *pol*, *nef* and *env* genes. We used longitudinal viral sequence data covering the first three years of infection to count escape events in each of 46 epitopes in all available patient samples, and only considered periods when patients were off therapy. Approximately one third of patients drove escape in an epitope for which they were HLA-matched within their first year of infection and escape continued to be seen into the second year. However an estimated 33% of patients had still not driven any escape in their HLA-restricted epitopes across *gag*, *pol* or *nef* by the end of their second year off therapy. In looking at whether escape was clustered in patients, we found little evidence to suggest that this was the case. We also observed that time to escape for individual epitopes was faster in HLA-matched patients and in patients who were able to mount a measurable $CD8^+$ T-cell response, and that patients with protective HLA alleles were more likely to have their first escape sooner.

3.2 Results

3.2.1 Cohort characteristics

The cohort consisted of 125 treatment-naive, HIV-1 subtype B infected adults who were recruited soon after the estimated date of seroconversion (median 11 weeks; range 1-20 weeks) as part of the SPARTAC clinical trial and followed for up to three years (see Methods, full details in [8], patient characteristics shown in Table 3.1). Participants were

randomised into one of three arms, which determined whether they received no treatment, 12 weeks antiretroviral therapy (ART) or 48 weeks ART. Consensus viral sequences for four immunogenic genes (*gag*, *pol*, *env* and *nef*), and IFN-γ CD8$^+$ T-cell ELISpot data were collected longitudinally. Participants were followed for up to three years whilst off ART (median 109 weeks, IQR 85-145 weeks); some participants initiated long-term ART before the end of the three years, upon reaching the trial clinical endpoint. The amount of data available at each time point is summarised in Table A.1.

Table 3.1: Patient characteristics table

Characteristic	Whole trial (N=366)	UK patients (N=125)
Sex – no. (%)		
Male	219 (60)	125 (100)
Female	147 (40)	0 (0)
Age – yr		
Median (interquartile range)	32 (25–40)	34 (29–42)
Range	19–63	19–60
Estimated time since seroconversion at randomisation – wk		
Median (interquartile range)	12 (9–15)	11 (7–14)
Range	1–24	1–20
CD4+ count – cells/mm^3		
Median (interquartile range)	559 (435–700)	550 (435–682)
Range	95–1399	130–1310
HIV RNA level – copies/ml		
Median (interquartile range)	4.53 (3.67–5.18)	4.78 (4.08–5.29)
Range	1.40–6.47	2.22–6.22

For this study, we took all the UK HIV-1 Subtype B infected participants that had been enrolled in the SPARTAC trial and for which exact times of initiation and cessation of both short course ART and, if applicable, long term ART were known. The resulting cohort of 125 participants had similar characteristics to the whole trial cohort except that all the UK HIV-1B infected participants recruited were male. Participants in the UK cohort were also recruited slightly earlier in infection on average, and (perhaps consequently) had slightly higher viral loads on average at recruitment compared to the trial as a whole.

3.2.2 Escape prevalence at baseline and after 1 year

A CTL escape mutation was defined as *any amino acid variation in previously identified (and phenotypically confirmed) escape sites within optimal defined epitopes* in *gag*, *pol*, *env* or *nef* (see Methods for more details). All analyses were also run using alternative, more lenient definitions of escape. Those additional analyses, which are shown in Figures A.7-A.12, confirm that the results presented here are not dependent on this definition of escape.

In addition to drawing on a large body of collated literature to form this definition we also validated it by analysing the strength of patients' $CD8^+$ T-cell responses to autologous epitope variants (see Methods and Table A.2).

At baseline (the first trial study visit) the data comprised a total of 3831 epitope sequences from 122 patients in which we were able to look for variation within known escape sites. The range of times from seroconversion amongst these patients matched that of the whole cohort. Of these, 1235 contained escape mutations. However, this escape at baseline was, for almost all epitopes, equally prevalent in HLA-matched and HLA-mismatched hosts (Figure 3.1A). This pattern is more consistent with variation that has been transmitted than variation that has been driven by within-host HLA-restricted immunity prior to the first sampling. In contrast, after one year, four epitopes derived from *gag*, *pol* and *nef* had markedly higher escape prevalence in HLA-matched hosts than in mismatched hosts (Figure 3.1B). Further analysis (see Methods for details) confirmed that the distribution of points in Fig. 3.1B (at one year) is significantly different from what would be expected under the null hypothesis that escape is randomly distributed between matched and mismatched hosts, whereas the distribution at baseline is not.

3.2.3 Incidence of escape during up to three years of observation

Of those epitopes sequenced, 2297 were initially wild-type and had at least one later sequence for comparison, and hence were candidates to allow the observation of incident escape (note that in a few cases this initial time point was after baseline due to sequence data being unavailable). Due to the high variability of the *env* gene, the vast majority of epitopes in *env* (all 32 HLA-matched patient-epitope pairs and 215/316 HLA-mismatched patient-epitope pairs) were already escaped at baseline, and hence whilst these were included in our analyses we were not able to comprehensively study incident escape in *env*. In the 2297 candidate epitopes, just 108 'escape' events were observed in patients studied while off ART and only 37 of those were in epitopes in an HLA-matched patient. To see if there was evidence for a separate group of particularly fast escaping patients we compared the distribution of the number of escape events per host (in their HLA-restricted epitopes) with a random distribution, calculated using a Poisson process, and found no significant difference between the distributions (Figure 3.2A). In fact this Poisson process in which

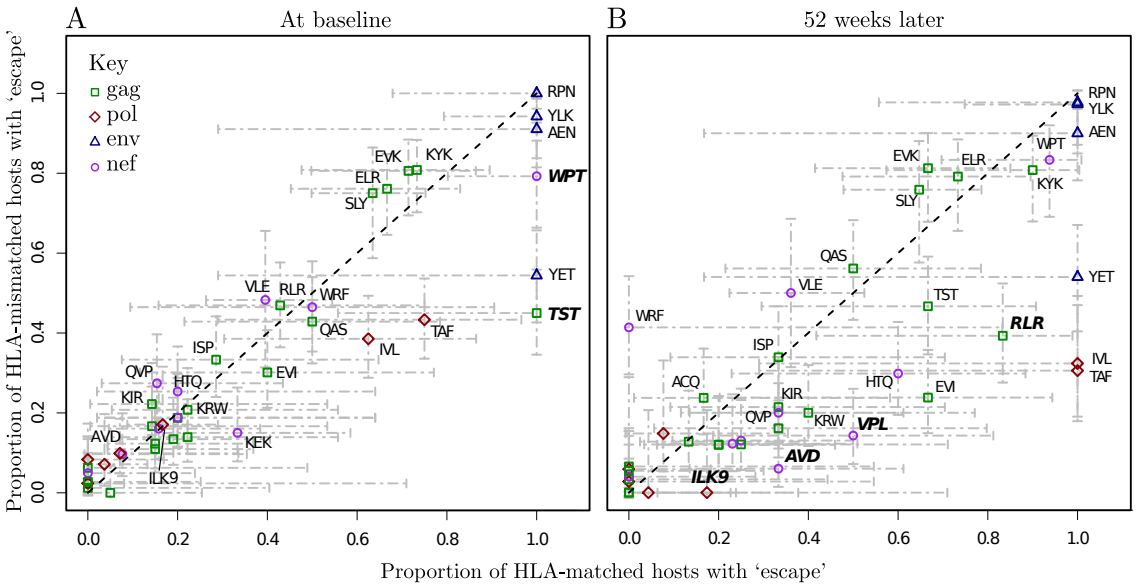


Figure 3.1: Escape prevalence in HLA-matched and -mismatched hosts. Epitopes are labelled where possible with their first three amino acids, and length if necessary to distinguish them. Bars represent 95% binomial confidence limits (Agresti-Coull method). The dotted black line is $y = x$. Epitopes labelled in bold have a significantly higher proportion of escape in matched hosts than in mismatched hosts (one-tailed Fisher's Exact test, $p < 0.1$, note that multiple testing was not corrected for since the purpose of these tests was simply to give a relative measure of significance). Raw data for the number of patients in each category can be found in Tables A.3 and A.4. First visit (baseline) sequence data was available in at least one gene for 122/125 patients. The range of time from seroconversion among these patients was 1-20 weeks, median 11. (A) At baseline the majority of epitopes have escape at equal prevalence in HLA-matched and -mismatched hosts (B) 52 weeks later within-host evolution has resulted in a higher prevalence of escape in HLA-matched hosts for many epitopes, and in the distribution as a whole HLA-matching and escape are now significantly associated ($p < 0.01$, permutation test, see Methods for details)

escape was driven at an average rate of 0.0018 per week across all HLA-matched patient-epitope pairs, described the distribution of incident escape across patients well. Since many patients had missing data, particularly at later time points (Table A.1) we used this average rate to construct a similar expected distribution supposing all patients had had a full set of sequence data for the first two years (whilst untreated) (Figure 3.2B). Even after accounting for the missing data in this way, only 12% of patients would have driven more than two escape variants in HLA-restricted epitopes and the median and modal numbers of incident escape events were one and zero respectively.

This analysis is meaningful if patients with missing data would have had similar rates of escape to those observed for a full two years whilst untreated. We believe this to be a

valid assumption and assess it in further detail later.

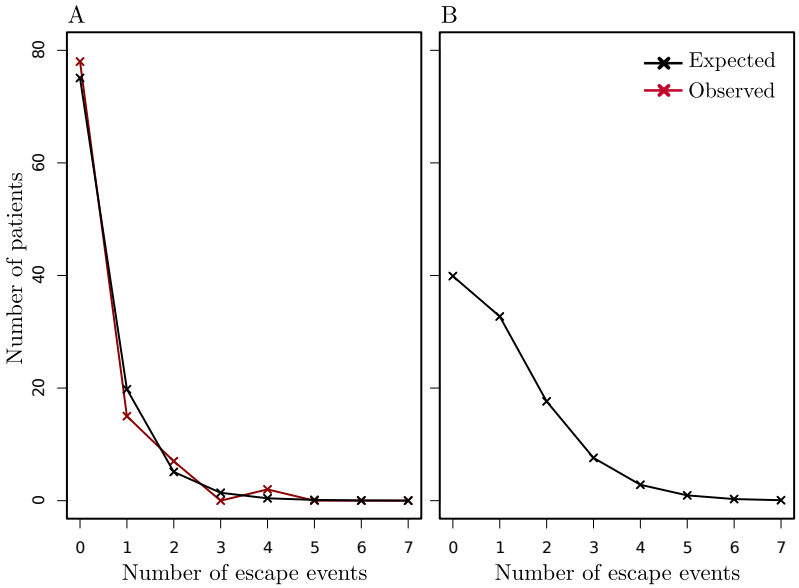


Figure 3.2: The distribution of incident escape across patients. (A) The observed distribution of incident escape (in HLA-matched patient-epitope pairs) across patients (red line) is similar to the distribution given by a Poisson process where the average rate of escape is constant across all patient-epitope pairs (black line). (B) The expected distribution of escape supposing all patients in (A) had a full set of sequence data and were observed for a full 2 years whilst off-ART. A goodness-of-fit test showed that there was no significant difference between the observed and expected distributions in (A) ($p > 0.1$). Details of calculations for the expected distributions are given in the Methods.

3.2.4 When does escape happen?

Time to escape can be described either for each patient in a population (how long does it take until a viral variant with a new escape mutation is detectable in a patient?) or for each epitope within each patient (how long does it take until an escape mutation appears in an initially wild-type epitope?). By considering the first such escape event (in patients or in epitopes) the well-developed statistical tools of survival analysis become applicable. Since only 9% of patients have more than one incident escape event in an epitope for which they are HLA-matched (Figure 3.2A) very little information is lost in such analysis.

In assessing the suitability of these analyses we also needed to address the question of whether the time at which patients are censored from the survival analysis (which occurs when they have no further sequence data) is independent of the rate at which they drive escape mutations. For some patients the fact that we were unable to obtain sequence data at later time points was a direct consequence of the fact that they had reached the trial

primary endpoint (a CD4 cell count < 350 cells/μl or commencing long-term ART) within the time frame of our observation period. Hence if, as some might hypothesise, escape events can drive clinical failure, it is possible that censored patients would have high rates of escape that we'd fail to observe.

We looked in more detail at those patients who reached the trial endpoint (or clinically 'failed') within our three-year observation period. An incident escape was observed in 6/20 patients for whom we had no sequence data after clinical failure compared to 7/24 patients who did have sequence data after clinical failure. In the 7 patients in the latter group who drove at least one escape event, there were just two cases where an escape mutation was first seen at the time point after clinical failure (see Appendix A and Figure A.2 for more details). Therefore the extent to which escape is linked to censoring time is small, and it is fair to assume that the (unobserved) rate of escape in patients who are censored from the analysis is the same as that of those who continue to be observed.

Figure 3.3 shows time to first escape for patients whilst they were off ART. Only patients with at least two time points of sequence data for both *nef* and *gag* (the genes for which the most data were available) were used to avoid underestimating the occurrence of escape due to missing data. This left 65 patients for this analysis. Note that this number includes both treated and untreated patients (range of previous ART duration 2 - 12 months). We also considered these patient groups separately (Figures A.4-A.6) and this did not change our conclusions. Multivariate Cox models for time to escape confirmed that the impact of early limited treatment on CTL escape was negligible (Appendix A).

The Kaplan-Meier plot for time to first escape in an HLA-restricted epitope shows that there is large variation between patients in time to first escape, with some patients who received ~ 12 weeks of therapy escaping before the 24 week time point (so that the midpoint approximation gives the therapy-adjusted time to escape as around 6 weeks, assuming no viral evolution on ART) whilst an estimated 33% of patients did not drive any new escape in their HLA-restricted epitopes in 92 weeks off ART (95% C.I. (16,70) %). Note also that the slope of the curve is close to constant; there is no indication of a propensity for many incident escape events to arise early during the observation period and fewer later.

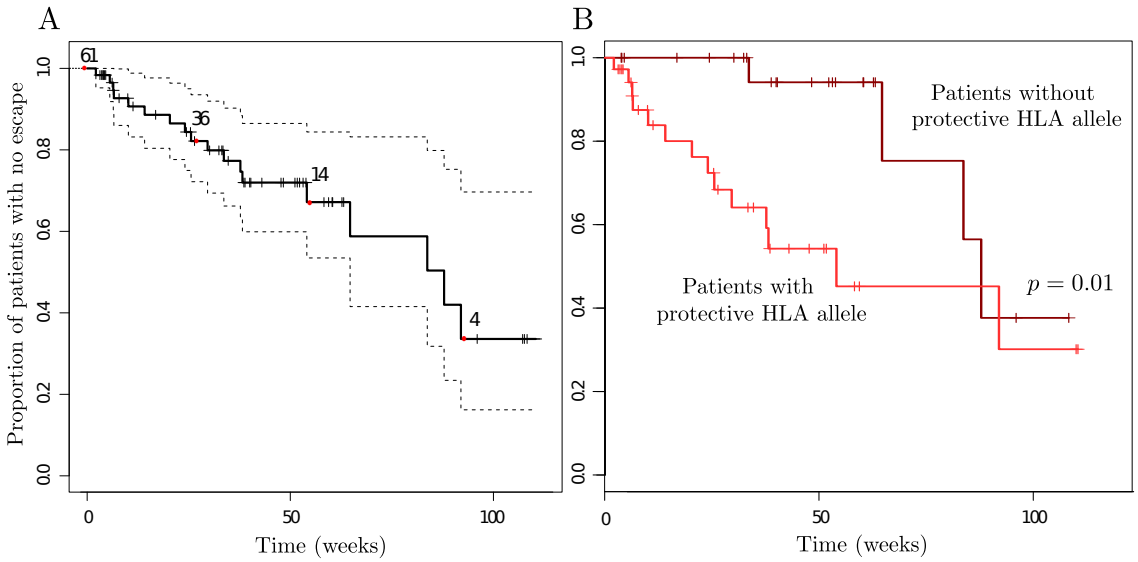


Figure 3.3: Kaplan-Meier plots of time to first escape using a midpoint approximation. Patients who were either missing data for *gag* or *nef*, the two genes for which the most data was available, were not included so as not to skew the results due to lack of data. 4 of these patients had no epitopes restricted by their HLA types that were WT at baseline, so $n = 61$ initially here. (A) Time to first escape in an HLA-restricted epitope (solid line) is plotted along with the 95% confidence intervals (dotted lines). (B) Patients are split according to whether they have one of the more 'protective' HLA alleles or not. The set of beneficial alleles was taken to be B*58, B*27, B*57, A*26, B*51, A*11, B*14, B*18, B*08 (all the HLA-A and -B alleles down to B*08 that are present in our data, taken from the ranking in [334]) as this split the patients approximately in half. Having a protective HLA resulted in a significantly increased risk of HLA-matched escape (p=0.01, Likelihood Ratio test on Cox Proportional Hazards model with single predictor. Hazard ratio = 3.7, 95% C.I. = (1.2, 11.3)). In both plots the x-axis represents the time since cessation of treatment, or baseline for those not receiving treatment, and vertical checks mark time points at which patients were censored (either because they began long term ART or because there was no further sequence data available for them). Numbers indicate the number of patients who have not yet escaped or been censored at the corresponding time points marked by red dots (0, 27, 55, 93 wks).

3.2.5 Having a protective HLA type is associated with earlier first escape

Although there was no evidence for a separate group of patients with a high frequency of escape (Figure 3.2), there was evidence that some patients had a tendency to drive escape mutations sooner than others. Figure 3.3B shows a Kaplan-Meier plot for time to first HLA-matched escape event for patients split according to whether or not they have one of the more protective HLA types. First escape is earlier in patients with a 'protective' HLA allele than in those without.

3.2.6 Waiting time to escape for a wild-type epitope

Figure 3.4 records Kaplan-Meier survival curves for wild-type epitopes. This analysis included all patient epitope pairs which were observed whilst the patient was off ART (i.e. in which it would have been possible to observe escape), giving a total of 46 epitopes and 114 patients. Here 'failure' is the appearance of an escape mutation in an epitope. The characteristic time to escape for a wild-type epitope is of the order of months or years. It is faster in HLA-matched hosts (Figure 3.4A), and amongst epitopes in HLA-matched hosts it is faster if there is a detectable $CD8^+$ T-cell ELISpot response to that epitope in that host (Figure 3.4B). Yet even in a host with the epitope's restricting HLA and a detectable $CD8^+$ T-cell response more than half of wild-type epitopes still show no escape after two years' observation (Figure 3.4B, survival = 0.69 between 84 and 115 weeks).

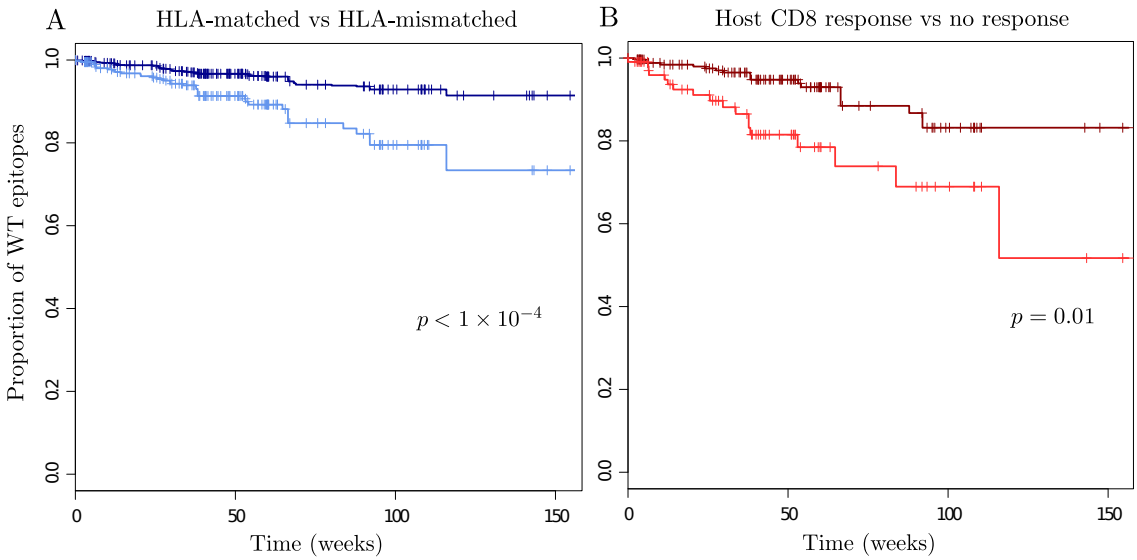


Figure 3.4: Kaplan-Meier survival curves for wild-type epitopes. For the 114 patients and 46 epitopes for which appropriate sequence data was available: (A) Time to escape in epitopes within HLA-mismatched (dark blue) and -matched (light blue) hosts is shown. (B) Epitopes in HLA-matched hosts are split according to whether they have a measurable $CD8^+$ T-cell ELISpot response to them (light red) or not (dark red). Escape is strongly significantly faster in epitopes within HLA-matched hosts ($p < 1 \times 10^{-4}$, hazard ratio = 2.6, 95% C.I. = (1.7, 4.2)) and then faster again if the host has a measurable $CD8^+$ T-cell ELISpot response to that epitope ($p = 0.013$, hazard ratio = 3.0, 95% C.I = (1.3, 7.0)). Note that p-values and hazard ratios were calculated using a mixed effects model with random intercept terms for both patient and epitope ID, to account for correlation of observations within patients and within epitopes (see Methods).

3.3 Discussion

The literature on CTL escape in HIV-1 infection is dominated by studies of small numbers of individuals [27–31]. Several publications describe single patients in whom many CTL escape mutations arise and recent papers have described very active, rapid outgrowth of many escape mutations in a small number of patients studied intensively in the first weeks of infection [134, 160]. It has been known for some time that escape mutations that arise in early infection have a faster fixation rate than those that arise during chronic infection [133, 170]. These observations lead to a natural set of questions about the timing of CTL escape in HIV-1 infection. What is a normal number of escape events observable in a patient during the first few years of infection? Is escape very concentrated amongst a subset of patients so that patients fall into two groups – one with lots of escape and one with little? Are escape events also focussed in time so that much escape occurs early in infection and very little later on?

To address questions like this properly it is necessary to follow a large number of patients through time, so that those in whom nothing happens are given proper attention. This study of 125 patients in the first few years of untreated infection from a large randomised controlled trial does just that. It finds that the incidence of escape is very low; after two years of observation an estimated 33% of patients had not seen a first escape incident in *gag*, *pol* or *nef*. The observed frequency of incident escape across all epitopes in HLA-matched hosts translated to an estimated 12% of patients driving more than 2 escape mutations within 2 years (Figure 3.2B). The inevitable conclusion is that patients with many escape events are unusual and, further, there was no evidence for a separate group of patients with a very high number of escape events (Figure 3.2A). Equally, the distribution of escape through time showed no evidence for much escape early on and little later; the Kaplan Meier survival curves for the proportion of patients without an escape, and the proportion of epitopes without escape both have constant slopes (Figures 3.3 & 3.4).

It has long been known that some HLA types confer a survival advantage upon their host. The relationship between the restricting HLA type and the propensity for an epitope to escape has been contentious. We previously [335] analysed the prevalence of escape in 84

chronically infected patients and concluded that protective T-cell responses were associated with more frequent viral escape, hypothesising that this result was due to a high fitness cost of mutations in epitopes restricted by protective alleles. However, Asquith [336], in a study that involved measuring the entropy of epitopes across sequences in the LANL HIV database, found that epitope entropy was significantly positively correlated with relative hazard of the restricting HLA allele, concluding that protective HLA alleles restricted epitopes that escape less frequently than average. In this cohort patients with protective HLA alleles escape significantly sooner (Figure 3.3B), and epitopes restricted by protective HLAs escape faster (although not significantly so) than others (Figure A.3). Further, all patients with escape in two or more HLA restricted epitopes had at least one of our defined list of protective HLAs. This large cohort study thus supports our previous finding that protective HLAs are associated with more frequent escape.

At first glance it seems counterintuitive that patients with some HLA types escape sooner and more frequently than others but that there was no evidence for a separate group of patients with much escape. However this apparent conflict is easily resolved; it is likely that patients with protective HLAs drive escape more frequently but do not have so much escape as to form a distinct subset of patients. They just lie at the top end of the distribution.

Why is escape in this cohort so slow? Is it because we missed very early escape events that occurred before patients were recruited? Is it that escape is concentrated in a small number of epitopes in which the process of escape is already largely complete? Or is it that escape is rare because responses are rare? Finally, is the definition of escape used here too restrictive?

Liu et al [160] have documented the presence of minor epitope variants within days of seroconversion, rising to fixation quickly in the first few weeks. However our results, presented in Figure 3.1A, suggest that there was little escape happening this early on. Since reversion of escape mutations in mismatched hosts is relatively slow [171] we used the proportion of escape in HLA-mismatched hosts at first time point as an estimate of the prevalence of transmitted escape for each epitope, and hence by comparison with the proportion of escape in HLA-matched hosts obtained a quantitative estimate for the frequency of escape before the first time point. As an example, for TST (an epitope that is

known to escape particularly early [172]), at the first time point 45% of HLA-mismatched patients had an escaped form of the epitope. We therefore assume that 45% of the 7 HLA-matched patients would have been infected with an escaped epitope. Hence, with reference to Table A.5, the estimated number of escape events in TST that have arisen since baseline is $6 - 7 \times 0.45 = 2.9$. Summing over all epitopes, these calculations gave the estimated 'survival' of wild-type epitopes in the weeks between seroconversion and first available sequence data (an average of 18.5 weeks) as 98.9% compared to 97.1% in the first 12 weeks of observation in which patients were off ART (see Appendix A for further details). Hence, whilst we have missed a handful of escape events ($\sim$ 6 in total), these data do not support the idea that the majority of escape happens very early, within the first few weeks or months of infection.

The high prevalence of escape at baseline might suggest that the incidence of escape is low because many of the epitopes that are prone to acquire escape mutations already have them transmitted at baseline. This was true of the *env* epitopes we studied, which is unsurprising given the various and strong selection pressured on *env*, and a few others such as Gag TST. However, whilst there were epitopes in which the process of escape was complete even at baseline, this was not the general rule; Figure 3.4 shows that more than 70% of HLA-matched patient-epitope pairs remain unescaped throughout the three-year observation period. Nor is it the case that all of the fastest escaping epitopes end up escaping in all HLA-matched patients. In these data only two epitopes (KYK and TAF) escape in all HLA-matched patients within the observation period.

The fastest rate of escape was seen within epitopes against which a positive $CD8^+$ T-cell response had been measured (a group comprising $\sim$ 30% of HLA-matched host-epitope pairs). Even here the incidence of escape was low (Figure 3.4B). Hence we cannot conclude that it was a lack of strong $CD8^+$ T-cell responses in the hosts to the set of epitopes we studied that led to few escape events being observed. However, as only IFN-γ production was measured to indicate the strength of the response we cannot tell whether or not the responses measured were qualitatively good in other ways.

Lastly, the definition of escape that we have used may have prevented some true escape from being classified as such. We were able expand the definition in two ways: by considering amino acid mutations that occur outside of known escape sites (but still within the

epitope), and by extending the list of epitopes beyond the set of optimal defined epitopes (see Appendix A and Table A.6). Repeated analyses given these less stringent definitions are presented in Figures A.7-A.12. Both of these amendments reduce the time to first escape in a patient so that an estimated $\sim 10\%$ (down from $\sim 30\%$) of patients have driven no escape in HLA-restricted epitopes within the first two years. Changing the definition does not change the conclusion that the majority of escape at baseline is transmitted, or that escape mutations rise to fixation with a roughly uniform frequency across the observation period. However, extending the list of epitopes diminishes the association between HLA relative hazard and time to escape, suggesting that the strength of this association is sensitive to the set of epitopes considered.

We acknowledge that even this extended epitope list is unlikely to be complete, and that the Los Alamos 'A-list' will evolve to include new peptides and HLA-restrictions [337,338]. Indeed, when using the extended list we observe 144 vs. 69 incident 'escapes' in HLA-mismatched vs. -matched patient-epitope pairs (Figure A.12). Many of these 'escapes' in supposedly unrestricted epitopes cannot be accounted for by overlap with another, HLA-restricted epitope. Some of these may be indicative of immune escape driven by other components of the immune response such as NK cells, $CD4^+$ T-cells or the antibody response. But understanding the impact of these alternative selective pressures is not necessary for assessing the concern that our methods are blind to CTL escape occurring in previously unidentified epitopes. We have previously shown that HLA-association studies favour the detection of rapid escape mutations. Hence any escape in unknown or poorly characterised epitopes that we have not looked in is likely to be slower than the time frame of this study and consequently not affect our conclusions [339].

Our definition of escape was also based on consensus viral sequence data; hence we were unable to detect the presence of any low frequency variants unlike with deep sequencing methods [29,134]. However, variants that never rise to a majority in the population are of limited interest since they lack biological significance in terms of being unlikely to effect viral dynamics or the course of the disease in the long term. Variants that do rise to greater than 50% prevalence would be detectable with our methods. Therefore our use of consensus viral sequence is not problematic.

The final aspect of our definition of escape to address is the use of HXB2 as our com-

parison sequence. Although there is no 'gold standard' comparator for this analysis, there were only four epitopes in which HXB2 differed from the 'A list' optimal at a documented escape site. We therefore re-ran the analysis re-classifying these four epitopes and found no significant difference in the distribution of baseline escape prevalence between HLA-matched and -mismatched hosts. We did identify 4 new incident escapes (3 in EVK, 1 in RPN). Although the EVK escape variant is only poorly defined, its inclusion would mean that an estimated 25% of patients had not driven an escape by the end of 2 years off-therapy (as opposed to 33%).

In conclusion, this study of a cohort from a randomised controlled trial, the proper design for assessing rates of escape across a population, reveals that escape is on average both less frequent and less concentrated in the first few months of infection than would be expected from recent intense studies of much smaller numbers of acutely infected individuals.

3.4 Materials and Methods

3.4.1 Ethics Statement

The SPARTAC trial was approved by the following authorities: Medicines and Healthcare products Regulatory Agency (UK), Ministry of Health (Brazil), Irish Medicines Board (Ireland), Medicines Control Council (South Africa), and The Uganda National Council for Science and Technology (Uganda). It was also approved by the following ethics committees in the participating countries: Central London Research Ethics Committee (UK), Hospital Universitario Clementino Fraga Filho Ethics in Research Committee (Brazil), Clinical Research and Ethics Committee of Hospital Clinic in the province of Barcelona, Spain, The Adelaide and Meath Hospital Research Ethics Committee (Ireland), University of Witwatersrand Human Research Ethics Committee, University of Kwazulu-Natal Research Ethics Committee and University of Cape Town Research Ethics Committee (South Africa), Uganda Virus Research Institute Science and ethics committee (Uganda), The Prince Charles Hospital Human Research Ethics Committee and St Vincent's Hospital Human Research Ethics Committee (Australia), and the National Institute for Infectious Diseases Lazzaro Spallanzani, Institute Hospital and the Medical Research Ethics Com-

mittee, and the ethical committee Of the Central Foundation of San Raffaele, MonteTabor (Italy). All participants signed a written informed consent.

3.4.2 Participants and Trial Design

The design of the SPARTAC trial is reported in [8]. In brief, SPARTAC was an international open Randomised Controlled Trial enrolling adults with primary HIV infection (PHI) within 6 months of a last negative, equivocal or incident HIV-1 test. All participants gave written informed consent. The trial was approved by research ethics committees in each country. Time of seroconversion was estimated as the midpoint of last negative/equivocal and first positive tests, or date of incident test. Participants were randomised to receive ART for 48 weeks (ART-48), 12 weeks (ART-12) or no therapy (standard of care, SOC). The primary endpoint was a composite of two events: if participants either reached a CD4 count of < 350 cells/mm^3 (> 3 months after randomisation and confirmed within 4 weeks) or initiated long-term ART. This provided an immunological surrogate of clinical progression, but also allowed inclusion of those participants who commenced ART at CD4 cell counts greater than 350 cells/mm^3.

The participants studied here consisted of a sub-group of125 HIV-1 subtype B positive individuals of whom 42, 41 and 42 were randomised to ART-12, ART-48 and SOC, respectively. Peripheral blood mononuclear cells (PBMCs) were collected at regular intervals during the treatment period and follow-up. The sub-group of 125 participants was based on those individuals infected with subtype B HIV-1 for whom both sequence and ELISpot data were available, predominantly determined by specimen availability.

3.4.3 Sequences

Viral RNA was extracted from patient plasma (Qiagen Viral RNA extraction kit) and the HIV-1 *pol*, *gag*, *nef* and *env* genes were amplified separately using nested PCR reactions and primers described previously [164, 335, 340]. The PCR products were purified and sequenced using Big Dye dideoxy terminator chemistry (ABI). Sequences are therefore presented as the consensus from a bulk PCR product for each time-point. Sequence data were available for each patient at a subset of the following time points: 0, 16 or 24, 52 or 60, 108 and 156 weeks following recruitment onto the trial (see Table A.1 for details).

3.4.4 CD8$^+$ T cell ELISpot assays

Quantification of CD8$^+$ T-cell response was performed by interferon gamma ELISpot analysis in all subtype B patients, using methods described elsewhere [112]. Responses were determined to 181 subtype B optimal peptides covering the Gag (n=67), Pol (n=47), Nef (n=30) and Env (n=37) proteins and 195 autologous variants synthesised followed sequence analysis. The optimal peptides tested were derived from the "best-defined 'A list' CTL epitope" database accessed from the Los Alamos HIV Immunology Website. Analyses were performed singly, but in duplicate for the negative control, and results expressed as spot forming units (SFU) per 10^6 cells. ELISpot responses were measured at 0, 24 and 60 weeks post-recruitment.

3.4.5 HLA genotyping

Patients' HLA type was determined to the oligo-allelic level using Dynal RELITM Reverse Sequence-Specific Oligonucleotide kits for the HLA-A, -B and -C loci (Dynal Biotech). To obtain four-digit typing, Dynal Biotech Sequence-Specific priming kits were used, in conjunction with the Sequence-Specific Oligonucleotide type.

3.4.6 Defining escape

A CTL escape mutation was defined as *any amino acid variation in previously identified (and phenotypically confirmed) escape sites within an 'optimal' defined epitope.* Known escape sites were defined as within-epitope sites for which escape (E), calculated escape (CE), inferred escape (IE) or literature escape (LE) had been documented in the 'CTL/CD8$^+$ Epitope Variants and Escape Mutations' HIV database table, as downloaded on 05/11/12 [341]. Any amino acid difference between autologous sequence and HXB2 in one of the sites under consideration was classed as escape. The list of 'optimal' defined epitopes was initially drawn from the set of epitopes for which ELISpot assays had been conducted (see above) though this was later extended (Appendix A and Table A.6). The 4-digit HLA-type restricting each epitope was determined using the 'Best-defined' epitope summary table on the Los Alamos HIV Immunology Database [341] downloaded on 01/03/2013. 2-digit HLA types were used only where 4-digit HLA types were not avail-

able. Only epitopes restricted by HLA-A and -B alleles were included since data on patient HLA-C alleles was not initially available. However a subsequent analysis found there were no incident escape mutations observed in any of these patients in epitopes restricted by their HLA-C alleles, so the exclusion of these epitopes is not problematic.

This intentionally stringent definition of escape was chosen to optimise the balance between including all relevant variation available in sequence data whilst excluding variation that is not escape. This definition does not include escape mutations that lie outside the epitope and disrupt proteasomal processing or antigen presentation pathways. It also excludes escape that occurs in poorly studied or unknown epitopes [342]. To complement the published data available and to check that mutations classed as 'escape' genuinely did result in diminished IFN-γ production by $CD8^+$ T-cells, a comparison was made between the magnitudes of $CD8^+$ T-cell ELISpot responses for the pre-defined optimal peptides with those for autologous epitope variants observed in the population at baseline. Variants for 7 Gag and 2 Pol epitopes were tested. In all cases except Gag EVD (where the optimal peptide differed from the HXB2 sequence) the major variant(s) elicited a diminished response. In 6/9 cases responses to all 'escape' variants were reduced by at least 90% (Table A.2).

3.4.7 Identification of escape in the data

Firstly, the sequence data was subjected to quality control: A phylogenetic tree was constructed for all sequences of each gene in turn so that patients whose sequences did not cluster with each other could be identified and removed from the dataset if necessary. Due to difficulties in aligning all regions of all genes, epitopes were located using a string-matching search, allowing for 4 amino acid differences between the HXB2 epitope sequence and the patient sequence. Spurious matches were identified by hand and removed. Missing data resulted in escape being classed as 'not determined' if the HXB2 and viral sequence matched at all of the defined escape sites in the epitope except those where data was missing.

3.4.8 Statistics

Permutation test on the distribution of escape between HLA-matched and -mismatched hosts. We wished to test the null hypothesis that escape is equally likely to be present in HLA-matched and -mismatched hosts against the alternative hypothesis that there is more escape in HLA-matched hosts. The statistic used for this was the mean (across all epitopes) of the Fisher's exact test p-values for whether escape was independent of HLA-matching for that epitope. A permutation test was used to calculate the distribution of this mean under the null hypothesis; 2,000 random data sets were generated by permuting which patients the escape events occurred in for each epitope (i.e. there was no permutation between epitopes). The mean of the p-values for the observed data was then calculated and compared to the null distribution (Figure A.1).

Poisson process for calculation of expected escape distributions. For each epitope in each patient in which an incident escape could have been observed, the total amount of time for which the patient was observed whilst off ART was calculated. Let E be the total number of escape events observed in the population, T be the total observation time (whilst off ART) across all epitopes in all patients and t_p be the total observation time for all epitopes of a particular patient, p. Then, under the assumption that the average rate of incidence of escape in all patients is $r = E/T$, the probability of patient p driving i escape events is:

$$\Pr(p \text{ drives } i \text{ escape events during observation}) = \frac{e^{-t_p r}(t_p r)^i}{i!}$$

The expected number of patients with i incident escape events is then the sum over all patients of these probabilities. The expected distribution of escape across different epitopes is calculated similarly.

To account for missing data (for Figure 3.2B), it was supposed that each patient had 108 weeks of data, during which time they were off ART. Where an epitope sequence was entirely missing (so that whether or not the epitope was initially wild-type could not be determined), the probability of it being wild-type at baseline was taken to be equal to the prevalence of escape at the first time point, as in Table A.5 (this was necessary for a total of 203 HLA-matched patient-epitope pairs). We could then calculate $t_p =$

(# HLA-matched, initially wild-type epitopes) $\times$ 108.

Note that this model does not impose the condition that only one escape is possible in each patient-epitope pair. We believe this to be a reasonable simplification given that the total number of escape events is small.

A χ^2 goodness-of-fit test with 4 degrees of freedom (i.e. categories for 0, 1, 2, 3, and ≥ 4 escaped epitopes) was used to test the null hypothesis that the observed data followed the expected distribution.

Survival analysis. For the survival analysis shown in Figures 3.3 and 3.4 only patient-epitope pairs in which it would have been possible to observe an escape were considered. This included all patient-epitope pairs that were wild-type in known escape sites at the first data point and had data available at a second data point. For each patient-epitope pair where an incident escape occurred, escape times were estimated as the midpoint between the last wild-type observation (or if that observation was during therapy, the therapy end time) and the first appearance of the escape mutant in the consensus sequence (or the clinical endpoint, whichever was earlier). Escape events occurring during treatment were discarded. Where no incident escape occurred, right-censoring started at the last sequence data time point or clinical endpoint, whichever was earlier. In Figure 3.3, hazard ratios were calculated using a simple Cox Proportional Hazards model with a single predictor - the variable of interest. p-values relate to the Likelihood Ratio test comparing the one-predictor model with the null model. In Figure 3.4, where observations from all patients and epitopes were pooled, hazard ratios and associated p-values were calculated using a mixed effects Cox model with a single predictor but also random intercept terms for patient and epitope ID. This was implemented with the package 'coxme' in R.

3.5 Questions addressed in this chapter

- What is the prevalence at the time of infection and incidence thereafter of CTL escape in these patients?

  CTL escape is found in 1235/3831 epitope sequences at baseline. Data were consistent with the majority of this escape having been present in the transmitted virus. Prevalence varied widely amongst the epitopes studied (Figure 3.1A; section 3.4.2). The incidence of escape across all epitopes and all patients studied was low (Figure 3.2, Figure 3.4; section 3.4.3).

- When during infection does CTL escape tend to occur?

  There were only 2 (out of 43) epitopes in which escape routinely occurred very early in infection (Figure 3.1A, Table A.3). Escape was observed to occur at a fairly constant frequency throughout the first 5 years of infection, and there was large inter-patient variability in time to first escape event (Figure 3.3A, Figure 3.4; sections 3.4.4 and 3.4.6).

- Is there evidence for a disproportionately high or low number of escape events in some patients?

  No. The distribution of 'number of escape events per patient' was not statistically significantly different from what would be expected if all patients had an equal propensity to drive escape events (Figure 3.2; section 3.4.3).

- Are there any host immunity factors associated with a greater incidence of escape?

  Yes. The presence of a $CD8^+$ T-cell response towards an epitope and possession of a 'protective' HLA allele were significantly associated with a greater incidence of escape and shorter time to first observed escape, respectively (Figure 3.3B, Figure 3.4; sections 3.4.5 and 3.4.6).

- Is there any evidence that CTL escape reduces a patient's ability to control the virus?

  We found no evidence for immune escape impacting disease progression or for an increase in viral load following an observed incident escape (Figures A.13 and A.14, Appendix). However, our study was underpowered to look at this question, particularly in terms of the relationship between incident escape and viral load.

4

Early initiation of ART

4.1 Introduction

The HIV reservoir is a barrier to cure. By definition, the reservoir consists of virus (in large part harboured by latently infected resting $CD4^+$ T-cells) which persists during anti-retroviral therapy (ART) and can cause viral rebound if ART is discontinued [343]. Indeed, in the majority of patients cessation of ART results in viral rebound within 4 weeks [23,280]. In one study, of 164 patients who interrupted ART initiated during primary HIV infection, only 14 had viral loads (VL) that remained undetectable (<50 copies/ml) 1 year later, but four of those patients were found to be still controlling the virus 5 years post treatment interruption [286].

The VISCONTI patients are a well-studied group of 14 so-called post-treatment controllers (PTCs; not the exact same 14 patients as above) [11]. All started ART during primary infection, were treated with combination ART for a median of 36.5 months and had maintained undetectable VL for several years post treatment interruption (median 7.4, IQR 6.1-8.6, at time of study). Evidence suggests that they are not simply patients who would have been able to spontaneously control the virus without ART. The characteristics of PTCs and spontaneous HIV controllers differ on several points [21]. For example, spontaneous controllers had significantly lower viral loads and higher CD4 counts in primary infection compared to the VISCONTI PTCs, and protective HLA alleles are consistently over-represented in cohorts of spontaneous controllers but not amongst the PTCs [11].

The existence of such PTCs raises the possibility that ART cessation, perhaps following additional reservoir-reducing interventions, may in the future be a desirable and feasible

option. However post-treatment control is currently poorly understood. We are unable to predict which patients will go on to control the virus after ART interruption and will need to understand the underlying factors and mechanisms much better before this is possible [21]. Substantial attention has been given to the *size* of the reservoir and how that is affected by ART and may itself affect post-treatment control. In this chapter I focus on the *size and quality* of the reservoir. In particular I explore the distribution of turnover rates as one aspect of reservoir quality.

4.1.1 Data review: factors contributing to post-treatment control

Many studies seeking to uncover the correlates of post-treatment control ask, "What are the determinants of time to viral rebound post treatment interruption?". These studies may include very few genuine PTCs who control for clinically significant periods of time (> 2 years is generally considered significant [21]). However, the mechanisms behind even very transient periods of control may be similar to those that enable years of control.

The size of the HIV reservoir is one of the clearest factors influencing post treatment control. Various assays exist for determining the size of the reservoir. The viral outgrowth assay is considered to be the 'gold standard', but it is resource intensive and is also likely to be an underestimate of reservoir size [219]. PCR-based assays such as total or integrated HIV DNA in PBMCs are much more feasible for large studies but are known to be overestimates since a large proportion of proviruses are replication incompetent [220]. A comparative study found that PCR-based assays estimated infected cell numbers at least two logs higher than those estimated using the viral outgrowth assay [32]. The ratio of PCR-based to outgrowth estimates varies a lot between patients but all three assays (total, integrated and viral outgrowth) have been found to be significantly correlated [344]. The VISCONTI PTCs all had remarkably low levels of cell-associated HIV DNA post-treatment (median 1.71 log copies/10^6 PBMCs), more than ten times lower than in patients with uncontrolled infection [11, 345]. Aside from this observation, there is now a body of other studies showing an association between PCR-based measures of the size of the reservoir at treatment interruption and time to viral rebound [22, 23, 286–288]. However, HIV DNA level is not a straightforward predictor of whether or not a patient will exhibit post-treatment control; even patients with undetectable HIV DNA have been known to

experience viral rebound within weeks of treatment interruption [256, 285].

The second well-studied correlate of time to viral rebound is the timing of ART initiation and, additionally in some studies, the duration for which patients have received ART. Table 4.1 summarises studies in which patients underwent ART interruption and outcomes post-treatment were recorded and related to the timing or duration of ART. It shows that patients treated in chronic infection rebound sooner than those treated early in infection (where 'early' is usually defined as within the first 6 months) [23, 280, 291]. Note that a significant association between ART initiation time and viral rebound time is not seen in all studies in Table 4.1 – not all studies include both early- and chronic- treated patients. A significant effect of ART duration was found in only one study [289]. Table 4.2 summarises studies relating the timing or duration of ART with reservoir size on treatment. It shows that patients who started ART later in infection are consistently found to have higher levels of HIV DNA after months to years of treatment [225, 256, 258, 259, 262, 292]. Studies estimated a $0.7 - 2.3\,\log$ difference in median on-treatment levels of HIV DNA between early- and chronic- treated patients [256, 258, 262, 292]. Very few studies have looked at the effect of duration of ART on reservoir levels, one found a significant negative correlation between ART duration and HIV DNA levels [258]. All these observations taken together suggest that *there is a positive effect of early ART on viral rebound time, which is at least partly mediated via a smaller reservoir in early ART starters.*

It is not clear whether the strength of the immune response plays any role in determining post treatment control but since it has received much attention it is worth mentioning here. Some have suggested that strong $CD4^+$ T cell responses maintain an effective cytotoxic T-lymphocyte response and are linked to a patient's ability to control viraemia post-treatment [294, 346], but others have found contrasting results [347]. In the VISCONTI PTCs, both the number of HIV-specific $CD8^+$ T-cells making an IFN-gamma response and the capacity of the $CD8^+$ T cells to suppress infection *ex vivo* were low, significantly weaker than in a comparison group of spontaneous controllers [11].

Table 4.1: A table summarising data on the relationship between ART initiation and duration and viral rebound

Paper	*N*	ART initiation	Duration of ART	ART Regimen	Rebound defn	Results
Harrigana 1999 [348]	6	Not reported	1-20 mo.	HAART	VL measured every few days post-TI and rate of rebound calculated.	No correlation between rate of rebound or duration for which patients had suppressed on ART ($r^2 = 0.01$). NB: All patients stopped ART due to side-effects or complications.
Steingrover 2008 [291]	24 primary + 48 chronic	Primary: < 6 mo post infection. Chronic: not reported	Primary: 1-2 yrs. Chronic: 4-6 yrs	Intensive HAART (5-drug) simplified after 1 yr, various 3-drug regimen	VL >50, 500, 5000 copies/ml all used	**Initiation** of ART during chronic as opposed to primary infection was related to faster rebound ($p < 0.001$, hazard ratio 2.3). ART **duration** was not associated with time to rebound once corrected for primary/chronic group.
Goujard 2012 [286]	164	<3 mo post infection	1-3 yrs	Two RTIs + PI or EFV	Classify into VL < 50 ($n = 14$), VL maintained > 50 and < 500 ($n = 14$) , VL rebounds above 500 ($n = 136$)	No significant difference in **timing** ($p = 0.74$) or **duration** ($p = 0.27$) of ART between the three groups. Note that there is little variation in ART initiation time amongst these patients.
Hamlyn 2012 [280]	182 primary (SPARTAC) + 1450 chronic (SMART)	Primary: < 6 mo post s/c Chronic: median ≈ 2 yrs post infection	Primary: median 3 mo. Chronic: median 72 mo.	Various	VL > 400	ART **initiation time**: some evidence of faster rebound in chronic patients - the probability of rebound by 4 wks post-ART was similar for chronic and primary patients but the slope of VL over 48 wks post-ART was steeper in chronic than primary patients (adjusted $p < 0.0001$)

Table 4.1 (contd.). A table summarising data on the relationship between ART initiation and duration and viral rebound

Paper	*N*	ART initiation	Duration of ART	ART Regimen	Rebound defn	Results
Stohr 2013 [289]	167 (SPARTAC)	$<$ 6 mo post s/c	12 wks or 48 wks	Two NRTIs + ritonavir-boosted PI recommended	VL $>$ 400	ART **initiation time** not significantly associated with probability of rebound ($p = 0.25$). VL at baseline was significantly associated with chance of rebound within 12 weeks of treatment interruption though ($p < 0.001$). **Duration:** Those on ART for $>$ 12 wks had lower probabilities of rebounding within 12 wks than those on ART for $\leq$ 12 wks ($p < 0.001$, odds ratio 0.11).
Li 2016 [23]	155 chronic + 48 early + 32 acute, from 6 studies	Acute: $<$ 4 wks post infection. Early: 2 wks - 6 mo post infection. Chronic: not given	Acute/early: 52 weeks or $>$ 6 mo for the two studies. Chronic: median 5.1 yrs	They look at NNRTI regimen as a predictor	Two definitions: two conseq VL $>$ 200 or one VL $>$ 1000. VL is measured at least fortnightly for up to 16 weeks in most cases.	ART **initiation time**: Proportion of patients with VL$<$ 200 at wk 12 was significantly smaller for chronic than acute/early starters (chronic vs. acute vs. early: 3 vs. 9 vs. 15%, $p < 0.01$). In a two-covariate cox model including cell-associated RNA at ART-interruption, ART initiation in acute/early did not significantly predict viral rebound time but had an odds ratio of 0.4 ($p = 0.1$).

Table 4.2: A table summarising data on the relationship between ART initiation and duration and reservoir size

Paper	N	ART initiation	Duration at sampling	'Reservoir' measure	Results
Chun 1998 [203]	10	0.3 - 4.4 months after onset of symptoms	0.2 - 17.0 months	Total and integrated HIV DNA per million resting CD4s. Infectious units per million resting CD4s.	Neither time of **initiation** nor **duration** of ART correlated with any of the reservoir measures ($p > 0.5$)
Chomont 2009 [225]	34	Mean 38 months post infection	Mean 45 months	Integrated HIV DNA copies per million CD4s	ART **initiation time**: Patients who started ART within a year of infection had significantly lower levels of HIV DNA than those who initiated ART after > 1 year ($p < 0.0001$).
Chun 2010 [256]	44	9 early (< 6 mo since infection), 35 chronic (> 6 mo).	Median 7.7 years (range 3.0-10.5)	HIV proviral DNA per million CD4s	ART **initiation time**: Patients that initiated ART early had significantly lower levels of HIV DNA ($p = 0.003$, median in early vs chronic: 4.6 vs 949.4)
Gianella 2011 [259]	24 acute, 8 early chronic	Acute: < 60 days from infection. Early chronic: 61-120 days from infection	Median 18 months	HIV DNA per million PBMCs, mean post-cessation value across up to 1 year.	ART **initiation time**: Post-cessation HIV-1 DNA setpoints were statistically lower in early compared to later starters (2.3 vs 2.7 log copies; $p = 0.03$).
Watanabe 2011 [258]	61	6 pre s/c, 55 post s/c (chronic)	> 4 months	HIV-DNA per million CD4s	ART **initiation time**: Pre s/c (early treated) patents had significantly lower levels of HIV DNA ($p = 0.016$, > 1 log difference in medians). The **duration** of ART correlated negatively with levels of HIV DNA ($\rho = -0.3, p = 0.03$).
Hocqueloux 2013 [262]	35 primary + 272 chronic	Primary: < 4 mo since infection. Chronic: > 4 mo since infection.	Median time suppressed on ART: 3.1 yrs (primary), 3.9 yrs (chronic)	Total HIV DNA per million PBMCs	ART **initiation time**: Primary treated patients had lower levels of HIV DNA than chronic patients (2.15 vs 2.84 log copies, $p < 0.0001$).

Table 4.2 (contd.). A table summarising data on the relationship between ART initiation and duration and reservoir size

Paper	N	ART initiation	Duration at sampling	'Reservoir' measure	Results
Jain 2013 [257]	34 early + 32 chronic	Early: $<$ 6 months since infection. Chronic: $>$ 2 years since infection	$>$ 2 years	Total HIV DNA and cell-associated HIV RNA, per million PBMCs	ART **initiation time**: Early ART starters had significantly lower levels of HIV DNA and cell-associated RNA.
Ananworanich 2012 [260]	30	Fiebig stage IV or earlier [88]	24 wks	Total HIV DNA per million PBMCs and per million CD4s, at ART initiation (wk 0) and wk 24	At ART **initiation**, Fiebig I patients had lower total HIV DNA than Fiebig III and Fiebig II patients ($p \leq 0.02$). HIV DNA at wk 0 and wk 24 was significantly correlated ($p < 0.001$).
Buzon 2014 [292]	9 early + 26 chronic	Early: within 6 mo of infection. Chronic: $>$ 2 yrs since diagnosis	$>$ 10 years	Total and integrated HIV-DNA per CD4	ART **initiation time**: Early treated patients had lower levels of total DNA ($p = 0.001$) and integrated DNA (p not reported) than chronic patients. Within early-treated patients, those who initiated ART closer to the estimated date of infection had significantly lower levels of total and integrated DNA ($p = 0.05, r = 0.68$ and $p = 0.02, r = 0.75$ resp.)
Crooks 2015 [349]	17 acute (HIV Western Blot negative) + 20 chronic	Acute: within 45 days of infection, one exception. Chronic: not reported	Median duration at first measurement was 21 mo. (acute patients) and 78 mo. (chronic)	Decay of resting cell infection (using Quantitative Viral Outgrowth Assay) after patients have been suppressed for $\geq$ 6 months	ART **initiation time**: No evidence for more rapid decay in acute patients compared with chronic patients (during follow up of median 1.2 years, $p = 0.99$).

4.1.2 Data motivating this chapter

There are two particular sets of data that have motivated my focus on T-cell turnover rates within the latently infected reservoir. The first dataset of interest is that presented in Hocqueloux et al [262], reproduced in Figure 4.1A. This is currently unique in its size, timespan, and the inclusion of both primary-treated and chronic-treated patients. HIV DNA load per million PBMCs was measured in just under 300 patients from the time of viral suppression on ART and for up to 14 years following. Patients treated earlier had lower HIV DNA levels initially and faster decay on ART so that after many years on treatment the average HIV DNA load was much smaller in the primary-treated patients than in the chronic-treated patients. These data suggest that *there are fewer latently infected cells with a very long half-life (i.e. slow turnover) in primary-treated individuals compared to in chronic-treated individuals.* I shall refer to this as the Hocqueloux data.

Secondly, deep sequencing of latently infected cells coupled with longitudinal viral RNA sequence prior to ART has provided information on when those cells were infected. It can therefore also be used to give estimates of the turnover of the reservoir at the point when it was laid down (i.e. in untreated infection). Recent unpublished data of this sort from Brodin et al shows that a disproportionately high number of sequences from latently infected cells sampled after more than three years of ART match viral strains that were circulating immediately prior to ART. Using this they estimate that *the half life of the latently infected cells in untreated infection is* ≈ 1 *year*, as represented in Figure 4.1B. This study was done in patients who had initiated ART in chronic infection, after approximately five years of infection. I shall refer to this as the Brodin data.

4.1.3 Questions addressed in this chapter

Motivated by these data, I ask the following questions to inform our understanding of the dynamics of the latent reservoir before and during ART and hence of post-treatment control. Firstly, based on the Hocqueloux decay data, might early-treated patients experience a faster decay of their HIV-DNA load on ART as a result of a smaller slow-turnover population of latently infected cells being present early in infection? If so, then does this explanation still hold when I account for a large portion of the HIV DNA load being repli-

cation incompetent, or, could replication incompetent DNA alone explain the data? By developing a simple linear model of T-cell dynamics I find that the explanation holds in both cases and also generate a testable prediction about the proportion of replication incompetent HIV DNA over time. I then ask whether the mechanism described by my model is also compatible with the Brodin sequence data. Initially the results are not compatible and so I investigate further: could falling activation rates in treated infection enable the model to fit with these data? Though this is possible, changing the model in this way means it is no longer compatible with the Hocqueloux DNA decay data and so I conclude by asking what it is about my model that means it is unable to fit both data sets at once.

4.2 Results

The patterns of HIV DNA decay seen in the Hocqueloux data [262] (Figure 4.1A) led me to reason that early treated patients might have a particularly small portion of the reservoir that has slow-turnover and is therefore slow-decaying on ART. If we assume that this is the case and fit a model with two distinct populations of T-cells, slow-turnover and medium-turnover, to this data, we find that the slow-turnover population is approximately 8-fold smaller in the primary-treated patients than the chronic-treated patients, at the time virus becomes undetectable on ART (Figure 4.1A and Table 4.3). In contrast, the medium-turnover population is not even 2-fold smaller in the earlier-treated patients. Note that this data starts at the point at which virus becomes undetectable, by which point the fastest turnover cells will have largely decayed. The first question I ask is, is it possible that as untreated infection progresses there could be an 8-fold increase in the size of the slow-turnover population of latently infected cells between primary (median 1.9 months) and chronic (median 4.7 years) infection?

4.2.1 Model development

I apply a simple linear ODE model to this question, encapsulating the basic dynamics of resting (R), activated (T) and latently infected (L) $CD4^+$ T cells (model diagram in Figure 4.2A). Since I am only concerned with how the number of latently infected cells changes over time I do not explicitly model the dynamics of productively infected cells or

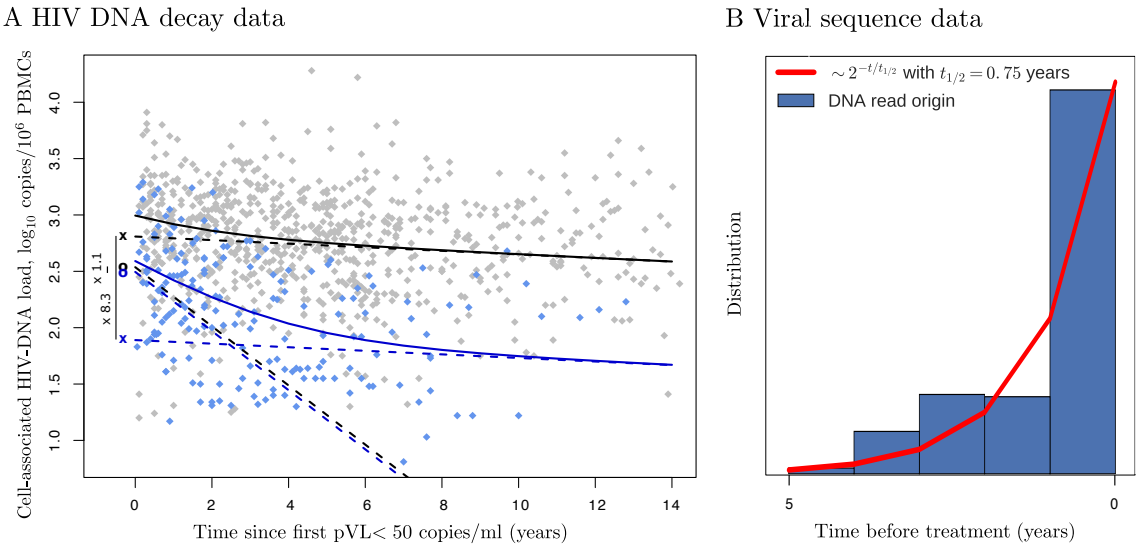


Figure 4.1: Collated data on the dynamics of the latent reservoir (A) HIV DNA decay data originally published in Hocqueloux et al [262]. Patients were stratified according to whether they initiated cART in primary (Fiebig stages I-V, $n = 34$, blue dots) or chronic ($n = 262$, grey dots) infection. In the primary HIV infection group, median time from estimated date of infection to first ART was 1.9 months (IQR: 1.4, 3.0). In the chronic HIV infection group, median time from estimated date of infection to first ART was 4.7 years (IQR: 3.0, 7.2). The lines show a bi-exponential mixed-effects model fitted to the data. The model fitted is $\log_{10}(L(t)) = \log_{10}(A_2e^{-b_2t} + A_3e^{-b_3t})$ with an intercept term as a random effect to account for multiple, longitudinal measures per patient (mean 3.2 measures per patient). The rate parameters b_2 and b_3 are fixed between primary and chronic groups whereas the intercept parameters A_2 and A_3 may vary. To achieve convergence of the model fitting algorithm, b_3 had to be fixed; a value of 0.0001 is used here. Fitted values for this fit along with those corresponding to different b_3 values are shown in Table 4.3 . The solid lines show the fitted curves for $L(t)$ (primary in blue, chronic in black) and the dashed lines show the decay of the medium (b_2) and slow (b_3) populations separately. The blue and black circles and crosses on the left hand side of the graph indicate the values of A_2 (circles) and A_3 (crosses) for primary- (blue) and chronic- (black) treated patients. (B) A representation of the result from Brodin et al [250]. The distribution of the origin of 'reservoir variants' (proviral sequences from latently infected cells sampled after at least 3 years of ART) is skewed so that the majority match most closely to viral RNA circulating immediately prior to ART initiation. This leads to an estimated half-life of the 'reservoir' prior to ART of less than one year, as represented by the curve plotted in red here.

Table 4.3: Fitted values for the size of the slow- and medium-turnover populations at the point when VL becomes undetectable on ART

Decay rates		Size of medium (A_2) in		Size of slow (A_3) in		**Fold change**	
Slow (b_3)	Medium (b_2)	Primary	Chronic	Primary	Chronic	Medium	Slow
$\mathbf{5 \times 10^{-5}}$	1.5×10^{-3}	318	442	65	564	**1.39**	**8.65**
-	$(1.2, 1.9) \times 10^{-3}$	(255, 396)	(330, 592)	(49, 85)	(519, 612)	-	-
$\mathbf{1 \times 10^{-4}}$	1.7×10^{-3}	312	344	78	644	**1.10**	**8.29**
-	$(1.3, 2.1) \times 10^{-3}$	(248, 392)	(233, 507)	(60, 101)	(595, 696)	-	-
$\mathbf{2 \times 10^{-4}}$	1.9×10^{-3}	295	124	104	819	**0.42**	**7.87**
-	$(1.4, 2.5) \times 10^{-3}$	(230, 378)	(39, 393)	(81, 133)	(761, 882)	-	-

Numbers in brackets are the coefficient minus and plus standard error. Fold change is the chronic value divided by the primary value. Note that b_3 is set while b_2, A_2, A_3 are fitted. The shaded row corresponds to the fitted values as shown in Figure 4.1A.

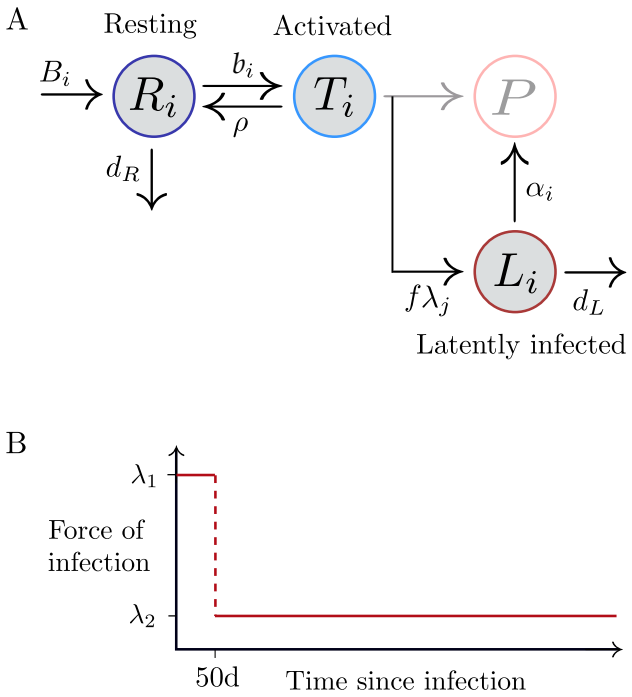


Figure 4.2: A model of T cell activation and latent cell infection (A) Model diagram, in which i indexes different CD4$^+$ T-cell populations with different expected times to activation. The dynamics of any one particular population are shown. In this basic model, uninfected resting cells (R_i) may become activated at rate b_i (to T_i) and are susceptible to infection while they remain activated. A fraction, f of newly infected cells become latently infected. Latently infected cells may become re-activated at rate α_i. Throughout this chapter we assume that $\alpha_i = b_i$. B_i is the rate at which new naive cells are created and migrate into the blood. ρ is the rate at which activated cells return to a resting state. The decay rates in this model ($d_R, d_L + \alpha_i$) are an aggregate of death and proliferation for each T-cell population. The behaviour of productively infected cells (P) and virions is not simulated because it is not the focus of this study. (B) The force of infection, λ_j, is fixed, with a higher value in acute infection lasting 50 days, as shown.

free virus. Instead the force of infection, λ_j, is fixed but is higher in acute than in chronic infection ($\lambda_1 > \lambda_2$), to mimic the effect of peak viraemia (Figure 4.2B).

The model includes two key assumptions. Firstly, only activated (not resting) $CD4^+$ T-cells are susceptible to HIV infection [350]. Secondly, the rate of activation of resting (uninfected cells) is linked to the rate of re-activation of latently infected cells. In other words, I assume that there is some factor intrinsic to each cell, such as its antigen specificity, which determines how frequently it is activated, relating to both activation from a resting uninfected state and viral reactivation from a latently infected state. My intuition is that the resulting rarely activated, rarely re-activated populations would be both laid down gradually during untreated infection (as a result of being rarely activated) *and* decay slowly during treated infection (as a result of being rarely re-activated). I hypothesise that this mechanism explains the larger size of the slow turnover, persistent portion of the reservoir in chronically infected patients. Hence, to investigate the separate behaviour of slow and fast-turnover latently infected T-cell subpopulations under this model, I categorise $CD4^+$ T-cells into three classes (denoted using the subscript i) with separate activation rates, b_i (b_1 ='frequent', b_2 ='intermediate', b_3='rare'). The most rarely activated cells ($i = 3$) are rarely susceptible to infection but also have a long half-life once latently infected, since viral reactivation is assumed to lead to cell death. Hence the frequent/intermediate/rare activation latently infected populations have fast/medium/slow turnover respectively. I will use these terms interchangeably throughout this chapter. The model equations are as follows:

$$\begin{aligned}
\frac{dR_i}{dt} &= B_i - (d_R + b_i)R_i + \rho T_i \\
\frac{dT_i}{dt} &= b_i R_i - (\rho + \lambda_j)T_i \\
\frac{dL_i}{dt} &= f\lambda_j T_i - d_L L_i - \alpha_i L_i
\end{aligned}$$

Resting cells are sourced at rate B_i, die at rate d_R and become activated at rate b_i. Activated cells return to a resting state at rate ρ (note the average time spent activated is independent of the activation class) and become infected at rate λ_j. In line with Ribeiro et al's modelling work on T-cell turnover [96] I set the death rate of activated cells to be

equal to their proliferation rate, hence neither are included in the model equations. A fraction, f, of newly infected cells become latently infected. Latently infected cells have an activation-independent decay rate, d_L, and an activation-related decay rate, α_i. In line with my second assumption the activation-related decay rate should be proportional to b_i, throughout this chapter I make the simplifying assumption that $\alpha_i = b_i$. Both of the decay rates represent an aggregate of death and proliferation. I assume that ART has 100% efficacy and so the force of infection during ART is zero.

I sought to use data from T-cell stable isotope labelling experiments to parameterise the turnover rates of uninfected $CD4^+$ T-cells in the model. Because the labelling and de-labelling periods of these studies are relatively short compared to the timescales I am considering (of the order of days or weeks as opposed to months or years) I cannot use these data to infer turnover rates for each of the three (frequent/intermediate/rare activation) populations separately. Instead, I choose parameters for my model such that the three populations as a whole have average turnover rates that match those seen in stable isotope labelling data. By assuming that the system is in steady state prior to infection I am able to apply parameter estimates from the healthy patients in the modelling study by Ribeiro et al [96] directly to my model and also use it to inform the initial relative abundances of the frequent/intermediate/rare activation populations. Table 4.4 provides more details on how this was done.

Values for the parameters relating to the dynamics of infection and the decay of latently infected cells were taken from previous studies of viral dynamics in the literature, as detailed in Table 4.4.

Figure 4.3 shows the simulated dynamics of the latently infected populations in the model during untreated primary and chronic infection, treated primary infection and treated chronic infection. The values corresponding to L_2 and L_3 at viral suppression in primary- and chronic-treated patients, as estimated from the Hocqueloux data, are also plotted for comparison (blue and black circles and crosses). In the top panel, comparing the dark red line (L_3, rarely activated population) with the crosses, and the violet line (L_2, intermediate activation population) with the circles we see that the model was able to reproduce the main features of the Hocqueloux data well. In both the model and the data the slow-turnover (rarely activated) population is much smaller in primary infection

Table 4.4: Parameter values and their source

Parameter	Description	Value or calculation	Reasoning
ρ	The rate at which activated cells revert to a resting state	0.026 day^{-1}	In [96] this is estimated as 0.026 ± 0.018 in healthy controls
d_R	Death rate of resting cells	0.001 day^{-1}	[96] states that "preliminary data fitting showed that the value of d_R was very small in all cases, of the order of 10^{-3}"
α_1, α_3 $(= b_1, b_3)$	Activation rates of fast and slow pool	0.1, 0.00005 day^{-1} resp	α_1 chosen so that cells in the fast-turnover population are activated once every ten days on average. α_3 chosen subject to the following constraints (1) $\alpha_3 + d_L = 0.0001$, to match the decay rate of the slow-turnover population fitted to the Hocqueloux data. (2) $\alpha_3 > 0.00001$, since this corresponds to a cell being activated less than once every 200 years on average, which is very low
α_2 $(= b_2)$	Activation rate of medium pool	Varies	Fit using decay data in [262]. $\alpha_2 + d_L = b_2$.
$T_i(0)$	Initial values for numbers of activated cells in each class. $T_1(0) : T_2(0) : T_3(0)$ determines the activation rate distribution of the CD4$^+$ T-cell pool as a whole	The $T_i(0)$ values are determined according to the constraint: $\frac{T_1(0)}{\alpha_1} + \frac{T_2(0)}{\alpha_2} + \frac{T_3(0)}{\alpha_3} = \frac{T}{0.002}$. $\frac{T_1(0)}{T_2(0)} = 10, 0.5, 3$ in Figures 4.3, 4.6, 4.7 respectively. The total size, $T = \sum T_i(0)$, is scaled so that $L_2(50) + L_3(50) + L_2(1850) + L_3(1850) = A_2(\text{PHI}) + A_3(\text{PHI}) + A_2(\text{CHI}) + A_3(\text{CHI})$.	The constraint ensures that the average activation rate is 0.002, as estimated in [96]. $\frac{T_1(0)}{T_2(0)}$ is chosen based on initial runs of the model so that the results best fit the Hocqueloux data. The scaling of T also ensures that the model best fits the data, so that patterns of growth and decay can be easily compared
$R_i(0)$	Initial values for numbers of resting cells in each class	$R_i(0) = \frac{\rho}{b_i} T_i(0)$	Prior to infection the system is at equilibrium
B_i	Inflow of resting cells per day	$d_R R_i(0)$	Prior to infection the system is at equilibrium
λ_j	Force of infection during acute (λ_1) and chronic (λ_2) infection	$\lambda_1 = 0.1$, $\lambda_2 = 0.01$ day^{-1}	From the work in Appendix 0.1 I consider any λ_2 in the range 0.0005-0.01 reasonable. I also estimated that λ_1 is a little over 10 times λ_2
f	Fraction of new infections that become latent	0.0001	Since we are not concerned with absolute numbers but rather relative patterns of growth and decay, the value of f is inconsequential
d_L	Activation-independent decay rate of latently infected cells	0.00005 day^{-1} (Figs. 4.3 & 4.9), 0.0001 day^{-1} (Fig. 4.6)	As described for α_3, the decay rate of the slow-turnover population should be 0.0001, to match the Hocqueloux data

than it is in chronic infection (model: 7.9 fold change, data: 8.3 fold change) whereas the medium-turnover population is more similar is size between the two time points (model: 2.0 fold change, data: 1.1 fold change). As shown in the bottom two panels, these small discrepancies result in similar but not identical patterns of decay of $L_2 + L_3$ on ART seen in the model (grey lines) and in the curves that were fitted to the data (blue and black lines). Since the fold difference in the L_i populations between acute and chronic infection determines the potential benefit of early treatment, I wished to gain a greater understanding of which parameters affect the patterns of growth of L_i. In particular, which aspects of the model are necessary to get a large increase in the size of the slow-turnover population between primary and chronic infection?

In order to answer these questions, which involve exploring a large parameter space, I turned to analytics. The questions relate to the relative difference in the size of the latently infection populations between primary and chronic infection, i.e. $L_i(t = 5\text{yrs})/L_i(t = 50\text{d})$. Since the model is a linear model we may solve the ODEs and write down an explicit expression for this ratio in terms of the model parameters. Having done this I seek to describe which parameters have the greatest effect on $L_i(5\text{yrs})/L_i(50\text{d})$ and understand why. I also wished to know what the range of $L_i(5\text{yrs})$ vs $L_i(50\text{d})$ could be, within the space of realistic parameters for my model.

Full workings for solving the set of ODEs for R, T, L are given in the appendix. In brief, when $t < 50\text{d}$ $(j = 1)$ we find

$$L = \lambda_1 \left(\frac{\nu_{12}}{\mu_1 + d_L + \alpha} e^{\mu_1 t} + \frac{\nu_{22}}{\mu_2 + d_L + \alpha} e^{\mu_2 t} + \frac{Bb}{(d_L + \alpha)((d_R + b)(\rho + \lambda_1) - \rho b)} \right) + c_L e^{-(d_L + \alpha)t}$$

where μ_1, μ_2 are the solutions to the quadratic

$$\mu^2 + (d_R + b + \rho + \lambda_1)\mu + b\lambda_1 + d_R(\rho + \lambda_1) = 0$$

and ν_{12}, ν_{22}, c_L are determined by the initial conditions as follows:

$$\nu_{12} + \nu_{22} + \frac{Bb}{(d_R + b)(\rho + \lambda_1) - \rho b} = T_0$$

$$\frac{\rho}{d_R + b + \mu_1}\nu_{12} + \frac{\rho}{d_R + b + \mu_2}\nu_{22} + \frac{B(\rho + \lambda_1)}{(d_R + b)(\rho + \lambda_1) - \rho b} = R_0.$$

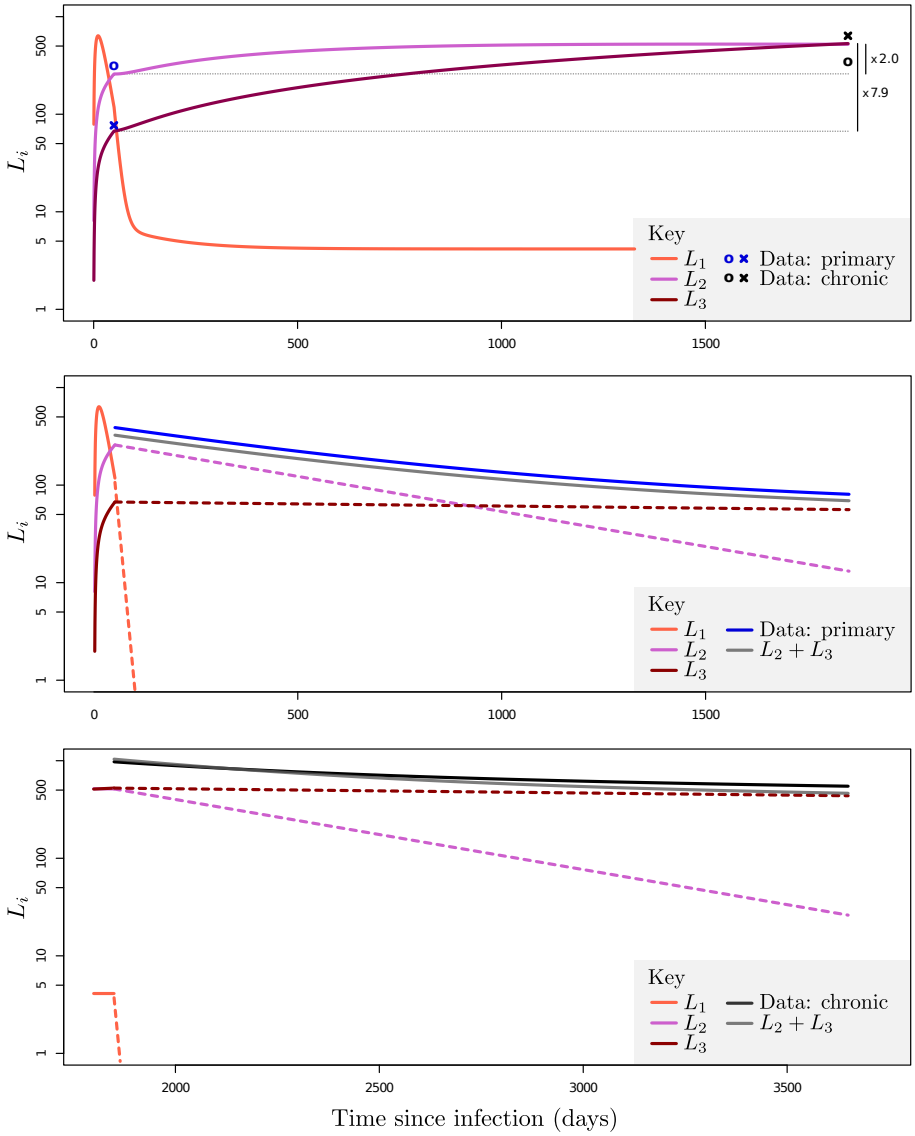


Figure 4.3: Could early-ART be beneficial because it restricts the size of the slow-decaying latently infected pool? Top panel: The simulated patterns of growth of the separate portions of the reservoir during untreated infection are compared with the sizes of the medium- and slow-decaying pools as estimated from the Hoqueloux data. For the model output, L_1 is shown in light red, L_2 in violet and L_3 in dark red. The estimated sizes of the medium-turnover population (same decay rate as L_2) and slow-turnover population (same decay rate as L_3), in primary and chronic infection, are shown by the circles and crosses, as in Figure 4.1. The fold-increase in L_2 and L_3 between primary and chronic infection is indicated on the right hand side of the graph. Middle panel: Resulting patterns of decay in the latently infected HIV reservoir when ART is initiated in primary infection. In the model simulation ART is initiated at 50 days, at the end of acute infection. The simulated decay of L_1, L_2 and L_3 is shown by the corresponding dotted lines (colours as in top panel). The decay of $L_2 + L_3$ under the model is shown in grey for comparison with the decay curve as fitted to the primary patients in the Hocqueloux data, shown in blue. Note that L_1 is not included when comparing with the data because the data starts from the point at which the patients suppress viral load < 50 copies/ml, by which point L_1 would have significantly decayed. Bottom panel: As for middle panel but with ART initiated in chronic infection (1850 days $\approx$ 5 years in model). The decay curve fitted to the chronic patients in the Hocqueloux data is shown in black. Parameters used for the model simulation are given in Table 4.4.

$$c_L = 0 - \lambda_1 \left(\frac{\nu_{12}}{(\mu_1 + d_L + \alpha)} + \frac{\nu_{22}}{(\mu_2 + d_L + \alpha)} + \frac{Bb}{(d_L + \alpha)((d_R + b)(\rho + \lambda_1) - \rho b)} \right)$$

When $t > 50$d ($j = 2$) we may write $\tau = t - 50$ and find

$$L = \lambda_2 \left(\frac{\nu_{12}}{\mu_1 + d_L + \alpha} e^{\mu_1 \tau} + \frac{\nu_{22}}{\mu_2 + d_L + \alpha} e^{\mu_2 \tau} + \frac{Bb}{(d_L + \alpha)((d_R + b)(\rho + \lambda_2) - \rho b)} \right) + c_L e^{-(d_L + \alpha)\tau}$$

where μ_1, μ_2 are the solutions to the quadratic

$$\mu^2 + (d_R + b + \rho + \lambda_2)\mu + b\lambda_2 + d_R(\rho + \lambda_2) = 0$$

and ν_{12}, ν_{22}, c_L are now determined according to

$$\nu_{12} + \nu_{22} + \frac{Bb}{(d_R + b)(\rho + \lambda_2) - \rho b} = T(\lambda_1, 50)$$

$$\frac{\rho}{d_R + b + \mu_1}\nu_{12} + \frac{\rho}{d_R + b + \mu_2}\nu_{22} + \frac{B(\rho + \lambda_2)}{(d_R + b)(\rho + \lambda_2) - \rho b} = R(\lambda_1, 50),$$

$$c_L = L(\lambda_1, 50) - \lambda_2 \left(\frac{\nu_{12}}{(\mu_1 + d_L + \alpha)} + \frac{\nu_{22}}{(\mu_2 + d_L + \alpha)} + \frac{Bb}{(d_L + \alpha)((d_R + b)(\rho + \lambda_2) - \rho b)} \right)$$

These expressions are too complicated to gain understanding from their form alone, even after attempts to simplify them using approximations. In order to study the effect of each of the parameters on $L_i(5\text{yrs})/L_i(50\text{d})$ I plot it against each of the parameters in turn. I wish to do this for several values of α (not restricted to those used in Figure 4.3) and so I denote the ratio as $L_\alpha(5\text{yrs})/L_\alpha(50\text{d})$.

The graphs in Figure 4.4 show how $L_\alpha(5\text{yrs})/L_\alpha(50\text{d})$ varies with ρ, d_R, $d_L + \alpha$ (the decay rate of L_α) and λ_1 (given fixed λ_2 and where $\lambda_2 = \lambda_1/10$). In each case several values of α are used ($\alpha = 0.1, 0.01, 0.001, 0.0001, 0.00001$). Recall that since I have set $b = \alpha$, different values of α also correspond to different values of b. The plots show that the value of α has a large effect on the patterns of growth of the latently infected populations. For the more rarely activated populations ($\alpha \leq 0.001$, blue-purple lines), $L_\alpha(5\text{yrs}) < L_\alpha(50\text{d})$, whereas for the frequently activated populations ($\alpha > 0.01$, turquoise-green lines), $L_\alpha(5\text{yrs}) > L_\alpha(50\text{d})$, i.e. the reservoir in this subpopulation of T-cells peaks in acute infection and is then smaller in chronic infection. Linked to this, the decay rate of L_α has a large influence on the patterns of growth of L_α during untreated infection. Figure

4.4C shows that both $d_L + \alpha$ must be small and b must be small in order to get a greater than 5 fold increase in L_α from acute to chronic infection. In other words, it is the low rate at which cells become susceptible to infection combined with the slow turnover of that latently infected population that results in the slow accumulation of latently infected cells within the rarely activated population. As an aside, note that in separating the effect of the decay rate, $d_L + \alpha$, from the activation rate of uninfected cells, b, Figure 4.4C enables us to infer the behaviour of a model in which the rates of activation and reactivation are not assumed to be equal.

Focussing solely on the more rarely activated populations ($\alpha \leq 0.001$, since these are the ones that persist on ART), we see that $L_\alpha(5\text{yrs})/L_\alpha(50\text{d})$ is not particularly sensitive to changes in ρ or d_R (Figure 4.4A, B resp.). The force of infection, λ_j, has a larger effect on $L_\alpha(5\text{yrs})/L_\alpha(50\text{d})$ (Figure 4.4D). The left hand plot shows that the higher λ_1 is compared to λ_2, the greater the proportion of latent infections occurring in acute infection and hence the lower $L_\alpha(5\text{yrs})/L_\alpha(50\text{d})$ is. Also, still considering only low α, when λ_1/λ_2 is fixed (right hand plot), the higher the value of λ_j the greater $L_\alpha(5\text{yrs})/L_\alpha(50\text{d})$ is. This is because when λ_j is high, an activated cell is very likely to become infected before it returns to a resting state again. The low value of b ($= \alpha$) means cells rarely become susceptible and so limits the rate at which infection can spread through the T-cell pool, but the higher value of λ_2 means that latent infection stabilises at higher levels in chronic infection.

The plots also suggest that it is only by making the force of infection in acute and chronic infection larger or more similar that we can simulate populations in which $L_\alpha(5\text{yrs})/L_\alpha(50\text{d})$ is 10 or greater. Otherwise, the maximum difference in the size of of L_α between primary and chronic infection is approximately 8-9 fold, and this is only attainable for $\alpha \leq 0.0001$. With further thought, this makes intuitive sense. Even when the force of infection is no higher in acute than chronic infection the growth of L will be faster initially and then level off later on. For very small $\alpha + d_L$ the growth may approximate a linear curve and hence $L(50\text{d})$ could be at most $\approx 1/40$ of the size of $L(5\text{yrs})$ (5 yrs $\approx 40 \times 50$ days). However when $\lambda_1 = 10\lambda_2$ and λ_j is low, the growth would be approximately 10 times faster in acute infection than at the start of chronic infection and so we would expect the maximum difference in $L(50\text{d})$ and $L(5\text{yrs})$ to be around 4-fold. When λ_j is high, the five times higher value of λ_j in acute infection may only accelerate the growth of L during

that phase by more like 4-fold and hence the maximum difference in $L(50\text{d})$ and $L(5\text{yrs})$ is around 10-fold.

In conclusion, only rarely activated (low b) slow turnover (low $d_L + \alpha$) populations of latently infected cells accumulate significantly between acute and chronic infection. The force of infection also influences the patterns of growth of the latently infected populations. Assuming λ_j is within what I consider to be a reasonable range (see Appendix B), the potential benefit of early treatment predicted by the model is that it could limit the size of the slow turnover latently infected population by approximately one order of magnitude compared to treating in chronic infection.

4.2.2 Accounting for replication incompetent provirus

Up to this point I have been making the assumption that the HIV DNA measured in the Hocqueloux data is all replication competent. This assumption is not problematic so long as (1) the dynamics of cells with replication incompetent provirus match those of cells with replication competent provirus, and (2) the proportion of replication competent infections is independent of the activation-class (it is the same for all i). However there is good reason to believe that the first statement may not be true. Cells latently infected with replication competent, as opposed to incompetent, provirus are by definition more likely to produce viral proteins upon re-activation and hence die as a result of the viral cytopathic effect or the action of the immune response. Therefore, I adapted my model to include the generation of replication incompetent latent infections, in order to study whether with this additional complexity a new model would remain consistent with the the Hocqueloux data.

In the new model (Figure 4.5), a constant fraction, f_{RI}, of all new infections are replication incompetent. I study the simple case in which the decay rate of replication incompetent latent infections is unrelated to the re-activation rate and hence equal to d_L. The model equations are as follows:

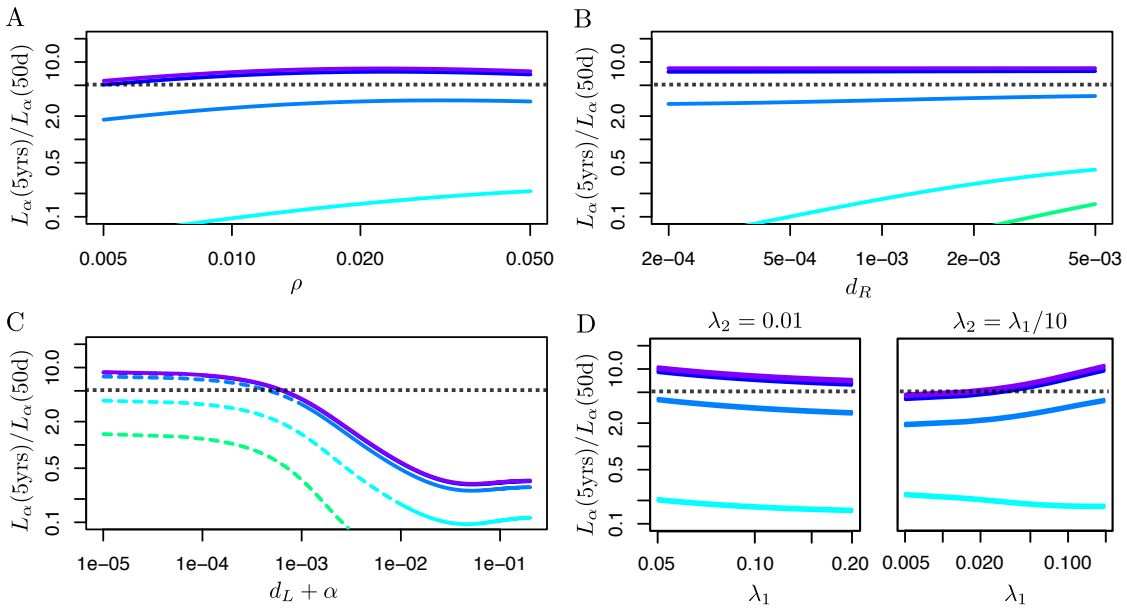


Figure 4.4: How does the fold change in L_α between acute and chronic infection depend on the model parameters? In each case $L_\alpha(t = 1850)/L_\alpha(t = 50)$ is plotted (1850d $\approx$ 5 yrs) for several values of α: $\alpha = 0.00001$(purple), 0.0001 (dark blue), 0.001 (mid blue), 0.01 (turquoise), 0.1 (green). Note that because we are largely interested in the upper end of the y-axis scale, the green line is not within the range of the axis in some plots. The dotted black line on each plot indicates a 5-fold difference between L_α(50d) and L_α(5yrs). Ranges for parameter values were chosen as follows (see also Table 4.4). (A) ρ is varied from 0.005 to 0.05. This range includes the estimate $\pm$ standard error found in [96]. (B) d_R is varied from 0.0002 to 0.005 since estimates for d_R are of the order of 10^{-3}. (C) $d_L + \alpha$ is varied from 0.00001 to 0.5 to include the full range for α used in the model. Where $d_L + \alpha < b$ (i.e. $d_L + \alpha < \alpha$) the curve is plotted with a dotted line – these values are useful for inferring how the model would behave if I had set activation and re-activation rates as proportional instead of equal. (D) Left hand plot: λ_1 is varied from $5\lambda_2$ to $20\lambda_2$, so the the force of infection in acute infection is between 5 and 20 times higher than that in chronic infection. Right hand plot: λ_1 is varied from 0.005 to 0.2 so that λ_2 ranges from 0.0005 to 0.02. This incorporates the reasonable range of λ_j, as found in the appendix. In all plots, when parameters are not being varied they are set as in Figure 4.3 and Table 4.4.

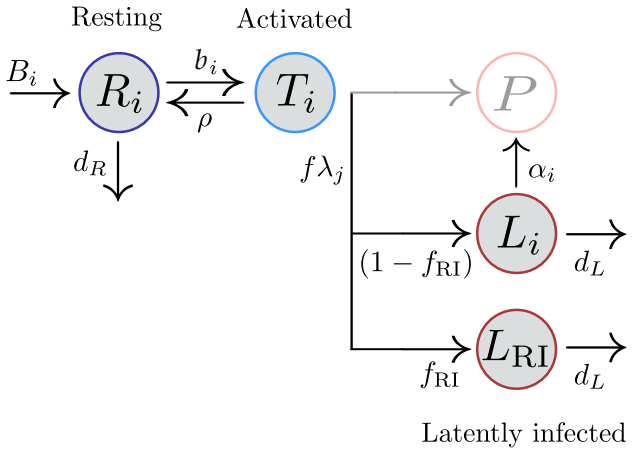


Figure 4.5: An extended model with replication incompetent latent infections The model is identical to that in Figure 4.2 except that only a fraction, $(1 - f_{\mathrm{RI}})$, of new latent infections are replication competent with the remainder being replication incompetent. Replication incompetent latently infected cells, L_{RI}, decay at rate d_L, i.e. they have no net decay related to re-activation.

$$\begin{aligned}
\frac{dR_i}{dt} &= B_i - (d_R + b_i)R_i + \rho T_i \\
\frac{dT_i}{dt} &= b_i R_i - (\rho + \lambda_j)T_i \\
\frac{dL_i}{dt} &= (1 - f_{\mathrm{RI}})f\lambda_j T_i - d_L L_i - \alpha_i L_i \\
\frac{dL_{\mathrm{RI}}}{dt} &= f_{\mathrm{RI}} f\lambda_j \sum_i T_i - d_L L_{\mathrm{RI}}
\end{aligned}$$

The slow-turnover portion of latently infected cells now includes both those cells which are infrequently activated (L_3) and those cells infected with replication incompetent provirus (L_{RI}). The medium-turnover population is L_2, as before. Figure 4.6 compares the behaviour of $L_3 + L_{\mathrm{RI}}$ and L_2 with the estimated dynamics of the slow- and medium-turnover populations in primary- and chronic- treated patients in the Hocqueloux data. It shows that, similarly to the previous model, the model with replication incompetent provirus reproduces the much greater increase of the slow-turnover population during untreated infection (compared to the medium-turnover population). Comparing the brown line ($L_3 + L_{\mathrm{RI}}$) in the top panel of Figure 4.6 with the violet line (L_2) we see that the slow-turnover population increases by 6.5-fold while the medium-turnover population increases by 2.6-fold.

This model does not fit the data as well as the original model – the difference in the

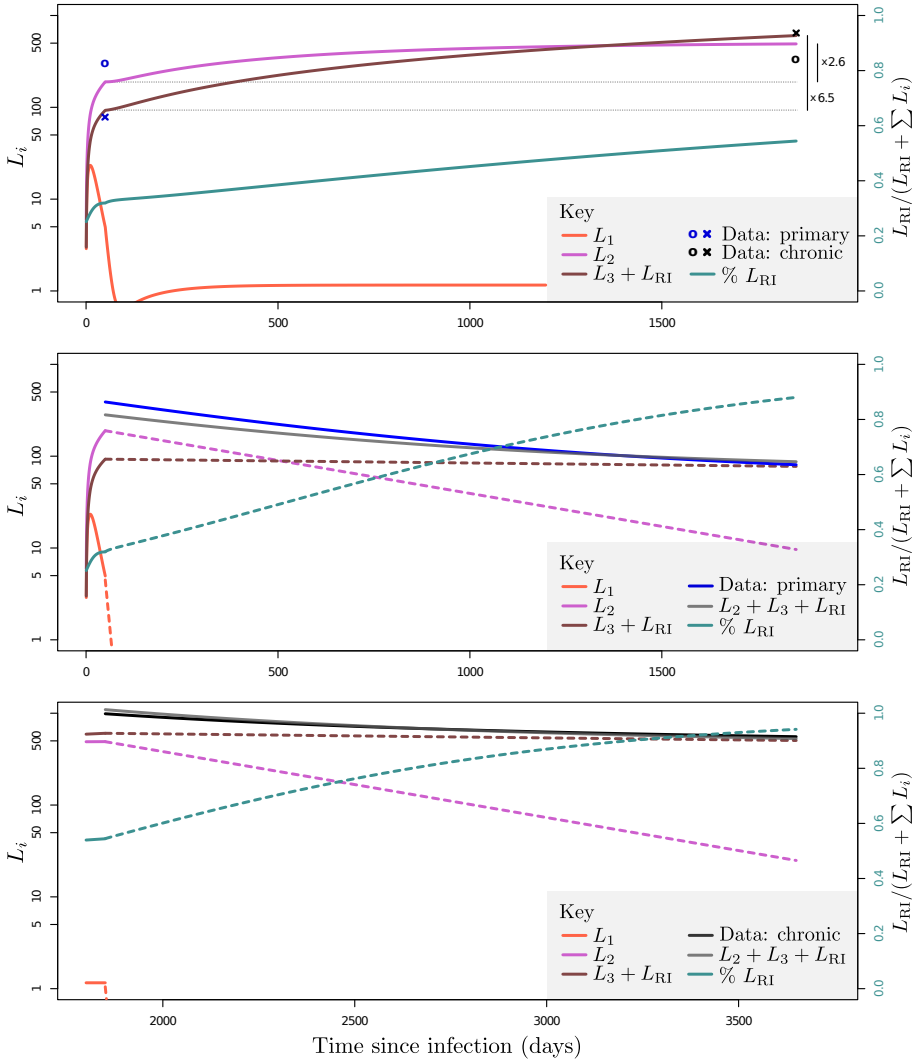


Figure 4.6: Can a model accounting for replication incompetent infections still explain the Hocqueloux data? In all three panels, the blue and black crosses and lines show the patterns observed in the Hocqueloux data, identically to in Figure 4.3. The proportion of replication competent latent infections predicted by the model is shown in turquoise, with reference to the right hand axes. Top panel: The simulated patterns of growth of the separate portions of the reservoir during untreated infection. L_1 is shown in light red, L_2 in violet and $L_3 + L_{RI}$ in brown. The fold-increase in L_2 and $L_3 + L_{RI}$ between primary and chronic infection is indicated on the right hand side of the graph. Middle panel: ART initiated in primary infection (= 50 days in the model). The simulated decay of L_1, L_2 and $L_3 + L_{RI}$ is shown by the corresponding dotted lines (colours as in top panel). The decay of $L_2 + L_3 + L_{RI}$ under the model is shown in grey for comparison with the decay curve as fitted to the primary patients in the Hocqueloux data, shown in blue. Bottom panel: ART initiated in chronic infection (= 1850 days in the model). The decay of $L_2 + L_3 + L_{RI}$ under the model is again shown in grey for comparison with the decay curve as fitted to the chronic patients in the Hocqueloux data, shown in black. Parameters used for the model simulation are given in Table 4.4. Additionally, $f_{RI} = 0.25$. Note that for $L_3 + L_{RI}$ to be smaller than L_2 in primary infection (as seen in the data), the initial size of T_3 must be much lower than that of T_2. Hence, the activation rate distribution used in this run of the model is different to that in Figure 4.3, where the initial size of T_3 was much more similar to that of T_2.

dynamics of the medium- and slow- turnover populations is not stark enough – but recall that I have considered the extreme case where there is no activation-related decay of the replication incompetent population.

The value of f_{RI} used is 0.25. This may seem low given that an average of more than 80% of proviruses have been found to be defective, measured in patients who had been on suppressive ART for > 6 months [219]. However, note that the proportion of replication incompetent latent infections only remains low during primary infection and has increased to around 90% after 5 years of ART in primary- and chronic-treated patients (turquoise line, Figure 4.6). The longer half-life of the replication incompetent infected cells means that they accumulate to greater levels than their replication competent counterparts. Consequently the model predicts that the proportion of replication incompetent latent infections increases during untreated infection and increases even faster once the patient initiates ART.

These positive results raise the following question: *could the Hoqueloux data be compatible with a model which includes replication incompetent virus (and replication competent virus) but only one, universal activation rate*? In short, it could, but it does not fit with the observations on correlates of time to rebound. In such a model the replication competent fraction would constitute the medium-turnover population and would behave as L_2 does in Figure 4.6. The behaviour of the replication incompetent fraction, which would constitute the slow-turnover population, can be inferred from the bottom left hand plot in Figure 4.4. This population would have an activation rate of ≈ 0.002, closer to that of the medium-blue line than the turquoise line, and a decay rate (denoted $d_L + \alpha$ in this plot) of 10^{-4}. Hence the rise in the slow turnover population between primary and chronic infection would still be around 6-7 fold. However, under this model the true 'reservoir' – the replication competent fraction – decays very noticeably during ART since a decay rate of 0.002 corresponds to a half-life of approximately one year. Hence, under this model I would expect the duration of ART to be one of the strongest factors influencing time to rebound after ART-cessation, while ART initiation time or PCR-based measures of reservoir size would be weakly correlated, if at all. This is not what is seen in the data (see Data review on factors influencing post-treatment control and Tables 4.1 & 4.2 - in Table 4.1 only one of the four studies looking at the relationship between ART duration

and rebound time found a significant correlation).

4.2.3 Is this mechanism compatible with the Brodin data?

Recent unpublished data that used proviral sequences to determine the time at which the cells in the reservoir were infected estimated the turnover of the reservoir pre-treatment to have a half life of the order of one year. This study by Brodin et al. was done in patients who were treated in chronic infection and had been on ART for more than three years. I wished to know whether the mechanistic explanation for the Hocqueloux data encapsulated by my model could also explain the Brodin data.

Figure 4.7 plots the distribution of times at which the cells in the model-simulated latently infected reservoir were laid down – akin to an 'age-distribution' for cells in the reservoir. Each solid line corresponds to the reservoir at a different time point during ART. The dotted line represents the distribution as estimated from the Brodin data, calculated assuming a homogeneous latently infected pool with a half-life of one year pre-ART. These distributions are plotted for both the original model (A) and the model with replication-incompetent infections (B), assuming that a patient initiates ART after five years of infection. At all time points, from ART initiation to 10 years following, the cells in the model-simulated reservoir are on average much older than seen in the Brodin data. This is particularly true for later time points. In the model, viruses from acute infection are over-represented in the reservoir and then there is little difference in the proportion of reservoir cells that were laid down early in chronic infection vs immediately prior to ART initiation.

The source of the discrepancy is that in my model the turnover *prior to ART* of the 'reservoir' cells is low compared to in the Brodin data. Therefore I wondered whether adjusting my model so that activation rates are higher in untreated infection than on ART (see Figure 4.8) would produce reservoir age-distributions that are consistent with the Brodin data. There is experimental data to support this adjustment: levels of immune activation are higher in viraemic patients than in those that are suppressing the virus on ART, as seen in stable isotope labelling studies of T-cell turnover [96]. We see in Figure 4.7C that if I allow the activation rates to vary in this way then I can closely reproduce the age-distribution seen in the Brodin data. However, the output of this simulation fits

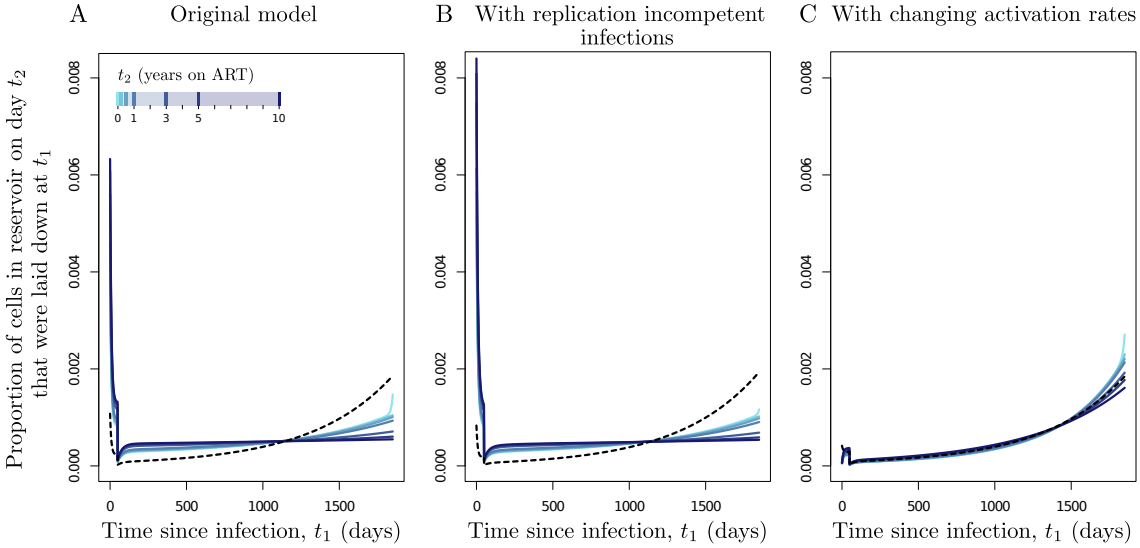


Figure 4.7: Simulated age-distributions of cells in the reservoir, compared with that of the Brodin data. The reservoir in patients who initiated ART in chronic infection is sampled at several different time points during ART (t_2 = 0, 3, 6 months, 1, 3, 5, 10 years; darker blue for later time points). For each one, the distribution of when (prior to ART) the cells were infected and became latent is plotted, with time since infection, t_1 along the x-axis. This distribution is the normalised value of $\lambda_j \sum_i T_i e^{-(\alpha_i+d_L)(1850-t_1+t_2)}$. The black dotted line shows a representation of the Brodin data – the distribution that would be expected if the cells in the reservoir had a half-life of one year prior to ART (equivalent to a decay rate of 0.0019). This is the normalised value of $\lambda_j T_2 e^{-0.0019(1850-t_1+t_2)}$. The higher force of infection in acute infection results in a peak early on for all distributions (A) Simulations using my original model. (B) Simulations using the model with replication incompetent infections. In both (A) and (B), the distributions predicted by the model are older on average than in the Brodin data. (C) Simulations in which the activation rates vary between untreated and treated infection, as in Figure 4.8.

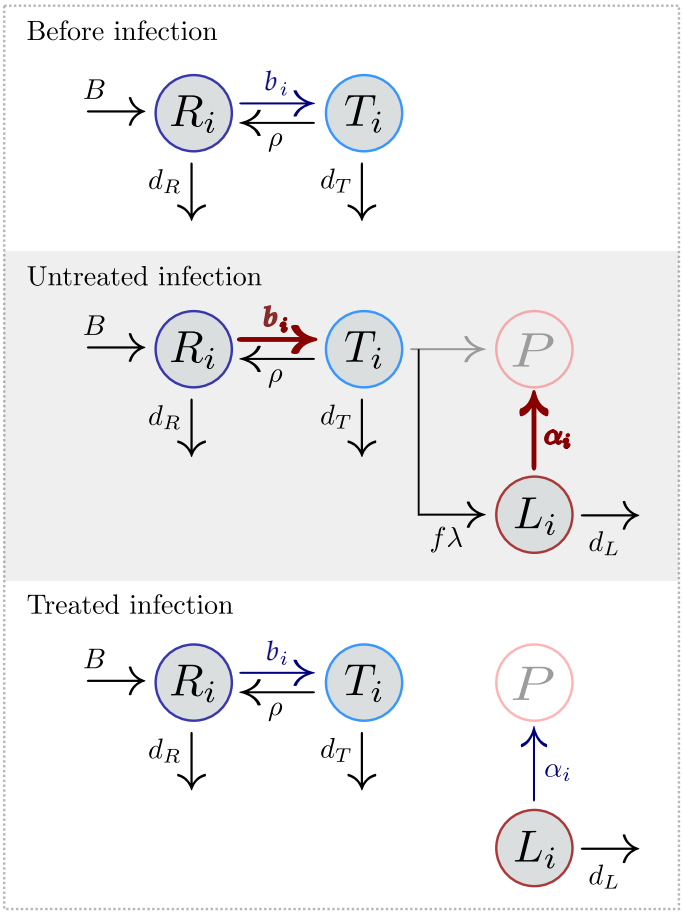


Figure 4.8: A model with changing activation rates. This third version of the model, is identical to the original model but with elevated activation rates during untreated infection (indicated by red arrows). This reflects the increase in immune activation that is seen in HIV-infected patients, which decreases towards the level seen in healthy patients once suppressive ART has been initiated. The rates used for the simulations are $b_1 = \alpha_1 = 0.08, b_2 = \alpha_2 = 0.003, b_3 = \alpha_3 = 0.0015$ in untreated infection (chosen to fit the Brodin data) and $b_1 = \alpha_1 = 0.02, b_2 = \alpha_2 = 0.001, b_3 = \alpha_3 = 0.00005$ (chosen to fit patterns of decelerating decay seen in the Hocquloux data).

the Hoqueloux data less well – in particular, there is only a 3.8-fold rise in the size of the slow-decaying population between primary and chronic infection because the turnover of this population is relatively fast (see Figure 4.9).

In fact, under the mechanism encapsulated by my model, the Hocqueloux data and Brodin data are fundamentally difficult to reconcile. Assuming that the reservoir contains slow- and medium-turnover populations of cells which differ in terms of their activation rates leads to the following observations: The reservoir in chronic treated patients after three years of ART will consist largely of slowly decaying latently infected cells (see Figure 4.1A and note the difference of one $\log_{10}$ between the two black dotted lines after three

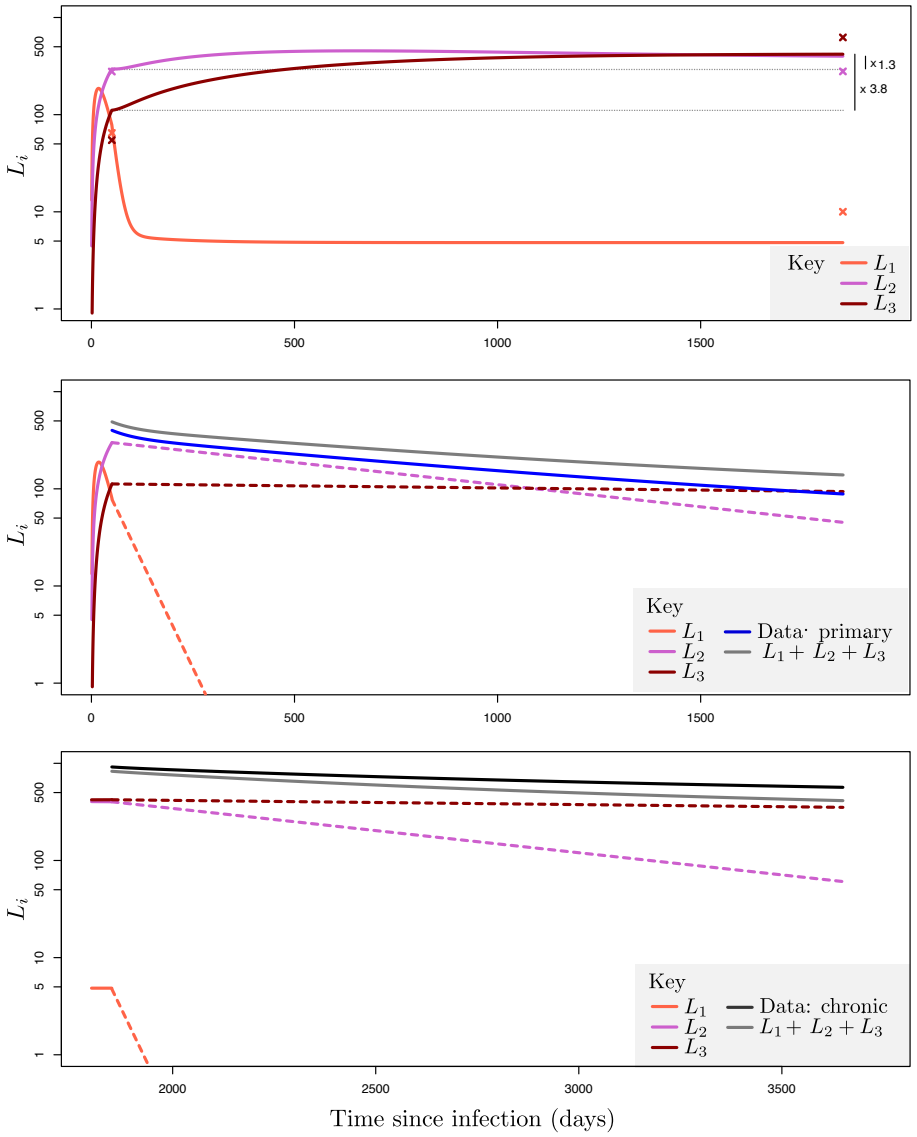


Figure 4.9: The model with changing activation rates does not reproduce the slow rise in the slow-decaying pool. Simulations of the model with changing activation rates are shown by the light red, violet and dark red lines, with colours as in Figure 4.3. Top panel: untreated infection. Middle panel: ART initiated at 50 days. Bottom panel: ART initiated at 1850 days ($\approx$ 5 years). The activation rates in untreated infection are higher than before infection or during ART, as described in Figure 4.8. The remaining parameters are as described in Table 4.4. Note that because L_1 now decays slower during ART than in previous models, a tri-exponential decay curve is fitted to the Hocqueloux data. In order for the non-linear model fitting routine to converge it was necessary to fix the decay rates ($d_L + \alpha_i$) and also fix L_1(chronic)/L_1(primary). The fit gives estimated values for L_1, L_2, and L_3 in primary and chronic infection, shown by the crosses in the top panel. The fitted curves for primary- and chronic-treated patients are shown by the blue and black lines in the middle and bottom panels respectively.

years). The Hocqueloux data shows an $\approx$ 8-fold rise in the size of the slowly decaying population between primary and chronic infection. My analytic work demonstrated that a fold-increase of this size requires the pool to have a low decay rate ($d_L + \alpha$) *prior to ART*, in other words a low rate of turnover (rate of decay equates to turnover in chronic infection when all populations are relatively stable). Note from the bottom right plot in Figure 4.4 that when the decay rate is 0.001 (medium blue line), then even raising λ_j to the top of the reasonable range only results in a 5-fold increase in L_α between primary and chronic infection. Hence 'low' here means less than 0.001. The half-life of less than one year estimated from the Brodin data equates to a turnover rate prior to ART that is higher than this (> 0.0019). Consequently I cannot reproduce both the substantial increase in the slow-decaying pool between primary and chronic infection and the relatively fast turnover of the same pool prior to ART.

4.3 Discussion

Understanding the persistence of the latently infected HIV reservoir will be essential for advancing towards a cure for HIV. This present study is the first that I am aware of to seek a formal mechanistic explanation for observations relating the timing of ART initiation and the long-term effects of treatment on the reservoir. Given the multiple possible explanations for why early ART results in prolonged control, a natural question might be "why have I started with this hypothesis relating to activation rates?". Firstly, note that the most basic model of latent reservoir dynamics (as presented in [306]) does not fit well with patterns of HIV DNA decay seen on ART [229, 267] (see also Appendix B, section B.3). Since we prefer simple models, a sensible way to begin searching for models that do fit the collection of available data is by removing the assumptions in the basic model one at a time. I chose to remove the assumption of homogeneity in the dynamics of the latent pool because it has previously been shown that incorporating so-called 'kinetic heterogeneity' can reproduce decelerating decay of latently infected cells [229]. More generally, it seems likely that latently infected cells do have a range of propensities for activation, and others have suggested this could be an important aspect of reservoir dynamics [229, 320]. This starting point also makes sense when viewed from perspective of wanting to better predict

time to viral rebound: we know that measures of reservoir size are significant but not adequate predictors of time to rebound [22, 23, 288, 311] – considering aspects of reservoir 'quality' might help us do better.

Using my model I have been able to show that rarely activated populations of latently infected cells would be expected to accumulate more slowly in the reservoir (compared to frequently-activated populations) and also decay more slowly on ART. Hence while there may be only a small change in the total size of the reservoir between primary and chronic infection, there could be much greater growth in the size of the most persistent portion of the reservoir. These dynamics fit the patterns of HIV DNA decay seen in the Hoqueloux data well [262]. They are also consistent with other studies which have found evidence that more recently infected cells decay at a faster rate [320].

My model results may help to explain why the beneficial effects of early, long-duration ART have not been clearly seen in all studies. Firstly, as I have stated, early ART most restricts the laying down of the rarely-activated cells. Consequently, the beneficial effects of early ART initiation would be most clearly seen when all patients have been on ART for a few years or more, by which point only the rarely-activated population remains. It is difficult to discern whether such a pattern exists in the data summarised in Tables 4.1 & 4.2 since not all studies correct for varying duration of ART. Secondly, since the decay of the reservoir is decelerating, the effect of ART duration is most obvious in the first few years, while the difference between those treated for 4 vs 10 years, for example, may be negligible. This could explain why the only study in Table 4.1 to find a significant association between ART duration and time to rebound involved the shortest treatment period (12 weeks versus 48 weeks, [289]). Large inter-patient variability may also mean that studies with smaller numbers of patients are not powered to detect even the larger effects predicted by my model.

The model-predicted combined effect of ART initiation time and duration is summarised in the Figures in Appendix B.4. A particularly striking implication of these model simulations is that preventing the laying down of the reservoir involves treating very early. More precisely, all three latently infected populations in my model grow very rapidly at the start of infection and even the slow-decaying population is more than 1/50th of its eventual size in chronic infection after just a few days (Figure 4.3, top panel). This

is in agreement with studies in rhesus monkeys which found that the reservoir was seeded within 3 days of mucosal SIV infection [255], and with early studies in humans [203].

My analysis showed that the rarely-activated portion of the latent reservoir must be turning over very slowly *prior to ART* in order to see a large increase in its size between primary and chronic infection. The low rates of turnover needed are reasonable when we consider that they are aggregates of proliferation and death. However, they mean that my model hypothesis is not compatible with the Brodin data, which found a faster rate of turnover than this prior to ART. Is this conclusion (that a low turnover rate is required for the slow rise in the rarely-activated pool) dependent on the form of my model? Is there an alternative mechanistic explanation that would fit with all the available data?

Firstly: Is this conclusion dependent on the specific form of my model? In order to build a clear understanding of the dynamics of a heterogeneous latent reservoir I have kept the model as simple as possible. I have assumed linear rates of growth and decline for the T-cell populations, however, homeostatic proliferation is thought to be an important process contributing to the maintenance of the latent reservoir [225]. In Appendix B.5 I incorporate homeostatic proliferation into my model and show that it does not affect my conclusions. I also assumed 100% efficacy of ART and consequently the absence of ongoing replication. The presence of ongoing replication under combination ART is debated, but if present it is likely to occur within drug sanctuaries [20,351]. Adding compartments into my model would introduce many additional parameters for which the value is uncertain. Therefore, analysing the effect that ongoing replication would have on my model results is not within the scope of this study. Whilst I have investigated varying the activation rates between untreated and treated infection, I have not allowed any variation in activation during untreated infection. This is a limitation of my model, and future work could investigate the behaviour of a model in which activation is dependent upon the amount of virus present (i.e. upon the force of infection). However, allowing this variation would not affect the conclusion that a low turnover rate during chronic infection (which is when the Brodin patients initiated ART) is required for the slow rise in the rarely activated pool.

Secondly: Is there an alternative mechanistic explanation that would fit with all the available data? There are aspects of reservoir 'quality' that I have not yet considered. High levels of immune checkpoint markers, in particular exhaustion markers such as PD-

1, have recently been found to be positively associated with short waiting times to viral rebound [293] and with levels of integrated HIV DNA during ART [352]. Distinguishing between activated and exhausted cells in the model could contribute to the slow rise of the slow-decaying pool if exhausted cells increased steadily during infection and persisted for longer in the reservoir. I suggest this as an interesting avenue for further investigation.

Turning aside from aspects of reservoir quality, the strength of the T-cell mediated immune response may play a role in determining whether post-treatment control is possible [294, 346]. Further, the timing of ART initiation may have an effect on the strength of the response, either because very early ART prevents the evolution of immune escape mutations or because early ART preserves the numbers and function of HIV-specific T-cells [346, 353, 354]. However, the role of the immune response is debated [11, 347], and at present a lack of accurate data on *in vivo* strength is a barrier to using models to quantify the role of the immune response and parameterise a formal mechanism for its action [294].

In fitting models to data such as the Hocqueloux and Brodin data we must bear in mind that a large proportion of latently infected cells harbour replication incompetent virus and so are not part of the "true" HIV reservoir. Accounting for this is challenging because it is not clear how the dynamics of these cells would differ from those of cells infected with replication competent virus, and measures of the replication competent fraction of the reservoir vary [219]. I considered it reasonable to assume that replication incompetent latently infected cells would have a lower activation-related death rate than replication competent latently infected cells. This gave rise to a testable prediction: we would expect the proportion of cell-associated HIV DNA that is replication incompetent to increase during untreated infection, because those infected cells have a longer half-life, and for this increase to be even more pronounced once patients have started ART. A recent study found a slightly higher proportion of defective proviruses in chronic- vs. acute-treated patients (98% vs. 93%) [220]. Additional, longitudinal data would be needed to test the predictions of the model and assess what the simulated dynamics of replication incompetent infections should be. New assays are being developed for more precise quantitation of the "true" reservoir, however the availability of a precise assay that can be feasibly performed on large cohorts is still a way off [221, 355].

The limitations associated with the Brodin data include the small sample size and the

inherent difficulty of determining the source of variation in sequence haplotype abundance, as discussed by the authors [250]. Given these, I am not convinced that the discrepancy between my model and the turnover rates suggested by the Brodin data is severe enough to reject my hypothesised mechanism at the present time. However, if there were evidence to contradict either a greater proportion of rarely-activated cells being present in the reservoir in chronic vs primary infection or slower decay of the rarely-activated cells on ART then my hypothesis would clearly be wrong. Hence, the most straightforward way to test my hypothesis would be to collect longitudinal measures of the activation rate distribution of the reservoir in infected patients. In theory this could be done either directly or indirectly (through measuring the underlying intrinsic factors that cause cells to be classified as frequently- or rarely- activated), but in both cases further assay development is required. If my hypothesis is correct, then measuring the activation rate distribution prior to treatment interruption could be used to provide more accurate predictions of time to viral rebound or the probability of post-treatment control.

4.4 Questions addressed in this chapter

- Does a model with heterogeneity in activation rates fit the different patterns of HIV DNA decay seen in early vs late treated-patients?

  Yes, the model shows much slower growth (pre-ART) of the slow-decaying (on ART) latently infected population, fitting the data well (Figure 4.3; section 4.4.1).

- Does this mechanistic explanation for the data still hold when we account for a majority of the HIV DNA being replication incompetent, defective provirus?

  The adapted model fits the data moderately well. The pre-ART dynamics of the medium- vs. slow-turnover populations are not as starkly different in the model as in the data. However, it is unclear how the dynamics of replication incompetent infected cells and replication competent infected cells differ and so I am unable to give a complete answer to this question at this point. (Figure 4.6; section 4.4.2).

- Is the model compatible with the estimate of pre-ART turnover of latently infected cells derived from viral sequence data?

  No, the model with heterogeneity in activation rates cannot simultaneously explain the differing patterns of HIV DNA decay seen in early vs late treated-patients *and* the high rate of pre-ART turnover estimated from the Brodin data. (Figures 4.7 & 4.9; section 4.4.3). However, the robustness of the estimate given in the Brodin data is unclear.

5

Viral evolution

This work has been published in Journal of the Royal Society Interface (as detailed in section 1.2: *Contributions to this thesis*).

5.1 Introduction

During a typical HIV-1 infection, viral load rises sharply to a peak in the first few weeks, then decreases to the set point viral load (SPVL) and is relatively stable thereafter [87]. The end of this long period of chronic asymptomatic infection is marked by an increase in viral load and progression to AIDS [356]. The term 'virulence' relates to a microorganism's capacity to cause disease and so for HIV, virulence is defined as the rate of progression to AIDS [35, 357].

Time between seroconversion and progression to AIDS varies greatly between HIV-1 infected individuals. Some experience rapid CD4+ T-cell decline and develop AIDS within a few months or years whereas others remain AIDS-free for over 35 years [92, 93]. It is likely that the course of disease within an individual is determined by an interplay between host factors (including host genetics) and viral genetic factors [93, 190]. There is ongoing debate about how much of the variation in time to progression can be attributed to each set of factors but recently the nature of the role played by virus genetics has received particular attention [194, 358].

HIV-1 is a relatively recent infection of humans, having crossed over from non-human primates in the last century [24], and it is likely to still be adapting to its new host. As is often the case with host-parasite interactions, there are constraints upon the virulence

evolution of HIV. The level of SPVL is highly predictive of time to AIDS [186] but high SPVL is also linked to an increased risk of transmission during chronic infection [187]. The proportion of transmissions that occur during acute vs chronic infection likely varies between settings [180, 181] but, given revised estimates of infectivity during the acute phase, it seems reasonable to expect that the majority of transmissions occur during chronic infection (see [180] for a full discussion). Therefore, the evolutionarily optimal value of SPVL balances duration of infectiousness and transmission rate, a concept termed the 'trade-off hypothesis' [184]. The trade-off hypothesis has been applied previously to the specific problem of HIV virulence evolution, with SPVL used as a marker for virulence [25].

Whilst there has been much work looking at whether the virulence of HIV-1 might be changing [35], there has been less on the possible impact of anti-retroviral therapy (ART) on virulence evolution. Yet given the widespread use of ART and the striking reduction in infectiousness of ART-treated patients [359,360], there is clearly the potential for ART to have evolutionary consequences beyond those of drug resistance. Coupled with the fact that patients are not treated at random but often according to their CD4 count, ART could be an added selection pressure on the evolution of HIV virulence. Indeed, it has been speculated that widespread ART could drive either increases [190,361] or decreases [357] in virulence. The benefits of ART to the individual and to epidemic control are so spectacular that they are going to be paramount in importance to any effects of ART on virulence evolution. However the epidemic is still far from over and increased coverage of ART does not yet imply the end of HIV transmission [362]. Hence it is still important to understand what might be the implications of widespread ART for future patterns of virulence change.

In this paper we first examine the observed patterns of changing HIV virulence, and then introduce two models to answer the following questions; in the absence of ART how would we expect the virulence of a novel infection to change? Would we expect widespread ART to drive changes in HIV virulence evolution and if so what is the expected magnitude and direction of any ART effect? Our analysis is based on an ODE model and a PDE model where time since infection is introduced as a second independent variable and which is equivalent to the ODE model at epidemic equilibrium. For clarity in the main text we start with the simplest form of the model and build it up in stages. The PDE model is employed specifically to help our understanding of the equilibrium effects of ART on

population average SPVL.

5.2 Modelling and results

5.2.1 What are the observed patterns of changing HIV virulence?

Individual studies based on measurement of either baseline CD4 count or SPVL have reported statistically significant trends in virulence in both directions [363,364]. The overall picture is confounded by the differing measures of virulence used, substantial changes in standards of assays, possible sampling biases, and the distinct character of separate sub-epidemics. In particular, it is important to note that the definition of SPVL varies between studies. In reality, viral load fluctuates during chronic infection and increases towards the onset of AIDS. Hence, the most precise measures of SPVL, such as those used in genome wide association studies [129], take an average of several longitudinal viral load measures from a defined window post seroconversion, filtering for outlier values. Most empirical studies of changing virulence simply use either a single viral load measure or an average of a few values [35, 189]. When it comes to assessing trends in virulence, single viral load measures may be acceptable (although they will introduce more variation and so require a larger sample size for adequate power), so long as sampling bias can be eliminated. This is only possible in seroincident cohorts, where the timing of measurements following the known date of seroconversion can be controlled for.

When we restrict our attention to studies of seroincident cohorts using SPVL as a proxy for virulence, the pattern is still unclear, but the results more consistently indicate an overall increase in SPVL during the past few decades across populations with a majority European ancestry (Figure 5.1A) [35,189]. In contrast, in a recent study of HIV-1 infected mothers in Botswana and South Africa, data describing viral replicative capacity (VRC), an *in vitro* measure of viral fitness, pointed to a decrease in virulence over time. In Gaberone, Botswana where the epidemic is 10 years older, median VRC of the cohort was significantly lower than in Durban, South Africa (Figure 5.1B). We will refer back to these data later when we come to set our modelling results in the context of observed trends.

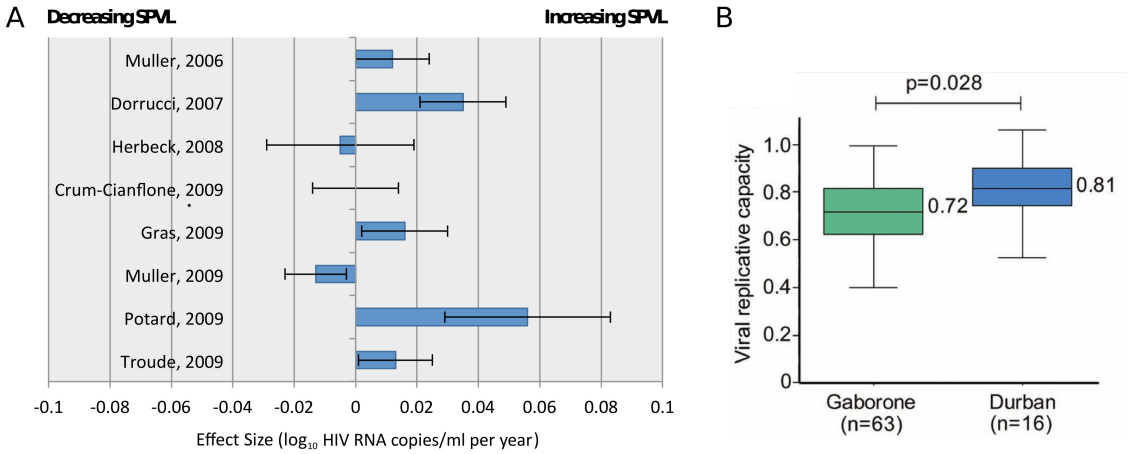


Figure 5.1: A collection of empirical data, reproduced from a meta-analysis by Herbeck et al [35] (A) and from Payne et al [357] (B). A: Results from eight studies measuring population-level trends in SPVL, showing significant trends in both directions. The effect sizes, i.e. the estimated per-year change in SPVL, and 95% confidence intervals (error bars) are shown. Criteria for inclusion of these studies in the meta analysis were that they controlled for ART use and reported data with which regression slopes could be estimated. SPVL was defined in most studies as the first measurement taken after seroconversion (but prior to the onset of clinical AIDS), approximately one year post-seroconversion. Note that Muller 2006 and 2009 are seroprevalent cohorts, the rest are seroincident. Herbeck et al calculated a summary estimate using a weighted least squares approach as 0.013 (95% CI [-0.001,0.027]), which increased after the removal of the seroprevalent cohorts, full details in [35]. B: The viral replicative capacity (VRC) of viruses isolated from mothers in Gaberone compared with Durban is significantly lower in Gaberone where the epidemic is around 10 years older and ART was introduced 5 years earlier. VRC was measured in identical conditions and normalised to NL4-3 comparator virus for these CD4-matched groups (CD4 300-500 per mm^3).

5.2.2 In the absence of treatment, how would we expect the virulence of a novel infection to change?

There is a received wisdom that successful parasites are relatively harmless to their hosts, and therefore that new infectious diseases of humans will evolve to avirulence. This general assumption has been challenged by the "trade-off hypothesis" - virulence is often linked to the chance of onward transmission, as is the case with HIV, and hence the 'optimal' level of virulence must balance transmissibility and duration of infectiousness [34,184]. We have encapsulated this virulence trade-off in a simple two-strain model. For simplicity we assume that the SPVL of a new infection is entirely determined by the genotype of the infecting strain (analyses with this assumption relaxed are shown in Appendix C, section C.2). Accordingly, infection with strain 1 results in high SPVL infections which have both a high transmission coefficient ($\beta_H c$) and high AIDS-related death rate (a_H). Infection with strain 2 results in low SPVL infections with low transmission coefficient ($\beta_L c$) and AIDS-related death rate (a_L). Note that for the purposes of this model we need not have a particular, precise definition of SPVL in mind. The important qualities of 'SPVL' as used here are that higher values are correlated with both a higher risk of transmission and faster progression to AIDS and death – our conclusions will apply to any definition of SPVL that meets those criteria.

The two strains in this model are in competition and low numbers of infections of both are introduced into an initially susceptible population. Strain switching within host occurs at a low rate, m, to avoid one strain necessarily becoming extinct, and SPVL is preserved within that host when this happens. Hence, an individual's disease course and infectiousness is determined entirely by the infecting strain, but strain switching can lead to them passing on the opposite strain. Biologically, this strain switching could go some way towards accounting for the effects of within host mutation and superinfection (we do not directly model superinfection). For example, an individual who is infected with a high virulence strain might drive viral escape mutations that lead to them transmitting an attenuated, low virulence strain. Alternatively, an individual infected with a low virulence strain might become superinfected with a very different strain and transmit that strain or a high virulence recombinant. The assumption that SPVL is preserved within the infecting

host in both of these cases is a simplification and limitation of our model, but reflects the possibility that the genotype of early viruses has a particular influence on disease outcome [196]. The model equations, in the absence of ART, are:

$$\begin{aligned}
\frac{dS}{dt} &= B - (\lambda_{S1} + \lambda_{S2})S - \mu S \\
\frac{dI^H_{S1}}{dt} &= \lambda_{S1}S - (\mu + a_H)I^H_{S1} - mI^H_{S1} + mI^H_{S2} \\
\frac{dI^H_{S2}}{dt} &= - (\mu + a_H)I^H_{S2} - mI^H_{S2} + mI^H_{S1} \\
\frac{dI^L_{S2}}{dt} &= \lambda_{S2}S - (\mu + a_L)I^L_{S2} - mI^L_{S2} + mI^L_{S1} \\
\frac{dI^L_{S1}}{dt} &= - (\mu + a_L)I^L_{S1} - mI^L_{S1} + mI^L_{S2}
\end{aligned} \tag{5.1}$$

S represents susceptible (uninfected) individuals and the I^j_i represent the different infected classes, where i denotes strain type and j denotes SPVL (H=high and L=low). All new infections are either in class I^H_{S1} or I^L_{S2} but, partway through an infection, strain switching can lead to these switching to become I^H_{S2} and I^L_{S1} infections respectively. The parameters are fully described in Table 5.1. Briefly, B is the rate at which new susceptibles are added to the population, μ is the death rate of uninfected individuals and $\lambda_i = (\beta_H c I^H_i + \beta_L c I^L_i)/N$ is the force of infection of each strain (where $N = S + \sum_{i,j} I^j_i$). A model diagram is shown in Figure 5.2A. Since m is small, the R_0s for both strains are approximated by

$$R_0^{S1} = \frac{\beta_H c}{\mu + a_H} \quad , \qquad R_0^{S2} = \frac{\beta_L c}{\mu + a_L}$$

(this calculation is exact when $m = 0$).

Model simulations of the epidemic with initial conditions $S = 40000, I^H_{S1} = 1, I^L_{S2} = 1, I^L_{S1} = 0, I^H_{S2} = 0$ are shown in Figure 5.3 (solid lines). Note that the underlying population size makes no difference to the dynamics of our model because we have used the standard assumption that transmission of a sexually transmitted disease is proportional to $\beta SI/N$ [184]. We simulate two scenarios: $R_0^{S1} > R_0^{S2}$ (Figure 5.3A,C) and $R_0^{S1} < R_0^{S2}$ (Figure 5.3B,D). Throughout the results, the number of AIDS-related deaths per untreated infected person per year is used as a proxy for virulence (Figure 5.3C,D).

In the first few decades of the epidemic, the virulent strain (S1) spreads faster through the population due to its high transmissibility and hence dominates. Following this, the

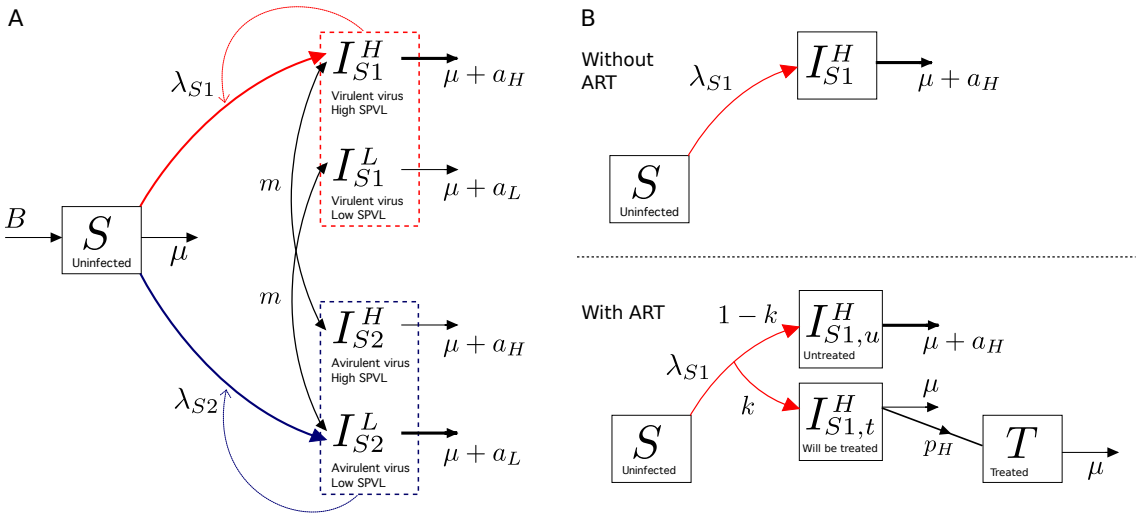


Figure 5.2: A model diagram, (A) for the basic model in the absence of ART (equations 1) and (B) showing the incorporation of ART into the model (equations 2). (A) Uninfected individuals, S, enter the population at rate B and die at rate μ. They may be infected with either strain, S1 (red) or S2 (blue). All infections initiated by strain S1 have high SPVL (H) and all infections initiated by S2 have low SPVL (L). Within host strain switching occurs at a low rate, m, and SPVL within that host is preserved when this happens. The force of infection for each strain is given by $\lambda_i = (\beta_H c I_i^H + \beta_L c I_i^L)/N$, where $N = S + \sum_{i,j} I_i^j$. Infected individuals have an accelerated death rate due to AIDS of $\mu + a_j$, where $a_H > a_L$. (B) Use of ART at $100k\%$ coverage is reflected by a proportion k of individuals entering the 'will be treated' class upon infection and progressing on to treatment at rate p_j, where $p_H > p_L$. Treated individuals, T, are assumed to be non-infectious and die at rate μ. Model parameters are fully described in Table 5.1.

slow growth of the low virulence strain (S2) and peaking of S1 infections leads to a second phase in which average virulence falls. The long-term equilibrium behaviour of the model constitutes a third phase in which the strain balance is determined by the R_0s (the whole of the third phase can be seen in Figure C.16). Since equilibrium is not reached for hundreds of years, the decline of virulence during the second phase is seen clearly whatever the balance of the $R_0 s$ (Figure 5.3C,D). Even when the virulence/transmissibility trade off means that S1 will predominate in the long run, the proportion of infections caused by this higher virulence strain still decreases for a while after the peak. The characteristic first, second and third phase behaviour described above is robust to changes in the R_0 values and initial conditions of the model (Figures C.11–C.13 & C.16). The values used in Figure 5.3 were chosen because they produce results that are representative of the middle of the range.

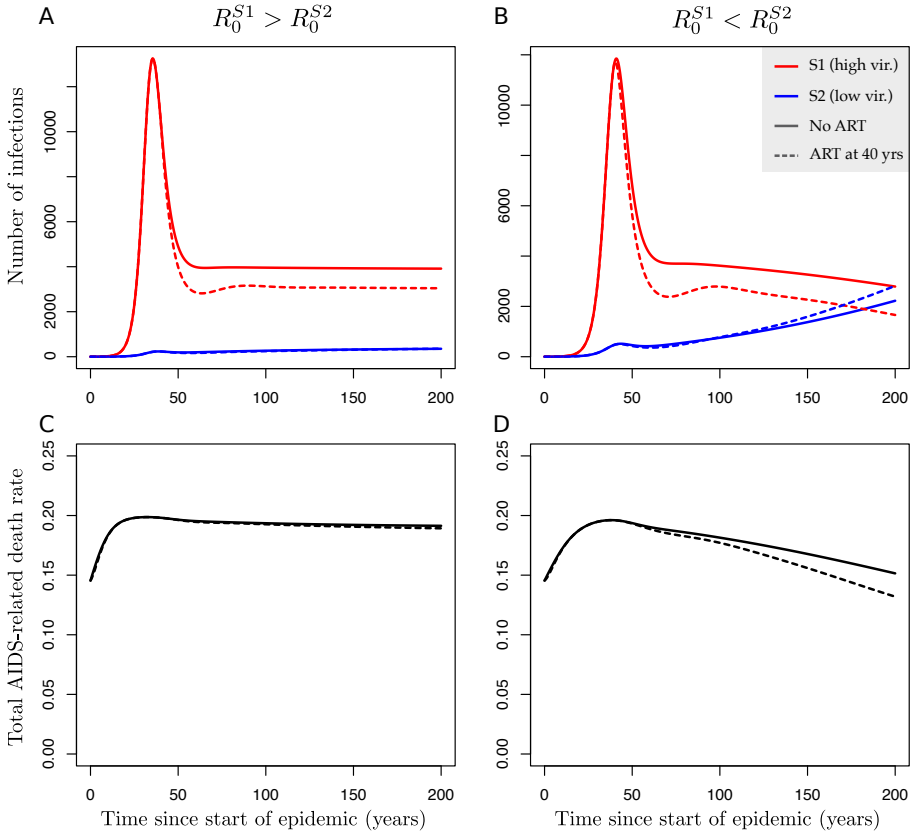


Figure 5.3: Behaviour of the two strain model with and without ART. A, C: The transmission coefficients, $\beta_H c$ and $\beta_L c$, are chosen so that in the absence of ART S1 will dominate at equilibrium ($R_0^{S1} = 2.4, R_0^{S2} = 2.2$). B, D: $\beta_H c$ and $\beta_L c$ chosen so that in the absence of ART S2 will dominate at equilibrium ($R_0^{S1} = 2.2, R_0^{S2} = 2.4$). The initial conditions are $S(0) = 40000, I^H_{S1,u}(0) = 1, I^L_{S2,u}(0) = 1$, all other populations equal to zero. The remaining parameter values are given in Table 5.1. Solid lines show results of the model simulation with no ART, dotted lines show the results when ART is introduced at 30% coverage 40 years into the epidemic. A, B: The numbers of strain S1 (red) and strain S2 (blue) infections during the course of the epidemic. C, D: Average virulence, measured in terms of the total number of AIDS-related deaths per untreated infected person per year and calculated as $\sum_i (a_H I^H_{i,u} + a_L I^L_{i,u}) / \sum_i (I^H_{i,u} + I^L_{i,u})$, through time. Early in the epidemic the spread of infection is dominated by the more virulent strain because it has a higher force of infection. However the slow growth of the less virulent strain and peak of virulent infections (A, B) leads to a second phase during which average virulence falls (C, D). Simulations of the model with a range of initial conditions and spanning the first 1000 years of the epidemic are shown in Figure C.16.

Table 5.1: Parameter values and references

Symbol	Description	Value used	Interpretation
μ	Death rate of uninfected individuals	1/40	The life expectancy of an HIV-uninfected individual in the population is on average 40 years, after reaching adulthood. This estimate is based on the WHO African Region [359].
B	Population birth rate	$\mu S(0)$	The population size is constant in the absence of infection.
a_H, a_L	AIDS-related death rates of high and low (resp.) SPVL infections	1/5, 1/11	In the model, an infected individual with high SPVL dies on average 5 years after infection, an infected individual with low SPVL dies on average 11 years after infection. In an HIV-infected Ugandan population, 81% survived 5 years post-seroconversion and 48% survived 10 years post-seroconversion [365].
p_H, p_L	Rates at which high and low (resp.) SPVL infections progress to the CD4 count threshold for commencing ART	In Fig. 5.3 these are set at 1/4 and 1/10. In Figs 5.5 & 5.6 p_H and p_L vary.	In Fig. 5.3, patients are treated on average a year before they would otherwise have died of AIDS. In Figs 5.5 & 5.6 the 'low CD4' period is at least a year. The lower bound estimate of one year for the 'low CD4' period is based on rates of CD4 count decline [366] and CD4 count treatment thresholds of 200 cells/mm^3 or greater [367].
$\beta_H c$, $\beta_L c$	Transmission coefficients of high and low (resp.) SPVL infections. Composed of c (contact rate) and β_j (probability of transmission upon contact of infectious and non-infections individuals)	$\approx$ 0.52, $\approx$ 0.26	Values are chosen to yield $R_0^{S1} = 2.2$ and $R_0^{S2} = 2.4$, or vice versa, in an untreated population. This puts the peak of the epidemic at 40 years in, consistent with estimates from Botswana and South Africa where epidemic emergence occurred in the 1950s - 1960s [46] and the epidemics peaked around 2000-5 [368]. A wider range of R_0 values is considered in Figures C.11–C.13.
k	ART coverage	In Figure 5.3, $k = 0.3$. In Figs 5.5 & 5.6, k varies.	From 40 years into the epidemic $100k$% of new infections will eventually receive treatment [359]. The introduction of ART coincides with the peak of the epidemic, reflecting the situation in South Africa [368,369]. Changing the timing of ART introduction relative to the peak has a negligible effect on virulence evolution (Figures C.14 & C.15).
m	Strain switching rate	0.001	Strain switching will occur in approximately 1 in every 1000 infections each year. We choose $m > 0$ simply so that both strains can be present at equilibrium.

5.2.3 Would we expect widespread ART to drive changes in HIV virulence evolution?

We incorporate ART into the model by supposing that a proportion, k, of individuals will eventually be treated, with the rest remaining untreated until death. Therefore, we split each infected class, I_i^j, into $I_{i,t}^j$ (treated) and $I_{i,u}^j$ (untreated), with $I_i^j = I_{i,t}^j + I_{i,u}^j$. The extended set of model equations is

$$\begin{aligned}
\frac{dS}{dt} &= B - (\lambda_{S1} + \lambda_{S2})S - \mu S \\
\frac{dI_{S1,u}^H}{dt} &= (1-k)\lambda_{S1}S - (\mu + a_H)I_{S1,u}^H - mI_{S1,u}^H + mI_{S2,u}^H \\
\frac{dI_{S1,t}^H}{dt} &= k\lambda_{S1}S - (\mu + p_H)I_{S1,t}^H - mI_{S1,t}^H + mI_{S2,t}^H \\
\frac{dI_{S1,u}^L}{dt} &= -(\mu + a_L)I_{S1,u}^L - mI_{S1,u}^L + mI_{S2,u}^L \\
\frac{dI_{S1,t}^L}{dt} &= -(\mu + p_L)I_{S1,t}^L - mI_{S1,t}^L + mI_{S2,t}^L \\
\frac{dI_{S2,u}^H}{dt} &= -(\mu + a_H)I_{S2,u}^H - mI_{S2,u}^H + mI_{S1,u}^H \\
\frac{dI_{S2,t}^H}{dt} &= -(\mu + p_H)I_{S2,t}^H - mI_{S2,t}^H + mI_{S1,t}^H \\
\frac{dI_{S2,u}^L}{dt} &= (1-k)\lambda_{S2}S - (\mu + a_L)I_{S2,u}^L - mI_{S2,u}^L + mI_{S1,u}^L \\
\frac{dI_{S2,t}^L}{dt} &= k\lambda_{S2}S - (\mu + p_L)I_{S2,t}^L - mI_{S2,t}^L + mI_{S1,t}^L \\
\frac{dT}{dt} &= p_H(I_{S1,t}^H + I_{S2,t}^H) + p_L(I_{S1,t}^L + I_{S2,t}^L) - \mu T
\end{aligned} \tag{5.2}$$

Once treated, patients are assumed to become noninfectious. We model treating based on CD4 count [367], by assuming that individuals with high SPVL will be treated sooner than those with low SPVL, at rates p_H and p_L respectively ($p_H > p_L$). See Figure 5.2B for a model diagram.

In Figure 5.3 we see that introducing ART 40 years into the epidemic (to roughly coincide with the peak, as in data from South Africa – see Table 5.1) slightly decreases virulence in the decades after it is introduced. We ask, is this indicative of a general pattern?

Intuitively, we might expect treatment based on patient CD4 count to favour less virulent viruses since it is only the most sick patients that get treated. Expressing this

intuitive argument formally allows us to examine exactly when this is true: *If* a randomly chosen infected person with 'low' CD4 count (i.e. a person eligible for treatment) is more likely to be infected with virulent virus than a person chosen at random from the entire infected pool, then treating 'low' CD4 count patients will favour the less virulent virus. This 'if' clause holds when the following inequality is satisfied:

$$\Pr(\text{infected with strain S1} \mid \text{low CD4}) > \Pr(\text{infected with strain S1}) \tag{5.3}$$

In order to calculate the sizes of the infected, 'low CD4' populations at equilibrium for both strains, we now introduce an infection-age dependent model (which we will refer to as the 'PDE model') and relate it back to the original ODE model.

5.2.4 Defining the infection-age dependent model

Let τ denote time since infection, and define $y^H_{S1}(t,\tau)$ to be the number of high SPVL, virulent strain (S1) infections of infection-age τ at time t, so that

$$\int_0^\infty y^H_{S1}(t,\tau)\mathrm{d}\tau = I^H_{S1}(t).$$

We assume that patient CD4 count drops below the 'low' threshold T_H years after infection with S1 or T_L years after infection with S2 ($T_L > T_H$). In this model the death rate is dependent on time since infection; the parameter d_j is the additional AIDS-related death rate of patients who have crossed the low CD4 count threshold. A proportion, k, of patients are treated at the point ($\tau = T_j$) when they reach the low CD4 count threshold, resulting

in a discontinuity in $y_i^j(\tau)$ at T_j (Figure 5.4A). The model equations are as follows:

$$
\begin{aligned}
\frac{dS}{dt} &= B - (\lambda_{S1} + \lambda_{S2})S - \mu S \\
\frac{\partial y_{S1}^H}{\partial t} + \frac{\partial y_{S1}^H}{\partial \tau} &= \begin{cases} -(\mu + m)y_{S1}^H(t,\tau) + m y_{S2}^H(t,\tau) & \text{if } \tau \le T_H \\ -(\mu + d_H + m)y_{S1}^H(t,\tau) + m y_{S2}^H(t,\tau) & \text{if } \tau > T_H \end{cases} \qquad y_{S1}^H(t,0) = \lambda_{S1} S \\
\frac{\partial y_{S1}^L}{\partial t} + \frac{\partial y_{S1}^L}{\partial \tau} &= \begin{cases} -(\mu + m)y_{S1}^L(t,\tau) + m y_{S2}^L(t,\tau) & \text{if } \tau \le T_L \\ -(\mu + d_L + m)y_{S1}^L(t,\tau) + m y_{S2}^L(t,\tau) & \text{if } \tau > T_L \end{cases} \qquad y_{S1}^L(t,0) = 0 \\
\frac{\partial y_{S2}^H}{\partial t} + \frac{\partial y_{S2}^H}{\partial \tau} &= \begin{cases} -(\mu + m)y_{S2}^H(t,\tau) + m y_{S1}^H(t,\tau) & \text{if } \tau \le T_H \\ -(\mu + d_H + m)y_{S2}^H(t,\tau) + m y_{S1}^H(t,\tau) & \text{if } \tau > T_H \end{cases} \qquad y_{S2}^H(t,0) = 0 \\
\frac{\partial y_{S2}^L}{\partial t} + \frac{\partial y_{S2}^L}{\partial \tau} &= \begin{cases} -(\mu + m)y_{S2}^L(t,\tau) + m y_{S1}^L(t,\tau) & \text{if } \tau \le T_L \\ -(\mu + d_L + m)y_{S2}^L(t,\tau) + m y_{S1}^L(t,\tau) & \text{if } \tau > T_L \end{cases} \qquad y_{S2}^L(t,0) = \lambda_{S2} S
\end{aligned}
\tag{5.4}
$$

where λ_{S1} and λ_{S2} are defined as before. At equilibrium, when $\frac{\partial y_i^j}{\partial t} = 0$, the above reduce to a set of ODEs in τ which we may solve to obtain $y_{S1}^j + y_{S2}^j$ and $y_{S1}^j - y_{S2}^j$. Combining these simultaneous equations appropriately yields

$$
\begin{aligned}
2y_{S1}^H &= \lambda_{S1} S^* [e^{-\mu\tau} + e^{-(\mu+2m)\tau}] \times \begin{cases} 1 & \text{if } \tau \le T_H \\ (1-k)e^{-d_H(\tau - T_H)} & \text{if } \tau > T_H \end{cases} \\
2y_{S2}^H &= \lambda_{S1} S^* [e^{-\mu\tau} - e^{-(\mu+2m)\tau}] \times \begin{cases} 1 & \text{if } \tau \le T_H \\ (1-k)e^{-d_H(\tau - T_H)} & \text{if } \tau > T_H \end{cases} \\
2y_{S1}^L &= \lambda_{S2} S^* [e^{-\mu\tau} - e^{-(\mu+2m)\tau}] \times \begin{cases} 1 & \text{if } \tau \le T_L \\ (1-k)e^{-d_L(\tau - T_L)} & \text{if } \tau > T_L \end{cases} \\
2y_{S2}^L &= \lambda_{S2} S^* [e^{-\mu\tau} + e^{-(\mu+2m)\tau}] \times \begin{cases} 1 & \text{if } \tau \le T_L \\ (1-k)e^{-d_L(\tau - T_L)} & \text{if } \tau > T_L \end{cases}
\end{aligned}
\tag{5.5}
$$

where S^* is the equilibrium value of S, and so $\lambda_{S1} S^*$ and $\lambda_{S2} S^*$ are constants (independent of τ).

In applying the PDE model later on, it will be useful to be able to relate the parameters T_j and d_j to the parameters a_j and p_j in the ODE model. We may do this by equating the two models at equilibrium, i.e. ensuring that at equilibrium the sizes of both the high SPVL and low SPVL infected classes in the ODE model match those in the PDE model. Hence, we require that, for $j = H, L$:

$$\begin{aligned}\int_0^\infty y^j_{S1}(t,\tau) + y^j_{S2}(t,\tau)\mathrm{d}\tau &= I^j_{S1,u} + I^j_{S1,t} + I^j_{S2,u} + I^j_{S2,t} \\ &= \frac{(1-k)\lambda_i S^*}{\mu + a_j} + \frac{k\lambda_i S^*}{\mu + p_j}\end{aligned}$$

After substituting in the solutions to the PDE model at equilibrium in (5.5) and integrating, this reduces to

$$e^{-\mu T_j}\left[\frac{1-k}{\mu + d_j} - \frac{1}{\mu}\right] - \frac{1}{\mu} = \frac{(1-k)}{\mu + a_j} + \frac{k}{\mu + p_j}.$$

Substituting in $k = 0$ and $k = 1$ shows that in order to obtain a condition that is independent of k we must have $\mu + d_j = p_j(\mu + a_j)/(p_j - a_j)$. In this case, the above simplifies to $e^{-\mu T_j} = p_j/(\mu + p_j)$.

In conclusion, the parameters in the two models are related according to

$$e^{-\mu T_j} = \frac{p_j}{\mu + p_j} \quad \text{and} \quad d_j = \frac{a_j(\mu + p_j)}{p_j - a_j} \quad .$$

A simple example shows that the parameters seem to correspond as we would expect: Take $\mu = 1/40$, $T_j = 4$ years (= time to reaching 'low CD4' treatment threshold), $d_j = 1$ per year (= AIDS-related death rate), then the calculations give $p_j \approx 9/40$ and $a_j \approx 9/50$. So average time to progression is just over 4 years and average time to death in an untreated patient is just over 5 years.

5.2.5 When does ART favour less virulent viruses?

We now apply this infection-age dependent model to calculating when the inequality in (5.3) holds. In terms of the populations in the infection-age dependent model, (5.3) is

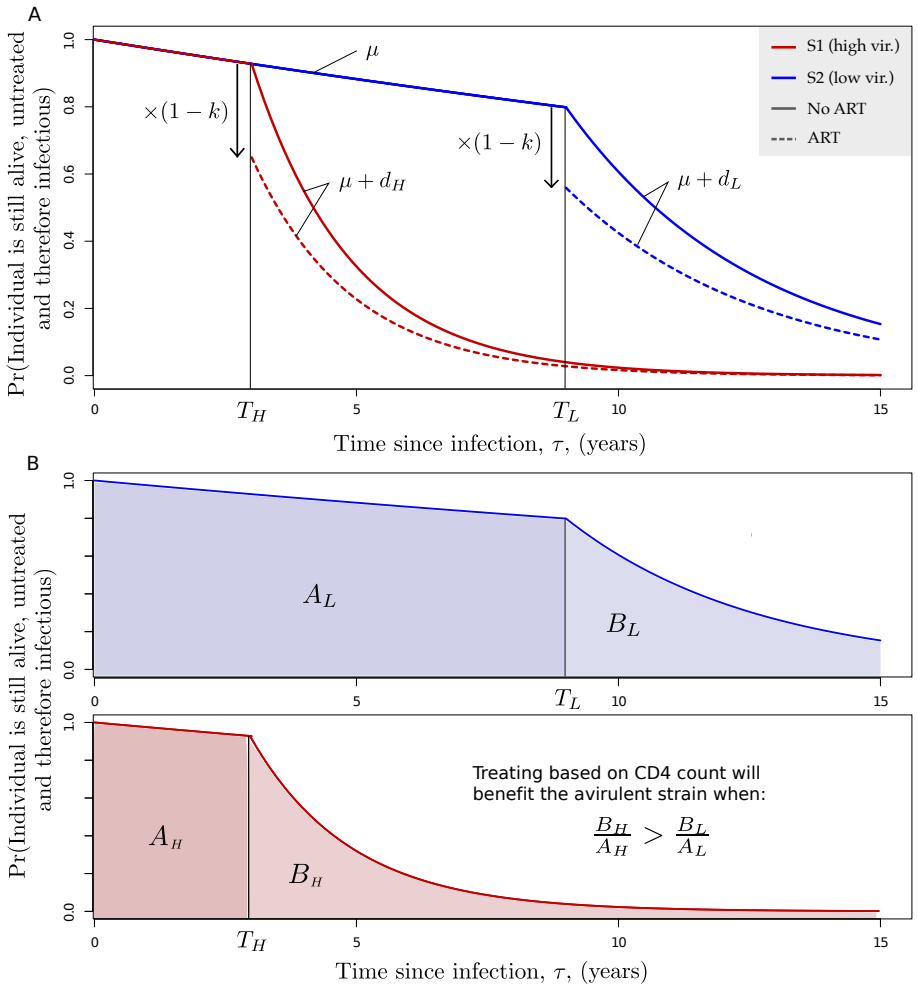


Figure 5.4: Diagrams representing the PDE version of the model and the relative importance of low CD4 infections. The graphs show the probability that an individual will still be alive and untreated and hence infectious τ years into their infection, plotted against τ. As in Figure 5.3 the high virulence strain (S1) is shown in red and the low virulence strain (S2) in blue. We here assume S1 infections always have high SPVL and S2 infections always have low SPVL (i.e. $m = 0$, as in the PDE model calculations in the main text). A: In the PDE model AIDS-related death of an individual is dependent on time since infection and only occurs after the low CD4 threshold has been crossed. A proportion, k, of treated patients are removed from the infectious class as they reach this threshold, giving rise to the discontinuity. Solid line; no ART, dotted line; ART at 30% coverage. B: Similar to (A) but split by strain. Shaded areas are proportional to the contribution of that period of the infection to onward transmissions of that strain in a model without treatment. When patients are treated they are no longer infectious (after T_j) and the same proportion are treated for each strain, therefore the effect of ART on the strain balance at equilibrium is determined by the relative importance of low CD4 transmissions, $\frac{B_H}{A_H}$ compared with $\frac{B_L}{A_L}$.

equivalent to:

$$\frac{\int_{T_H}^{\infty} y_{S1}^{H}\mathrm{d}\tau + \int_{T_L}^{\infty} y_{S1}^{L}\mathrm{d}\tau}{\int_{T_H}^{\infty} y_{S1}^{H} + y_{S2}^{H}\mathrm{d}\tau + \int_{T_L}^{\infty} y_{S1}^{L} + y_{S2}^{L}\mathrm{d}\tau} > \frac{\int_{0}^{\infty} y_{S1}^{H}\mathrm{d}\tau + \int_{0}^{\infty} y_{S1}^{L}\mathrm{d}\tau}{\int_{0}^{\infty} y_{S1}^{H} + y_{S2}^{H}\mathrm{d}\tau + \int_{0}^{\infty} y_{S1}^{L} + y_{S2}^{L}\mathrm{d}\tau}$$

Assuming that the strain switching rate, m, is negligible, so that $y_{S1}^{L} \approx y_{S2}^{H} \approx 0$, this becomes:

$$\frac{\int_{T_H}^{\infty} y_{S1}^{H}\mathrm{d}\tau}{\int_{T_H}^{\infty} y_{S1}^{H} + y_{S2}^{L}\mathrm{d}\tau} > \frac{\int_{0}^{\infty} y_{S1}^{H}\mathrm{d}\tau}{\int_{0}^{\infty} y_{S1}^{H} + y_{S2}^{L}\mathrm{d}\tau} \tag{5.6}$$

The integrals in this inequality are represented graphically in Figure 5.4B. Note that in this figure time since infection (τ) is on the x-axis, and so the figure shows the different progress of individual high and low virulence infections (whereas Figure 5.3 showed the progress of the epidemic as a whole through calendar time). In the notation of the figure, inequality (5.6) is equivalent to:

$$\frac{B_H}{A_H} > \frac{B_L}{A_L} \tag{5.7}$$

To describe this inequality in an intuitively appealing way, we note that it relates to 'the relative importance of low CD4 transmissions' for each strain: When ART is introduced, a proportion, k, of transmissions caused by individuals who have passed beyond the low CD4 threshold are effectively removed for each strain. The strain that is most severely affected by ART will be the one for which these 'low CD4' transmissions made up the greatest proportion of the overall number of transmissions. Hence, we find that the intuition that treatment will favour the low virulence viruses is true in the long run (at equilibrium) in the case where the proportion of low CD4 transmissions (B_i/A_i) is greater for high SPVL infections. This is when (5.7) holds.

If expected survival time after progressing to 'low CD4' count is the same for high and low SPVL infections, or if it is longer for low SPVL infections but only in proportion to the additional time taken to reach the low CD4 threshold, then (5.7) holds. In these cases, the latter of which seems consistent with available data [366], treatment will favour the low virulence viruses. Indeed, for this not to hold it must be the case that individuals with low SPVL continue to survive with low CD4 count for a disproportionately long time

(compared to individuals with low CD4 counts caused by high SPVL infections).

5.2.6 What is the expected magnitude and direction of this ART effect?

The equilibrium calculations above are not the whole picture and the magnitude and direction of this ART-effect may be influenced by considering the effect soon after the introduction of ART as opposed to at equilibrium. We may rewrite (5.6) in terms of the parameters of the PDE model by substituting in the solutions for the populations at equilibrium given in (5.5) (full workings in Appendix C, section C.3):

$$\frac{e^{\mu T_L} - 1}{e^{\mu T_H} - 1} > \frac{\mu + d_H}{\mu + d_L} \tag{5.8}$$

Then, utilising the relationship between the ODE and PDE model parameters, we are able to use the ODE model to confirm this analytical result at equilibrium (Figure 5.5) and see how it compares to the short-term ART-effect (Figure 5.6).

Figure 5.5 shows the effect of ART on virulence at equilibrium for a range of different values of T_j and d_j which we believe to span the reasonable parameter space. As expected, the direction of the ART-effect is determined by the relative importance of low CD4 transmissions. To understand the magnitude of the effect, note that the equilibrium virulence tends to rest at one of two extremes, determined by which strain dominates in the absence of ART. The values are extreme because the frequency of the subdominant strain is at mutation-selection balance which is very low when m is small, as here. Therefore, the magnitude of the ART-effect is largely determined by whether there is potential for ART to cause the strain balance to switch to the other extreme. For example, when $R_0^{S1} > R_0^{S2}$ (Figure 5.5A) then a large ART-effect is only seen when ART exerts a downward pressure on virulence, i.e. when low CD4 transmissions are of greater importance to S1. These results are summarised in Table 5.2.

Fifty years after the peak of the epidemic, the high virulence strain (which has the larger growth rate) always dominates in the absence of treatment (Figure 5.6). The effect of ART seen at this time point is to decrease virulence for almost all sets of parameters considered. This transient decrease in virulence, which masks any selective pressure exerted by the 'relative importance of low CD4 transmissions', is a result of the more immediate impact of ART on S1. Since the S1-infected population has a higher turnover, the effect of reducing

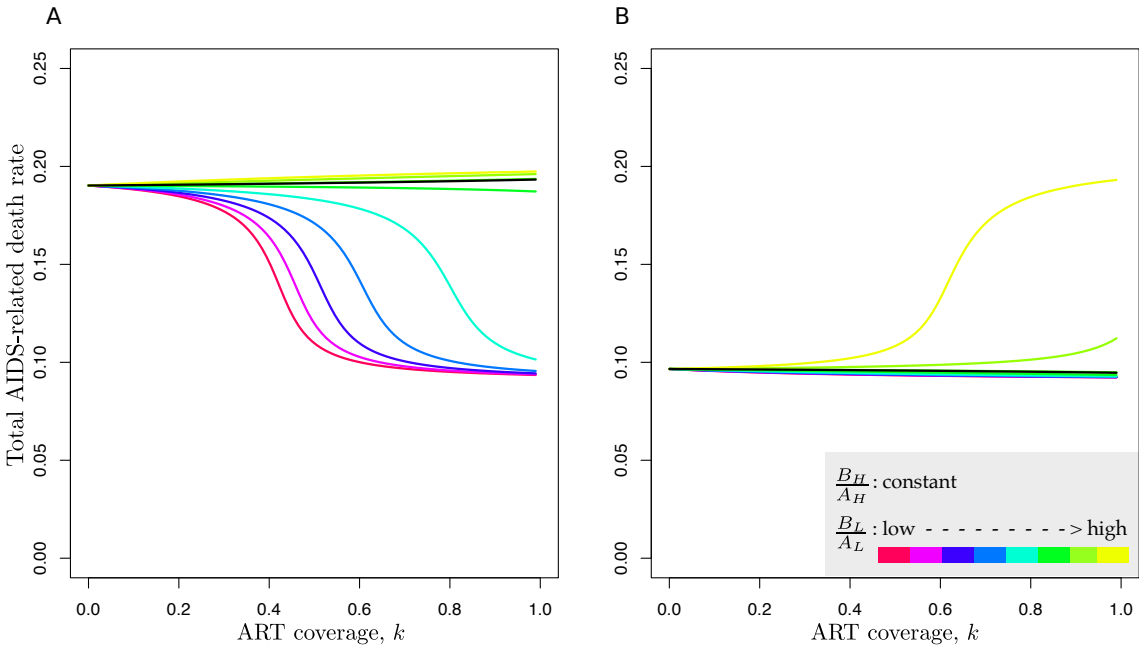


Figure 5.5: The relationship between ART coverage and virulence at equilibrium, for different parameter sets. A: $R_0^{S1} = 2.4, R_0^{S2} = 2.2$. B: $R_0^{S1} = 2.2, R_0^{S2} = 2.4$ (R_0s calculated in the absence of ART). Different coloured lines represent different proportions of S2 transmissions removed as a result of ART. So, with reference to Figure 5.4B, $\frac{B_H}{A_H}$ is kept constant (parameters $T_H = 3, d_H = 0.57$) while $\frac{B_L}{A_L}$ is varied from low (red line; parameters $T_L = 8, d_L = 0.57$) to high (yellow line; parameters $T_L = 5, d_L = 0.2$). The ODE model parameters corresponding to these PDE model parameters were calculated as set out in the main text and then the equilibrium position of the ODE model was computed (Appendix C, section C.1.4) to produce these plots. The black line corresponds to the parameter set in which ART has no effect at equilibrium (equality in (5.8)). Inequality (5.8) was obtained under the assumption that the switching rate, m, is negligible whereas these calculations of the equilibrium behaviour use $m = 0.001$, hence this black line deviates marginally from the horizontal. Total number of AIDS-related deaths per untreated infected person per year is calculated as in Figure 5.3. The extreme values of this are $a_H = 1/5$ and $a_L = 1/11$ and these are approached when S1 and S2 (resp.) completely dominate at equilibrium. A: In the absence of ART, S1 dominates at equilibrium. Hence, when $\frac{B_L}{A_L} < \frac{B_H}{A_H}$ then ART is able to switch the ordering of the R_0s so that S2 dominates at equilibrium. The more severe the inequality between $\frac{B_L}{A_L}$ and $\frac{B_H}{A_H}$, the lower the ART coverage needed to cause this switch. B: In the absence of ART, S2 dominates at equilibrium, and so this situation is the reverse of (A).

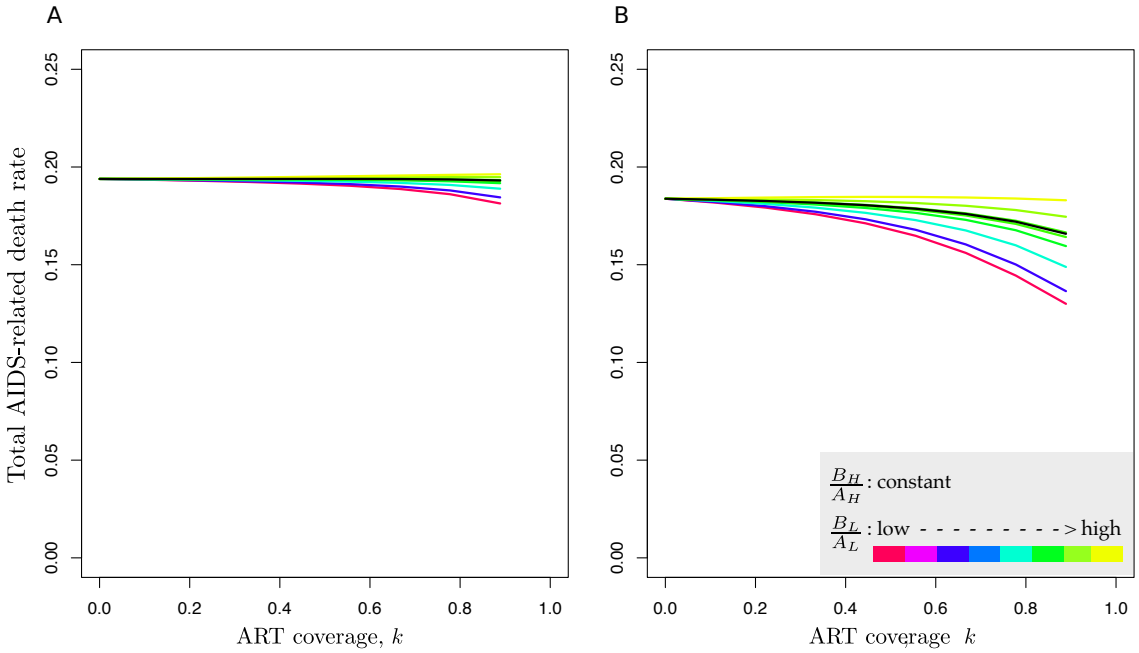


Figure 5.6: The effect of ART on virulence in the short term, 50 years after the introduction of ART. The results of model simulations, in which ART is introduced 40 years into the epidemic, are shown, with total number of AIDS-related deaths per untreated infected person per year once again used as a proxy for virulence. A: $R_0^{S1} = 2.4, R_0^{S2} = 2.2$. B: $R_0^{S1} = 2.2, R_0^{S2} = 2.4$ (R_0s calculated in the absence of ART). Different coloured lines correspond to different sets of model parameters which determine the effect of ART on the balance of removed transmissions, as described in Figure 5.5. Initial conditions and fixed parameters are as given in Figure 5.3 and Table 5.1. Note that points are not plotted for $k = 1$ because when all patients are treated there are no AIDS-related deaths and so overall virulence is not well defined at this point. The similarity of the results in (A) and (B) shows that changes in the balance of the R_0 values have little effect on model behaviour 90 years into the epidemic. S1 dominates in both scenarios in the absence of ART and the effect of ART is, in almost all cases considered, to benefit the low virulence strain at this point. The ART-effect is stronger for any given level of coverage when $\frac{B_L}{A_L} < \frac{B_H}{A_H}$ (red-blue lines).

the number of onward transmissions is seen more immediately in this population. The magnitude of the short term ART effect is smaller than at equilibrium and is greatest when low CD4 transmissions are of greater importance to the high virulence strain (S1). The results are again summarised in Table 5.2.

5.2.7 Can we find data to test these model predictions?

Since the HIV epidemic is only decades old and widespread ART is relatively recent, we expect that only the short term effects can be observed at present. Inferring the ART-effect from data from a single epidemic is not feasible. Instead we require comparable data

from two similar epidemics that differ in their ART use (though it will not be possible to ensure that all other differences are negligible). Previously published data of this sort was introduced at the beginning of the results (Figure 5.1B). Viral replicative capacity, an *in vitro* measure of viral fitness, was found to be significantly lower in data from Botswana than in South Africa, where the epidemic is ≈ 10 years younger. ART had been introduced ≈ 5 years previously in Botswana but was very limited in South Africa at the time the data was collected. This would suggest a decrease in virulence over time in the presence of ART, as we would expect from our model predictions. However it is not possible to conclude that ART was a causal effector in that decrease.

Table 5.2: Summary results table.

	Early		Late	
	$R_0^{S1} > R_0^{S2}$	$R_0^{S1} < R_0^{S2}$	$R_0^{S1} > R_0^{S2}$	$R_0^{S1} < R_0^{S2}$
$\frac{e^{\mu T_L}-1}{e^{\mu T_H}-1} > \frac{\mu+d_H}{\mu+d_L}$	Medium decrease in virulence	Medium decrease in virulence	Large decrease in virulence	Small decrease in virulence
$\frac{e^{\mu T_L}-1}{e^{\mu T_H}-1} < \frac{\mu+d_H}{\mu+d_L}$	Small decrease in virulence	Small decrease in virulence	Small increase in virulence	Medium increase in virulence

This table describes the magnitude and direction of the effect of ART on virulence depending on (i) whether it were to be measured soon after the introduction of ART ('Early' = within 50 years) or centuries later ('Late'), (ii) the balance of the R_0s of the two strains, (iii) the relative importance of 'low CD4' transmissions to both strains.

5.3 Discussion

Several large observational studies, each spanning of the order of 20 years and utilising various markers of virulence, have been conducted with the aim of determining whether the virulence of HIV is changing, and some have found significant trends [35]. Interpretation of these results is hampered in part by the various measurement and sampling biases that could cause spurious effects, as discussed in detail elsewhere [35, 188]. Additionally, there is perhaps an underlying assumption in the field that patterns of virulence change in a particular epidemic will be monotonic. In contrast, our model shows that the usual course of an epidemic and differing dynamics of the spread of high and low virulence viruses are likely to result in non-monotonic, transient changes in virulence. In particular it is possible that observed decreases in virulence a few decades into an epidemic would be caused by the steadier spread of low virulence viruses and hence not necessarily a sign that the virus

will eventually evolve to avirulence. Non-monotonic changes in mean SPVL have also been observed in agent-based model simulations [188], and very similar patterns to those described by our model have recently been seen in data pooled from seroconverter cohorts across Europe [189]. In this European study, SPVL was calculated as the average of the available viral load measurements taken 6-18 months after seroconversion. Measurements of SPVL in over 15,000 individuals with estimated seroconversion dates ranging from 1979-2008 showed patterns of increasing SPVL from 1980-2002 followed by a tendency of returning to lower levels in recent years. The global HIV-1 pandemic is composed of several sub-epidemics which differ in terms of the age of the epidemic, viral subtype, mode of transmission, population structure and virulence of the virus seeding the epidemic, amongst other factors. Therefore, given that our model shows non-monotonic patterns of virulence change we are not surprised that studies on different HIV-1 infected populations have found differing trends.

Our intuition was that treatment of the most sick patients would favour the less virulent viruses and that over time this might drive lower and lower average virulence. However, analysis with our PDE model suggested that we may better understand the effect of ART on virulence when we think in terms of the relative importance (to each strain) of 'low CD4' transmissions, i.e. the transmissions that no longer occur when a patient is on ART. We then see that the effects expected by our intuition could in theory come about. For example, low CD4 transmissions are of greater importance to the high virulence viruses if patients with low CD4 counts progress at the same rate, independent of SPVL. However it seems likely that 'low CD4' transmissions are of similar importance to both strains, and hence the resulting ART-effect may not be significant. In practice, we are also unlikely to observe a large effect of ART on virulence since these long-term effects materialise over the timescale of centuries and the largest effects also require high coverage of fully suppressive ART. Taking the epidemic in Africa as an example, ART coverage in the WHO African region was reported to be 37% in 2013 [359]. Yet, given that the HIV-1 epidemic is far from over in spite of substantial ART coverage [362], it is important to understand the size and direction of any putative ART effect.

We purposefully used an over-simplified model for the main analyses because it allowed us to gain an understanding of the key aspects of the dynamics. However, it is instructive

to consider further the following possibilities that were not initially allowed for: (i) Low heritability of SPVL. (ii) Varying infectiousness during the course of untreated infection and continued transmission in patients on treatment. (iii) Heterogeneity in contact rates. (iv) Early ART initiation, independent of CD4 count.

Firstly, we have assumed that the SPVL of a new infection is completely determined by the viral strain, and kept the strain switching rate, m, low. Consequently we have modelled a situation where heritability of SPVL is high and there is strong selection for virulence at the between-host level. The debate surrounding these two issues is still ongoing (see [25,190,193–195] for further detail). If there is no possibility of virulence adaptation in response to between-host selection pressures then our analysis, while valid, is redundant. However, ART could still have an effect on virulence evolution that is shaped by within-host selection pressures because the introduction of ART may increase the proportion of transmissions occurring earlier in infection. The other possibility is that there is selection for virulence at the between-host level but that heritability of SPVL is low (in other words, the percentage of the variation in SPVL that is explained by the viral strain is low). For example, heritability of SPVL across sub-Saharan Africa has been estimated at 20-46% [190]. We adapted our model to account for this – see section C.2 and Figures C.1–C.3. Reducing the heritability brings the two extremes of equilibrium strain balance closer together and so the magnitude of the ART-effect is reduced, both in the short- and long-term, while the direction is largely unchanged.

Secondly, we have assumed the probability of transmission to be constant throughout infection. In reality, the proportion of transmissions occurring in acute infection could be elevated as a result of higher infectiousness and also depending on underlying sexual mixing patterns. In Appendix C (section C.3, Figures C.4–C.6) the analyses are re-done under the assumption that 50% of onward transmissions occur in the first 6 months of infection, an approximate upper bound informed by the most recent analyses [180]. We have also made the assumption that patients in receipt of ART never transmit the virus again. This is optimistic given that continuous suppression of viral replication requires good adherence to medication that must be taken daily [370,371]. Allowing some individuals in the model to continue to transmit the virus at a lower rate would have effects akin to reducing the coverage of ART. Therefore we have not presented separate analyses with this assumption

relaxed.

Thirdly, it is known that differing modes of transmission or social factors influencing contact networks can have an effect on the progress of an epidemic [184]. We have assumed homogeneity of contacts in our model, whereas there may be situations in which a subset of the population (the 'core') have much higher contact rates. We may imagine that such a situation would result in differing patterns of virulence evolution in the core and in the 'periphery'. However, adding this core/periphery structure to our model has little affect on the overall patterns of virulence evolution seen both with and without ART (section C.4, Figures C.7–C.8).

Fourthly and finally, in light of recent evidence that treating early might reduce the size of the latent HIV reservoir and could possibly result in post-treatment control [372], some have suggested that all patients be treated as early as possible. Would we have seen a different pattern if we had modelled a set of treatment guidelines where patients are treated as soon as possible after diagnosis, regardless of CD4 count? Incorporating this method of treatment into our model, we see that it always favours the virulent strain in the long-term (i.e. at equilibrium, Figure C.9). However, in the short term the effect of ART is small at realistic levels of coverage (Figure C.10).

Table C.1 summarises the effect of all the additional considerations and modifications above relative to the main results of the original model. In almost all cases the modifications result in a less severe ART-effect, except when treatment efforts are concentrated towards those with more contacts. Indeed, since the relative importance of 'low CD4' transmissions has a tendency to be similar for both strains, it is hard to imagine a scenario or reasonable parameter regime that would result in drastically higher variations in virulence driven by treatment based on CD4 count. The results of a very recent independent study corroborate our main findings on the size and direction of the ART-effect using different methods [373].

In conclusion, should the results of this study alter how we treat? We believe not. Note that we may never be able to answer questions of how much impact ART has had on the shape of virulence evolution in a particular epidemic. Since we'll always be restricted to observational studies of virulence and no two epidemics differ only in ART coverage, we will not be able to use this data to establish causality. However, we have been able to use

our model to look at the range of feasible dynamics of the epidemic with varying coverage of ART. The intuition that ART initiation based on CD4 count would benefit less virulent viruses is correct when 'low CD4' transmissions bear greater importance for the spread of the higher virulence strains. But, though there are scenarios in which ART might cause a substantial effect in the long run, the effects on the timescales that we are concerned with are small. Finally, we emphasise that we believe the effects of ART on virulence are far outweighed by the benefits of treatment both to the individuals being treated and in terms of halting onward transmission to others [374, 375]. The overall effect of widespread ART is to decrease the numbers of people dying from AIDS. What fraction of those people died from high virulence infections is of secondary importance.

5.4 Questions addressed in this chapter

- What are the expected patterns of virulence change in the initial decades of an epidemic?

  We would expect an initial, somewhat transient increase in virulence during the first decades of an epidemic, irrespective of the evolutionarily stable value of virulence (Figure 5.3 and Figure C.13; section 5.4.2)

- Could administration of ART drive changes in virulence evolution?

  Yes. The administration of ART based on CD4 count threshold could drive eventual increases or decreases in virulence (Figures 5.3 and 5.5; section 5.4.3)

- What is the potential size and direction of any ART-effect?

  In the short term (on the timescale of decades), the ART-effect is likely to be small (in comparison to the fluctuations in virulence that would be expected in the absence of ART) and towards lesser virulence (Figures 5.5 and 5.6; Table 5.2; section 5.4.6).

- How does the effect vary according to different possible treatment guidelines?

  If ART is administered so that it is initiated upon diagnosis (or rather, if initiation time is independent of disease progression), then ART exerts an upward pressure on virulence in the long term. In the short term, the magnitude of the effect is similar to that for treatment based on CD4 count. However, ART can exert a short-term upward pressure on virulence if initiation is years into infection on average (Figures C.9 and C.10).

- Should these results alter how we treat?

  No. I believe that the effects of ART on virulence are far outweighed by the benefits of treatment, both the benefits to the treated individual and the positive impact of treatment as prevention.

6

Conclusion

In this thesis I have looked at three mechanisms or phenomena relating to drug-free control of HIV within infected individuals. What have we learnt, as a result of this work, about prospects for viral control? In Chapter 3 I found that across a large cohort of HIV-1 subtype B infected individuals, immune escape from $CD8^+$ T-cell responses was on average strikingly rare. Although we only studied previously characterised epitopes, we have good reason to expect that these are the most consistently targetted. The important question that this work feeds into is, how much are CTLs responsible for or capable of viral control? Data on the incidence and prevalence of CTL escape can be used to address this question in several ways. Firstly, rates of CTL killing have been estimated from escape rates and then used to quantify the contribution that this killing makes to infected cell clearance. In a recent review, Gadhamasetty et al conclude that CTL-mediated killing rates remain unknown [136]. The data presented in this thesis adds crucial information to this discussion; rare escape across the cohort as a whole despite the presence of detectable $CD8^+$ T-cell responses implies lower rates of CTL killing than those that have been estimated from patients with particularly frequent, early escape. Secondly, the question may be addressed by looking at the relationship between viral load and incident escape events, or between escape and disease progression. The study presented in Chapter 3 was underpowered to examine this relationship, however a recent analysis of longitudinal samples from a Zambian transmission pairs cohort showed that increasing adaptation to the host HLA profile significantly predicted subsequent increases in viral load [111]. This analysis also found that the extent to which the transmitted viral strain was adapted to the recipient's HLA alleles was predictive of disease progression, as measured by CD4 decline [111].

The question may also be addressed using assays that seek to measure the strength or quality of the CTL response directly. Routinely used measures of the strength of the response have been unable to explain the majority of the inter-patient variation in viral load and disease progression. However, this may be more of a reflection of the quality of the assays than the quality of the response. Assays poorly reflecting *in vivo* CTL strength could also account for the failure of vaccine candidates that initially seemed to elicit a 'strong' response [376]. Measures such as viral inhibition assays, that have been found to significantly correlate with $CD4^+$ T-cell decline, should be used more widely [124].

The accumulated evidence shows that the $CD8^+$ T-cell response has a significant and measurable role in viral control. However, so far, reliably moving individuals from non-controller to controller status with the use of preventative or therapeutic CTL-based vaccines has not been possible. Additionally, we know that the prevalence of CTL escape mutations in circulating viral strains is increasing, albeit slowly [182] (indeed, high prevalence of transmitted escape was observed in the data presented in chapter 3). Consequently, eliciting an effective CTL response against circulating virus will be an increasing challenge for vaccine design.

In Chapter 4 I showed that aspects of HIV reservoir 'quality', such as the distribution of expected times to activation of latently infected cells, could be important for post-treatment control. This first model of the impact of reservoir quality on post treatment control highlights the need for more precise data on reservoir dynamics (and, given inter-patient variability, lots of it). In particular, this work suggests that assays directly or indirectly measuring the size of the true HIV reservoir, as well as assays for per-cell viral activation probability, could be key. Yet even with our current level of understanding it is clear that new technologies will be needed to increase the number of patients who are able to control post-treatment. Results from trials of kick and kill therapies have so far not been promising. However, novel technologies aimed at reducing the reservoir or permanently silencing latent infections may have more chance of targetting the reservoir without resulting in new rounds of infection or encouraging proliferation of latently infected cells. Trials for new interventions, assay development and data collection should be undertaken alongside theoretical modelling work. In this way, mechanistic explanations for variation in the duration of post-treatment control can be developed and used to refine predictions

of time to viral rebound based on clinical markers at treatment interruption.

In Chapter 5 I made two important points that challenge intuitive ideas about expected trends in virulence: (1) an increase in virulence in the early stages of an epidemic will not necessarily be maintained, even in the absence of any change in external factors. (2) administering suppressive ART to the sickest individuals could place a small downwards *or* upwards pressure on virulence evolution in the long term – the effect depends on the relative importance of low CD4 transmissions. Two recent publications refine our expectation of the quantitative changes in set point viral load that may be seen within the next decades [191, 373]. The combined implications of these studies and my own work are that, while ART may result in selection for increased virulence at the population level, the overall effect of ART on the epidemic is still positive, resulting in decreased incidence and far fewer AIDS-related deaths. Also, decreasing virulence trends are now being observed and may aid efforts to control the epidemic, but predictions do not suggest that spontaneous HIV controllers will become anything more than a minority at any point in the foreseeable future. The development of interventions for viral control within infected individuals will still be necessary. Claims that the virus is becoming less virulent should be made with caution, lest they discourage the use of ART or hinder our efforts elsewhere.

In summary, I believe that the next major step forward for aiding viral control at the individual level is most likely to come from the development of novel methods to reduce the latent reservoir or permanently silence the provirus. These will need to be combined with early initiation of ART and be supported by better assays for measuring the true HIV reservoir. While a strengthened immune response may be able to play a role, it is still unclear what determines a reliably 'strong' response, and methods such as reversing immune exhaustion come with additional risks to the patient.

Finally, what relevance do these aspects of control in the individual have for tackling the HIV epidemic as a whole? More specifically, if post-treatment control were achievable in a majority of patients, what effect might this have on epidemic control? The Sustainable Development Goals (SDGs) contain a target for ending the HIV epidemic by 2030 [80]. In order to achieve this, UNAIDS has set an interim goal that involves 90% of people living with HIV knowing their status and 90% of those receiving ART, by 2020 [80]. The main barrier to achieving this goal will be the challenge of increasing the proportion

of individuals that know they are infected; this currently stands at around 50%. The development of new drugs or technologies for viral control could help increase the fraction of individuals knowing their status if it removed some of the stigma associated with HIV and encouraged voluntary testing, however it is unlikely to come soon enough to aid in achieving the SDGs. The extent to which such treatments would have a beneficial effect on epidemic control would also depend upon the probability of a functionally 'cured' patient becoming reinfected. In any case, whether or not the SDGs goals are achieved, we are looking at a situation extending decades into the future in which many millions of individuals will be receiving life-long ART. Given the chronic complications seen in ageing ART-treated individuals and the burden this places on the health systems of developing countries, the advent of a steralising cure or drug-free remission would be of huge benefit to managing the epidemic.

Bibliography

1. Joint United Nations Programme on HIV/AIDS (UNAIDS) (2016). Fact Sheet 2016. Available: `http://www.unaids.org/en/resources/fact-sheet`.

2. Fauci AS (1988) The human immunodeficiency virus: infectivity and mechanisms of pathogenesis. Science 239: 6l7–22.

3. World Health Organization (2015). Guideline on when to start antiretroviral therapy and on pre-exposure prophylaxis for HIV. Available: `http://www.who.int/hiv/pub/guidelines/earlyrelease-arv/en/`.

4. May MT, Gompels M, Delpech V, Porter K, Orkin C, et al. (2014) Impact on life expectancy of HIV-1 positive individuals of CD4+ cell count and viral load response to antiretroviral therapy. AIDS 28: 1193–1202.

5. Naik S, Das B (2016) New WHO Guidelines: Implications on Therapeutics and Monitoring of HIV Infections. HIV: Current Research 2016.

6. Finzi D, Blankson J, Siliciano JD, Margolick JB, Chadwick K, et al. (1999) Latent infection of CD4+ T cells provides a mechanism for lifelong persistence of HIV-1, even in patients on effective combination therapy. Nat Med 5: 512–517.

7. Oxenius A, Price DA, Günthard HF, Dawson SJ, Fagard C, et al. (2002) Stimulation of HIV-specific cellular immunity by structured treatment interruption fails to enhance viral control in chronic HIV infection. Proc Natl Acad Sci USA 99: 13747–13752.

8. SPARTAC Trial Investigators, et al (2013) Short-course antiretroviral therapy in primary HIV infection. N Engl J Med 2013: 207–217.

9. Allers K, Hütter G, Hofmann J, Loddenkemper C, Rieger K, et al. (2011) Evidence for the cure of HIV infection by CCR5Δ32/Δ32 stem cell transplantation. Blood 117: 2791–2799.

10. Deeks SG, Walker BD (2007) Human immunodeficiency virus controllers: mechanisms of durable virus control in the absence of antiretroviral therapy. Immunity 27: 406–416.

11. Sáez-Cirión A, Bacchus C, Hocqueloux L, Avettand-Fenoel V, Girault I, et al. (2013) Post-treatment HIV-1 controllers with a long-term virological remission after the interruption of early initiated antiretroviral therapy ANRS VISCONTI Study. PLoS Pathog 9: e1003211.

12. Okulicz JF, Marconi VC, Landrum ML, Wegner S, Weintrob A, et al. (2009) Clinical outcomes of elite controllers, viremic controllers, and long-term nonprogressors in the US Department of Defense HIV natural history study. J Infect Dis 200: 1714–1723.

13. Pereyra F, Addo MM, Kaufmann DE, Liu Y, Miura T, et al. (2008) Genetic and immunologic heterogeneity among persons who control HIV infection in the absence of therapy. J Infect Dis 197: 563–571.

14. O'Connell KA, Bailey JR, Blankson JN (2009) Elucidating the elite: mechanisms of control in HIV-1 infection. Trends in Pharmacological Sciences 30: 631–637.

15. Phillips RE, Rowland-Jones S, Nixon DF, Gotch FM, Edwards JP, et al. (1991) Human immunodeficiency virus genetic variation that can escape cytotoxic T cell recognition. Nature 354: 453–459.

16. Price DA, Goulder PJ, Klenerman P, Sewell AK, Easterbrook PJ, et al. (1997) Positive selection of HIV-1 cytotoxic T lymphocyte escape variants during primary infection. Proc Natl Acad Sci USA 94: 1890–1895.

17. Kelleher AD, Long C, Holmes EC, Allen RL, Wilson J, et al. (2001) Clustered mutations in HIV-1 gag are consistently required for escape from HLA-B27–restricted cytotoxic T lymphocyte responses. J Exp Med 193: 375–386.

18. Geels MJ, Jansen CA, Baan E, De Cuyper IM, van Schijndel GJ, et al. (2006) CTL escape and increased viremia irrespective of HIV-specific CD4+ T-helper responses in two HIV-infected individuals. Virology 345: 209–219.

19. Finzi D, Hermankova M, Pierson T, Carruth LM, Buck C, et al. (1997) Identification of a reservoir for HIV-1 in patients on highly active antiretroviral therapy. Science 278: 1295–1300.

20. Lorenzo-Redondo R, Fryer HR, Bedford T, Kim EY, Archer J, et al. (2016) Persistent HIV-1 replication maintains the tissue reservoir during therapy. Nature 530: 51–56.

21. Thornhill J, Frater J, Fidler S (2015) Post-treatment control: a functional cure for HIV. Future Virology 10: 1245–1256.

22. Williams JP, Hurst J, Stöhr W, Robinson N, Brown H, et al. (2014) HIV-1 DNA predicts disease progression and post-treatment virological control. eLife 3: e03821.

23. Li JZ, Etemad B, Ahmed H, Aga E, Bosch RJ, et al. (2016) The size of the expressed HIV reservoir predicts timing of viral rebound after treatment interruption. AIDS 30: 343–353.

24. Faria NR, Rambaut A, Suchard MA, Baele G, Bedford T, et al. (2014) The early spread and epidemic ignition of HIV-1 in human populations. Science 346: 56–61.

25. Fraser C, Hollingsworth TD, Chapman R, de Wolf F, Hanage WP (2007) Variation in HIV-1 set-point viral load: epidemiological analysis and an evolutionary hypothesis. Proc Natl Acad Sci USA 104: 17441–17446.

26. Kløverpris HN, Leslie A, Goulder P (2016) Role of HLA Adaptation in HIV Evolution. Frontiers in Immunology 6: 665.

27. Ferrari G, Korber B, Goonetilleke N, Liu MK, Turnbull EL, et al. (2011) Relationship between functional profile of HIV-1 specific CD8 T cells and epitope variability with the selection of escape mutants in acute HIV-1 infection. PLoS Pathog 7: e1001273.

28. Fischer W, Ganusov VV, Giorgi EE, Hraber PT, Keele BF, et al. (2010) Transmission of single HIV-1 genomes and dynamics of early immune escape revealed by ultra-deep sequencing. PLoS One 5: e12303.

29. Jones NA, Wei X, Flower DR, Wong M, Michor F, et al. (2004) Determinants of human immunodeficiency virus type 1 escape from the primary CD8+ cytotoxic T lymphocyte response. J Exp Med 200: 1243–1256.

30. Liu Y, McNevin J, Cao J, Zhao H, Genowati I, et al. (2006) Selection on the human immunodeficiency virus type 1 proteome following primary infection. J Virol 80: 9519–9529.

31. Salazar-Gonzalez JF, Salazar MG, Keele BF, Learn GH, Giorgi EE, et al. (2009) Genetic identity, biological phenotype, and evolutionary pathways of transmitted/founder viruses in acute and early HIV-1 infection. J Exp Med 206: 1273–1289.

32. Eriksson S, Graf EH, Dahl V, Strain MC, Yukl SA, et al. (2013) Comparative analysis of measures of viral reservoirs in HIV-1 eradication studies. PLoS Pathog 9: e1003174.

33. Svicher V, Ceccherini-Silberstein F, Antinori A, Aquaro S, Perno CF (2014) Understanding HIV compartments and reservoirs. Current HIV/AIDS Reports 11: 186–194.

34. Alizon S, Hurford A, Mideo N, Van Baalen M (2009) Virulence evolution and the trade-off hypothesis: history, current state of affairs and the future. J Evol Biol 22: 245–259.

35. Herbeck JT, Müller V, Maust BS, Ledergerber B, Torti C, et al. (2012) Is the virulence of HIV changing? A meta-analysis of trends in prognostic markers of HIV disease progression and transmission. AIDS 26: 193.

36. Roberts HE, Hurst J, Robinson N, Brown H, Flanagan P, et al. (2015) Structured observations reveal slow HIV-1 CTL escape. PLoS Genet 11: e1004914.

37. Roberts HE, Goulder PJ, McLean AR (2015) The impact of antiretroviral therapy on population-level virulence evolution of HIV-1. J R Soc Interface 12: 20150888.

38. Gallo RC, Montagnier L (2003) The discovery of HIV as the cause of AIDS. N Engl J Med 349: 2283–2285.

39. Hemelaar J (2012) The origin and diversity of the HIV-1 pandemic. Trends Mol Med 18: 182–192.

40. Quinn TC (1996) Global burden of the HIV pandemic. Lancet 348: 99–106.

41. Gouws E, Cuchi P (2012) Focusing the HIV response through estimating the major modes of HIV transmission: a multi-country analysis. Sexually Transmitted Infections 88: i76–i85.

42. Campbell-Yesufu OT, Gandhi RT (2011) Update on human immunodeficiency virus (HIV)-2 infection. Clin Infect Dis 52: 780–787.

43. Foley B, Pan H, Buchbinder S, Delwart E (2000) Apparent founder effect during the early years of the San Francisco HIV type 1 epidemic (1978-1979). AIDS Research and Human Retroviruses 16: 1463–1469.

44. Osmanov S, Pattou C, Walker N, Schwardländer B, Esparza J (2002) Estimated global distribution and regional spread of HIV-1 genetic subtypes in the year 2000. J Acquir Immune Defic Syndr 29: 184–190.

45. Hemelaar J, Gouws E, Ghys PD, Osmanov S, et al. (2011) Global trends in molecular epidemiology of HIV-1 during 2000–2007. AIDS 25: 679.

46. Walker PR, Pybus OG, Rambaut A, Holmes EC (2005) Comparative population dynamics of HIV-1 subtypes B and C: subtype-specific differences in patterns of epidemic growth. Infection, Genetics and Evolution 5: 199–208.

47. Abecasis AB, Wensing AM, Paraskevis D, Vercauteren J, Theys K, et al. (2013) HIV-1 subtype distribution and its demographic determinants in newly diagnosed patients in Europe suggest highly compartmentalized epidemics. Retrovirology 10: 1.

48. Selik RM, Haverkos HW, Curran JW (1984) Acquired immune deficiency syndrome (AIDS) trends in the United States, 1978–1982. The American Journal of Medicine 76: 493–500.

49. Joint United Nations Programme on HIV/AIDS (UNAIDS) and World Health Organization (2003). AIDS Epidemic Update 2003. Available: http://www.who.int/hiv/pub/epidemiology/epi2003/en/.

50. Abraha A, Nankya IL, Gibson R, Demers K, Tebit DM, et al. (2009) CCR5-and CXCR4-tropic subtype C human immunodeficiency virus type 1 isolates have a lower level of pathogenic fitness than other dominant group M subtypes: implications for the epidemic. J Virol 83: 5592–5605.

51. Murray CJ, Vos T, Lozano R, Naghavi M, Flaxman AD, et al. (2013) Disability-adjusted life years (DALYs) for 291 diseases and injuries in 21 regions, 1990–2010: a systematic analysis for the Global Burden of Disease Study 2010. Lancet 380: 2197–2223.

52. Buvé A, Bishikwabo-Nsarhaza K, Mutangadura G (2002) The spread and effect of HIV-1 infection in sub-Saharan Africa. Lancet 359: 2011–2017.

53. Joint United Nations Programme on HIV/AIDS (UNAIDS) (2010). Global report: UNAIDS report on the global AIDS epidemic 2010. Available: http://www.unaids.org/globalreport/Global_report.htm.

54. Joint United Nations Programme on HIV/AIDS (UNAIDS) (2016). AIDS by the numbers. Available: http://www.unaids.org/en/resources/documents/2016/AIDS-by-the-numbers.

55. Joint United Nations Programme on HIV/AIDS (UNAIDS) (2013). Global report: UNAIDS report on the global AIDS epidemic 2013. Available: http://www.who.int/hiv/pub/me/unaids_global_report/en/.

56. Joint United Nations Programme on HIV/AIDS (UNAIDS) (2013). Location, location: Connecting people to faster HIV services. Available: http://www.unaids.org/en/resources/documents/2013/location-location.

57. Joint United Nations Programme on HIV/AIDS (UNAIDS) (2016). Global AIDS update 2016. Available: `http://www.unaids.org/en/resources/documents/2016/Global-AIDS-update-2016`.

58. Ross DA (2010) Behavioural interventions to reduce HIV risk: what works? AIDS 24: S4–S14.

59. Potts M, Halperin DT, Kirby D, Swidler A, Marseille E, et al. (2008) Rethinking HIV prevention: Public health. Science 320: 749.

60. Stoneburner RL, Low-Beer D (2004) Population-level HIV declines and behavioral risk avoidance in Uganda. Science 304: 714–718.

61. Gray RH, Serwadda D, Kigozi G, Nalugoda F, Wawer MJ (2006) Uganda?s HIV prevention success: The role of sexual behavior change and the national response. Commentary on Green et al.(2006). AIDS and Behavior 10: 347–350.

62. Green EC, Halperin DT, Nantulya V, Hogle JA (2006) Uganda's HIV prevention success: the role of sexual behavior change and the national response. AIDS and Behavior 10: 335–346.

63. Shelton JD, Thomas G, Kongolo M, Bojuwoye O, Singh N, et al. (2006) Confessions of a condom lover. Lancet 368: 1947–1949.

64. Hallett TB, Gregson S, Mugurungi O, Gonese E, Garnett GP (2009) Assessing evidence for behaviour change affecting the course of HIV epidemics: a new mathematical modelling approach and application to data from Zimbabwe. Epidemics 1: 108–117.

65. Gregson S, Garnett GP, Nyamukapa CA, Hallett TB, Lewis JJ, et al. (2006) HIV decline associated with behavior change in eastern Zimbabwe. Science 311: 664–666.

66. Katz MH (1997) AIDS epidemic in San Francisco among men who report sex with men: successes and challenges of HIV prevention. J Acquir Immune Defic Syndr 14: S38–S46.

67. Morin SF, Vernon K, Harcourt JJ, Steward WT, Volk J, et al. (2003) Why HIV infections have increased among men who have sex with men and what to do about it: Findings from California focus groups. AIDS and Behavior 7: 353–362.

68. Winkelstein Jr W, Samuel M, Padian NS, Wiley JA, Lang W, et al. (1987) The San Francisco Men's Health Study: III. Reduction in human immunodeficiency virus transmission among homosexual/bisexual men, 1982-86. American Journal of Public Health 77: 685–689.

69. Joint United Nations Programme on HIV/AIDS (UNAIDS), et al. (1999). Trends in HIV Incidence and Prevalence: Natural Course of the Epidemic Or Results of Behavioural Change? Available: `http://www.who.int/hiv/strategic/surveillance/pubincprev/en/`.

70. Day TA, Kublin JG (2013) Lessons learned from HIV vaccine clinical efficacy trials. Curr HIV Res 11: 441–449.

71. Gilbert PB, Berger JO, Stablein D, Becker S, Essex M, et al. (2011) Statistical interpretation of the RV144 HIV vaccine efficacy trial in Thailand: a case study for statistical issues in efficacy trials. J Infect Dis 203: 969–975.

72. Attia S, Egger M, Müller M, Zwahlen M, Low N (2009) Sexual transmission of HIV according to viral load and antiretroviral therapy: systematic review and meta-analysis. AIDS 23: 1397–1404.

73. Donnell D, Baeten JM, Kiarie J, Thomas KK, Stevens W, et al. (2010) Heterosexual HIV-1 transmission after initiation of antiretroviral therapy: a prospective cohort analysis. Lancet 375: 2092–2098.

74. Cohen MS, Chen YQ, McCauley M, Gamble T, Hosseinipour MC, et al. (2016) Antiretroviral therapy for the prevention of HIV-1 transmission. N Engl J Med 375: 830–839.

75. Joint United Nations Programme on HIV/AIDS (UNAIDS) (Accessed Oct. 2016) World DataBank: World Development Indicators. http://dataworldbankorg/indicator/SHHIVARTCZS?contextual=region .

76. Montaner JS, Lima VD, Harrigan PR, Lourenço L, Yip B, et al. (2014) Expansion of HAART coverage is associated with sustained decreases in HIV/AIDS morbidity, mortality and HIV transmission: the 'HIV Treatment as Prevention' experience in a Canadian setting. PLoS One 9: e87872.

77. Tanser F, Bärnighausen T, Grapsa E, Zaidi J, Newell ML (2013) High coverage of ART associated with decline in risk of HIV acquisition in rural KwaZulu-Natal, South Africa. Science 339: 966–971.

78. Eaton JW, Menzies NA, Stover J, Cambiano V, Chindelevitch L, et al. (2014) Health benefits, costs, and cost-effectiveness of earlier eligibility for adult antiretroviral therapy and expanded treatment coverage: a combined analysis of 12 mathematical models. The Lancet Global Health 2: e23–e34.

79. Joint United Nations Programme on HIV/AIDS (UNAIDS) (2016). Prevention gap report. Available: `http://www.unaids.org/en/resources/documents/2016/prevention-gap`.

80. Joint United Nations Programme on HIV/AIDS (UNAIDS) (2015). On the Fast-Track to end AIDS. Available: `http://www.unaids.org/en/resources/documents/2015/UNAIDS_PCB37_15-18`.

81. Sawires SR, Dworkin SL, Fiamma A, Peacock D, Szekeres G, et al. (2007) Male circumcision and HIV/AIDS: challenges and opportunities. Lancet 369: 708.

82. Coates TJ, Richter L, Caceres C (2008) Behavioural strategies to reduce HIV transmission: how to make them work better. Lancet 372: 669–684.

83. Deeks SG, Lewin SR, Havlir DV (2013) The end of AIDS: HIV infection as a chronic disease. Lancet 382: 1525–1533.

84. Sattentau QJ, Weiss RA (1988) The CD4 antigen: physiological ligand and HIV receptor. Cell 52: 631–633.

85. Wilen CB, Tilton JC, Doms RW (2012) HIV: cell binding and entry. Cold Spring Harbor Perspectives in Medicine 2: a006866.

86. Laskey SB, Siliciano RF (2014) A mechanistic theory to explain the efficacy of antiretroviral therapy. Nature Reviews Microbiology 12: 772–780.

87. McMichael AJ, Borrow P, Tomaras GD, Goonetilleke N, Haynes BF (2010) The immune response during acute HIV-1 infection: clues for vaccine development. Nat Rev Immunol 10: 11–23.

88. Fiebig EW, Wright DJ, Rawal BD, Garrett PE, Schumacher RT, et al. (2003) Dynamics of HIV viremia and antibody seroconversion in plasma donors: implications for diagnosis and staging of primary HIV infection. AIDS 17: 1871–1879.

89. Ananworanich J, Fletcher JL, Pinyakorn S, Van Griensven F, Vandergeeten C, et al. (2013) A novel acute HIV infection staging system based on 4 th generation immunoassay. Retrovirology 10: 56.

90. Mellors JW, Rinaldo Jr CR, Gupta P, White RM, et al. (1996) Prognosis in HIV-1 infection predicted by the quantity of virus in plasma. Science 272: 1167.

91. de Wolf F, Spijkerman I, Schellekens PT, Langendam M, Kuiken C, et al. (1997) AIDS prognosis based on HIV-1 RNA, CD4+ T-cell count and function: markers with reciprocal predictive value over time after seroconversion. AIDS 11: 1799–1806.

92. Mclean KA, Holmes DA, Evans BA, McAlpine L, Thorp R, et al. (1990) Rapid clinical and laboratory progression of HIV infection. AIDS 4: 369–370.

93. Walker BD, Xu GY (2013) Unravelling the mechanisms of durable control of HIV-1. Nat Rev Immunol 13: 487–498.

94. Gurdasani D, Iles L, Dillon DG, Young EH, Olson AD, et al. (2014) A systematic review of definitions of extreme phenotypes of HIV control and progression. AIDS 28: 149–162.

95. Hill AL, Rosenbloom DI, Nowak MA (2012) Evolutionary dynamics of HIV at multiple spatial and temporal scales. Journal of Molecular Medicine 90: 543–561.

96. Ribeiro RM, Mohri H, Ho DD, Perelson AS (2002) In vivo dynamics of T cell activation, proliferation, and death in HIV-1 infection: why are CD4+ but not CD8+ T cells depleted? Proc Natl Acad Sci USA 99: 15572–15577.

97. Sousa AE, Carneiro J, Meier-Schellersheim M, Grossman Z, Victorino RM (2002) CD4 T cell depletion is linked directly to immune activation in the pathogenesis of HIV-1 and HIV-2 but only indirectly to the viral load. J Immunol 169: 3400–3406.

98. Chiu YL, Soros VB, Kreisberg JF, Stopak K, Yonemoto W, et al. (2005) Cellular APOBEC3G restricts HIV-1 infection in resting CD4+ T cells. Nature 435: 108–114.

99. Zinkernagel RM, Doherty PC (1974) Immunological surveillance against altered self components by sensitised T lymphocytes in lymphocytes choriomeningitis. Nature 251: 547–548.

100. Townsend A, Bodmer H (1989) Antigen recognition by class I-restricted T lymphocytes. Annual Review of Immunology 7: 601–624.

101. Rock KL, Goldberg AL (1999) Degradation of cell proteins and the generation of MHC class I-presented peptides. Annual Review of Immunology 17: 739–779.

102. Rudensky AY, Preston-Hurlburt P, Hong SC, Barlow A, Janeway CA (1991) Sequence analysis of peptides bound to MHC class II molecules. Nature 353: 622–627.

103. Carmichael A, Jin X, Sissons P, Borysiewicz L (1993) Quantitative analysis of the human immunodeficiency virus type 1 (HIV-1)-specific cytotoxic T lymphocyte (CTL) response at different stages of HIV-1 infection: differential CTL responses to HIV-1 and Epstein-Barr virus in late disease. J Exp Med 177: 249–256.

104. Borrow P, Lewicki H, Hahn BH, Shaw GM, Oldstone M (1994) Virus-specific CD8+ cytotoxic T-lymphocyte activity associated with control of viremia in primary human immunodeficiency virus type 1 infection. J Virol 68: 6103–6110.

105. Koup R, Safrit JT, Cao Y, Andrews CA, McLeod G, et al. (1994) Temporal association of cellular immune responses with the initial control of viremia in primary human immunodeficiency virus type 1 syndrome. J Virol 68: 4650–4655.

106. Hoffenbach A, Langlade-Demoyen P, Dadaglio G, Vilmer E, Michel F, et al. (1989) Unusually high frequencies of HIV-specific cytotoxic T lymphocytes in humans. J Immunol 142: 452–462.

107. Oxenius A, Fidler S, Brady M, Dawson SJ, Ruth K, et al. (2001) Variable fate of virus-specific CD4+ T cells during primary HIV-1 infection. Eur J Immunol 31: 3782–3788.

108. Gloster SE, Newton P, Cornforth D, Lifson JD, Williams I, et al. (2004) Association of strong virus-specific CD4 T cell responses with efficient natural control of primary HIV-1 infection. AIDS 18: 749–755.

109. Walker B, McMichael A (2012) The T-cell response to HIV. Cold Spring Harbor Perspectives in Medicine 2: a007054.

110. Carrington M, O'Brien SJ (2003) The Influence of HLA Genotype on AIDS. Annual Review of Medicine 54: 535–551.

111. Carlson JM, Du VY, Pfeifer N, Bansal A, Tan VY, et al. (2016) Impact of pre-adapted HIV transmission. Nat Med 22: 606–613.

112. Frater J, Ewings F, Hurst J, Brown H, Robinson N, et al. (2014) HIV-1-specific CD4+ responses in primary HIV-1 infection predict disease progression. AIDS 28: 699–708.

113. Fox A, Wolbers M, Hang NLK, Thai PQ, Yen NTT, et al. (2015) Hemagglutination inhibiting antibodies and protection against seasonal and pandemic influenza infection. Journal of Infection 70: 187–196.

114. Hedestam GBK, Fouchier RA, Phogat S, Burton DR, Sodroski J, et al. (2008) The challenges of eliciting neutralizing antibodies to HIV-1 and to influenza virus. Nature Reviews Microbiology 6: 143–155.

115. Richman DD, Wrin T, Little SJ, Petropoulos CJ (2003) Rapid evolution of the neutralizing antibody response to HIV type 1 infection. Proc Natl Acad Sci USA 100: 4144–4149.

116. Tomaras GD, Haynes BF (2009) HIV-1-specific antibody responses during acute and chronic HIV-1 infection. Current Opinion in HIV and AIDS 4: 373.

117. Tomaras GD, Yates NL, Liu P, Qin L, Fouda GG, et al. (2008) Initial B-cell responses to transmitted human immunodeficiency virus type 1: virion-binding immunoglobulin M (IgM) and IgG antibodies followed by plasma anti-gp41 antibodies with ineffective control of initial viremia. J Virol 82: 12449–12463.

118. Wikramaratna PS, Lourenço J, Klenerman P, Pybus OG, Gupta S (2015) Effects of neutralizing antibodies on escape from CD8+ T-cell responses in HIV-1 infection. Phil Trans R Soc B 370: 20140290.

119. Huang KHG, Bonsall D, Katzourakis A, Thomson EC, Fidler SJ, et al. (2010) B-cell depletion reveals a role for antibodies in the control of chronic HIV-1 infection. Nature Communications 1: 102.

120. Douek DC, Brenchley JM, Betts MR, Ambrozak DR, Hill BJ, et al. (2002) HIV preferentially infects HIV-specific CD4+ T cells. Nature 417: 95–98.

121. Schmitz JE, Kuroda MJ, Santra S, Sasseville VG, Simon MA, et al. (1999) Control of viremia in simian immunodeficiency virus infection by CD8+ lymphocytes. Science 283: 857–860.

122. Addo M, Yu X, Rathod A, Cohen D, Eldridge R, et al. (2003) Comprehensive epitope analysis of human immunodeficiency virus type 1 (HIV-1)-specific T-cell responses directed against the entire expressed HIV-1 genome demonstrate broadly directed responses, but no correlation to viral load. J Virol 77: 2081–2092.

123. Phillips AN (1996) Reduction of HIV concentration during acute infection: independence from a specific immune response. Science 271: 497.

124. Yang H, Wu H, Hancock G, Clutton G, Sande N, et al. (2012) Antiviral inhibitory capacity of CD8+ T cells predicts the rate of CD4+ T-cell decline in HIV-1 infection. J Infect Dis 206: 552–561.

125. Migueles SA, Osborne CM, Royce C, Compton AA, Joshi RP, et al. (2008) Lytic granule loading of CD8+ T cells is required for HIV-infected cell elimination associated with immune control. Immunity 29: 1009–1021.

126. Hersperger AR, Pereyra F, Nason M, Demers K, Sheth P, et al. (2010) Perforin expression directly ex vivo by HIV-specific CD8+ T-cells is a correlate of HIV elite control. PLoS Pathog 6: e1000917.

127. Kiepiela P, Ngumbela K, Thobakgale C, Ramduth D, Honeyborne I, et al. (2007) CD8+ T-cell responses to different HIV proteins have discordant associations with viral load. Nat Med 13: 46–53.

128. Streeck H, Jolin JS, Qi Y, Yassine-Diab B, Johnson RC, et al. (2009) Human immunodeficiency virus type 1-specific CD8+ T-cell responses during primary infection are major determinants of the viral set point and loss of CD4+ T cells. J Virol 83: 7641–7648.

129. Fellay J, Shianna KV, Ge D, Colombo S, Ledergerber B, et al. (2007) A whole-genome association study of major determinants for host control of HIV-1. Science 317: 944–947.

130. Gao X, Nelson GW, Karacki P, Martin MP, Phair J, et al. (2001) Effect of a single amino acid change in MHC class I molecules on the rate of progression to AIDS. N Engl J Med 344: 1668–1675.

131. Scherer A, Frater J, Oxenius A, Agudelo J, Price DA, et al. (2004) Quantifiable cytotoxic T lymphocyte responses and HLA-related risk of progression to AIDS. Proc Natl Acad Sci USA 101: 12266–12270.

132. Emu B, Sinclair E, Hatano H, Ferre A, Shacklett B, et al. (2008) HLA class I-restricted T-cell responses may contribute to the control of human immunodeficiency virus infection, but such responses are not always necessary for long-term virus control. J Virol 82: 5398–5407.

133. Asquith B, Edwards CT, Lipsitch M, McLean AR (2006) Inefficient cytotoxic T lymphocyte–mediated killing of HIV-1–infected cells in vivo. PLoS Biol 4: e90.

134. Goonetilleke N, Liu MK, Salazar-Gonzalez JF, Ferrari G, Giorgi E, et al. (2009) The first T cell response to transmitted/founder virus contributes to the control of acute viremia in HIV-1 infection. J Exp Med 206: 1253–1272.

135. Liu D, Zuo T, Hora B, Song H, Kong W, et al. (2014) Preexisting compensatory amino acids compromise fitness costs of a HIV-1 T cell escape mutation. Retrovirology 11: 1.

136. Gadhamsetty S, Beltman JB, De Boer RJ (2015) What do mathematical models tell us about killing rates during HIV-1 infection? Immunology Letters 168: 1–6.

137. Wong JK, Strain MC, Porrata R, Reay E, Sankaran-Walters S, et al. (2010) In vivo CD8+ T-cell suppression of SIV viremia is not mediated by CTL clearance of productively infected cells. PLoS Pathog 6: e1000748.

138. Oxenius A, McLean AR, Fischer M, Price DA, Dawson SJ, et al. (2002) Human immunodeficiency virus-specific CD8+ T-cell responses do not predict viral growth and clearance rates during structured intermittent antiretroviral therapy. J Virol 76: 10169–10176.

139. Freel SA, Saunders KO, Tomaras GD (2011) CD8+ T-cell-mediated control of HIV-1 and SIV infection. Immunologic Research 49: 135–146.

140. Los Alamos National Laboratory HIV Database (Accessed Oct 2016) Landmarks of the HIV genome. HIV sequence database https://www.hiv.lanl.gov/content/sequence/HIV/MAP/landmark.html.

141. Wain-Hobson S, Sonigo P, Danos O, Cole S, Alizon M (1985) Nucleotide sequence of the AIDS virus, LAV. Cell 40: 9–17.

142. Mansky LM (1996) Forward Mutation Rate of Human Immunodeficiency Virus Type 1 in a T Lymphoid Cell Line. AIDS Research and Human Retroviruses 12: 307–314.

143. Perelson AS, Neumann AU, Markowitz M, Leonard JM, Ho DD (1996) HIV-1 dynamics in vivo: virion clearance rate, infected cell life-span, and viral generation time. Science 271: 1582.

144. Henn MR, Boutwell CL, Charlebois P, Lennon NJ, Power KA, et al. (2012) Whole genome deep sequencing of HIV-1 reveals the impact of early minor variants upon immune recognition during acute infection. PLoS Pathog 8: e1002529.

145. Neher RA, Leitner T (2010) Recombination rate and selection strength in HIV intra-patient evolution. PLoS Comput Biol 6: e1000660.

146. Zanini F, Brodin J, Thebo L, Lanz C, Bratt G, et al. (2015) Population genomics of intrapatient HIV-1 evolution. eLife 4: e11282.

147. Wood N, Bhattacharya T, Keele BF, Giorgi E, Liu M, et al. (2009) HIV evolution in early infection: selection pressures, patterns of insertion and deletion, and the impact of APOBEC. PLoS Pathog 5: e1000414.

148. Kim EY, Bhattacharya T, Kunstman K, Swantek P, Koning FA, et al. (2010) Human APOBEC3G-mediated editing can promote HIV-1 sequence diversification and accelerate adaptation to selective pressure. J Virol 84: 10402–10405.

149. Ciurea A, Hunziker L, Martinic MM, Oxenius A, Hengartner H, et al. (2001) CD4+ T-cell–epitope escape mutant virus selected in vivo. Nat Med 7: 795–800.

150. Harcourt GC, Garrard S, Davenport MP, Edwards A, Phillips RE (1998) HIV-1 variation diminishes CD4 T lymphocyte recognition. J Exp Med 188: 1785–1793.

151. Erdmann N, Du VY, Carlson J, Schaefer M, Jureka A, et al. (2015) HLA Class-II Associated HIV Polymorphisms Predict Escape from CD4+ T Cell Responses. PLoS Pathog 11: e1005111.

152. Alter G, Heckerman D, Schneidewind A, Fadda L, Kadie CM, et al. (2011) HIV-1 adaptation to NK-cell-mediated immune pressure. Nature 476: 96–100.

153. Bar KJ, Tsao Cy, Iyer SS, Decker JM, Yang Y, et al. (2012) Early low-titer neutralizing antibodies impede HIV-1 replication and select for virus escape. PLoS Pathog 8: e1002721.

154. Moore PL, Ranchobe N, Lambson BE, Gray ES, Cave E, et al. (2009) Limited neutralizing antibody specificities drive neutralization escape in early HIV-1 subtype C infection. PLoS Pathog 5: e1000598.

155. Wei X, Decker JM, Wang S, Hui H, Kappes JC, et al. (2003) Antibody neutralization and escape by HIV-1. Nature 422: 307–312.

156. Rong R, Li B, Lynch RM, Haaland RE, Murphy MK, et al. (2009) Escape from autologous neutralizing antibodies in acute/early subtype C HIV-1 infection requires multiple pathways. PLoS Pathog 5: e1000594.

157. van Gils MJ, Bunnik EM, Burger JA, Jacob Y, Schweighardt B, et al. (2010) Rapid escape from preserved cross-reactive neutralizing humoral immunity without loss of viral fitness in HIV-1-infected progressors and long-term nonprogressors. J Virol 84: 3576–3585.

158. Pircher H, Moskophidis D, Rohrer U, Bürki K, Hengartner H, et al. (1990) Viral escape by selection of cytotoxic T cell-resistant virus variants in vivo. Nature 346: 629–633.

159. Zimbwa P, Milicic A, Frater J, Scriba TJ, Willis A, et al. (2007) Precise identification of a human immunodeficiency virus type 1 antigen processing mutant. J Virol 81: 2031–2038.

160. Liu MK, Hawkins N, Ritchie AJ, Ganusov VV, Whale V, et al. (2013) Vertical T cell immunodominance and epitope entropy determine HIV-1 escape. J Clin Invest 123: 380–393.

161. Troyer RM, McNevin J, Liu Y, Zhang SC, Krizan RW, et al. (2009) Variable fitness impact of HIV-1 escape mutations to cytotoxic T lymphocyte (CTL) response. PLoS Pathog 5: e1000365.

162. Martinez-Picado J, Prado JG, Fry EE, Pfafferott K, Leslie A, et al. (2006) Fitness cost of escape mutations in p24 Gag in association with control of human immunodeficiency virus type 1. J Virol 80: 3617–3623.

163. Leslie A, Pfafferott K, Chetty P, Draenert R, Addo M, et al. (2004) HIV evolution: CTL escape mutation and reversion after transmission. Nat Med 10: 282–289.

164. Duda A, Lee-Turner L, Fox J, Robinson N, Dustan S, et al. (2009) HLA-associated clinical progression correlates with epitope reversion rates in early human immunodeficiency virus infection. J Virol 83: 1228–1239.

165. Crawford H, Prado JG, Leslie A, Hué S, Honeyborne I, et al. (2007) Compensatory mutation partially restores fitness and delays reversion of escape mutation within the immunodominant HLA-B* 5703-restricted Gag epitope in chronic human immunodeficiency virus type 1 infection. J Virol 81: 8346–8351.

166. Jamieson BD, Yang OO, Hultin L, Hausner MA, Hultin P, et al. (2003) Epitope escape mutation and decay of human immunodeficiency virus type 1-specific CTL responses. J Immunol 171: 5372–5379.

167. Allen TM, Altfeld M, Yu XG, O'Sullivan KM, Lichterfeld M, et al. (2004) Selection, transmission, and reversion of an antigen-processing cytotoxic T-lymphocyte escape mutation in human immunodeficiency virus type 1 infection. J Virol 78: 7069–7078.

168. Brumme ZL, John M, Carlson JM, Brumme CJ, Chan D, et al. (2009) HLA-associated immune escape pathways in HIV-1 subtype B Gag, Pol and Nef proteins. PLoS One 4: e6687.

169. Allen TM, Altfeld M, Geer SC, Kalife ET, Moore C, et al. (2005) Selective Escape from CD8+ T-Cell Responses Represents a Major Driving Force of Human Immunodeficiency Virus Type 1 (HIV-1) Sequence Diversity and Reveals Constraints on HIV-1 Evolution. J Virol 79: 13239–13249.

170. Ganusov VV, Goonetilleke N, Liu MK, Ferrari G, Shaw GM, et al. (2011) Fitness costs and diversity of the cytotoxic T lymphocyte (CTL) response determine the rate of CTL escape during acute and chronic phases of HIV infection. J Virol 85: 10518–10528.

171. Fryer HR, Frater J, Duda A, Roberts MG, Phillips RE, et al. (2010) Modelling the evolution and spread of HIV immune escape mutants. PLoS Pathog 6: e1001196.

172. Palmer D, Frater J, Phillips R, McLean AR, McVean G (2013) Integrating genealogical and dynamical modelling to infer escape and reversion rates in HIV epitopes. Proc R Soc B 280: 20130696.

173. Yue L, Pfafferott KJ, Baalwa J, Conrod K, Dong CC, et al. (2015) Transmitted virus fitness and host T cell responses collectively define divergent infection outcomes in two HIV-1 recipients. PLoS Pathog 11: e1004565.

174. Geels MJ, Cornelissen M, Schuitemaker H, Anderson K, Kwa D, et al. (2003) Identification of sequential viral escape mutants associated with altered T-cell responses in a human immunodeficiency virus type 1-infected individual. J Virol 77: 12430–12440.

175. Cao J, McNevin J, Holte S, Fink L, Corey L, et al. (2003) Comprehensive analysis of human immunodeficiency virus type 1 (HIV-1)-specific gamma interferon-secreting CD8+ T cells in primary HIV-1 infection. J Virol 77: 6867–6878.

176. Oxenius A, Price DA, Trkola A, Edwards C, Gostick E, et al. (2004) Loss of viral control in early HIV-1 infection is temporally associated with sequential escape from CD8+ T cell responses and decrease in HIV-1-specific CD4+ and CD8+ T cell frequencies. J Infect Dis 190: 713–721.

177. Grenfell BT, Pybus OG, Gog JR, Wood JL, Daly JM, et al. (2004) Unifying the epidemiological and evolutionary dynamics of pathogens. Science 303: 327–332.

178. Ball SC, Abraha A, Collins KR, Marozsan AJ, Baird H, et al. (2003) Comparing the ex vivo fitness of CCR5-tropic human immunodeficiency virus type 1 isolates of subtypes B and C. J Virol 77: 1021–1038.

179. Lythgoe KA, Fraser C (2012) New insights into the evolutionary rate of HIV-1 at the within-host and epidemiological levels. Proc R Soc B 279: 3367–3375.

180. Bellan SE, Dushoff J, Galvani AP, Meyers LA (2015) Reassessment of HIV-1 acute phase infectivity: accounting for heterogeneity and study design with simulated cohorts. PLoS Med 12: e1001801.

181. Wawer MJ, Gray RH, Sewankambo NK, Serwadda D, Li X, et al. (2005) Rates of HIV-1 transmission per coital act, by stage of HIV-1 infection, in Rakai, Uganda. J Infect Dis 191: 1403–1409.

182. Cotton LA, Kuang XT, Le AQ, Carlson JM, Chan B, et al. (2014) Genotypic and functional impact of HIV-1 adaptation to its host population during the North American epidemic. PLoS Genet 10: e1004295.

183. Kawashima Y, Pfafferott K, Frater J, Matthews P, Payne R, et al. (2009) Adaptation of HIV-1 to human leukocyte antigen class I. Nature 458: 641–645.

184. Anderson R, May RM (1991) Infectious diseases of humans: dynamics and control. Oxford University Press.

185. Kerr PJ (2012) Myxomatosis in Australia and Europe: a model for emerging infectious diseases. Antiviral Research 93: 387–415.

186. Mellors JW, Munoz A, Giorgi JV, Margolick JB, Tassoni CJ, et al. (1997) Plasma viral load and CD4+ lymphocytes as prognostic markers of HIV-1 infection. Ann Intern Med 126: 946–954.

187. Quinn TC, Wawer MJ, Sewankambo N, Serwadda D, Li C, et al. (2000) Viral load and heterosexual transmission of human immunodeficiency virus type 1. N Engl J Med 342: 921–929.

188. Herbeck JT, Mittler JE, Gottlieb GS, Mullins JI (2014) An HIV epidemic model based on viral load dynamics: value in assessing empirical trends in HIV virulence and community viral load. PLoS Comput Biol 10: e1003673.

189. Pantazis N, Porter K, Costagliola D, De Luca A, Ghosn J, et al. (2014) Temporal trends in prognostic markers of HIV-1 virulence and transmissibility: an observational cohort study. Lancet HIV 1: e119–e126.

190. Fraser C, Lythgoe K, Leventhal GE, Shirreff G, Hollingsworth TD, et al. (2014) Virulence and pathogenesis of HIV-1 infection: an evolutionary perspective. Science 343: 1243727.

191. Blanquart F, Grabowski MK, Herbeck J, Nalugoda F, Serwadda D, et al. (2016) A transmission-virulence evolutionary trade-off explains attenuation of HIV-1 in Uganda. eLife 5: e20492.

192. Lythgoe KA, Pellis L, Fraser C (2013) Is HIV short-sighted? Insights from a multistrain nested model. Evolution 67: 2769–2782.

193. van Dorp CH, van Boven M, de Boer RJ (2014) Immuno-epidemiological modeling of HIV-1 predicts high heritability of the set-point virus load, while selection for CTL escape dominates virulence evolution. PLoS Comput Biol 10: e1003899.

194. Hodcroft E, Hadfield JD, Fearnhill E, Phillips A, Dunn D, et al. (2014) The Contribution of Viral Genotype to Plasma Viral Set-Point in HIV Infection. PLoS Pathog 10: e1004112.

195. Hool A, Leventhal GE, Bonhoeffer S (2013) Virus-induced target cell activation reconciles set-point viral load heritability and within-host evolution. Epidemics 5: 174–180.

196. Miura T, Brumme ZL, Brockman MA, Rosato P, Sela J, et al. (2010) Impaired replication capacity of acute/early viruses in persons who become HIV controllers. J Virol 84: 7581–7591.

197. Redd AD, Collinson-Streng AN, Chatziandreou N, Mullis CE, Laeyendecker O, et al. (2012) Previously transmitted HIV-1 strains are preferentially selected during subsequent sexual transmissions. J Infect Dis 206: 1433–1442.

198. World Health Organization (2016). Consolidated guidelines on the use of antiretroviral drugs for treating and preventing HIV infection. Chapter 4 – Clinical guidelines: antiretroviral therapy. Available: `http://www.who.int/hiv/pub/arv/arv-2016/en/`.

199. Chun TW, Stuyver L, Mizell SB, Ehler LA, Mican JAM, et al. (1997) Presence of an inducible HIV-1 latent reservoir during highly active antiretroviral therapy. Proc Natl Acad Sci USA 94: 13193–13197.

200. Blankson JN, Persaud D, Siliciano RF (2002) The challenge of viral reservoirs in HIV-1 infection. Annual Review of Medicine 53: 557–593.

201. Eisele E, Siliciano RF (2012) Redefining the viral reservoirs that prevent HIV-1 eradication. Immunity 37: 377–388.

202. Luzuriaga K, Gay H, Ziemniak C, Sanborn KB, Somasundaran M, et al. (2015) Viremic relapse after HIV-1 remission in a perinatally infected child. N Engl J Med 372: 786–788.

203. Chun TW, Engel D, Berrey MM, Shea T, Corey L, et al. (1998) Early establishment of a pool of latently infected, resting CD4+ T cells during primary HIV-1 infection. Proc Natl Acad Sci USA 95: 8869–8873.

204. Josefsson L, Von Stockenstrom S, Faria NR, Sinclair E, Bacchetti P, et al. (2013) The HIV-1 reservoir in eight patients on long-term suppressive antiretroviral therapy is stable with few genetic changes over time. Proc Natl Acad Sci USA 110: E4987–E4996.

205. Zhang L, Chung C, Hu BS, He T, Guo Y, et al. (2000) Genetic characterization of rebounding HIV-1 after cessation of highly active antiretroviral therapy. J Clin Invest 106: 839–845.

206. Kearney MF, Wiegand A, Shao W, Coffin JM, Mellors JW, et al. (2016) Origin of Rebound Plasma HIV Includes Cells with Identical Proviruses That Are Transcriptionally Active before Stopping of Antiretroviral Therapy. J Virol 90: 1369–1376.

207. Chun TW, Carruth L, Finzi D, Shen X, DiGiuseppe JA, et al. (1997) Quantification of latent tissue reservoirs and total body viral load in HIV-1 infection. Nature 387: 183–188.

208. Chun TW, Nickle DC, Justement JS, Meyers JH, Roby G, et al. (2008) Persistence of HIV in gut-associated lymphoid tissue despite long-term antiretroviral therapy. J Infect Dis 197: 714–720.

209. Gray LR, Roche M, Flynn JK, Wesselingh SL, Gorry PR, et al. (2014) Is the central nervous system a reservoir of HIV-1? Current Opinion in HIV and AIDS 9: 552.

210. Lamers SL, Rose R, Maidji E, Agsalda-Garcia M, Nolan DJ, et al. (2016) HIV DNA is frequently present within pathologic tissues evaluated at autopsy from combined antiretroviral therapy-treated patients with undetectable viral loads. J Virol 90: 8968–8983.

211. Lassen KG, Ramyar KX, Bailey JR, Zhou Y, Siliciano RF (2006) Nuclear retention of multiply spliced HIV-1 RNA in resting CD4+ T cells. PLoS Pathog 2: e68.

212. Pace MJ, Graf EH, Agosto LM, Mexas AM, Male F, et al. (2012) Directly infected resting CD4+ T cells can produce HIV Gag without spreading infection in a model of HIV latency. PLoS Pathog 8: e1002818.

213. Siliciano RF, Greene WC (2011) HIV latency. Cold Spring Harbor Perspectives in Medicine 1: a007096.

214. Saleh S, Solomon A, Wightman F, Xhilaga M, Cameron PU, et al. (2007) CCR7 ligands CCL19 and CCL21 increase permissiveness of resting memory CD4+ T cells to HIV-1 infection: a novel model of HIV-1 latency. Blood 110: 4161–4164.

215. Evans VA, Kumar N, Filali A, Procopio FA, Yegorov O, et al. (2013) Myeloid dendritic cells induce HIV-1 latency in non-proliferating CD4+ T cells. PLoS Pathog 9: e1003799.

216. Han Y, Lassen K, Monie D, Sedaghat AR, Shimoji S, et al. (2004) Resting CD4+ T cells from human immunodeficiency virus type 1 (HIV-1)-infected individuals carry integrated HIV-1 genomes within actively transcribed host genes. J Virol 78: 6122–6133.

217. Ruelas DS, Greene WC (2013) An integrated overview of HIV-1 latency. Cell 155: 519–529.

218. Donahue DA, Wainberg MA (2013) Cellular and molecular mechanisms involved in the establishment of HIV-1 latency. Retrovirology 10: 1–11.

219. Ho YC, Shan L, Hosmane NN, Wang J, Laskey SB, et al. (2013) Replication-competent noninduced proviruses in the latent reservoir increase barrier to HIV-1 cure. Cell 155: 540–551.

220. Bruner KM, Murray AJ, Pollack RA, Soliman MG, Laskey SB, et al. (2016) Defective proviruses rapidly accumulate during acute HIV-1 infection. Nat Med 22: 1043–1049.

221. Procopio FA, Fromentin R, Kulpa DA, Brehm JH, Bebin AG, et al. (2015) A novel assay to measure the magnitude of the inducible viral reservoir in HIV-infected individuals. EBioMedicine 2: 874–883.

222. Burbelo PD, Bayat A, Rhodes CS, Hoh R, Martin JN, et al. (2014) HIV antibody characterization as a method to quantify reservoir size during curative interventions. J Infect Dis 209: 1613–1617.

223. Barouch DH, Deeks SG (2014) Immunologic strategies for HIV-1 remission and eradication. Science 345: 169–174.

224. Dai J, Agosto LM, Baytop C, Jianqing JY, Pace MJ, et al. (2009) Human immunodeficiency virus integrates directly into naive resting CD4+ T cells but enters naive cells less efficiently than memory cells. J Virol 83: 4528–4537.

225. Chomont N, El-Far M, Ancuta P, Trautmann L, Procopio FA, et al. (2009) HIV reservoir size and persistence are driven by T cell survival and homeostatic proliferation. Nat Med 15: 893–900.

226. Hatano H, Jain V, Hunt PW, Lee TH, Sinclair E, et al. (2013) Cell-based measures of viral persistence are associated with immune activation and programmed cell death protein 1 (PD-1)–expressing CD4+ T cells. J Infect Dis 208: 50–56.

227. Buzon MJ, Sun H, Li C, Shaw A, Seiss K, et al. (2014) HIV-1 persistence in CD4+ T cells with stem cell-like properties. Nat Med 20: 139–142.

228. Banga R, Procopio FA, Noto A, Pollakis G, Cavassini M, et al. (2016) PD-1+ and follicular helper T cells are responsible for persistent HIV-1 transcription in treated aviremic individuals. Nat Med 22: 754–761.

229. Müller V, Vigueras-Gómez JF, Bonhoeffer S (2002) Decelerating decay of latently infected cells during prolonged therapy for human immunodeficiency virus type 1 infection. J Virol 76: 8963–8965.

230. Deeks SG, Lewin SR, Ross AL, Ananworanich J, Benkirane M, et al. (2016) International AIDS Society global scientific strategy: towards an HIV cure 2016. Nat Med 22: 839–850.

231. Sherrill-Mix S, Lewinski MK, Famiglietti M, Bosque A, Malani N, et al. (2013) HIV latency and integration site placement in five cell-based models. Retrovirology 10: 90.

232. Macallan DC, Wallace D, Zhang Y, de Lara C, Worth AT, et al. (2004) Rapid turnover of effector–memory CD4+ T cells in healthy humans. J Exp Med 200: 255–260.

233. Ahmed R, Westera L, Drylewicz J, Elemans M, Zhang Y, et al. (2015) Reconciling estimates of cell proliferation from stable isotope labeling experiments. PLoS Comput Biol 11: e1004355.

234. Pace MJ, Agosto L, Graf EH, O'Doherty U (2011) HIV reservoirs and latency models. Virology 411: 344–354.

235. Imamichi H, Natarajan V, Adelsberger JW, Rehm CA, Lempicki RA, et al. (2014) Lifespan of effector memory CD4+ T cells determined by replication-incompetent integrated HIV-1 provirus. AIDS 28: 1091–1099.

236. Wagner TA, McKernan JL, Tobin NH, Tapia KA, Mullins JI, et al. (2013) An increasing proportion of monotypic HIV-1 DNA sequences during antiretroviral treatment suggests proliferation of HIV-infected cells. J Virol 87: 1770–1778.

237. Maldarelli F, Wu X, Su L, Simonetti F, Shao W, et al. (2014) Specific HIV integration sites are linked to clonal expansion and persistence of infected cells. Science 345: 179–183.

238. Simonetti FR, Sobolewski MD, Fyne E, Shao W, Spindler J, et al. (2016) Clonally expanded CD4+ T cells can produce infectious HIV-1 in vivo. Proc Natl Acad Sci USA 113: 1883–1888.

239. Vandergeeten C, Fromentin R, DaFonseca S, Lawani MB, Sereti I, et al. (2013) Interleukin-7 promotes HIV persistence during antiretroviral therapy. Blood 121: 4321–4329.

240. Katlama C, Lambert-Niclot S, Assoumou L, Papagno L, Lecardonnel F, et al. (2016) Treatment intensification followed by interleukin-7 reactivates HIV without reducing total HIV DNA: a randomized trial. AIDS 30: 221–230.

241. Seddon B, Tomlinson P, Zamoyska R (2003) Interleukin 7 and T cell receptor signals regulate homeostasis of CD4 memory cells. Nat Immunol 4: 680–686.

242. Boritz EA, Darko S, Swaszek L, Wolf G, Wells D, et al. (2016) Multiple Origins of Virus Persistence during Natural Control of HIV Infection. Cell 166: 1004–1015.

243. Sedaghat AR, Siliciano RF, Wilke CO (2008) Low-level HIV-1 replication and the dynamics of the resting CD4+ T cell reservoir for HIV-1 in the setting of HAART. BMC Infectious Diseases 8: 1.

244. Fletcher CV, Staskus K, Wietgrefe SW, Rothenberger M, Reilly C, et al. (2014) Persistent HIV-1 replication is associated with lower antiretroviral drug concentrations in lymphatic tissues. Proc Natl Acad Sci USA 111: 2307–2312.

245. Buzon MJ, Massanella M, Llibre JM, Esteve A, Dahl V, et al. (2010) HIV-1 replication and immune dynamics are affected by raltegravir intensification of HAART-suppressed subjects. Nat Med 16: 460–465.

246. Llibre JM, Buzón MJ, Massanella M, Esteve A, Dahl V, et al. (2012) Treatment intensification with raltegravir in subjects with sustained HIV-1 viraemia suppression: a randomized 48-week study. Antiviral Therapy 17: 355.

247. Gandhi RT, Zheng L, Bosch RJ, Chan ES, Margolis DM, et al. (2010) The effect of raltegravir intensification on low-level residual viremia in HIV-infected patients on antiretroviral therapy: a randomized controlled trial. PLoS Med 7: e1000321.

248. Shen L, Siliciano RF (2008) Viral reservoirs, residual viremia, and the potential of highly active antiretroviral therapy to eradicate HIV infection. Journal of Allergy and Clinical Immunology 122: 22–28.

249. Kearney MF, Spindler J, Shao W, Yu S, Anderson EM, et al. (2014) Lack of detectable HIV-1 molecular evolution during suppressive antiretroviral therapy. PLoS Pathog 10: e1004010.

250. Brodin J, Zanini F, Thebo L, Lanz C, Bratt G, et al. (2016) Establishment and stability of the latent HIV-1 DNA reservoir. eLife : e18889.

251. Santangelo PJ, Rogers KA, Zurla C, Blanchard EL, Gumber S, et al. (2015) Whole-body immunoPET reveals active SIV dynamics in viremic and antiretroviral therapy-treated macaques. Nature Methods 12: 427–432.

252. Wagner TA, McLaughlin S, Garg K, Cheung CY, Larsen BB, et al. (2014) Proliferation of cells with HIV integrated into cancer genes contributes to persistent infection. Science 345: 570–573.

253. Shiu C, Cunningham CK, Greenough T, Muresan P, Sanchez-Merino V, et al. (2009) Identification of ongoing human immunodeficiency virus type 1 (HIV-1) replication in residual viremia during recombinant HIV-1 poxvirus immunizations in patients with clinically undetectable viral loads on durable suppressive highly active antiretroviral therapy. J Virol 83: 9731–9742.

254. Günthard HF, Wong JK, Spina CA, Ignacio C, Kwok S, et al. (2000) Effect of influenza vaccination on viral replication and immune response in persons infected with human immunodeficiency virus receiving potent antiretroviral therapy. J Infect Dis 181: 522–531.

255. Whitney JB, Hill AL, Sanisetty S, Penaloza-MacMaster P, Liu J, et al. (2014) Rapid seeding of the viral reservoir prior to SIV viraemia in rhesus monkeys. Nature 512: 74–77.

256. Chun TW, Justement JS, Murray D, Hallahan CW, Maenza J, et al. (2010) Rebound of plasma viremia following cessation of antiretroviral therapy despite profoundly low levels of HIV reservoir: implications for eradication. AIDS 24: 2803.

257. Jain V, Hartogensis W, Bacchetti P, Hunt PW, Hatano H, et al. (2013) Antiretroviral Therapy Initiated Within 6 Months of HIV Infection Is Associated With Lower T-Cell Activation and Smaller HIV Reservoir Size. J Infect Dis 208: 1202-1211.

258. Watanabe D, Ibe S, Uehira T, Minami R, Sasakawa A, et al. (2011) Cellular HIV-1 DNA levels in patients receiving antiretroviral therapy strongly correlate with therapy initiation timing but not with therapy duration. BMC Infectious Diseases 11: 1.

259. Gianella S, von Wyl V, Fischer M, Niederoest B, Battegay M, et al. (2011) Effect of early antiretroviral therapy during primary HIV-1 infection on cell-associated HIV-1 DNA and plasma HIV-1 RNA. Antiviral Therapy 16: 535.

260. Ananworanich J, Schuetz A, Vandergeeten C, Sereti I, De Souza M, et al. (2012) Impact of multi-targeted antiretroviral treatment on gut T cell depletion and HIV reservoir seeding during acute HIV infection. PLoS One 7: e33948.

261. Archin NM, Vaidya NK, Kuruc JD, Liberty AL, Wiegand A, et al. (2012) Immediate antiviral therapy appears to restrict resting CD4+ cell HIV-1 infection without accelerating the decay of latent infection. Proc Natl Acad Sci USA 109: 9523–9528.

262. Hocqueloux L, Avettand-Fènoël V, Jacquot S, Prazuck T, Legac E, et al. (2013) Long-term antiretroviral therapy initiated during primary HIV-1 infection is key to achieving both low HIV reservoirs and normal T cell counts. Journal of Antimicrobial Chemotherapy 68: 1169–1178.

263. Murray JM, McBride K, Boesecke C, Bailey M, Amin J, et al. (2012) Integrated HIV DNA accumulates prior to treatment while episomal HIV DNA records ongoing transmission afterwards. AIDS 26: 543–550.

264. Zhang L, Ramratnam B, Tenner-Racz K, He Y, Vesanen M, et al. (1999) Quantifying residual HIV-1 replication in patients receiving combination antiretroviral therapy. N Engl J Med 340: 1605–1613.

265. Siliciano JD, Kajdas J, Finzi D, Quinn TC, Chadwick K, et al. (2003) Long-term follow-up studies confirm the stability of the latent reservoir for HIV-1 in resting CD4+ T cells. Nat Med 9: 727–728.

266. Blankson JN, Finzi D, Pierson TC, Sabundayo BP, Chadwick K, et al. (2000) Biphasic decay of latently infected CD4+ T cells in acute human immunodeficiency virus type 1 infection. J Infect Dis 182: 1636–1642.

267. Strain MC, Little SJ, Daar ES, Havlir DV, Günthard HF, et al. (2005) Effect of treatment, during primary infection, on establishment and clearance of cellular reservoirs of HIV-1. J Infect Dis 191: 1410–1418.

268. Fischer M, Joos B, Niederöst B, Kaiser P, Hafner R, et al. (2008) Biphasic decay kinetics suggest progressive slowing in turnover of latently HIV-1 infected cells during antiretroviral therapy. Retrovirology 5: 107.

269. Besson GJ, Lalama CM, Bosch RJ, Gandhi RT, Bedison MA, et al. (2014) HIV-1 DNA decay dynamics in blood during more than a decade of suppressive antiretroviral therapy. Clin Infect Dis 59: 1312–1321.

270. Althaus CL, Joos B, Perelson AS, Günthard HF (2014) Quantifying the turnover of transcriptional subclasses of HIV-1-infected cells. PLoS Comput Biol 10: e1003871.

271. Deeks SG (2012) HIV: Shock and kill. Nature 487: 439–440.

272. Spivak AM, Planelles V (2016) HIV-1 eradication: early trials (and tribulations). Trends Mol Med 22: 10–27.

273. Archin NM, Liberty A, Kashuba AD, Choudhary SK, Kuruc J, et al. (2012) Administration of vorinostat disrupts HIV-1 latency in patients on antiretroviral therapy. Nature 487: 482–485.

274. Søgaard OS, Graversen ME, Leth S, Olesen R, Brinkmann CR, et al. (2015) The depsipeptide romidepsin reverses HIV-1 latency in vivo. PLoS Pathog 11: e1005142.

275. Elliott JH, McMahon JH, Chang CC, Lee SA, Hartogensis W, et al. (2015) Short-term administration of disulfiram for reversal of latent HIV infection: a phase 2 dose-escalation study. Lancet HIV 2: e520–e529.

276. Laird GM, Bullen CK, Rosenbloom DI, Martin AR, Hill AL, et al. (2015) Ex vivo analysis identifies effective HIV-1 latency–reversing drug combinations. J Clin Invest 125: 1901–1912.

277. Shan L, Deng K, Shroff NS, Durand CM, Rabi SA, et al. (2012) Stimulation of HIV-1-specific cytolytic T lymphocytes facilitates elimination of latent viral reservoir after virus reactivation. Immunity 36: 491–501.

278. Archin NM, Bateson R, Tripathy M, Crooks AM, Yang KH, et al. (2014) HIV-1 expression within resting CD4 T-cells following multiple doses of vorinostat. J Infect Dis 210: 728–735.

279. Byrareddy SN, Arthos J, Cicala C, Villinger F, Ortiz KT, et al. (2016) Sustained virologic control in SIV+ macaques after antiretroviral and $\alpha 4\beta 7$ antibody therapy. Science 354: 197–202.

280. Hamlyn E, Ewings FM, Porter K, Cooper DA, Tambussi G, et al. (2012) Plasma HIV viral rebound following protocol-indicated cessation of ART commenced in primary and chronic HIV infection. PLoS One 7: e43754.

281. Rothenberger MK, Keele BF, Wietgrefe SW, Fletcher CV, Beilman GJ, et al. (2015) Large number of rebounding/founder HIV variants emerge from multifocal infection in lymphatic tissues after treatment interruption. Proc Natl Acad Sci USA 112: E1126–E1134.

282. Bednar MM, Hauser BM, Zhou S, Jacobson JM, Eron JJ, et al. (2016) Diversity and Tropism of HIV-1 Rebound Virus Populations in Plasma Level After Treatment Discontinuation. J Infect Dis 214: 403–407.

283. Lerner P, Guadalupe M, Donovan R, Hung J, Flamm J, et al. (2011) The gut mucosal viral reservoir in HIV-infected patients is not the major source of rebound

plasma viremia following interruption of highly active antiretroviral therapy. J Virol 85: 4772–4782.

284. Horiike M, Iwami S, Kodama M, Sato A, Watanabe Y, et al. (2012) Lymph nodes harbor viral reservoirs that cause rebound of plasma viremia in SIV-infected macaques upon cessation of combined antiretroviral therapy. Virology 423: 107–118.

285. Henrich T, Hanhauser E, Sirignano M, Kuritzkes D (2014) HIV-1 rebound following allogeneic stem cell transplantation and treatment interruption. In: Conference on Retroviruses and Opportunistic Infections. pp. 3–6.

286. Goujard C, Girault I, Rouzioux C, Lécuroux C, Deveau C, et al. (2012) HIV-1 control after transient antiretroviral treatment initiated in primary infection: role of patient characteristics and effect of therapy. Antiviral Therapy 17: 1001.

287. Yerly S, Günthard HF, Fagard C, Joos B, Perneger TV, et al. (2004) Proviral HIV-DNA predicts viral rebound and viral setpoint after structured treatment interruptions. AIDS 18: 1951–1953.

288. Assoumou L, Weiss L, Piketty C, Burgard M, Melard A, et al. (2015) A low HIV-DNA level in peripheral blood mononuclear cells at antiretroviral treatment interruption predicts a higher probability of maintaining viral control. AIDS 29: 2003–2007.

289. Stöhr W, Fidler S, McClure M, Weber J, Cooper D, et al. (2013) Duration of HIV-1 viral suppression on cessation of antiretroviral therapy in primary infection correlates with time on therapy. PLoS One 8: e78287.

290. Fourati S, Flandre P, Calin R, Carcelain G, Soulie C, et al. (2014) Factors associated with a low HIV reservoir in patients with prolonged suppressive antiretroviral therapy. Journal of Antimicrobial Chemotherapy 69: 753–756.

291. Steingrover R, Pogány K, Garcia EF, Jurriaans S, Brinkman K, et al. (2008) HIV-1 viral rebound dynamics after a single treatment interruption depends on time of initiation of highly active antiretroviral therapy. AIDS 22: 1583–1588.

292. Buzon MJ, Martin-Gayo E, Pereyra F, Ouyang Z, Sun H, et al. (2014) Long-term antiretroviral treatment initiated at primary HIV-1 infection affects the size, composition, and decay kinetics of the reservoir of HIV-1-infected CD4 T cells. J Virol 88: 10056–10065.

293. Hurst J, Hoffmann M, Pace M, Williams JP, Thornhill J, et al. (2015) Immunological biomarkers predict HIV-1 viral rebound after treatment interruption. Nature Communications 6: 8495.

294. Conway JM, Perelson AS (2015) Post-treatment control of HIV infection. Proc Natl Acad Sci USA 112: 5467–5472.

295. Bolker BM (2008) Ecological models and data in R. Princeton University Press.

296. May RM, Anderson Rt (1983) Epidemiology and genetics in the coevolution of parasites and hosts. Proceedings of the Royal Society of London B: Biological Sciences 219: 281–313.

297. May RM, Anderson RM, et al. (1979) Population biology of infectious diseases: Part II. Nature 280: 455–461.

298. Wei X, Ghosh SK, Johnson VA, Emini EA, Deutsch P, et al. (1995) Viral dynamics in human immunodeficiency virus type 1 infection. Nature 373: 12.

299. Ho DD, Neumann AU, Perelson AS, Chen W, Leonard JM, et al. (1995) Rapid turnover of plasma virions and CD4 lymphocytes in HIV-1 infection. Nature 373: 123–126.

300. Granich RM, Gilks CF, Dye C, De Cock KM, Williams BG (2009) Universal voluntary HIV testing with immediate antiretroviral therapy as a strategy for elimination of HIV transmission: a mathematical model. Lancet 373: 48–57.

301. Eaton JW, Johnson LF, Salomon JA, Bärnighausen T, Bendavid E, et al. (2012) HIV treatment as prevention: systematic comparison of mathematical models of the potential impact of antiretroviral therapy on HIV incidence in South Africa. PLoS Med 9: e1001245.

302. Alizon S, Magnus C (2012) Modelling the course of an HIV infection: insights from ecology and evolution. Viruses 4: 1984–2013.

303. Wang S, Hottz P, Schechter M, Rong L (2015) Modeling the slow CD4+ T cell decline in HIV-infected individuals. PLoS Comput Biol 11: e1004665.

304. Huang G, Takeuchi Y, Korobeinikov A (2012) HIV evolution and progression of the infection to AIDS. J Theor Biol 307: 149–159.

305. Hernandez-Vargas EA, Middleton RH (2013) Modeling the three stages in HIV infection. J Theor Biol 320: 33–40.

306. Perelson AS, Essunger P, Cao Y, Vesanen M, Hurley A, et al. (1997) Decay characteristics of HIV-1-infected compartments during combination therapy. Nature 387: 188–191.

307. Kim H, Perelson AS (2006) Viral and latent reservoir persistence in HIV-1–infected patients on therapy. PLoS Comput Biol 2: e135.

308. Rong L, Perelson AS (2009) Modeling latently infected cell activation: viral and latent reservoir persistence, and viral blips in HIV-infected patients on potent therapy. PLoS Comput Biol 5: e1000533.

309. Rong L, Perelson AS (2009) Asymmetric division of activated latently infected cells may explain the decay kinetics of the HIV-1 latent reservoir and intermittent viral blips. Mathematical Biosciences 217: 77–87.

310. Hill AL, Rosenbloom DI, Fu F, Nowak MA, Siliciano RF (2014) Predicting the outcomes of treatment to eradicate the latent reservoir for HIV-1. Proc Natl Acad Sci USA 111: 13475–13480.

311. Hill AL, Rosenbloom DI, Goldstein E, Hanhauser E, Kuritzkes DR, et al. (2016) Real-time predictions of reservoir size and rebound time during antiretroviral therapy interruption trials for HIV. PLoS Pathog 12: e1005535.

312. Mclean AR, Michie CA (1995) In vivo estimates of division and death rates of human T lymphocytes. Proc Natl Acad Sci USA 92: 3707–3711.

313. McCune JM, Hanley MB, Cesar D, Halvorsen R, Hoh R, et al. (2000) Factors influencing T-cell turnover in HIV-1 seropositive patients. J Clin Invest 105: R1-R8.

314. Asquith B, Debacq C, Macallan DC, Willems L, Bangham CR (2002) Lymphocyte kinetics: the interpretation of labelling data. Trends in Immunology 23: 596–601.

315. Zhang J, Perelson AS (2013) Contribution of follicular dendritic cells to persistent HIV viremia. J Virol 87: 7893–7901.

316. Macallan DC, Asquith B, Irvine AJ, Wallace DL, Worth A, et al. (2003) Measurement and modeling of human T cell kinetics. Eur J Immunol 33: 2316–2326.

317. Vrisekoop N, den Braber I, de Boer AB, Ruiter AF, Ackermans MT, et al. (2008) Sparse production but preferential incorporation of recently produced naive T cells in the human peripheral pool. Proc Natl Acad Sci USA 105: 6115–6120.

318. De Boer RJ, Perelson AS (2013) Quantifying T lymphocyte turnover. J Theor Biol 327: 45–87.

319. Mohri H, Perelson AS, Tung K, Ribeiro RM, Ramratnam B, et al. (2001) Increased Turnover of T Lymphocytes in HIV-1 Infection and Its Reduction by Antiretroviral Therapy. J Exp Med 194: 1277-1288.

320. Strain M, Günthard H, Havlir D, Ignacio C, Smith D, et al. (2003) Heterogeneous clearance rates of long-lived lymphocytes infected with HIV: intrinsic stability predicts lifelong persistence. Proc Natl Acad Sci USA 100: 4819–4824.

321. Hethcote HW (2000) The mathematics of infectious diseases. SIAM review 42: 599–653.

322. Dodd PJ, Garnett GP, Hallett TB (2010) Examining the promise of HIV elimination by ?test and treat?in hyper-endemic settings. AIDS 24: 729.

323. Kretzschmar ME, van der Loeff MFS, Coutinho RA (2012) Elimination of HIV by test and treat: a phantom of wishful thinking? AIDS 26: 247–248.

324. Powers KA, Ghani AC, Miller WC, Hoffman IF, Pettifor AE, et al. (2011) The role of acute and early HIV infection in the spread of HIV and implications for transmission prevention strategies in Lilongwe, Malawi: a modelling study. Lancet 378: 256–268.

325. Osnas EE, Dobson AP (2010) Evolution of virulence when transmission occurs before disease. Biol Lett 6: 505–508.

326. Pereyra F, Jia X, McLaren PJ, Telenti A, De Bakker P, et al. (2010) The major genetic determinants of HIV-1 control affect HLA class I peptide presentation. Science 330: 1551–1557.

327. Altfeld M, Kalife ET, Qi Y, Streeck H, Lichterfeld M, et al. (2006) HLA Alleles Associated with Delayed Progression to AIDS Contribute Strongly to the Initial CD8+ T Cell Response against HIV-1. PLoS Med 3: e403.

328. Kaiser P, Joos B, Niederöst B, Weber R, Günthard HF, et al. (2007) Productive human immunodeficiency virus type 1 infection in peripheral blood predominantly takes place in CD4/CD8 double-negative T lymphocytes. J Virol 81: 9693–9706.

329. Brumme ZL, Brumme CJ, Carlson J, Streeck H, John M, et al. (2008) Marked epitope-and allele-specific differences in rates of mutation in human immunodeficiency type 1 (HIV-1) Gag, Pol, and Nef cytotoxic T-lymphocyte epitopes in acute/early HIV-1 infection. J Virol 82: 9216–9227.

330. Goulder PJ, Watkins DI (2004) HIV and SIV CTL escape: implications for vaccine design. Nat Rev Immunol 4: 630–640.

331. Klenerman P, Hill A (2005) T cells and viral persistence: lessons from diverse infections. Nat Immunol 6: 873–879.

332. Chopera DR, Mlotshwa M, Woodman Z, Mlisana K, de Assis Rosa D, et al. (2011) Virological and immunological factors associated with HIV-1 differential disease progression in HLA-B* 58: 01-positive individuals. J Virol 85: 7070–7080.

333. Herbeck JT, Rolland M, Liu Y, McLaughlin S, McNevin J, et al. (2011) Demographic processes affect HIV-1 evolution in primary infection before the onset of selective processes. J Virol 85: 7523–7534.

334. O'Brien SJ, Gao X, Carrington M (2001) HLA and AIDS: a cautionary tale. Trends Mol Med 7: 379–381.

335. Frater AJ, Brown H, Oxenius A, Günthard H, Hirschel B, et al. (2007) Effective T-cell responses select human immunodeficiency virus mutants and slow disease progression. J Virol 81: 6742–6751.

336. Asquith B (2008) The evolutionary selective advantage of HIV-1 escape variants and the contribution of escape to the HLA-associated risk of AIDS progression. PLoS One 3: e3486.

337. Llano A, Williams A, Olvera A, Silva-Arrieta S, Brander C (2013) Best-Characterized HIV-1 CTL Epitopes: The 2013 Update. HIV Molecular Immunology 2013 : 3–25.

338. Frahm N, Yusim K, Suscovich TJ, Adams S, Sidney J, et al. (2007) Extensive HLA class I allele promiscuity among viral CTL epitopes. Eur J Immunol 37: 2419–2433.

339. Fryer HR, Frater J, Duda A, Palmer D, Phillips RE, et al. (2012) Cytotoxic T-lymphocyte escape mutations identified by HLA association favor those which escape and revert rapidly. J Virol 86: 8568–8580.

340. English S, Katzourakis A, Bonsall D, Flanagan P, Duda A, et al. (2011) Phylogenetic analysis consistent with a clinical history of sexual transmission of HIV-1 from a single donor reveals transmission of highly distinct variants. Retrovirology 8: 54.

341. Los Alamos National Laboratory (2013). HIV Molecular Immunology Database. URL `http://www.hiv.lanl.gov/content/immunology`.

342. Schellens IM, Kesmir C, Miedema F, van Baarle D, Borghans JA (2008) An unanticipated lack of consensus cytotoxic T lymphocyte epitopes in HIV-1 databases: the contribution of prediction programs. AIDS 22: 33–37.

343. Barton K, Winckelmann A, Palmer S (2016) HIV-1 Reservoirs During Suppressive Therapy. Trends in Microbiology 24: 345–355.

344. Kiselinova M, De Spiegelaere W, Buzon MJ, Malatinkova E, Lichterfeld M, et al. (2016) Integrated and total HIV-1 DNA predict ex vivo viral outgrowth. PLoS Pathog 12: e1005472.

345. Lewin SR, Rouzioux C (2011) HIV cure and eradication: how will we get from the laboratory to effective clinical trials? AIDS 25: 885–897.

346. Rosenberg ES, Altfeld M, Poon SH, Phillips MN, Wilkes BM, et al. (2000) Immune control of HIV-1 after early treatment of acute infection. Nature 407: 523–526.

347. Jansen CA, De Cuyper IM, Steingrover R, Jurriaans S, Sankatsing SU, et al. (2005) Analysis of the effect of highly active antiretroviral therapy during acute HIV-1 infection on HIV-specific CD4 T cell functions. AIDS 19: 1145–1154.

348. Harrigana PR, Whaley M, Montaner JS (1999) Rate of HIV-1 RNA rebound upon stopping antiretroviral therapy. AIDS 13: F59–F62.

349. Crooks AM, Bateson R, Cope AB, Dahl NP, Griggs MK, et al. (2015) Precise quantitation of the latent HIV-1 reservoir: implications for eradication strategies. J Infect Dis 212: 1361–1365.

350. Siliciano JD, Siliciano RF (2006) The latent reservoir for HIV-1 in resting CD4+ T cells: a barrier to cure. Current Opinion in HIV and AIDS 1: 121–128.

351. Martinez-Picado J, Deeks SG (2016) Persistent HIV-1 replication during antiretroviral therapy. Current Opinion in HIV and AIDS 11: 417–423.

352. Fromentin R, Bakeman W, Lawani MB, Khoury G, Hartogensis W, et al. (2016) CD4+ T Cells Expressing PD-1, TIGIT and LAG-3 Contribute to HIV Persistence during ART. PLoS Pathog 12: e1005761.

353. Oxenius A, Price DA, Easterbrook PJ, O'Callaghan CA, Kelleher AD, et al. (2000) Early highly active antiretroviral therapy for acute HIV-1 infection preserves immune function of CD8+ and CD4+ T lymphocytes. Proc Natl Acad Sci USA 97: 3382–3387.

354. Deng K, Pertea M, Rongvaux A, Wang L, Durand CM, et al. (2015) Broad CTL response is required to clear latent HIV-1 due to dominance of escape mutations. Nature 517: 381–385.

355. De Spiegelaere W (2016) Viral markers for HIV cure trials: are we getting any closer? Journal of Virus Eradication 2: 55.

356. Katzenstein TL, Nielsen C, Lundgren JD, Jakobsen PH, Gerstoft J (1996) Longitudinal serum HIV RNA quantification: correlation to viral phenotype at seroconversion and clinical outcome. AIDS 10: 167–173.

357. Payne R, Muenchhoff M, Mann J, Roberts HE, Matthews P, et al. (2014) Impact of HLA-driven HIV adaptation on virulence in populations of high HIV seroprevalence. Proc Natl Acad Sci USA 111: E5393–E5400.

358. Müller V, Fraser C, Herbeck JT (2011) A strong case for viral genetic factors in HIV virulence. Viruses 3: 204–216.

359. World Health Organisation (2015). World Health Statistics 2015. Available: `http://www.who.int/whosis/whostat/en/`.

360. Cohen MS, Chen YQ, McCauley M, Gamble T, Hosseinipour MC, et al. (2011) Prevention of HIV-1 infection with early antiretroviral therapy. N Engl J Med 365: 493–505.

361. Helleberg M, Kronborg G, Larsen C, Pedersen G, Pedersen C, et al. (2013) No change in viral set point or CD4 cell decline among antiretroviral treatment-naïve, HIV-1-infected individuals enrolled in the Danish HIV Cohort Study in 1995–2010. HIV Med 14: 362–369.

362. Lowenthal ED, Bakeera-Kitaka S, Marukutira T, Chapman J, Goldrath K, et al. (2014) Perinatally acquired HIV infection in adolescents from sub-Saharan Africa: a review of emerging challenges. Lancet Infect Dis 14: 627–639.

363. Müller V, Maggiolo F, Suter F, Ladisa N, De Luca A, et al. (2009) Increasing clinical virulence in two decades of the Italian HIV epidemic. PLoS Pathog 5: e1000454.

364. Dorrucci M, Rezza G, Porter K, Phillips A, et al. (2007) Temporal trends in post-seroconversion CD4 cell count and HIV load: the Concerted Action on Seroconversion to AIDS and Death in Europe Collaboration, 1985–2002. J Infect Dis 195: 525–534.

365. Morgan D, Mahe C, Mayanja B, Okongo JM, Lubega R, et al. (2002) HIV-1 infection in rural Africa: is there a difference in median time to AIDS and survival compared with that in industrialized countries? AIDS 16: 597–603.

366. Lepri AC, Sabin CA, Pezzotti P, England PD, Phillips AN, et al. (1997) Is there a general tendency for CD4 lymphocyte decline to speed up during human immunodeficiency virus infection? Evidence from the Italian Seroconversion Study. J Infect Dis 175: 775–780.

367. Beck EJ, Vitoria M, Mandalia S, Crowley S, Gilks CF, et al. (2006) National adult antiretroviral therapy guidelines in resource-limited countries: concordance with 2003 who guidelines? AIDS 20: 1497–1502.

368. UN Joint Programme on HIV/AIDS (UNAIDS) (Accessed February 2015). South Africa country profile (2013). Available: `http://www.unaids.org/sites/default/files/epidocuments/ZAF.pdf`.

369. Johnson LF (2012) Access to antiretroviral treatment in South Africa, 2004-2011. South Afr J HIV Med 13: 22–27.

370. Paterson DL, Swindells S, Mohr J, Brester M, Vergis EN, et al. (2000) Adherence to protease inhibitor therapy and outcomes in patients with HIV infection. Ann Intern Med 133: 21–30.

371. Hardon AP, Akurut D, Comoro C, Ekezie C, Irunde HF, et al. (2007) Hunger, waiting time and transport costs: time to confront challenges to ART adherence in Africa. AIDS care 19: 658–665.

372. Ananworanich J, Dubé K, Chomont N (2015) How does the timing of antiretroviral therapy initiation in acute infection affect HIV reservoirs? Current Opinion in HIV and AIDS 10: 18.

373. Herbeck JT, Mittler JE, Gottlieb GS, Goodreau S, Murphy JT, et al. (2016) Evolution of HIV-1 virulence in response to widespread scale up of antiretroviral therapy: a modelling study. Virus Evolution 2: vew208.

374. Mahy M, Stover J, Stanecki K, Stoneburner R, Tassie JM (2010) Estimating the impact of antiretroviral therapy: regional and global estimates of life-years gained among adults. Sex Transm Infect 86: ii67–71.

375. Williams BG, Lima V, Gouws E (2011) Modelling the impact of antiretroviral therapy on the epidemic of HIV. Curr HIV Res 9: 367–382.

376. McElrath MJ, De Rosa SC, Moodie Z, Dubey S, Kierstead L, et al. (2008) HIV-1 vaccine-induced immunity in the test-of-concept Step Study: a case–cohort analysis. Lancet 372: 1894–1905.

377. Little SJ, McLean AR, Spina CA, Richman DD, Havlir DV (1999) Viral dynamics of acute HIV-1 infection. J Exp Med 190: 841–850.

378. Schacker TW, Hughes JP, Shea T, Coombs RW, Corey L (1998) Biological and virologic characteristics of primary HIV infection. Annals of Internal Medicine 128: 613–620.

A

Supplementary material relating to chapter 3

This appendix originally appeared as supplementary material for my PLoS Genetics paper [36]. I have added Figures A.13 and A.14 which were included in the response to the reviewers but not in the original publication of the paper.

A.1 Supplementary methods

A.1.1 Estimating the number of escape events before first time point

The data in Table A.5 was used for this analysis. The prevalence of escape in HLA-mismatched hosts was used as an estimate for the true prevalence of transmitted escape so that an estimate for the number of transmitted escaped epitopes in HLA-matched hosts could be inferred. We then calculated the number of escape events driven before baseline as

$$\sum_{\text{epitopes}} (\text{HLA-matched patients with escape at first time point} - \text{HLA matched patients with transmitted escape})$$

giving a total of 5.9 escape events in epitopes in HLA-matched hosts. Since there were 530 HLA-matched patient-epitope pairs that were wild-type at the first time point this is 5.9 out of a possible 530+5.9 = 535.9 (the estimated number of wild-type epitopes in HLA-matched hosts at infection). The mean time between seroconversion and first available sequence data across all patient-epitope pairs was found to be 18.5 weeks. Therefore

$(535.9 - 5.9)/535.9$ gives a survival percentage of 98.9% in the first 18.5 weeks.

A.1.2 Is escape associated with clinical failure and if so would this lead us to underestimate the rate of escape?

In the 'time to escape' analysis of Figures 3.3 and 3.4, patients are censored from the survival analysis if they have no further sequence data or if they start long term ART (usually because they have reached the primary endpoint of the trial). If escape plays a part in driving clinical failure then those patients that were censored due to clinical failure during the three-year observation period may have had high rates of escape that we were unable to observe, leading us to underestimate the rate of escape.

We initially split all HLA-matched patient-epitope pairs into those that were censored from the survival analysis as a result of clinical failure within the three-year observation period and those whose censoring was unrelated to clinical failure (Figure A.2C). This first group was further divided into those whose last sequence data sample was before clinical failure (Figure A.2A), and those whose last sample was after clinical failure (Figure A.2B). Most of the patient-epitope pairs fell in category C.

The escape events that we are concerned we may have been unable to observe are those that would have been driven soon before clinical failure but remained unobserved since the patient had no further sequence data after failure. There are 20 and 24 patients with final sequence data before and after clinical failure respectively, and incident escape events were observed in 6 and 7 of these patients resp. (Fig A.2). Examination of the patients in category B showed that 75 patient-epitope pairs were wild-type at the time point before clinical failure and of these only two were observed to escape. Hence only two incident escape events would have been missed had sequence data not been available at the post-clinical failure time point. Given the similar numbers of patients in groups A and B it is fair to assume that the number of escape events that went unobserved in patients that were censored due to clinical failure (in A) was also around two. Therefore the extent to which escape is linked to censoring time is small and we do not believe that patients being censored after clinical failure has lead us to underestimate the rate of escape.

A.1.3 Multivariate Cox models for time to escape

In order to see whether the association between HLA relative risk and time to escape persisted when other factors were taken into account that could be confounding, we made a multivariate Cox proportional hazards model. We included predictors for time spent on ART, baseline viral load (VL), baseline CD4 count, number of responses each patient made to wild-type epitopes at baseline, and whether or not the patient had a protective HLA type. The HLA predictor remained in the model along with baseline viral load and CD4 count, but neither VL nor CD4 count were associated with a non-negligible hazard ratio, hence the association between possession of a protective HLA allele and time to first escape seems genuine.

A.1.4 Extending the definition of escape

The first amendment to the definition of escape considers all within-epitope mutations as 'escape' and so the epitope list is also no longer restricted to include only those epitopes with phenotypically verified escape sites. The resulting list in Table A.6 is the intersection of the HIV database 'A-list' of best defined epitopes and the set of optimal epitopes for which ELISpot assays were conducted.

The second amendment extended the epitope list so that it was not restricted to peptides for which ELISpot assays had been performed and also included epitopes on the longer list of epitopes available from the LANL immunology database [341]. Where a 'best-defined' epitope HLA restriction was available it was used.

A.2 Tables

Table A.1: The number of individual patients for which viral sequence and CD8$^+$ T-cell ELISpot data is available

Gene	Week (approximate)	Number of UK patients with data for viral sequence	2 t.p.s + ELISpot
gag	0	89	83
	24	60	
	52	66	
	108	35	
	156	8	
pol	0	96	54
	16 or 24	30	
	52 or 60	41	
	108	17	
	156	1	
env	0	70	55
	24	38	
	52	51	
	108	0	
	156	0	
nef	0	76	54
	24	60	
	52	62	
	108	39	
	156	12	

Note that some sequences do not cover the whole gene and so the number given is an upper bound for the number of patients who have sequence data for any one epitope. For each patient ELISpot data was either available for all 181 optimal peptides across all four genes or not at all. Data was available in 115 patients at week 0, 109 patients at week 24 and 115 patients at week 60. The final column gives the number of patients with at least 2 time points of sequence data and ELISpot data at at least one of 0, 24 or 60 weeks.

Table A.2: Diminished responses to variants present in the population at baseline

Epitope	Escape?	Prevalence	HLA matched	ELISpot response (%)
S L Y N T V A T L	HXB2	28/84	0.68	100.0
- - - - - I - V -	Y	16/84	0.69	69.6
- - F - - - - - -	Y	12/84	0.42	0.0
- - - - - - - V -	Y	12/84	0.50	1.1
- - F - - - - V -	Y	9/84	0.56	31.6
- - F - A - - V -	Y	2/84	1.00	0.0
- - F - - I - V -	Y	2/84	1.00	31.6
- - - - - I - - -	Y	2/84	1.00	115.2
- - F - - I - - -	Y	1/84	0.00	0.0
R L R P G G K K K	HXB2	45/75	0.09	100.0
- - - - - - - - Q	Y	16/75	0.06	0.0
- - - - - - - - R	Y	5/75	0.20	0.0
- - - - - - R - -	Y	5/75	0.00	5.1
- - - - - - - - T	Y	3/75	0.00	0.0
- - - - - - - - N	Y	1/75	1.00	0.0
A C Q G V G G P G H K	HXB2	70/84	0.09	100.0
- - - - - - - - S - -	Y	14/84	0.07	0.0
K R W I I L G L N K	HXB2	67/81	0.10	100.0
- - - - - M - - - -	Y	11/81	0.09	0.0
- K - - - M - - - -	Y	3/81	0.00	0.0
N A N P D C K T I	HXB2	69/84	0.06	100.0
- S - - - - - - -	Y	13/84	0.08	0.0
- - - - - - - I -	Y	2/84	0.00	0.0
E V K D T K E A L	Y	25/83	0.36	100.0
D - - - - - - - -	Y	24/83	0.13	45.4
- I - - - - - - -	HXB2	14/83	0.36	62.8
D - R - - - - - -	Y	11/83	0.18	0.0
- I R - - - - - -	N	4/83	0.25	0.0
D I - - - - - - -	Y	3/83	0.00	41.9
- - Q - - - - - -	Y	2/83	0.50	0.0
I L K E P V H G V	HXB2	77/89	0.57	100.0
- - - - - - - - A	Y	7/89	0.57	0.0
- - R - - - - - -	Y	5/89	0.60	0.0
T S T L Q E Q I G W	HXB2	43/73	0.00	100.0
- - - - - - - - A -	Y	20/73	0.05	36.9
- - N - - - - - A -	Y	6/73	0.33	5.7
- - N - - - - - T -	Y	2/73	0.50	7.7
- - - - - - - - D -	Y	1/73	1.00	55.7
- - - - - - - - E -	Y	1/73	1.00	54.0
T A F T I P S I	HXB2	50/83	0.02	100.0
- - - - - - - T	Y	33/83	0.06	0.6

All epitopes for which $CD8^+$ T-cell responses to autologous variants were assessed and for which there was at least one HLA-matched patient with a positive response to the optimal epitope are shown. The top sequence for each epitope gives the pre-defined optimal ELISpot peptide, which is also the most prevalent variant in each case. The 'Escape' column records whether or not each variant is classified as escape according to our definition. The prevalence of each variant in the cohort at baseline and the proportion of patients with a particular variant who are HLA-matched for the epitope are also recorded. The final column gives the average ELISpot response to the variant (number of SFCs) in those that are HLA-matched and respond to the optimal, as a percentage of their response to the optimal.

Table A.3: The numbers of HLA-matched and -mismatched patients with escape at baseline

Epitope	HLA restriction	Matched	with escape	Mismatched	with escape	p
ACQGVGGPGHK	A*1101	7	1	78	13	
AENLWVTVY	B*1801	2	2	67	61	
AIFQSSMTK	A*0301, A*1101	23	0	72	6	
AVDLSHFLK	A*0301, A*1101	13	1	62	6	
DCKTILKAL	B*0801	20	1	65	0	
DRFYKTLRA	B*1402	5	0	80	5	
EIYKRWII	B*0801	20	3	65	8	
ELRSLYNTV	B*0801	21	14	67	51	
EVIPMFSAL	A*2601	5	2	83	25	
EVKDTKEAL	B*0801	21	15	67	54	
FLKEKGGL	B*0801	19	3	56	9	
GEIYKRWII	B*0801	20	3	64	7	
GELDRWEKI	B*4002	2	0	85	2	
GGKKKYKLK	B*0801	21	4	67	9	
HTQGYFPDWQ	B*5701	5	1	71	18	
ILKEPVHGV	A*0201	54	9	41	7	
ILKEPVHGVY	B*1501	14	1	81	8	
IRLRPGGKK	B*2705	9	2	79	11	
ISPRTLNAW	B*5701	7	2	81	27	
IVLPEKDSW	B*5701	8	5	83	32	0.17
KAFSPEVIPMF	B*5701, B*5703	7	0	81	1	
KEKGGLEGL	B*4001, B*4002	15	5	60	9	0.11
KIRLRPGGK	A*0301	7	1	81	18	
KRWIILGLNK	B*2705	9	2	77	16	
KYKLKHIVW	A*2402	15	11	73	59	
LVGPTPVNI	A*0201	53	0	42	1	
NANPDCKTI	B*5101	5	1	80	15	
QASQEVKNW	B*5301, B*5701	8	4	77	33	
QVPLRPMTYK	A*0301, A*1101	13	2	62	17	
RLRPGGKKK	A*0301	7	3	81	38	
RPNNNTRKSI	B*0702	10	10	59	59	
RPQVPLRPM	B*4201	0	0	75	3	
SFNCGGEFF	B*1516	0	0	70	9	
SLYNTVATL	A*0201, A*0202, A*0205	52	33	36	27	
TAFTIPSI	B*5101	4	3	90	39	
TPGPGVRYPL	B*0702,B*4201	15	0	61	3	
TPQDLNTML	B*0702, B*3910, B*4201, B*8101	14	0	73	2	
TSTLQEQIGW	B*5701, B*5801	6	6	80	36	0.01
VIYQYMDDL	A*0201	54	2	42	3	
VLEWRFDSRL	A*0201	43	17	29	14	
VPLRPMTY	B*3501	5	1	69	13	
WPTVRERM	B*0801	19	19	53	42	0.03
WRFDSRLAF	B*1503	2	1	71	33	
YETEVHNVW	B*1801	2	2	68	37	
YLKDQQLL	B*0801	18	18	52	49	
YPGIKVRQL	B*4201	0	0	96	90	
Totals		679	210	3152	1025	

All p-values < 0.2 are given for a Fisher's exact test with the alternative hypothesis that the proportion of escape in matched hosts is greater than that in mismatched hosts

Table A.4: The numbers of HLA-matched and -mismatched patients with escape after 1 year

Epitope	HLA restriction	Matched	with escape	Mismatched	with escape	p
ACQGVGGPGHK	A*1101	6	1	59	14	
AENLWVTVY	B*1801	1	1	50	45	
AIFQSSMTK	A*0301, A*1101	13	1	27	4	
AVDLSHFLK	A*0301, A*1101	12	4	50	3	0.02
DCKTILKAL	B*0801	15	0	50	0	
DRFYKTLRA	B*1402	4	0	61	4	
EIYKRWII	B*0801	15	3	50	6	
ELRSLYNTV	B*0801	15	11	48	38	
EVIPMFSAL	A*2601	3	2	63	15	0.16
EVKDTKEAL	B*0801	15	10	48	39	
FLKEKGGL	B*0801	16	4	46	6	
GEIYKRWII	B*0801	15	3	50	6	
GELDRWEKI	B*4002	2	0	59	0	
GGKKKYKLK	B*0801	15	2	47	6	
HTQGYFPDWQ	B*5701	5	3	57	17	0.19
ILKEPVHGV	A*0201	23	4	18	0	0.09
ILKEPVHGVY	B*1501	4	0	36	1	
IRLRPGGKK	B*2705	4	1	58	7	
ISPRTLNAW	B*5701	6	2	59	20	
IVLPEKDSW	B*5701	2	2	34	11	0.12
KAFSPEVIPMF	B*5701, B*5703	6	0	60	2	
KEKGGLEGL	B*4001, B*4002	13	3	49	6	
KIRLRPGGK	A*0301	6	2	56	12	
KRWIILGLNK	B*2705	5	2	60	12	
KYKLKHIVW	A*2402	10	9	52	42	
LVGPTPVNI	A*0201	21	0	17	1	
NANPDCKTI	B*5101	3	1	62	10	
QASQEVKNW	B*5301, B*5701	8	4	57	32	
QVPLRPMTYK	A*0301, A*1101	12	4	50	10	
RLRPGGKKK	A*0301	6	5	56	22	0.05
RPNNNTRKSI	B*0702	6	6	44	43	
RPQVPLRPM	B*4201	0	0	62	3	
SFNCGGEFF	B*1516	0	0	50	9	
SLYNTVATL	A*0201, A*0202, A*0205	34	22	29	22	
TAFTIPSI	B*5101	2	2	36	11	0.11
TPGPGVRYPL	B*0702, B*4201	12	0	50	2	
TPQDLNTML	B*0702, B*3910, B*4201, B*8101	11	0	55	3	
TSTLQEQIGW	B*5701, B*5801	6	4	60	28	
VIYQYMDDL	A*0201	23	1	18	0	
VLEWRFDSRL	A*0201	36	13	24	12	
VPLRPMTY	B*3501	6	3	56	8	0.06
WPTVRERM	B*0801	16	15	42	35	
WRFDSRLAF	B*1503	1	0	58	24	
YETEVHNVW	B*1801	1	1	50	27	
YLKDQQLL	B*0801	14	14	37	36	
YPGIKVRQL	B*4201	0	0	41	40	
Totals		449	165	2201	694	

All p-values < 0.2 are given for a Fisher's exact test with the alternative hypothesis that the proportion of escape in matched hosts is greater than that in mismatched hosts

Table A.5: The numbers of HLA-matched and -mismatched patients with escape at the first time point

Epitope	HLA restriction	Matched (escaped)	Mismatched (escaped)	Incident escape	
				Matched	Mismatched
ACQGVGGPGHK	A*1101	9 (1)	90 (16)	2	3
AENLWVTVY	B*1801	2 (2)	78 (71)	0	1
AIFQSSMTK	A*0301, A*1101	26 (1)	75 (7)	0	1
AVDLSHFLK	A*0301, A*1101	19 (2)	75 (6)	3	1
DCKTILKAL	B*0801	22 (1)	77 (1)	0	0
DRFYKTLRA	B*1402	9 (0)	90 (6)	1	0
EIYKRWII	B*0801	22 (3)	77 (9)	0	1
ELRSLYNTV	B*0801	22 (15)	77 (60)	1	3
EVIPMFSAL	A*2601	5 (2)	94 (28)	1	1
EVKDTKEAL	B*0801	22 (15)	77 (62)	0	2
FLKEKGGL	B*0801	23 (5)	71 (10)	4	3
GEIYKRWII	B*0801	22 (3)	76 (8)	0	1
GELDRWEKI	B*4002	2 (0)	96 (2)	0	0
GGKKKYKLK	B*0801	22 (4)	76 (11)	0	1
HTQGYFPDWQ	B*5701	8 (3)	86 (25)	1	0
ILKEPVHGV	A*0201	56 (10)	45 (7)	0	0
ILKEPVHGVY	B*1501	14 (1)	87 (8)	0	0
IRLRPGGKK	B*2705	9 (2)	89 (13)	0	1
ISPRTLNAW	B*5701	7 (2)	92 (30)	1	0
IVLPEKDSW	B*5701	8 (5)	91 (35)	0	1
KAFSPEVIPMF	B*5701, B*5703	7 (0)	92 (1)	0	2
KEKGGLEGL	B*4001, B*4002	16 (5)	78 (14)	2	3
KIRLRPGGK	A*0301	11 (2)	87 (20)	0	0
KRWIILGLNK	B*2705	9 (2)	90 (20)	3	1
KYKLKHIVW	A*2402	17 (13)	81 (67)	4	4
LVGPTPVNI	A*0201	55 (0)	46 (1)	0	0
NANPDCKTI	B*5101	5 (1)	94 (16)	0	0
QASQEVKNW	B*5301, B*5701	9 (4)	90 (41)	2	5
QVPLRPMTYK	A*0301, A*1101	19 (5)	75 (20)	2	5
RLRPGGKKK	A*0301	11 (5)	87 (39)	1	2
RPNNNTRKSI	B*0702	11 (11)	69 (67)	0	1
RPQVPLRPM	B*4201	0 (0)	94 (5)	0	1
SFNCGGEFF	B*1516	0 (0)	81 (10)	0	2
SLYNTVATL	A*0201, A*0202, A*0205	60 (39)	39 (27)	3	4
TAFTIPSI	B*5101	5 (3)	95 (40)	2	0
TPGPGVRYPL	B*0702, B*4201	18 (0)	76 (3)	0	0
TPQDLNTML	B*0702, B*3910, B*4201, B*8101	21 (1)	78 (2)	0	1
TSTLQEQIGW	B*5701, B*5801	7 (6)	92 (41)	0	1
VIYQYMDDL	A*0201	56 (2)	46 (3)	0	0
VLEWRFDSRL	A*0201	55 (23)	37 (16)	2	4
VPLRPMTY	B*3501	8 (2)	86 (17)	2	3
WPTVRERM	B*0801	23 (22)	67 (53)	0	1
WRFDSRLAF	B*1503	2 (1)	90 (40)	0	7
YETEVHNVW	B*1801	2 (2)	79 (41)	0	2
YLKDQQLL	B*0801	20 (20)	61 (58)	0	1
YPGIKVRQL	B*4201	0 (0)	102 (96)	0	1
Totals		776 (246)	3631 (1173)	37	71

Since a few patients did not have available sequence data at baseline, this table is similar but not identical to Table A.3. The number of incident escape events observed within HLA-matched and -mismatched patients is also given

Table A.6: All epitopes in first extended definition of escape

Gene	Epitopes			
gag	**ACQGVGGPGHK**	AEQASQDVKNW	AEWDRVHPV	**DCKTILKAL**
	DRFYKTLRA	EEKAFSPEV	**EIYKRWII**	**ELRSLYNTV**
	ETINEEAAEW	**EVIPMFSAL**	**EVKDTKEAL**	FRDYVDRFYK
	GEIYKRWII	**GELDRWEKI**	**GGKKKYKLK**	GHQAAMQML
	GHQAAMQMLKE	GLNKIVRMY	GPGHKARVL	GQMREPRGSDI
	GVGGPGHK	HAGPIAPGQMREPRG	HPVHAGPIA	HQAISPRTL
	IEIKDTKEAL	**IRLRPGGKK**	**ISPRTLNAW**	**KAFSPEVIPMF**
	KETINEEAA	**KIRLRPGGK**	KIRLRPGGKK	**KRWIILGLNK**
	KYKLKHIVW	LYNTVATLY	MTNNPPIPV	**NANPDCKTI**
	NSSKVSQNY	PPIPVGDIY	QAISPRTLNAW	**QASQEVKNW**
	RDYVDRFYKTL	**RLRPGGKKK**	RLRPGGKKKY	RMYSPTSI
	RSLYNTVATLY	SEGATPQDL	**SLYNTVATL**	SPRTLNAWV
	TLNAWVKVV	TLYCVHQK	TLYCVHQRI	**TPQDLNTML**
	TSTLQEQIGW	VKVIEEKAF	VQNLQGQMV	WASRELERF
	YVDRFYKTL			
nef	AALDLSHFL	**AVDLSHFLK**	**FLKEKGGL**	FPVTPQVPLR
	HTQGYFPDWQ	**KEKGGLEGL**	LEKHGAITS	PLRPMTYK
	PLTFGWCYKL	**QVPLRPMTYK**	RPMTYKAAL	**RPQVPLRPM**
	RQDILDLWV	RRQDILDLWI	RRQDILDLWVY	RYPLTFGW
	TPGPGVRYPL	TPQVPLRPM	TQGYFPDWQNY	**VLEWRFDSRL**
	VPLRPMTY	**WPTVRERM**	**WRFDSRLAF**	YPLTFGWCF
pol	**AIFQSSMTK**	ALVEICTEM	ALVEICTEMEK	EKEGKISKI
	GIPHPAGLK	GKKAIGTVL	GPKVKQWPL	HPDIVIYQY
	IEELRQHLL	IETVPVKL	**ILKEPVHGV**	**ILKEPVHGVY**
	IRYQYNVL	**IVLPEKDSW**	KLNWASQIY	KLVDFRELNK
	KQNPDIVIY	LVGKLNWASQIY	**LVGPTPVNI**	NETPGIRYQY
	NPEIVIYQY	QIYPGIKVR	RQYDQILIEI	SPAIFQSSM
	TAFTIPSI	TPVNIIGRNML	TVLDVGDAY	**VIYQYMDDL**
	VPLDEDFRKY	**YPGIKVRQL**	YTAFTIPSV	
env	**AENLWVTVY**	AENLWVTVYY	DPNPQEVVL	ERYLKDQQL
	EVAQRAYR	HIGPGRAFY	IPRRIRQGL	IVNRNRQGY
	IVTRIVELL	LFCASDAKAY	LPCRIKQII	MHEDIISLW
	RGPGRAFVTI	RIKQIINMW	RIRQGLERA	**RPNNNTRKSI**
	RQGLERALL	RVKEKYQHL	RYLKDQQLL	SFEPIPIHY
	SFNCGGEFF	SLLNATDIAV	SVITQACPK	TAVPWNASW
	TVYYGVPVWK	VPVWKEATTT	VPVWKEATTTL	**YETEVHNVW**
	YLKDQQLL			

Peptides that are also in the 'A-list' of optimal epitopes are shown in bold

A.3 Figures

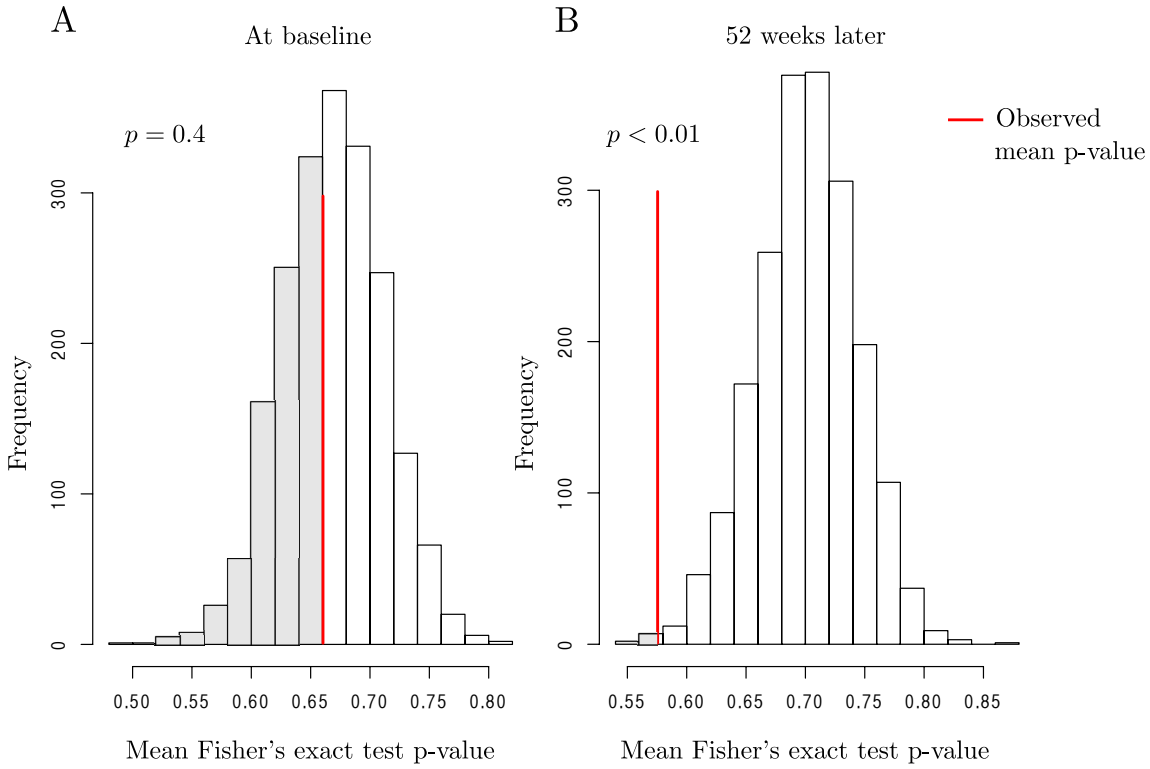


Figure A.1: The distribution of escape between HLA-matched and mismatched host-epitope pairs at baseline and 1 year later. Histograms show the distribution of the mean of the Fisher's exact test p-values for independence of HLA-matching and escape in each epitope, under the null hypothesis that 'escape' is equally likely to be seen in HLA-matched and -mismatched hosts. (A) at baseline, (B) at 52 weeks. The red lines show the observed mean of the p-values. 2000 random simulations were used to obtain the null distributions. There is significant evidence to reject the null hypothesis at 52 weeks but not baseline, suggesting that little escape has already been driven before baseline.

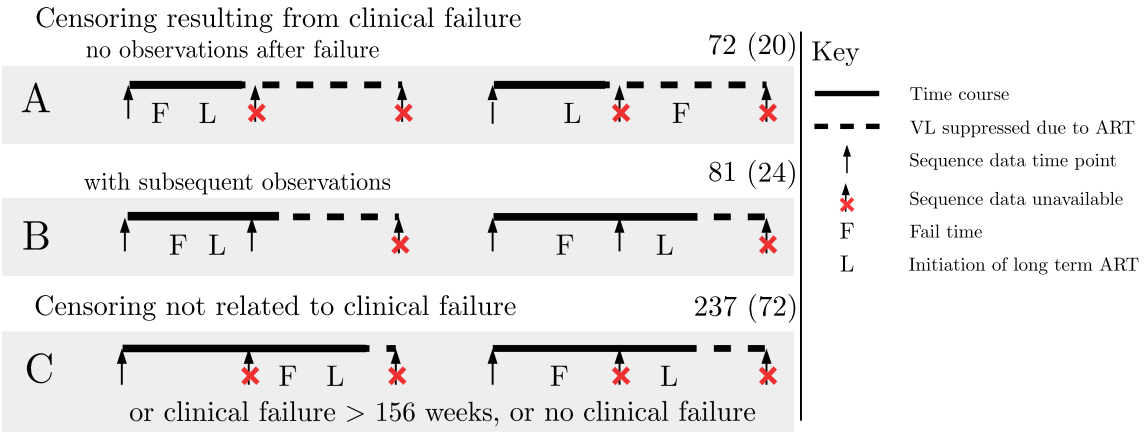


Figure A.2: Defining the relationship between clinical failure and censoring. Each patient-epitope pair was categorised according to if and when the patient reached the trial endpoint and how their time of clinical failure related to the last available sequence data point, as shown here diagrammatically. The three categories are (A) censoring may have resulted from clinical failure and there were no observations after failure, (B) censoring may have resulted from clinical failure but there was at least 1 further observation after failure, and (C) censoring is not related to clinical failure since long course ART was started after the last observed data point. Numbers on the right hand side represent the number of HLA-matched patient-epitope pairs and in brackets the number of distinct patients in each category. Note that three patients have epitopes in both A and B. One patient was removed as they were suspected to have been superinfected during the observation period.

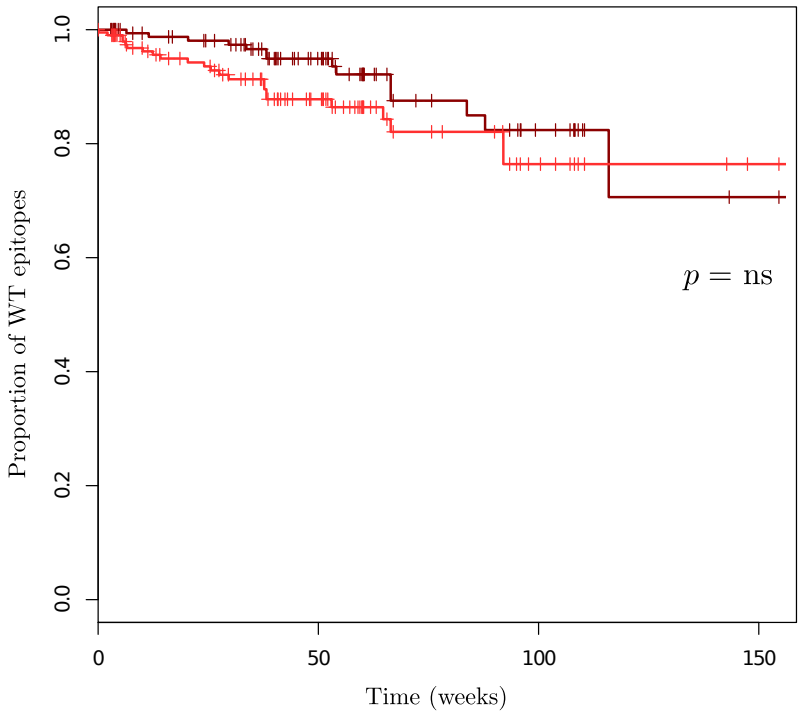


Figure A.3: Kaplan-Meier survival cure for wild-type epitopes, split by restricting HLA. All HLA-matched host-epitope pairs are considered. Epitopes restricted by a protective HLA-allele as defined in Figure 3.3 (light red) escape sooner than others (dark red). There is no significant increased risk associated with restriction by a protective allele here ($p = 0.3$, mixed effects Cox model as in Figure 3.4), though narrowing the definition of 'protective' does result in significance.

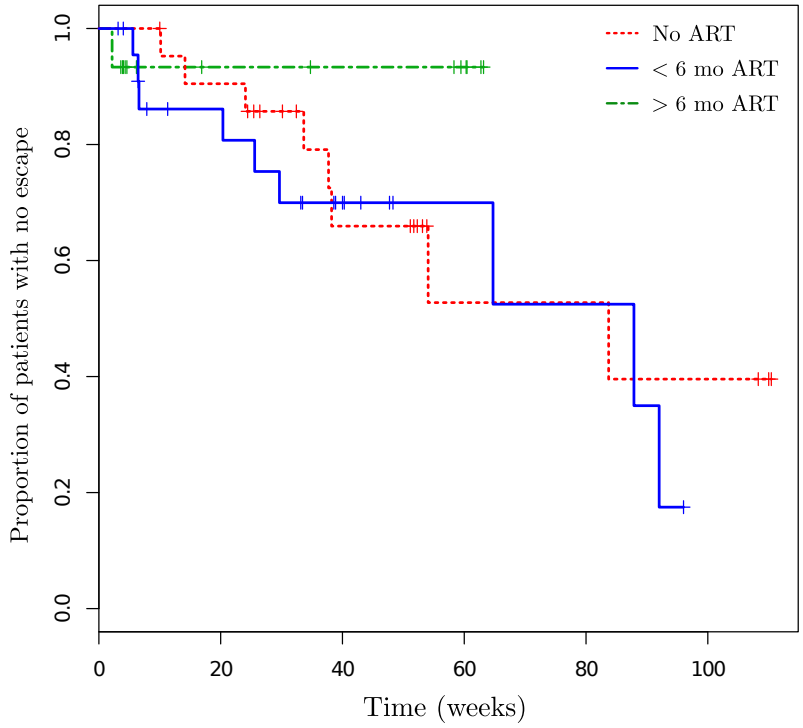


Figure A.4: Kaplan-Meier plots to show time to first escape (using midpoint approximation) within the patients of this cohort, split by the duration of therapy they have received. Patients who were either missing data for *gag* or *nef*, the two genes for which the most data was available, were not included so as not to skew the results due to lack of data. Time to first escape in an HLA-restricted epitope is plotted. These survival curves are very similar for the patients who have received no ART and who have received < 6 months of ART. Patients who have received > 6 mo ART were observed for less time off ART and hence the number of patients in this group with enough data to be included in the analysis is smaller (15 patients compared to 22 with no ART and 24 with < 6 mo ART). Therefore, while there appears to be a slower rate of escape in patients who have received > 6 months ART this difference is not significant ($p = 0.24$) and the effect of removing this group from the data is small (see Figure A.5).

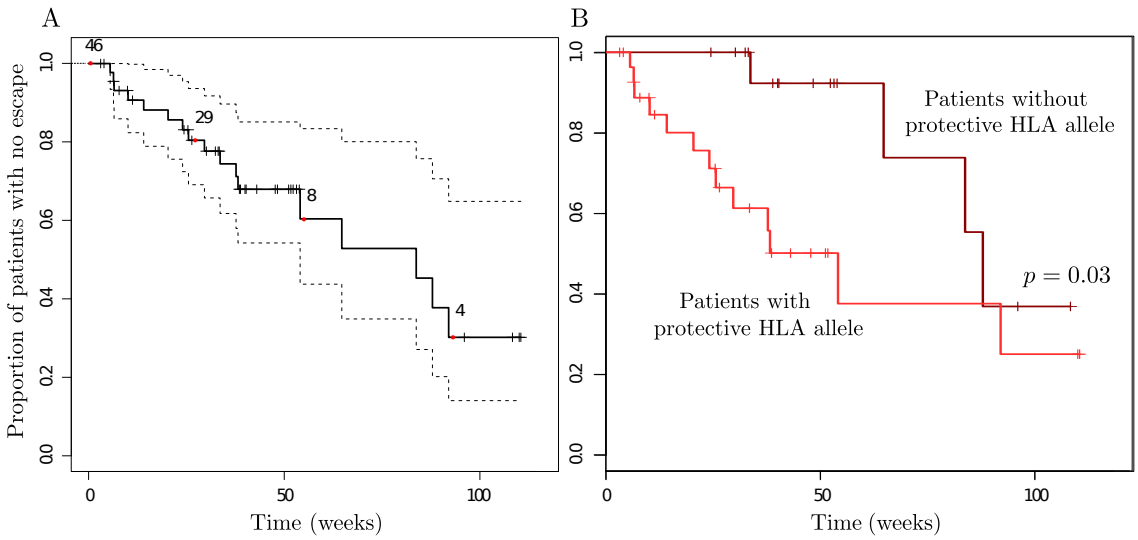


Figure A.5: Kaplan-Meier plots to show time to first escape (using midpoint approximation) within the patients of this cohort, excluding patients who have received > 6 mo ART. Patients who were either missing data for *gag* or *nef*, the two genes for which the most data was available, were not included so as not to skew the results due to lack of data. (A) Time to first escape in an HLA-restricted epitope (solid line) is plotted along with 95% confidence intervals (dotted line). (B) Patients are split according to whether they have one of the more 'protective' HLA alleles or not. The set of beneficial alleles was taken to be B*58, B*27, B*57, A*26, B*51, A*11, B*14, B*18, B*08 (all the HLA-A and -B alleles down to B*08 that are present in our data, taken from the ranking in [334]). Having a protective HLA resulted in a significantly increased risk of escape in an HLA-restricted epitope (p=0.03, HR = 3.3). In both plots the x-axis represents the time since cessation of ART, or baseline for those who did not receive ART, and vertical checks mark time points at which patients were censored (either because they began long term ART or because there was no further sequence data available for them). Numbers indicate the number of patients who have not yet escaped or been censored at the corresponding red dots (time points: 0, 27, 55, 93 wks).

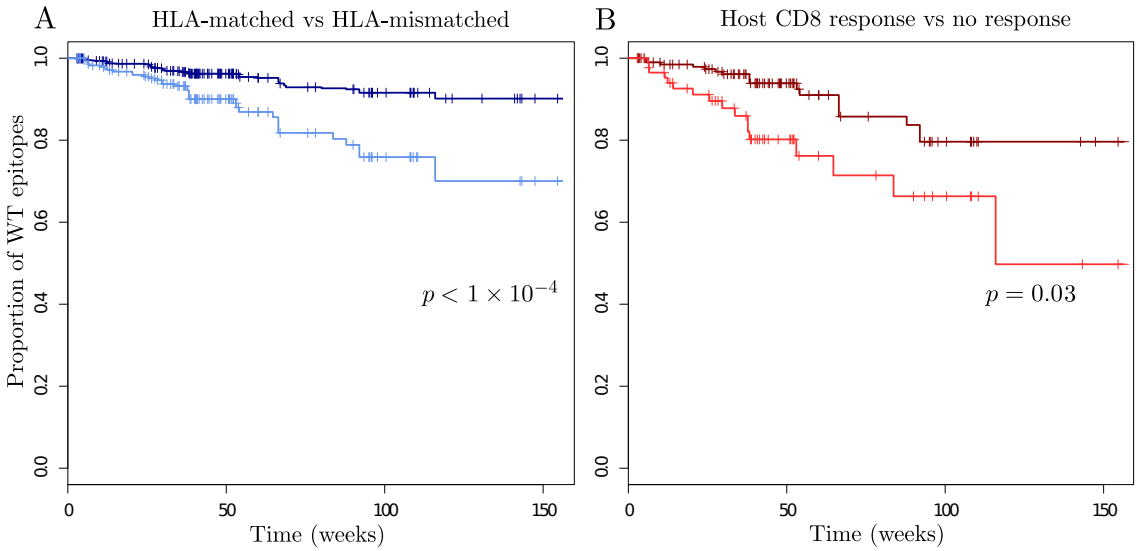


Figure A.6: Kaplan-Meier survival curves for wild-type epitopes, excluding patients who have received $>$ 6 mo ART. As with time to first escape in a patient, time to escape in epitopes was longer for epitopes in patients who have previously received $>$ 6 mo ART, but there was no difference between epitopes in those who had received no ART and in those who had received $<$ 6 mo ART. (A) Time to a first escape in epitopes within HLA-mismatched (dark blue) and -matched (light blue) hosts is shown. (B) Epitopes in HLA-matched hosts are split according to whether they have a measurable $CD8^+$ T-cell ELISpot response to them (light red) or not (dark red). As in Figure 3.4, escape is strongly significantly faster within epitopes in HLA-matched hosts ($p < 1 \times 10^{-4}$, HR = 2.5) and then faster again if the host has a measurable $CD8^+$ T-cell ELISpot response to that epitope ($p = 0.034$, HR = 2.7). p-values and hazard ratios were calculated using a mixed effects model as in Figure 3.4.

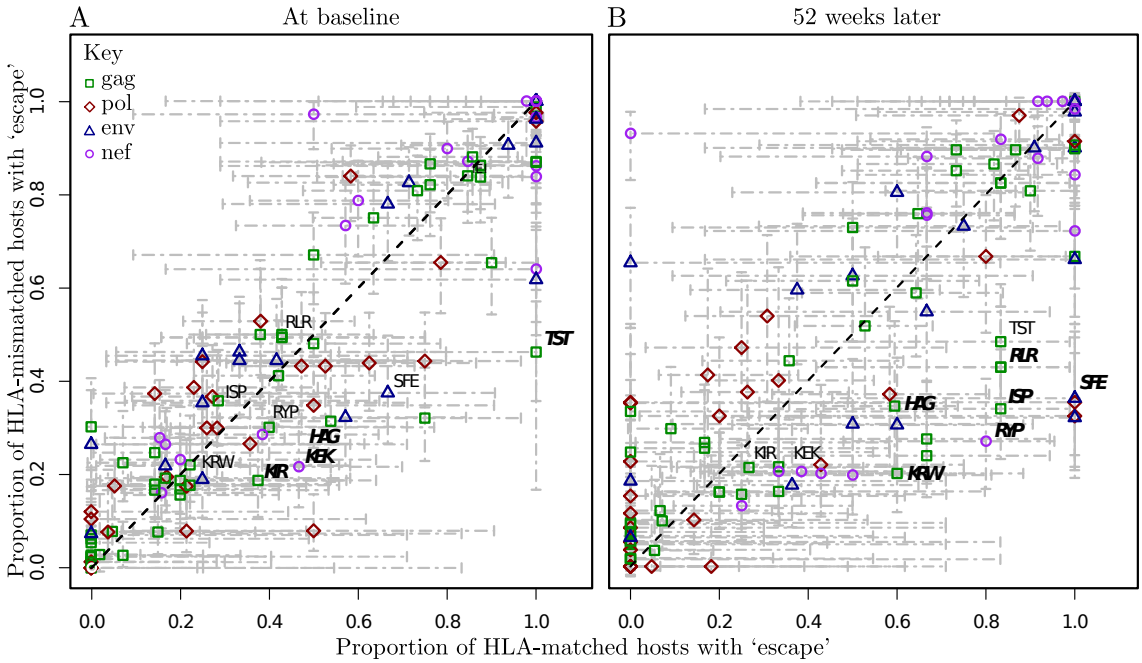


Figure A.7: Escape prevalence in HLA-matched and -mismatched hosts, where escape is defined as any mutation within the epitope. Epitopes are labelled where possible with their first three amino acids. Bars represent 95% binomial confidence limits (Agresti-Coull method). The dotted black line is $y = x$. Epitopes labelled in bold have a significantly higher proportion of escape in matched hosts than in mismatched hosts (one-tailed Fisher's Exact test, $p < 0.1$). Note that this plot is noisier than Figure 3.1 since a smaller proportion of the mutations classified as 'escape' are likely to be CTL related. Consequently the distribution at neither time point is significantly different from that under the null hypothesis that escape is equally likely to occur in HLA-matched and -mismatched hosts (permutation test, see Methods). (A) At baseline the majority of epitopes have escape at equal prevalence in HLA-matched and -mismatched hosts (B) 52 weeks later within host evolution has resulted in a higher prevalence of escape in HLA-matched hosts for many epitopes, with six lying significantly 'below the line' despite a decrease in the number of patients with sequence data available at 52 weeks.

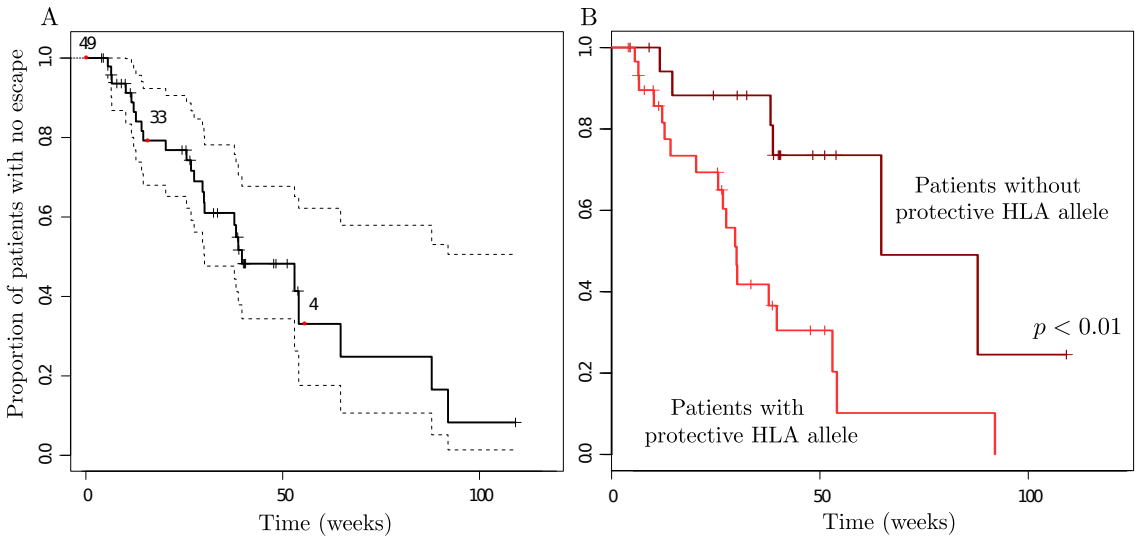


Figure A.8: Kaplan-Meier plots to show time to first escape (using midpoint approximation) within the patients of this cohort, excluding patients who have received > 6 mo ART, where escape is defined as any mutation within the epitope. Patients who were either missing data for *gag* or *nef*, the two genes for which the most data was available, were not included so as not to skew the results due to lack of data. (A) Time to first escape in an HLA-restricted epitope (solid line) is plotted along with 95% confidence intervals (dotted line). (B) Patients are split according to whether they have one of the more 'protective' HLA alleles or not. The set of beneficial alleles was taken to be all the HLA-A and -B alleles down to B*08 that are present in our data, taken from the ranking in [334]. Having a protective HLA resulted in a significantly increased risk of escape in an HLA-restricted epitope ($p = 0.003$, HR $= 3.6$). In both plots the x-axis represents the time since cessation of ART, or baseline for those who did not receive ART, and vertical checks mark time points at which patients were censored (either because they began long term ART or because there was no further sequence data available for them). Numbers indicate the number of patients who have not yet escaped or been censored at the corresponding red dots (time points: 0, 27, 55 wks).

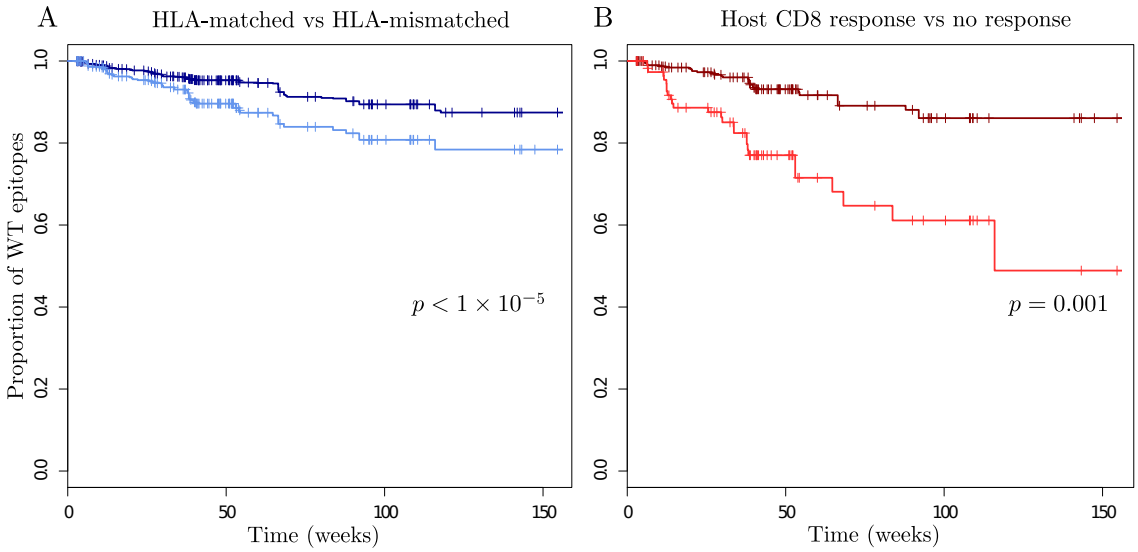


Figure A.9: Kaplan-Meier survival curves for wild-type epitopes, excluding patients who have received > 6 mo ART, where escape is defined as any mutation within the epitope. (A) Time to a first escape for epitopes in HLA-mismatched (dark blue) and -matched (light blue) hosts is shown. (B) Epitopes within HLA-matched hosts are split according to whether they have a measurable $CD8^+$ T-cell ELISpot response to them (light red) or not (dark red). As in Figure 3.4, escape is strongly significantly faster within epitopes in HLA-matched hosts ($p < 1 \times 10^{-5}$, HR=2.2) and then faster again if the host has a measurable $CD8^+$ T-cell ELISpot response to that epitope ($p = 0.001$, HR=2.9). p-values and hazard ratios were calculated using a mixed effects model as in Figure 3.4.

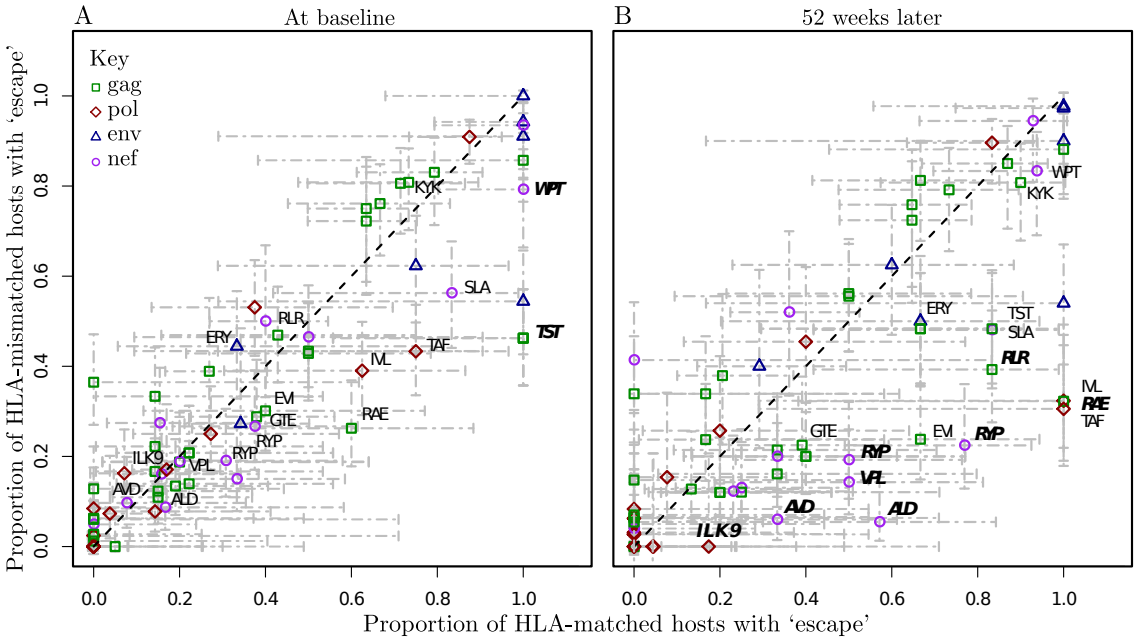


Figure A.10: Escape prevalence in HLA-matched and -mismatched hosts, where the escape list has been extended beyond the optimals to all epitopes $<$ 12aa in length with a 4-digit HLA restriction defined. Epitopes are labelled where possible with their first three amino acids. Bars represent 95% binomial confidence limits (Agresti-Coull method). The dotted black line is $y = x$. Epitopes labelled in bold have a significantly higher proportion of escape in matched hosts than in mismatched hosts (one-tailed Fisher's Exact test, $p < 0.1$). (A) At baseline the majority of epitopes have escape at equal prevalence in HLA-matched and -mismatched hosts and the distribution of points is not significantly different from as would be expected if escape was equally likely to occur in HLA-matched and -mismatched hosts ($p = 0.5$, permutation test) (B) 52 weeks later within host evolution has resulted in a higher prevalence of escape in HLA-matched hosts for many epitopes, with the eight epitopes and the distribution as a whole lying significantly 'below the line' ($p < 0.003$, permutation test, see Methods).

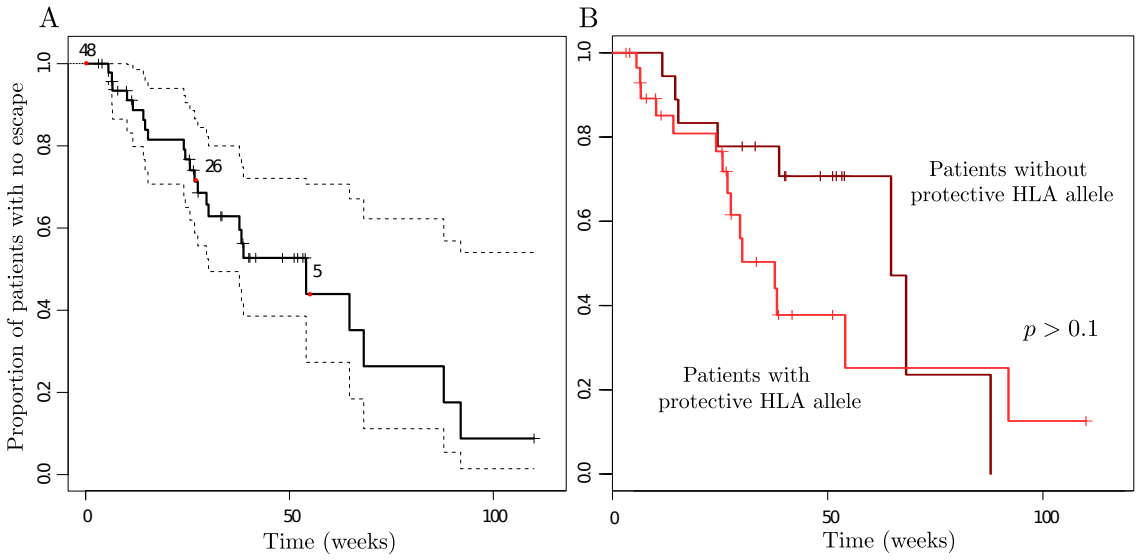


Figure A.11: Kaplan-Meier plots to show time to first escape (using midpoint approximation) within the patients of this cohort, excluding patients who have received > 6 mo ART, where the escape list has been extended beyond the optimals to all epitopes < 12 aa in length with a 4-digit HLA restriction defined. Patients who were either missing data for *gag* or *nef*, the two genes for which the most data was available, were not included so as not to skew the results due to lack of data. (A) Time to first escape in an HLA-restricted epitope (solid line) is plotted along with 95% confidence intervals (dotted line). (B) Patients are split according to whether they have one of the more 'protective' HLA alleles or not. The set of beneficial alleles was taken to be all the HLA-A and -B alleles down to B*08 that are present in our data, taken from the ranking in [334]. Having a protective HLA resulted in an increased risk of escape in an HLA-restricted epitope early on, but this was not significant. In both plots the x-axis represents the time since cessation of ART, or baseline for those who did not receive ART, and vertical checks mark time points at which patients were censored (either because they began long term ART or because there was no further sequence data available for them). Numbers indicate the number of patients who have not yet escaped or been censored at the corresponding time points marked by red dots 0, 27, 55 wks.

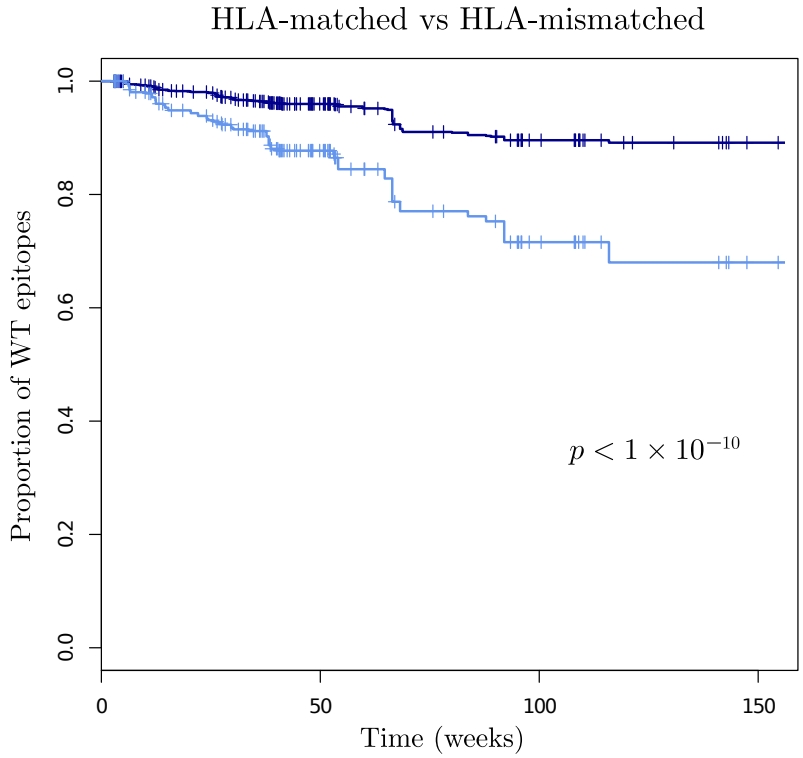


Figure A.12: Kaplan-Meier survival curves for wild-type, epitopes excluding patients who have received > 6 mo ART, where the escape list has been extended beyond the optimals to all epitopes < 12 aa in length with a 4-digit HLA restriction defined. Time to a first escape for epitopes in HLA-mismatched (dark blue) and -matched (light blue) hosts is shown. As in Figure 3.4, escape is strongly significantly faster within epitopes in HLA-matched hosts ($p < 1 \times 10^{-10}$, HR=3.2). The effect of a response could not be analysed as $CD8^+$ T-cell ELISpot responses were not measured for all of the extended list of epitopes. The p-value and hazard ratio was calculated using a mixed effects model as in Figure 3.4.

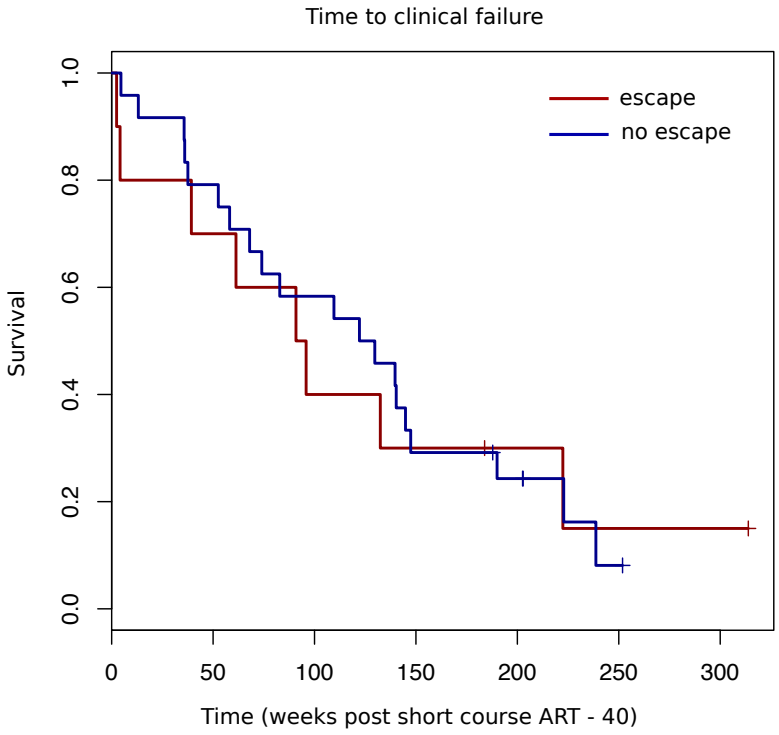


Figure A.13: No evidence for immune escape impacting disease progression. This analysis involved 34 patients for whom sequence data spanning at least 40 weeks off-therapy was available, and who do not reach the primary endpoint of the trial within 40 weeks of coming off any short term therapy. Patients are split according to whether an incident escape was estimated to occur within the first 40 weeks of off-therapy observation. The Kaplan-Meier shows time to primary endpoint (defined as reaching a CD4 count of < 350 cells/mm^3 or initiating long-term ART). Presence of an escape in the first 40 weeks (red) vs. no escape in that period (blue) had no significant effect on time to clinical failure in the trial. Adjusting the '40' threshold between 24 and 52 weeks always gave a similar result. A Cox proportional hazards test showed no significant difference between the two groups ($p = 0.86$).

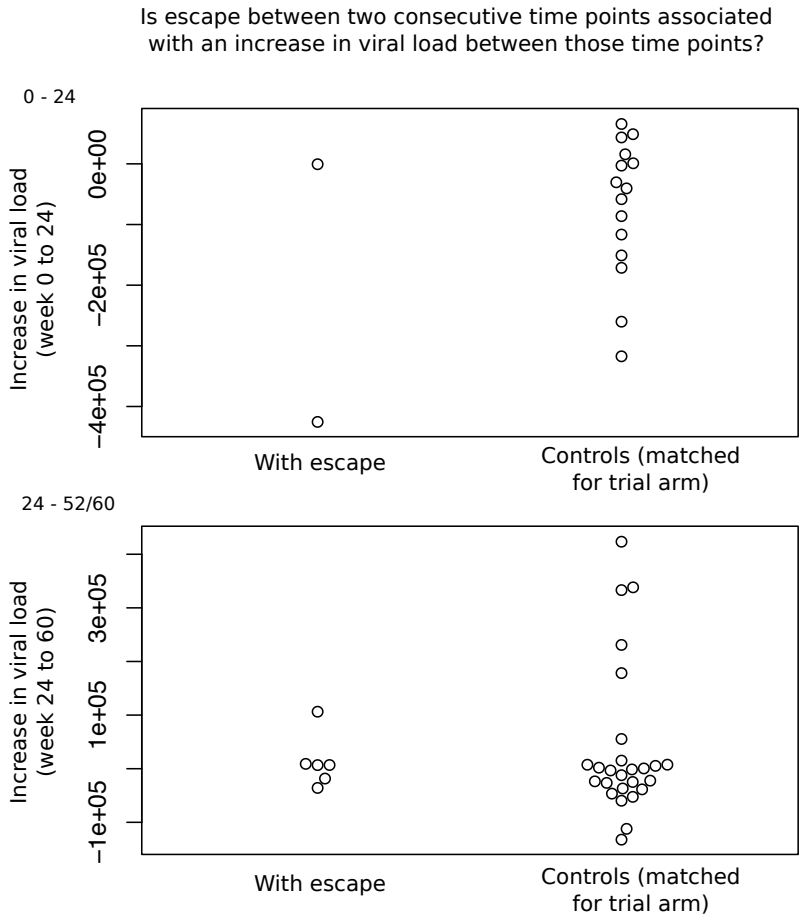


Figure A.14: No evidence for an increase in viral load following observed incident escape. Top panel: Patients who had sequence data for at least *gag* and *nef* at both 0 and 24 weeks, and viral load data at both time points, were selected for analysis. There were two patients with an incident escape between these time points. Controls were selected from those with no incident escape, matching for trial arm (short course ART or standard of care). The change in viral load between week 0 and 24 is plotted for both groups of patients. Bottom panel: The same analysis as above but using the 24 week and 52 or 60 week time points. Although there was only limited data to conduct the analysis, we found no evidence for a change in the viral load (either greater or lower) following the emergence of an escape mutation. We have no statistical support for this result, due to there being few patients with sequence data at consecutive time points in multiple genes.

B

Supplementary methods relating to chapter 4

B.1 Parameterising the force of infection

Several studies have estimated the value of the transmission coefficient, often termed β, from patient data. In chronic infection, when viral load, V, is stable, βV is equivalent to the force of infection, termed λ_2 in our model. However the structure of the models fitted to the data in these studies differs from our model in that they do not include susceptible cells becoming activated from a dynamic resting pool but rather have a constant rate of influx of new susceptible cells. Therefore we cannot simply take estimates of βV from the literature and use them for our analysis. Instead we first extend our set of ODEs to explicitly model the behaviour of productively infected cells and virions. We then work out for what range of values of β we get the following necessary dynamics: (1) peak vireamia of the order of 20 days after infection [377], (2) viral load reaches a (non-zero) set point, which we will denote V_{SP}, following acute infection [378].

The full model is as follows.

$$\frac{dR_i}{dt} = B_i - (d_R + b_i)R_i + \rho T_i$$
$$\frac{dT_i}{dt} = b_i R_i - (\rho + \beta V)T_i$$
$$\frac{dL_i}{dt} = f\beta V T_i - d_L L_i - \alpha_i L_i$$
$$\frac{dP_i}{dt} = (1-f)\beta V T_i - kP_i + \alpha_i L_i$$
$$\frac{dV}{dt} = Nk\sum_i P - cV$$

The parameters k, N and c are taken from the literature [308] ($k = 1, N = 2000, c = 23$). Figure B.1 shows timing of peak vireamia and the setpoint (calculated as the average value of V between 100 and 1000 days) for values of β in the range 0.00001 to 0.01. The values of β for which peak vireamia falls within 2 and 50 days are indicated by the red shaded area. On the right hand plot the value of the viral load set point is shown in blue. The dotted line indicates that a β value of 0.0005 results in a set point of 1. This absolute number is fairly arbitrary but plotting the behaviour of V with time shows that when β is this low, viral load oscillates by more than one order of magnitude in chronic infection. Hence this seems like a reasonable lower limit for β. The upper limit is given by the peak viral load timing being later than 2 days - this corresponds to $\beta \approx 0.002$. βV_{SP} is plotted in purple; this allows us to translate the reasonable range for β into a reasonable range for $\lambda_2 = \beta V_{\mathrm{SP}}$. This is indicated by the dotted lines to the right hand axis and is approximately 0.0005 – 0.01.

Figure B.2 shows the viral load curves from model simulations using the values of β and corresponding values of λ_2 at the top and bottom of the reasonable range described (left hand plots). It also shows the simulated behaviour of the three latently infected populations, similarly to in the figures of the main text, for the value of λ_2 at the top of the range. This is the value used in the main text.

In order to parameterise λ_1/λ_2 we calculated the area under the viral load curve in the simulation of the full model with $\beta = 0.0018$ (light pink line, corresponding $\lambda_2 = 0.01$). The area under the curve in the first 50 days was 7600 whereas from day 50 to 100 it was 520. Hence in this simulation the average force of infection falls by more than 10-fold

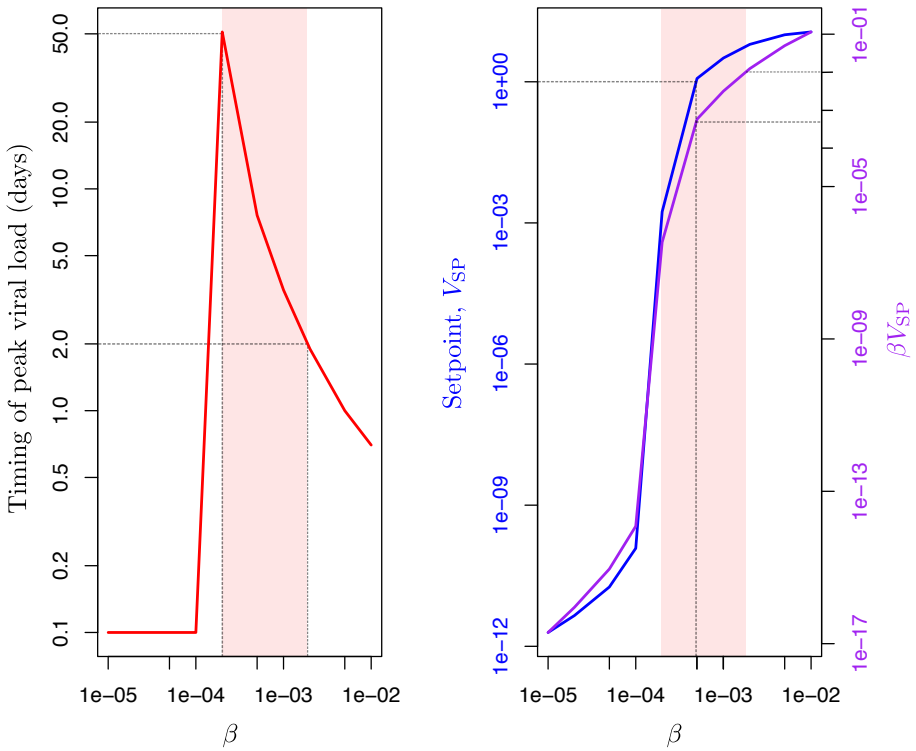


Figure B.1: The timing of peak viraemia and set point viral load as a function of the transmission coefficient, β. The red shaded area on both plots indicates the values of β for which peak viraemia occurs between 2 and 50 days. On the right hand plot set point viral load is plotted in blue, calculated as the average value of V between 100 and 1000 days. The product of β and the viral set point is shown in purple (right hand axis). The dotted lines to the right hand axis indicate the values of βV_{SP} for which both (1) peak viraemia occurs within the realistic time frame and (2) set point viral load is greater than 1.

between acute ($t < 50$) and chronic infection. Note that setting $\lambda_1 = 10\lambda_2$ results in similar values of $L_i(5\text{yrs})/L_i(50\text{d})$ in the model with fixed λ_j and the model with β – these values are indicated on the right hand side of the plots.

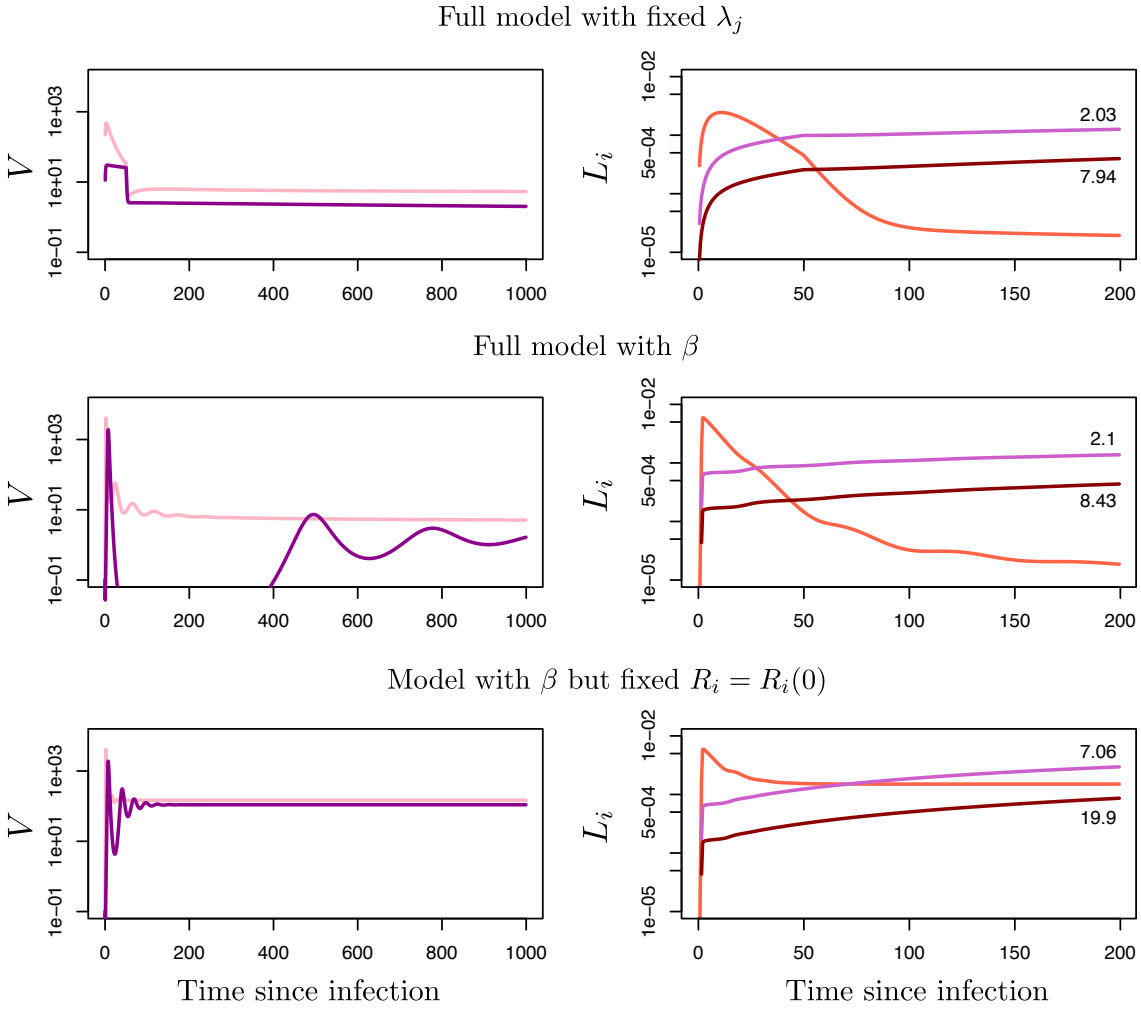


Figure B.2: Simulations of three different models for high and low values of β. On the left hand plots V is plotted against time for simulations with a high (light pink) and low (purple) force of infection. On the left hand plots L_1 (light red), L_2 (violet), and L_3 (dark red) are plotted against time. For L_2 and L_3, $L_i(5\text{yrs})/L_i(50\text{d})$ is calculated and indicated on the plots. Top: model with fixed force of infection (as used in main chapter) but with virion production simulated, for $\lambda_2 = 0.01$ (light pink) and $\lambda_2 = 0.0005$ (purple), $\lambda_1 = 10\lambda_2$. Middle: the full model with force of infection dependent on V, as detailed in section B.1, with $\beta = 0.0018$ (light pink) and $\beta = 0.0005$ (purple). Bottom: as middle panel but using a model in which R is fixed at its initial value.

B.2 Full solution to ODEs

We wish to solve the set of linear ODEs:

$$\begin{aligned}\frac{dR}{dt} &= B - (d_R + b)R + \rho T \\ \frac{dT}{dt} &= bR - (\rho + \lambda_j)T \\ \frac{dL}{dt} &= f\lambda_j T - (d_L + \alpha)L\end{aligned}$$

Let us solve first the equations for R and T. We may write

$$\mathbf{y} = \begin{pmatrix} R \\ T \end{pmatrix}, \quad \mathbf{A} = \begin{pmatrix} -(d_R + b) & \rho \\ b & -(\rho + \lambda_j) \end{pmatrix}$$

so that

$$\dot{\mathbf{y}} = \mathbf{A}\mathbf{y} + \begin{pmatrix} B \\ 0 \end{pmatrix}$$

Then if μ_1 and μ_2 are the eigenvalues of $\mathbf{A}$ and $\boldsymbol{\nu_1}$ and $\boldsymbol{\nu_2}$ are the corresponding eigenvectors, the solutions for R and T have the form

$$\mathbf{y} = \boldsymbol{\nu_1} e^{\mu_1 t} + \boldsymbol{\nu_2} e^{\mu_2 t} + \begin{pmatrix} g(t) \\ h(t) \end{pmatrix}$$

The eigenvalues of $\mathbf{A}$ satisfy

$$\mu^2 + (d_R + b + \rho + \lambda_j)\mu + b\lambda_j + d_R(\rho + \lambda_j) = 0$$

while eigenvectors satisfy

$$-(d_R + b)\nu_{i1} + \rho\nu_{i2} = \mu_i \nu_{i1} \quad \Rightarrow \quad \nu_{i1} = \frac{\rho}{b + d_R + \mu_i}\nu_{i2}$$

for $i = 1, 2$.

So the solutions are of the form

$$R = \frac{\rho}{d_R + b + \mu_1}\nu_{12}e^{\mu_1 t} + \frac{\rho}{d_R + b + \mu_2}\nu_{22}e^{\mu_2 t} + g(t)$$
$$T = \nu_{12}e^{\mu_1 t} + \nu_{22}e^{\mu_2 t} + h(t)$$

Substituting these into the differential equations shows that we can take $g(t)$ and $h(t)$ as constants:

$$g = \frac{B(\rho + \lambda_j)}{(d_R + b)(\rho + \lambda_j) - \rho b}, \quad h = \frac{Bb}{(d_R + b)(\rho + \lambda_j) - \rho b}.$$

During acute infection ($t < 50$), $\lambda_j = \lambda_1$ and the initial conditions give

$$\nu_{12} + \nu_{22} + \frac{Bb}{(d_R + b)(\rho + \lambda_1) - \rho b} = T_0,$$

$$\frac{\rho}{d_R + b + \mu_1}\nu_{12} + \frac{\rho}{d_R + b + \mu_2}\nu_{22} + \frac{B(\rho + \lambda_1)}{(d_R + b)(\rho + \lambda_1) - \rho b} = R_0.$$

During chronic infection ($t >50$), $\lambda_j = \lambda_2$, we may write the solutions in terms of $\tau = t - 50$,

$$R = \frac{\rho}{d_R + b + \mu_1}\nu_{12}e^{\mu_1 t} + \frac{\rho}{d_R + b + \mu_2}\nu_{22}e^{\mu_2 \tau} + g$$
$$T = \nu_{12}e^{\mu_1 t} + \nu_{22}e^{\mu_2 \tau} + h$$

and the 'initial' conditions give

$$\nu_{12} + \nu_{22} + \frac{Bb}{(d_R + b)(\rho + \lambda_2) - \rho b} = T(\lambda_1, t = 50),$$

$$\frac{\rho}{d_R + b + \mu_1}\nu_{12} + \frac{\rho}{d_R + b + \mu_2}\nu_{22} + \frac{B(\rho + \lambda_2)}{(d_R + b)(\rho + \lambda_2) - \rho b} = R(\lambda_1, t = 50).$$

Now if we substitute the solution for T into the differential equation for L the we can use an integrating factor to solve for L, first for $t < 50$:

$$\frac{dL}{dt} = f\lambda_1 T - (d_L + \alpha)L$$

$$\frac{d}{dt}\left[e^{(d_L+\alpha)t}L\right] = e^{(d_L+\alpha)t}\lambda_1\left(\nu_{12}e^{\mu_1 t} + \nu_{22}e^{\mu_2 t} + \frac{Bb}{(d_R+b)(\rho+\lambda_1)-\rho b}\right)$$

$$L = \lambda_1\left(\frac{\nu_{12}}{\mu_1+d_L+\alpha}e^{\mu_1 t} + \frac{\nu_{22}}{\mu_2+d_L+\alpha}e^{\mu_2 t} + \frac{Bb}{(d_L+\alpha)((d_R+b)(\rho+\lambda_1)-\rho b)}\right) + c_L e^{-(d_L+\alpha)t}$$

where $c_L = 0 - \lambda_1\left(\nu_{12}/(\mu_1+d_L+\alpha) + \nu_{22}/(\mu_2+d_L+\alpha) + \frac{Bb}{(d_L+\alpha)((d_R+b)(\rho+\lambda_1)-\rho b)}\right)$.

Similarly, when $t > 50$ we find

$$L = \lambda_2\left(\frac{\nu_{12}}{\mu_1+d_L+\alpha}e^{\mu_1\tau} + \frac{\nu_{22}}{\mu_2+d_L+\alpha}e^{\mu_2\tau} + \frac{Bb}{(d_L+\alpha)((d_R+b)(\rho+\lambda_2)-\rho b)}\right) + c_L e^{-(d_L+\alpha)\tau}$$

where

$$c_L = L(\lambda_1, t=50) - \lambda_2\left(\frac{\nu_{12}}{(\mu_1+d_L+\alpha)} + \frac{\nu_{22}}{(\mu_2+d_L+\alpha)} + \frac{Bb}{(d_L+\alpha)((d_R+b)(\rho+\lambda_2)-\rho b)}\right)$$

.

B.3 A homogeneous model does not suffice

I wished to compare the fits, to the Hocqueloux HIV DNA decay data, of a homogeneous model (in which the decay of the latently infected population can be described by an average parameter), and a model where the total latently infected population is described as the sum of two populations with different average activation rates. This latter model is the one fitted to the HIV DNA decay data in the main chapter. To do this I used the 'nlme' package in R to fit both a linear mixed effects model and the original non-linear model using maximum likelihood methods. In both cases the model is fitted to data from primary- and chronic-treated patients simultaneously with different intercepts allowed for the two groups. The results are shown graphically in Figure B.3 and show that the homogeneous model is a particularly poor fit to the HIV DNA data from primary-treated patients in particular. The homogenous (single-population) model has an Akaike Information Criterion (AIC) of 691 whereas the heterogeneous, two-population model has

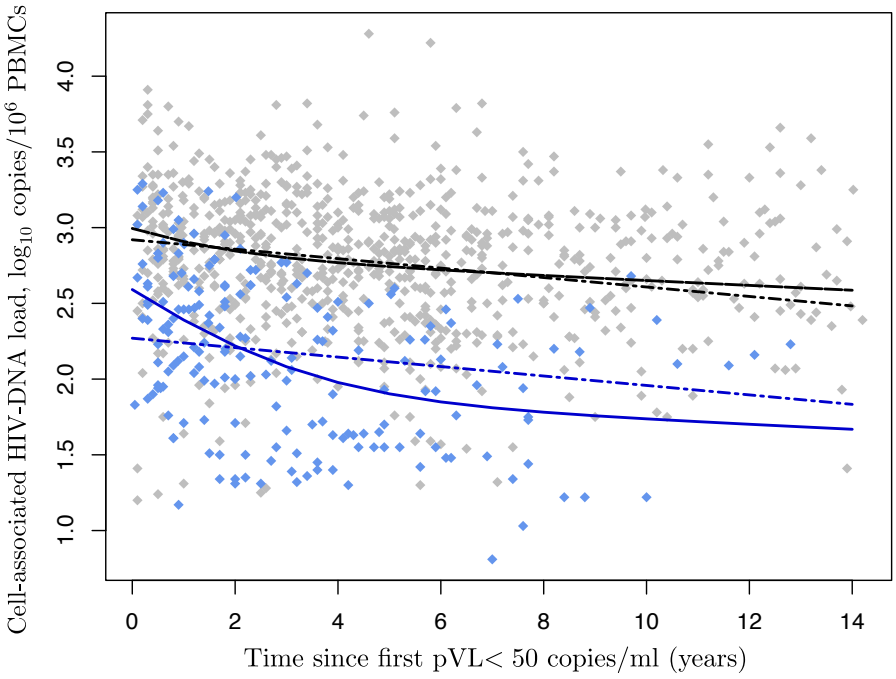


Figure B.3: A homogeneous model and the original model, fitted to DNA decay data. A comparison of the patterns of decay described by a single exponential model (linear mixed effects model fitted to the log-transformed data; dot-dashed lines) and the original bi-exponential model (non-linear mixed effects model; solid lines). The Hocqueloux HIV DNA decay data is plotted as described in Figure 4.1; blue indicates patients treated in primary infection and black/grey indicates chronic-treated patients.

an AIC of 645. A lower value of the AIC indicates a better fit, accounting for the number of parameters used in the model, and so this confirms that the original two-population model is preferred.

B.4 Effect of ART initiation time and duration

The plot in Figure B.4 shows how the size of the reservoir varies for different ART initiation and duration times. It shows that both early initiation and long duration of ART are necessary to get a large reduction in the size of the reservoir. Under my original model, a reduction by at least 100-fold (dark orange to red) compared to the reservoir size in a chronically infected, untreated patient requires an ART initiation time of around 10 days post-infection, followed by of the order of 5000 days ($>$ 10 years) of ART.

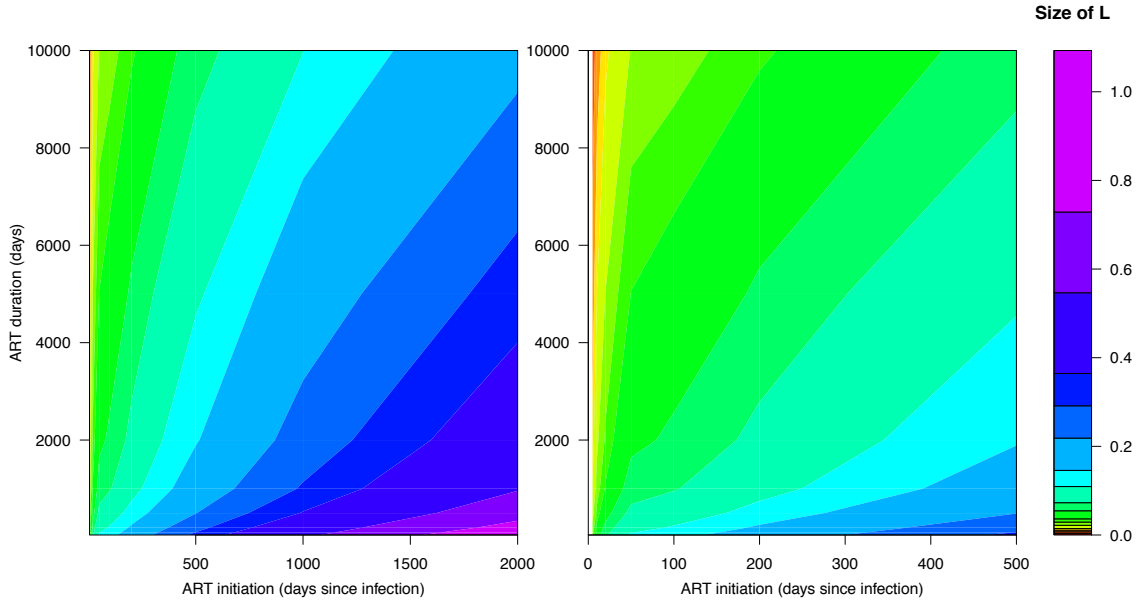


Figure B.4: The reduction in the reservoir that can be achieved under the model for a range of ART initiation and duration times. For each ART initiation time and ART duration, the simulated size of the reservoir at the end of ART ($L_1+L_2+L_3$) is indicated. The sizes given in the key on the right hand side are normalised relative to the model-simulated size in a patient who has been infected for 2000 days and is treatment naive. The right hand contour plot is identical to the left hand plot except for the x-axis, which is zoomed in to focus on early ART initiation times. Parameters are as used in Figure 4.3 and Table 4.4

B.5 Homeostatic proliferation

I stimulate homeostatic maintenance of the size of the total CD4$^+$ T cell pool, $R+T+L$, by adding in logistic growth terms, as detailed below:

$$\frac{dR_i}{dt} = B - (d_R + b_i)R_i + \rho T_i + r_i R_i \left(1 - \frac{R+T+L}{T_{\max}}\right)$$
$$\frac{dT_i}{dt} = b_i R_i - \lambda T_i - \rho T_i - dT_i + r_i T_i \left(1 - \frac{R+T+L}{T_{\max}}\right)$$
$$\frac{dL_i}{dt} = f_L \lambda T_i - (\alpha_i + d_L)L_i + r_i L_i \left(1 - \frac{R+T+L}{T_{\max}}\right)$$

In these equations, $T_{\max} = R(0) + T(0)$. Death of the activated CD4$^+$ T cell pool is added in and set as $d = 0.06$, as measured in Ribeiro et al [96]. I found that varying the r_i values had little effect on the model output. Results from simulations with this model are presented in Figure B.5, for comparison with Figure 4.3 in the main chapter. The main differences are that the peak of L_1 in acute infection is lower, and there is slightly less change in L_3 between primary and chronic infection (6.5 fold instead of 7.9 fold).

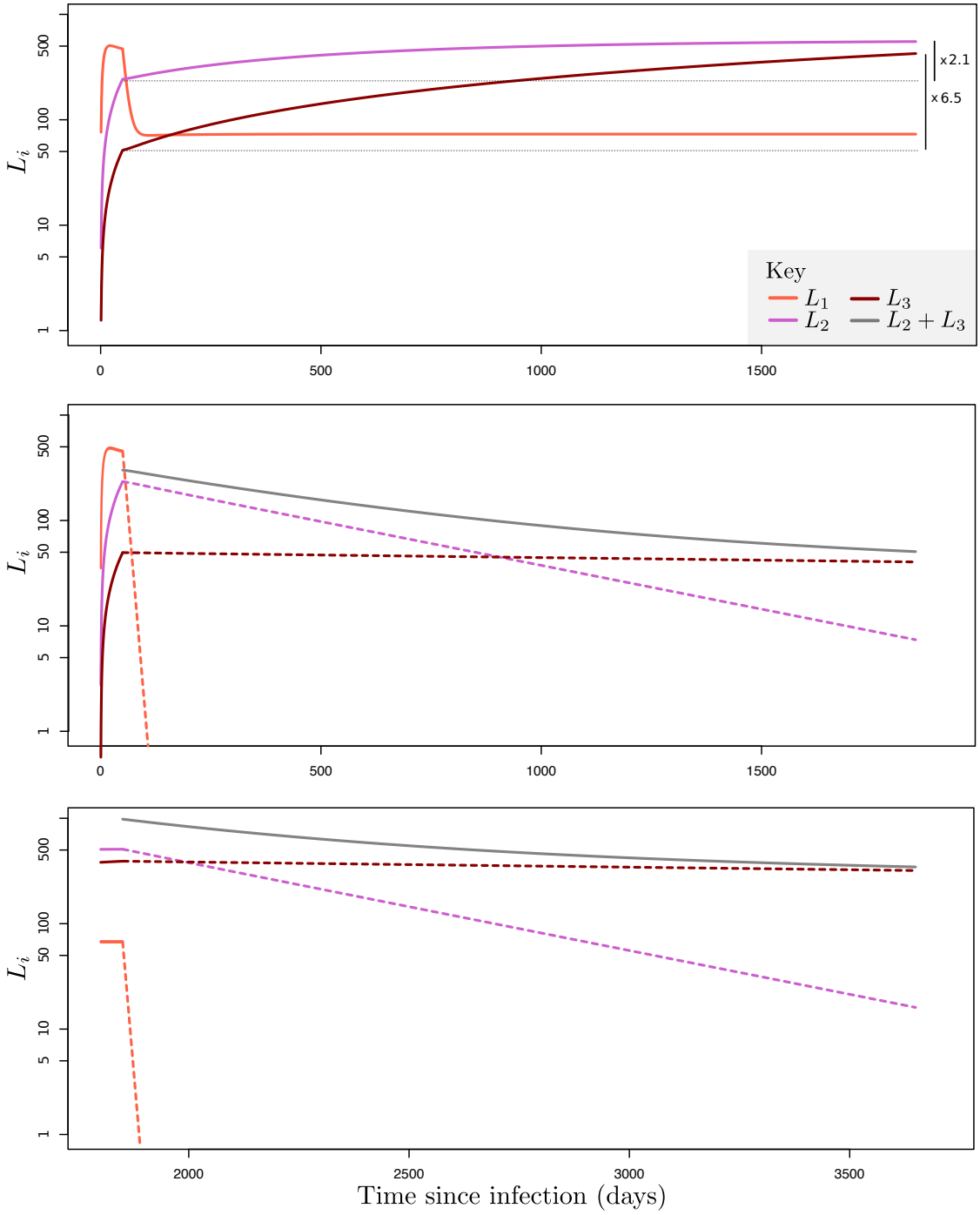


Figure B.5: A model with homeostatic proliferation produces similar results to the original model. The model described in section B.5 is simulated and the output plotted as in Figure 4.3. Parameters are as used in Figure 4.3 and Table 4.4, with the addition of $d = 0.06$, $r_1 = 0.5, r_2 = 0.05, r_3 = 0.005$. The r_i are chosen so that the faster turnover populations have higher logistic growth rate, but setting $r_1 = r_2 = r_3$ produced very similar results. The total size of the $CD4^+$ T-cell pool stabilises quickly so that $r_i \left(1 - \frac{R+T+L}{T_{\max}}\right)$ is soon very small compared to the other rates.

C

Supplementary methods relating to chapter 5

This appendix originally appeared as supplementary material for my Journal of the Royal Society Interface paper [37].

C.1 Supplementary methods relating to the original model

In this section we cover in more detail the calculations using the PDE model that help us to understand when ART is expected to favour the less virulent strain. We then relate the PDE model to the ODE model at equilibrium and solve the full ODE model at equilibrium. This is done in order to calculate 'total number of AIDS-related deaths per untreated infected person per year' at equilibrium and its relation to the relative importance of low CD4 transmissions.

C.1.1 ODE model equations

Recall the equations for the ODE model with ART as presented in (5.2) in the main text. S represents the population of susceptible (uninfected) individuals, I are the various infected classes, where the superscripts H and L indicate high and low (resp.) SPVL and the subscripts S1 and S2 index strain type, with u and t distinguishing between individuals who will remain untreated or will be treated with ART. To shorten notation we denote $I_i^j = I_{i,t}^j + I_{i,u}^j$ and define $\lambda_i = (\beta_H c I_i^H + \beta_L c I_i^L)/N$. T is the population of individuals

receiving ART, assumed to be noninfectious.

$$\begin{aligned}
\frac{dS}{dt} &= B - (\lambda_{S1} + \lambda_{S2})S - \mu S \\
\frac{dI^H_{S1,u}}{dt} &= (1-k)\lambda_{S1}S - (\mu + a_H)I^H_{S1,u} - mI^H_{S1,u} + mI^H_{S2,u} \\
\frac{dI^H_{S1,t}}{dt} &= k\lambda_{S1}S - (\mu + p_H)I^H_{S1,t} - mI^H_{S1,t} + mI^H_{S2,t} \\
\frac{dI^L_{S1,u}}{dt} &= -(\mu + a_L)I^L_{S1,u} - mI^L_{S1,u} + mI^L_{S2,u} \\
\frac{dI^L_{S1,t}}{dt} &= -(\mu + p_L)I^L_{S1,t} - mI^L_{S1,t} + mI^L_{S2,t} \\
\frac{dI^H_{S2,u}}{dt} &= -(\mu + a_H)I^H_{S2,u} - mI^H_{S2,u} + mI^H_{S1,u} \\
\frac{dI^H_{S2,t}}{dt} &= -(\mu + p_H)I^H_{S2,t} - mI^H_{S2,t} + mI^H_{S1,t} \\
\frac{dI^L_{S2,u}}{dt} &= (1-k)\lambda_{S2}S - (\mu + a_L)I^L_{S2,u} - mI^L_{S2,u} + mI^L_{S1,u} \\
\frac{dI^L_{S2,t}}{dt} &= k\lambda_{S2}S - (\mu + p_L)I^L_{S2,t} - mI^L_{S2,t} + mI^L_{S1,t} \\
\frac{dT}{dt} &= p_H(I^H_{S1,t} + I^H_{S2,t}) + p_L(I^L_{S1,t} + I^L_{S2,t}) - \mu T
\end{aligned} \tag{C.1}$$

C.1.2 PDE model definition and solution at epidemic equilibrium

To recap, in the PDE model both treatment and AIDS-related death are dependent on age of infection. Therefore each infected class is no longer split into 'treated' and 'untreated'. Let τ denote time since infection, and define $y^H_1(t,\tau)$ to be the number of high SPVL virulent strain (S1) infections of infection-age τ at time t, so that

$$\int_0^\infty y^H_{S1}(t,\tau)\mathrm{d}\tau = I^H_{S1}(t)$$

and similarly for y^L_{S1}, y^H_{S2}, y^L_{S2}.

Let an average person with a high SPVL infection become classified as 'low CD4' at $\tau = T_H$ and an average person with a low SPVL infection become classified as 'low CD4' at $\tau = T_L$. Let d_H and d_L be the AIDS-related death rates of patients with high and low SPVL infections respectively. Then the full set of PDEs describing the spread of the two strains is:

$$\frac{dS}{dt} = B - (\lambda_{S1} + \lambda_{S2})S - \mu S$$

$$\frac{\partial y^H_{S1}}{\partial t} + \frac{\partial y^H_{S1}}{\partial \tau} = \begin{cases} -(\mu + m)y^H_{S1}(t,\tau) + m y^H_{S2}(t,\tau) & \text{if } \tau \leq T_H \\ -(\mu + d_H + m)y^H_{S1}(t,\tau) + m y^H_{S2}(t,\tau) & \text{if } \tau > T_H \end{cases} \qquad y^H_{S1}(t,0) = \lambda_{S1} S$$

$$\frac{\partial y^L_{S1}}{\partial t} + \frac{\partial y^L_{S1}}{\partial \tau} = \begin{cases} -(\mu + m)y^L_{S1}(t,\tau) + m y^L_{S2}(t,\tau) & \text{if } \tau \leq T_L \\ -(\mu + d_L + m)y^L_{S1}(t,\tau) + m y^L_{S2}(t,\tau) & \text{if } \tau > T_L \end{cases} \qquad y^L_{S1}(t,0) = 0$$

$$\frac{\partial y^H_{S2}}{\partial t} + \frac{\partial y^H_{S2}}{\partial \tau} = \begin{cases} -(\mu + m)y^H_{S2}(t,\tau) + m y^H_{S1}(t,\tau) & \text{if } \tau \leq T_H \\ -(\mu + d_H + m)y^H_{S2}(t,\tau) + m y^H_{S1}(t,\tau) & \text{if } \tau > T_H \end{cases} \qquad y^H_{S2}(t,0) = 0$$

$$\frac{\partial y^L_{S2}}{\partial t} + \frac{\partial y^L_{S2}}{\partial \tau} = \begin{cases} -(\mu + m)y^L_{S2}(t,\tau) + m y^L_{S1}(t,\tau) & \text{if } \tau \leq T_L \\ -(\mu + d_L + m)y^L_{S2}(t,\tau) + m y^L_{S1}(t,\tau) & \text{if } \tau > T_L \end{cases} \qquad y^L_{S2}(t,0) = \lambda_{S2} S$$

where $\lambda_{S1} = (\beta_H c I_H^{S1} + \beta_L c I_L^{S1})/N$ and $\lambda_{S2} = (\beta_H c I_H^{S2} + \beta_L c I_L^{S2})/N$. There is also a discontinuity at $\tau = T_i$ where a proportion k of infected patients reaching that infected age are put onto treatment (and hence removed from the infectious class):

$$\lim_{\tau \to T_j^+} y_i^j(\tau) = (1-k) \lim_{\tau \to T_j^-} y_i^j(\tau)$$

At equilibrium, when $\frac{\partial y_i^j}{\partial t} = 0$, the above reduce to a set of ODEs in τ:

$$\frac{\mathrm{d}y^H_{S1}}{\mathrm{d}\tau} = \begin{cases} -(\mu+m)y^H_{S1}(\tau) + my^H_{S2}(\tau) & \text{if } \tau \le T_H \\ -(\mu+d_H+m)y^H_{S1}(\tau) + my^H_{S2}(\tau) & \text{if } \tau > T_H \end{cases} \qquad y^H_{S1}(0) = \lambda_{S1}S^*$$

$$\frac{\mathrm{d}y^L_{S1}}{\mathrm{d}\tau} = \begin{cases} -(\mu+m)y^L_{S1}(\tau) + my^L_{S2}(\tau) & \text{if } \tau \le T_L \\ -(\mu+d_L+m)y^L_{S1}(\tau) + my^L_{S2}(\tau) & \text{if } \tau > T_L \end{cases} \qquad y^L_{S1}(0) = 0$$

$$\frac{\mathrm{d}y^H_{S2}}{\mathrm{d}\tau} = \begin{cases} -(\mu+m)y^H_{S2}(\tau) + my^H_{S1}(\tau) & \text{if } \tau \le T_H \\ -(\mu+d_H+m)y^H_{S2}(\tau) + my^H_{S1}(\tau) & \text{if } \tau > T_H \end{cases} \qquad y^H_{S2}(0) = 0$$

$$\frac{\mathrm{d}y^L_{S2}}{\mathrm{d}\tau} = \begin{cases} -(\mu+m)y^L_{S2}(\tau) + my^L_{S1}(\tau) & \text{if } \tau \le T_L \\ -(\mu+d_L+m)y^L_{S2}(\tau) + my^L_{S1}(\tau) & \text{if } \tau > T_L \end{cases} \qquad y^L_{S2}(0) = \lambda_{S2}S^*$$

where S^* is the equilibrium value of S and so $\lambda_{S1}S^*, \lambda_{S2}S^*$ are now constants (independent of τ). We may solve these for $y^j_{S1} + y^j_{S2}$ and $y^j_{S1} - y^j_{S2}$:

$$y^H_{S1} + y^H_{S2} = \begin{cases} \lambda_{S1}S^*e^{-\mu\tau} & \text{if } \tau \le T_H \\ (1-k)\lambda_{S1}Se^{-\mu T_H}e^{-(\mu+d_H)(\tau-T_H)} & \text{if } \tau > T_H \end{cases}$$

$$y^H_{S1} - y^H_{S2} = \begin{cases} \lambda_{S1}S^*e^{-(\mu+2m)\tau} & \text{if } \tau \le T_H \\ (1-k)\lambda_{S1}Se^{-(\mu+2m)T_H}e^{-(\mu+2m+d_H)(\tau-T_H)} & \text{if } \tau > T_H \end{cases}$$

$$y^L_{S1} + y^L_{S2} = \begin{cases} \lambda_{S2}S^*e^{-\mu\tau} & \text{if } \tau \le T_L \\ (1-k)\lambda_{S2}Se^{-\mu T_L}e^{-(\mu+d_L)(\tau-T_L)} & \text{if } \tau > T_L \end{cases}$$

$$y^L_{S1} - y^L_{S2} = -\begin{cases} \lambda_{S2}S^*e^{-(\mu+2m)\tau} & \text{if } \tau \le T_L \\ (1-k)\lambda_{S2}Se^{-(\mu+2m)T_L}e^{-(\mu+2m+d_L)(\tau-T_L)} & \text{if } \tau > T_L \end{cases}$$

Then

$$
\begin{aligned}
2y^H_{S1} &= \lambda_{S1}S^*[e^{-\mu\tau} + e^{-(\mu+2m)\tau}] \times \begin{cases} 1 & \text{if } \tau \le T_H \\ (1-k)e^{-d_H(\tau-T_H)} & \text{if } \tau > T_H \end{cases} \\
2y^H_{S2} &= \lambda_{S1}S^*[e^{-\mu\tau} - e^{-(\mu+2m)\tau}] \times \begin{cases} 1 & \text{if } \tau \le T_H \\ (1-k)e^{-d_H(\tau-T_H)} & \text{if } \tau > T_H \end{cases} \\
2y^L_{S1} &= \lambda_{S2}S^*[e^{-\mu\tau} - e^{-(\mu+2m)\tau}] \times \begin{cases} 1 & \text{if } \tau \le T_L \\ (1-k)e^{-d_L(\tau-T_L)} & \text{if } \tau > T_L \end{cases} \\
2y^L_{S2} &= \lambda_{S2}S^*[e^{-\mu\tau} + e^{-(\mu+2m)\tau}] \times \begin{cases} 1 & \text{if } \tau \le T_L \\ (1-k)e^{-d_L(\tau-T_L)} & \text{if } \tau > T_L \end{cases}
\end{aligned}
\tag{C.2}
$$

Recall that the purpose of introducing age-of-infection dependent death rates and treatment was to determine for which parameter sets the following inequality is true

$$\text{Pr(infected with strain S1} \mid \text{low CD4)} > \text{Pr(infected with strain S1)}$$

Here the sample space is the population of currently infected individuals and we are concerned with how these probabilities compare in the absence of ART ($k = 0$). This can be written as:

$$
\frac{\int_{T_H}^{\infty} y^H_{S1}\mathrm{d}\tau + \int_{T_L}^{\infty} y^L_{S1}\mathrm{d}\tau}{\int_{T_H}^{\infty} y^H_{S1} + y^H_{S2}\mathrm{d}\tau + \int_{T_L}^{\infty} y^L_{S1} + y^L_{S2}\mathrm{d}\tau} > \frac{\int_{0}^{\infty} y^H_{S1}\mathrm{d}\tau + \int_{0}^{\infty} y^L_{S1}\mathrm{d}\tau}{\int_{0}^{\infty} y^H_{S1} + y^H_{S2}\mathrm{d}\tau + \int_{0}^{\infty} y^L_{S1} + y^L_{S2}\mathrm{d}\tau} \tag{C.3}
$$

We may now use the expressions in (C.2) for $y^H_{S1}(\tau)$ etc., with $k = 0$, to calculate both

sides of (C.3) at equilibrium. First the left hand side:

$$\begin{aligned}
\int_{T_H}^{\infty} y_{S1}^{H} \mathrm{d}\tau &= \frac{1}{2}\lambda_{S1}S^* \int_{T_H}^{\infty} \left(e^{-\mu\tau} + e^{-(\mu+2m)\tau}\right) e^{-a_h(\tau - T_H)} \mathrm{d}\tau \\
&= \frac{1}{2}\lambda_{S1}S^* e^{d_H T_H} \int_{T_H}^{\infty} e^{-(\mu+d_H)\tau} + e^{-(\mu+2m+d_H)\tau} \mathrm{d}\tau \\
&= \frac{1}{2}\lambda_{S1}S^* \left[-\frac{e^{-(\mu+d_H)\tau}}{\mu + d_H} - \frac{e^{-(\mu+2m+d_H)\tau}}{\mu + 2m + d_H} \right]_{T_H}^{\infty} \\
&= \frac{1}{2}\lambda_{S1}S^* \left[\frac{e^{-(\mu+d_H)T_H}}{\mu + d_H} + \frac{e^{-(\mu+2m+d_H)T_H}}{\mu + 2m + d_H} \right] \\
&= \frac{1}{2}\lambda_{S1}S^* \left(\frac{e^{-\mu T_H}}{\mu + d_H} + \frac{e^{-(\mu+2m)T_H}}{\mu + 2m + d_H} \right)
\end{aligned}$$

Similarly

$$\begin{aligned}
\int_{T_H}^{\infty} y_{S2}^{H} \mathrm{d}\tau &= \frac{1}{2}\lambda_{S1}S^* \left(\frac{e^{-\mu T_H}}{\mu + d_H} - \frac{e^{-(\mu+2m)T_H}}{\mu + 2m + d_H} \right) \\
\int_{T_L}^{\infty} y_{S1}^{L} \mathrm{d}\tau &= \frac{1}{2}\lambda_{S2}S^* \left(\frac{e^{-\mu T_L}}{\mu + d_L} - \frac{e^{-(\mu+2m)T_L}}{\mu + 2m + d_L} \right) \\
\int_{T_L}^{\infty} y_{S2}^{L} \mathrm{d}\tau &= \frac{1}{2}\lambda_{S2}S^* \left(\frac{e^{-\mu T_L}}{\mu + d_L} + \frac{e^{-(\mu+2m)T_L}}{\mu + 2m + d_L} \right)
\end{aligned}$$

Therefore

$$\int_{T_H}^{\infty} y_{S1}^{H} + y_{S2}^{H} \mathrm{d}\tau + \int_{T_L}^{\infty} y_{S1}^{L} + y_{S2}^{L} \mathrm{d}\tau = \lambda_{S1}S^* \frac{e^{-\mu T_H}}{\mu + d_H} + \lambda_{S2}S^* \frac{e^{-\mu T_L}}{\mu + d_L}$$

Also, for the right hand side

$$\begin{aligned}
\int_{0}^{\infty} y_{S1}^{H} \mathrm{d}\tau &= \int_{T_H}^{\infty} y_{S1}^{H} \mathrm{d}\tau + \int_{0}^{T_H} y_{S1}^{H} \mathrm{d}\tau \\
&= \int_{T_H}^{\infty} y_{S1}^{H} \mathrm{d}\tau + \frac{1}{1}\lambda_{S1}S^* \left[-\frac{e^{-\mu\tau}}{\mu} - \frac{e^{-(\mu+2m)\tau}}{\mu + 2m} \right]_{0}^{T_H} \\
&= \int_{T_H}^{\infty} y_{S1}^{H} \mathrm{d}\tau + \frac{1}{2}\lambda_{S1}S^* \left[\frac{1}{\mu} + \frac{1}{\mu + 2m} - \frac{e^{-\mu T_H}}{\mu} - \frac{e^{-(\mu+2m)T_H}}{\mu + 2m} \right] \\
&= \frac{1}{2}\lambda_{S1}S^* \times \\
&\quad \left[\frac{1}{\mu} + \frac{1}{\mu + 2m} + e^{-\mu T_H} \left(\frac{1}{\mu + d_H} - \frac{1}{\mu} \right) + e^{-(\mu+2m)T_H} \left(\frac{1}{\mu + 2m + d_H} - \frac{1}{\mu + 2m} \right) \right]
\end{aligned}$$

and similarly to before the integral of all four populations is:

$$\lambda_{S1}S^*\left[\frac{1}{\mu}+e^{-\mu T_H}\left(\frac{1}{\mu+d_H}-\frac{1}{\mu}\right)\right]+\lambda_{S2}S^*\left[\frac{1}{\mu}+e^{-\mu T_L}\left(\frac{1}{\mu+d_L}-\frac{1}{\mu}\right)\right]$$

Substituting these all into equation C.3, cross multiplying and comparing the $\lambda_{S1}\lambda_{S1}$, $\lambda_{S1}\lambda_{S2}$ and $\lambda_{S2}\lambda_{S2}$ terms on both sides we obtain

$$\begin{aligned}&\frac{1}{\mu}\left[\left(\lambda_{S1}+\lambda_{S2}-\lambda_{S1}e^{-\mu T_H}-\lambda_{S2}e^{-\mu T_L}\right)\left(\lambda_{S1}\frac{e^{-(\mu+2m)T_H}}{\mu+2m+d_H}-\lambda_{S2}\frac{e^{-(\mu+2m)T_L}}{\mu+2m+d_L}\right)\right]\\ >&\frac{1}{\mu+2m}\left[\left(\lambda_{S1}\frac{e^{-\mu T_H}}{\mu+d_H}+\lambda_{S2}\frac{e^{-\mu T_L}}{\mu+d_L}\right)\left(\lambda_{S2}e^{-(\mu+2m)T_L}-\lambda_{S1}e^{-(\mu+2m)T_H}+\lambda_{S1}-\lambda_{S2}\right)\right]\end{aligned}$$

To simplify further we set $m=0$, which is reasonable when m is very small compared to μ. So, with this assumption we are able to obtain

$$\begin{aligned}&\left[\left(\lambda_{S1}+\lambda_{S2}-\lambda_{S1}e^{-\mu T_H}-\lambda_{S2}e^{-\mu T_L}\right)\left(\lambda_{S1}\frac{e^{-\mu T_H}}{\mu+d_H}-\lambda_{S2}\frac{e^{-\mu T_L}}{\mu+d_L}\right)\right]\\ &\quad>\left[\left(\lambda_{S1}\frac{e^{-\mu T_H}}{\mu+d_H}+\lambda_{S2}\frac{e^{-\mu T_L}}{\mu+d_L}\right)\left(\lambda_{S2}e^{-\mu T_L}-\lambda_{S1}e^{-\mu T_H}+\lambda_{S1}-\lambda_{S2}\right)\right]\\ \Rightarrow\quad&2\lambda_{S2}\lambda_{S1}\frac{e^{-\mu T_H}}{\mu+d_H}-2\lambda_{S1}\lambda_{S2}\frac{e^{-\mu T_L}}{\mu+d_L}>2\lambda_{S1}\lambda_{S2}\frac{e^{-\mu T_L}e^{-\mu T_H}}{\mu+d_H}-2\lambda_{S1}\lambda_{S2}\frac{e^{-\mu T_H}e^{-\mu T_L}}{\mu+d_L}\\ \Rightarrow\quad&\frac{e^{\mu T_L}}{\mu+d_H}-\frac{e^{\mu T_H}}{\mu+d_L}>\frac{1}{\mu+d_H}-\frac{1}{\mu+d_L}\\ \Rightarrow\quad&\frac{e^{\mu T_L}-1}{e^{\mu T_H}-1}>\frac{\mu+d_H}{\mu+d_L}\end{aligned}$$

C.1.3 Relating the ODE and PDE models at equilibrium

As covered briefly in the main text, we wish to relate the parameters a_j and p_j in the ODE model to the parameters T_j and d_j in the PDE model. We do this by equating the two models at equilibrium, i.e. ensuring that at equilibrium the sizes of both the high SPVL and low SPVL infected classes in the ODE model match those in the PDE model. So, for $j=H,L$:

$$\int_0^\infty y^j(t,\tau)\mathrm{d}\tau = I_u^j + I_t^j$$

$$\Leftrightarrow \quad \int_0^{T_j} \lambda S^* e^{-\mu\tau}\mathrm{d}\tau + \int_{T_j}^\infty (1-k)\lambda S^* e^{-\mu T_j} e^{-(\mu+d_j)(\tau-T_j)}\mathrm{d}\tau = \frac{(1-k)\lambda S^*}{\mu+a_j} + \frac{k\lambda S^*}{\mu+p_j}$$

$$\Leftrightarrow \quad \frac{\lambda S^*}{\mu} - \frac{\lambda S^*}{\mu}e^{-\mu T_j} + \frac{(1-k)\lambda S^*}{\mu+d_j}e^{-\mu T_j} = \frac{(1-k)\lambda S^*}{\mu+a_j} + \frac{k\lambda S^*}{\mu+p_j}$$

$$\Leftrightarrow \quad e^{-\mu T_j}\left[\frac{1-k}{\mu+d_j} - \frac{1}{\mu}\right] = \frac{(1-k)}{\mu+a_j} + \frac{k}{\mu+p_j} + \frac{1}{\mu}$$

Substituting in $k = 0$ and $k = 1$ shows that in order to obtain a condition that is independent of k we must have $\mu + d_j = p_j(\mu + a_j)/(p_j - a_j)$. Substituting this back in:

$$e^{-\mu T_j}\left[\frac{(1-k)(p_j-a_j)}{p_i(\mu+a_j)} - \frac{1}{\mu}\right] = \frac{1-k}{\mu+a_j} + \frac{k}{\mu+p_j} - \frac{1}{\mu}$$

$$\Leftrightarrow \quad e^{-\mu T_j}\left[-\frac{\mu(kp_j+(1-k)a_j)+a_jp_j}{\mu p_j(\mu+a_j)}\right] = -\frac{\mu(kp_j+(1-k)a_j)+a_jp_j}{(\mu+a_j)\mu(\mu+p_j)}$$

$$\Leftrightarrow \quad e^{-\mu T_j} = \frac{p_j}{\mu+p_j}$$

So we must choose a_i and p_j to satisfy

$$e^{-\mu T_j} = \frac{p_j}{\mu+p_j} \quad \text{and} \quad d_j = \frac{a_j(\mu+p_j)}{p_j-a_j}$$

C.1.4 Equilibrium population size calculations for the ODE model

To find the equilibrium population class sizes we first re-write the model equations in (C.1) in matrix notation. Let $\mathbf{dy}$ be the vector of derivatives of the untreated infected classes, ordered as in (C.1). Similarly let $\mathbf{y}$ be the vector of population sizes. Then define the matrices $\mathbf{\Lambda}$ and $\mathbf{M}$ such that

$$\mathbf{dy} = \mathbf{\Lambda y} S/N + \mathbf{M y}$$

At equilibrium $\mathbf{dy} = \mathbf{0}$ and so we wish to solve $\mathbf{\Lambda y} S^*/N^* = -\mathbf{M y}$, where S^* and N^* are the equilibrium values of S and N. The solution for $\mathbf{y}$ that we want is the eigenvector of $\mathbf{M^{-1}\Lambda}$ corresponding to the eigenvalue with the largest absolute value.

Now let $\delta_1 = \mu + a_H + m$, $\delta_2 = \mu + p_H + m$, $\delta_3 = \mu + a_L + m$, $\delta_4 = \mu + p_L + m$ so that

$$\mathbf{M} = \begin{pmatrix} -\delta_1 & 0 & 0 & 0 & m & 0 & 0 & 0 \\ 0 & -\delta_2 & 0 & 0 & 0 & m & 0 & 0 \\ 0 & 0 & -\delta_3 & 0 & 0 & 0 & m & 0 \\ 0 & 0 & 0 & -\delta_4 & 0 & 0 & 0 & m \\ m & 0 & 0 & 0 & -\delta_1 & 0 & 0 & 0 \\ 0 & m & 0 & 0 & 0 & -\delta_2 & 0 & 0 \\ 0 & 0 & m & 0 & 0 & 0 & -\delta_3 & 0 \\ 0 & 0 & 0 & m & 0 & 0 & 0 & -\delta_4 \end{pmatrix}$$

and we can calculate the inverse

$$\mathbf{M^{-1}} = \begin{pmatrix} m_1 & 0 & 0 & 0 & n_1 & 0 & 0 & 0 \\ 0 & m_2 & 0 & 0 & 0 & n_2 & 0 & 0 \\ 0 & 0 & m_3 & 0 & 0 & 0 & n_3 & 0 \\ 0 & 0 & 0 & m_4 & 0 & 0 & 0 & n_4 \\ n_1 & 0 & 0 & 0 & m_1 & 0 & 0 & 0 \\ 0 & n_2 & 0 & 0 & 0 & m_2 & 0 & 0 \\ 0 & 0 & n_3 & 0 & 0 & 0 & m_3 & 0 \\ 0 & 0 & 0 & n_4 & 0 & 0 & 0 & m_4 \end{pmatrix}$$

where $m_i = \frac{\delta_i}{m^2 - \delta_i^2}$, $n_i = \frac{m}{\delta_i^2 - m^2}$ for $i \in \{1, 2, 3, 4\}$. This gives

$$\mathbf{M^{-1}\Lambda} = c \begin{pmatrix} m_1\bar{k}\beta_H & m_1\bar{k}\beta_H & m_1\bar{k}\beta_L & m_1\bar{k}\beta_L & 0 & 0 & 0 & 0 \\ m_2k\beta_H & m_2k\beta_H & m_2k\beta_L & m_2k\beta_L & 0 & 0 & 0 & 0 \\ 0 & 0 & 0 & 0 & n_3\bar{k}\beta_H & n_3\bar{k}\beta_H & n_3\bar{k}\beta_L & n_3\bar{k}\beta_L \\ 0 & 0 & 0 & 0 & n_4k\beta_H & n_4k\beta_H & n_4k\beta_L & n_4k\beta_L \\ n_1\bar{k}\beta_H & n_1\bar{k}\beta_H & n_1\bar{k}\beta_L & n_1\bar{k}\beta_L & 0 & 0 & 0 & 0 \\ n_2k\beta_H & n_2k\beta_H & n_2k\beta_L & n_2k\beta_L & 0 & 0 & 0 & 0 \\ 0 & 0 & 0 & 0 & m_3\bar{k}\beta_H & m_3\bar{k}\beta_H & m_3\bar{k}\beta_L & m_3\bar{k}\beta_L \\ 0 & 0 & 0 & 0 & m_4k\beta_H & m_4k\beta_H & m_4k\beta_L & m_4k\beta_L \end{pmatrix}$$

where $\bar{k} = (1 - k)$. We can calculate the eigenvalues and eigenvectors of this matrix computationally. If $\mathbf{y}^*$ is the eigenvector corresponding to the largest eigenvalue then the equilibrium value of total AIDS-related deaths per untreated infected person per year is $\sum_i (a_H y_{i,u}^{*H} + a_L y_{i,u}^{*L}) / \sum_i (y_{i,u}^{*H} + y_{i,u}^{*L})$, as plotted in Figure 5.5.

C.2 Low heritability of SPVL

C.2.1 Methods

In this new model an infection initiated with strain S1 has high SPVL with frequency $f \in (0.5, 1)$ (whereas before $f = 1$) and remains at the same SPVL regardless of within host strain switching (as before). The same is true for infections initiated by strain S2 and low SPVL. The lower f is, the lower the heritability of SPVL in the model. The adjusted model equations are:

$$\begin{aligned}
\frac{dS}{dt} &= B - (\lambda_{S1} + \lambda_{S2})S - \mu S \\
\frac{dI^H_{S1,u}}{dt} &= f(1-k)\lambda_{S1}S - (\mu + a_H)I^H_{S1,u} - mI^H_{S1,u} + mI^H_{S2,u} \\
\frac{dI^H_{S1,t}}{dt} &= fk\lambda_{S1}S - (\mu + p_H)I^H_{S1,t} - mI^H_{S1,t} + mI^H_{S2,t} \\
\frac{dI^L_{S1,u}}{dt} &= (1-f)(1-k)\lambda_{S1}S - (\mu + a_L)I^L_{S1,u} - mI^L_{S1,u} + mI^L_{S2,u} \\
\frac{dI^L_{S1,t}}{dt} &= (1-f)k\lambda_{S1}S - (\mu + p_L)I^L_{S1,t} - mI^L_{S1,t} + mI^L_{S2,t} \\
\frac{dI^H_{S2,u}}{dt} &= (1-f)(1-k)\lambda_{S2}S - (\mu + a_H)I^H_{S2,u} - mI^H_{S2,u} + mI^H_{S1,u} \\
\frac{dI^H_{S2,t}}{dt} &= (1-f)k\lambda_{S2}S - (\mu + p_H)I^H_{S2,t} - mI^H_{S2,t} + mI^H_{S1,t} \\
\frac{dI^L_{S2,u}}{dt} &= f(1-k)\lambda_{S2}S - (\mu + a_L)I^L_{S2,u} - mI^L_{S2,u} + mI^L_{S1,u} \\
\frac{dI^L_{S2,t}}{dt} &= fk\lambda_{S2}S - (\mu + p_L)I^L_{S2,t} - mI^L_{S2,t} + mI^L_{S1,t} \\
\frac{dT}{dt} &= p_H(I^H_{S1,t} + I^H_{S2,t}) + p_L(I^L_{S1,t} + I^L_{S2,t}) - \mu T
\end{aligned} \tag{C.4}$$

Note that a low strain switching rate, m, is still required to avoid one strain necessarily becoming extinct.

The R_0 values are now calculated as (approximating using $m = 0$ again):

$R_0 =$ Pr(new infection has high SPVL) $\times$ (avg. # infections generated by high SPVL infection)
+ Pr(new infection has low SPVL) $\times$ (avg. # infections generated by low SPVL infection)

Hence:

$$R_0^{S1} = f\beta_H c\left(\frac{(1-k)}{\mu+a_H}+\frac{k}{\mu+p_H}\right)+(1-f)\beta_L c\left(\frac{(1-k)}{\mu+a_L}+\frac{k}{\mu+p_L}\right)$$
$$R_0^{S2} = (1-f)\beta_H c\left(\frac{(1-k)}{\mu+a_H}+\frac{k}{\mu+p_H}\right)+f\beta_L c\left(\frac{(1-k)}{\mu+a_L}+\frac{k}{\mu+p_L}\right)$$

And the equilibrium matrix becomes: $\mathbf{M^{-1}\Lambda} =$

$$c\begin{pmatrix}
m_1f\bar{k}\beta_H & m_1f\bar{k}\beta_H & m_1f\bar{k}\beta_L & m_1f\bar{k}\beta_L & n_1\bar{f}\bar{k}\beta_H & n_1\bar{f}\bar{k}\beta_H & n_1\bar{f}\bar{k}\beta_L & n_1\bar{f}\bar{k}\beta_L\\
m_2fk\beta_H & m_2fk\beta_H & m_2fk\beta_L & m_2fk\beta_L & n_2\bar{f}k\beta_H & n_2\bar{f}k\beta_H & n_2\bar{f}k\beta_L & n_2\bar{f}k\beta_L\\
m_3\bar{f}\bar{k}\beta_H & m_3\bar{f}\bar{k}\beta_H & m_3\bar{f}\bar{k}\beta_L & m_3\bar{f}\bar{k}\beta_L & n_3f\bar{k}\beta_H & n_3f\bar{k}\beta_H & n_3f\bar{k}\beta_L & n_3f\bar{k}\beta_L\\
m_4\bar{f}k\beta_H & m_4\bar{f}k\beta_H & m_4\bar{f}k\beta_L & m_4\bar{f}k\beta_L & n_4fk\beta_H & n_4fk\beta_H & n_4fk\beta_L & n_4fk\beta_L\\
n_1f\bar{k}\beta_H & n_1f\bar{k}\beta_H & n_1f\bar{k}\beta_L & n_1f\bar{k}\beta_L & m_1\bar{f}\bar{k}\beta_H & m_1\bar{f}\bar{k}\beta_H & m_1\bar{f}\bar{k}\beta_L & m_1\bar{f}\bar{k}\beta_L\\
n_2fk\beta_H & n_2fk\beta_H & n_2fk\beta_L & n_2fk\beta_L & m_2\bar{f}k\beta_H & m_2\bar{f}k\beta_H & m_2\bar{f}k\beta_L & m_2\bar{f}k\beta_L\\
n_3\bar{f}\bar{k}\beta_H & n_3\bar{f}\bar{k}\beta_H & n_3\bar{f}\bar{k}\beta_L & n_3\bar{f}\bar{k}\beta_L & m_3f\bar{k}\beta_H & m_3f\bar{k}\beta_H & m_3f\bar{k}\beta_L & m_3f\bar{k}\beta_L\\
n_4\bar{f}k\beta_H & n_4\bar{f}k\beta_H & n_4\bar{f}k\beta_L & n_4\bar{f}k\beta_L & m_4fk\beta_H & m_4fk\beta_H & m_4fk\beta_L & m_4fk\beta_L
\end{pmatrix}$$

where $\bar{f} = (1-f)$.

C.2.2 Results: Magnitude and direction of the ART effect

We have not re-done the PDE analysis for this model since we expect the direction of the ART-effect at equilibrium to remain the same as in the original model. This is because, even though high SPVL infections don't correspond exactly to strain S1 infections, it is still the case that if 'low CD4' transmissions occur proportionally more in high SPVL infections (compared to low SPVL infections) then they are of greater importance to the onward transmission of S1. Therefore, so long as $f > 0.5$, the direction of the long-term ART-effect will remain the same.

In Figures C.1–C.3 we have redone Figures 5.3, 5.5 and 5.6 (resp.) of the main text using this model and $f = 0.8$. We see that, in both the short- and the long-term, the magnitude of the ART-effect on virulence is lessened. This is because reducing the heritability brings the number of high and low SPVL infections closer together, and so there is less scope for change in overall virulence. Aside from this the results are qualitatively the same; the figures show that the patterns of virulence change in the absence of ART

and the direction of the ART-effect in the short- and long-term are all very similar to in the original model.

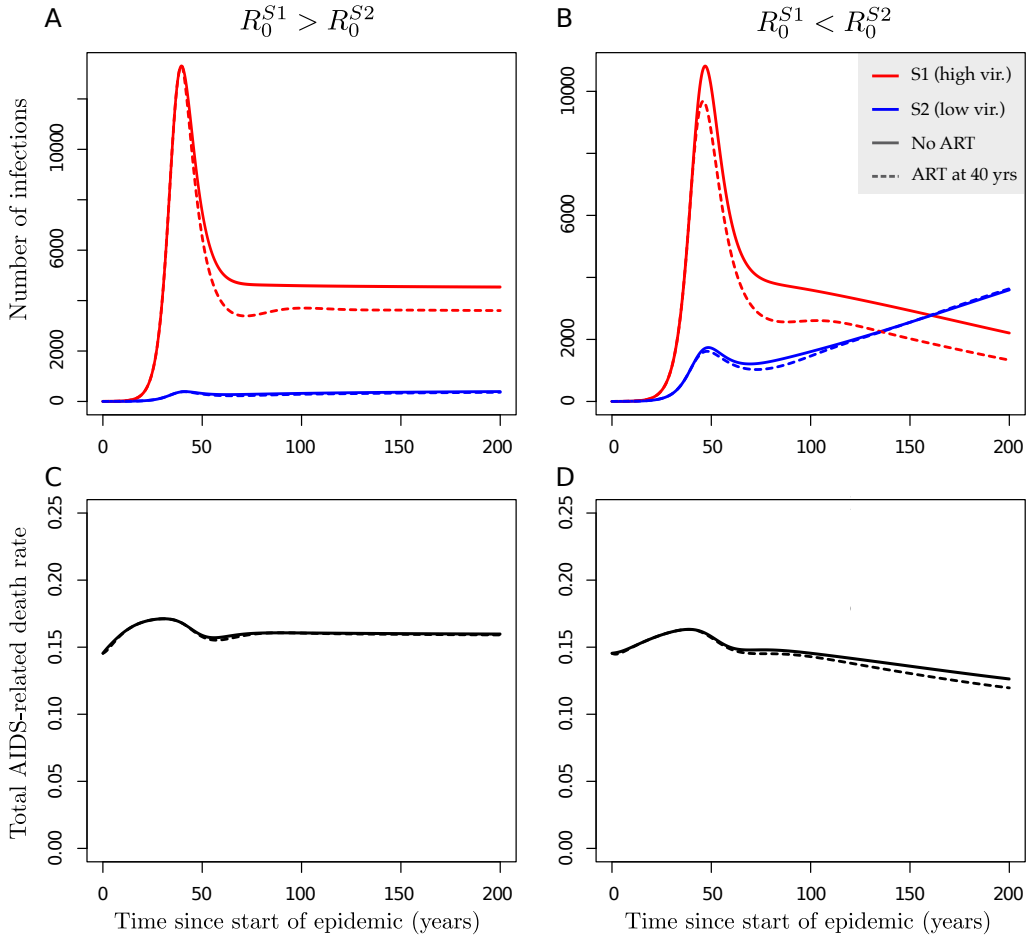


Figure C.1: Behaviour of the model with reduced heritability, with and without ART. Parameters and initial conditions are as in Figure 5.3 but with $f = 0.8$. A, C: In the absence of ART $R_0^{S1} = 2.4, R_0^{S2} = 2.2$. B, D: In the absence of ART $R_0^{S1} = 2.2, R_0^{S2} = 2.4$. Solid lines show the output of the model without ART while dotted lines plot trajectories for the model when ART is introduced at 30% coverage 40 years into the epidemic. A, B: The number of strain S1 infections through time is shown in red and the number of strain S2 infections in blue. With reduced heritability, the numbers of S1 and S2 infections are similar to in the case where $f = 1$ (Figure 5.3). C, D: However since each strain now gives rise to a mixture of high and low SPVL infections, the numbers of high and low SPVL infections are closer to each other and this results in the smaller magnitude variations in virulence. The shape of virulence change over time is similar to when $f = 1$. The effect of ART is still to increase virulence compared to the model without ART, but this effect is also reduced in magnitude when heritability is reduced.

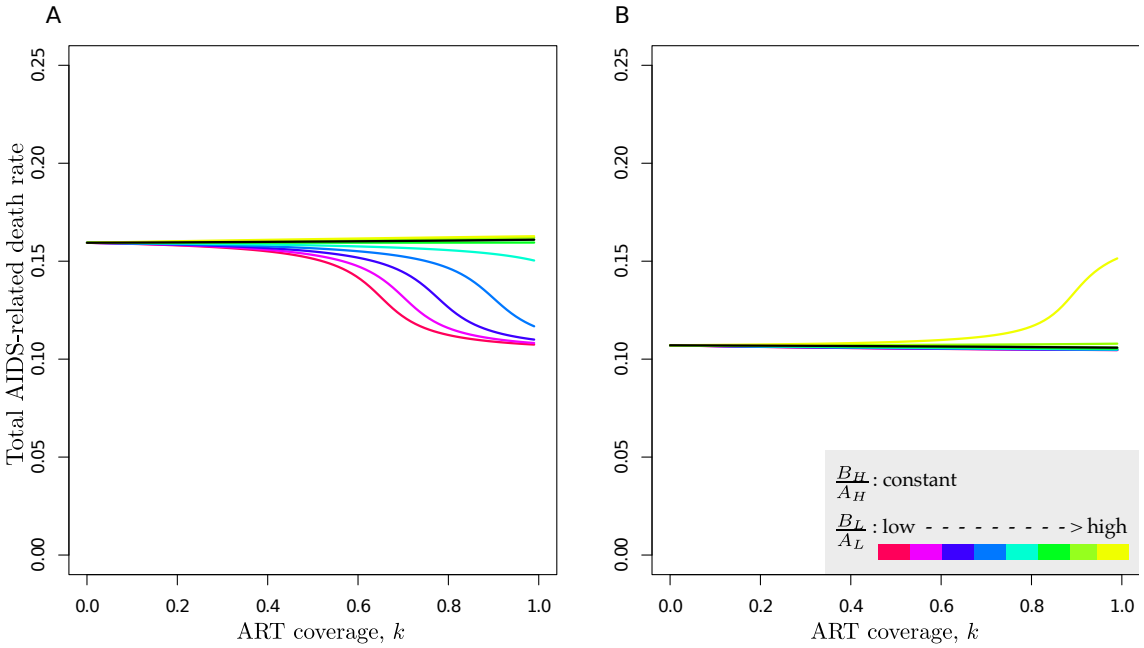


Figure C.2: The relationship between ART coverage and virulence at equilibrium for different parameter sets, when $f = 0.8$. Parameters and colours as in Figure 5.5 but with the heritability parameter $f = 0.8$. Recall $\frac{B_H}{A_H}$ is kept constant while $\frac{B_L}{A_L}$ is varied from low (red line) to high (yellow line). A: $R_0^{S1} = 2.4, R_0^{S2} = 2.2$. B: $R_0^{S1} = 2.2, R_0^{S2} = 2.4$. Total number of AIDS-related deaths per untreated infected person per year is plotted on the y axis. Since each strain now gives rise to a mixture of high and low virulence infections, the overall virulence values that occur when one strain dominates and the other is maintained at mutation-selection balance are less extreme than in Figure 5.5 when $f = 1$. Hence the potential effect of ART is reduced in magnitude while the direction of the effect remains the same.

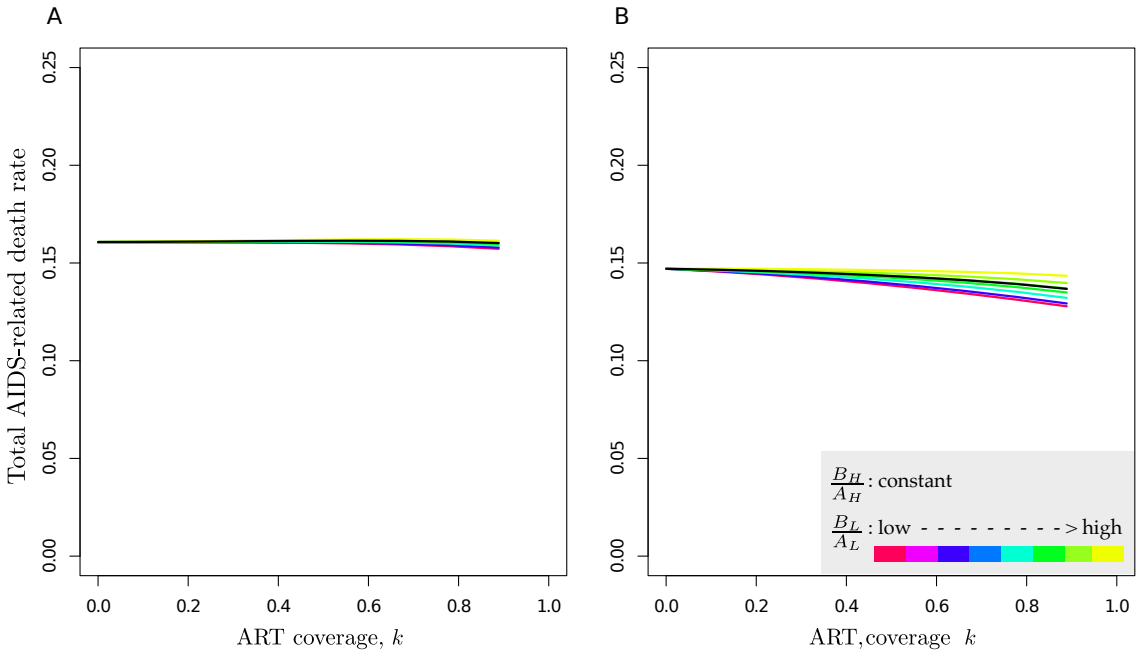


Figure C.3: The effect of ART on virulence in the short term, 50 years after the introduction of ART, when $f = 0.8$. The results of model simulations in which ART is introduced 40 years into the epidemic are shown. Parameters and colours are as in Figure 5.5 but with the heritability parameter $f = 0.8$. Recall $\frac{B_H}{A_H}$ is kept constant while $\frac{B_L}{A_L}$ is varied from low (red line) to high (yellow line). Initial conditions are as given in Figure 5.3. A: $R_0^{S1} = 2.4, R_0^{S2} = 2.2$. B: $R_0^{S1} = 2.2, R_0^{S2} = 2.4$. Total number of AIDS-related deaths per untreated infected person per year is plotted on the y axis. Note that points are not plotted for $k = 1$ because when all patients are treated there are no AIDS-related deaths and so overall virulence is not well defined at this point. Since each strain now gives rise to a mixture of high and low virulence infections, changes in the strain balance have a less severe effect on overall virulence and so the potential effect of ART is reduced compared to in Figure 5.6 when $f = 1$. The direction of the ART-effect is to decrease overall virulence at this point in time for all parameter sets, as before.

C.3 Model with increased transmission in acute infection

C.3.1 Methods

In this model we add in an 'acute' stage of infection, A, which lasts for on average $1/\alpha$ years. Individuals in the acute classes have γ-fold higher infectiousness. When these individuals transition into the standard infected classes they are at that point subdivided unto those who will or won't later receive treatment. The ODE model equations are shown below.

$$
\begin{aligned}
\frac{dS}{dt} &= B - (\beta_H c(I_\cdot^H + \gamma A_\cdot^H) + \beta_L c(I_\cdot^L + \gamma A_\cdot^L))S/N && - \mu S \\
\frac{dA_{S1}^H}{dt} &= f(\beta_H c(I_{S1}^H + \gamma A_{S1}^H) + \beta_L c(I_{S1}^L + A_{S1}^L))S/N && - (\mu + a_H + \alpha)A_{S1}^H \\
\frac{dA_{S1}^L}{dt} &= (1-f)(\beta_H c(I_{S1}^H + \gamma A_{S1}^H) + \beta_L c(I_{S1}^L + A_{S1}^L))S/N && - (\mu + a_L + \alpha)A_{S1}^L \\
\frac{dA_{S2}^H}{dt} &= (1-f)(\beta_H c(I_{S2}^H + \gamma A_{S2}^H) + \beta_L c(I_{S2}^L + A_{S2}^L))S/N && - (\mu + a_H + \alpha)A_{S2}^H \\
\frac{dA_{S2}^L}{dt} &= f(\beta_H c(I_{S2}^H + \gamma A_{S2}^H) + \beta_L c(I_{S2}^L + A_{S2}^L))S/N && - (\mu + a_L + \alpha)A_{S2}^L \\
\frac{dI_{S1,u}^H}{dt} &= (1-k)\alpha A_{S1}^H && - (\mu + a_H)I_{S1,u}^H - mI_{S1,u}^H + mI_{S2,u}^H \\
\frac{dI_{S1,t}^H}{dt} &= k\alpha A_{S1}^H && - (\mu + p_H)I_{S1,t}^H - mI_{S1,t}^H + mI_{S2,t}^H \\
\frac{dI_{S1,u}^L}{dt} &= (1-k)\alpha A_{S1}^L && - (\mu + a_L)I_{S1,u}^L - mI_{S1,u}^L + mI_{S2,u}^L \\
\frac{dI_{S1,t}^L}{dt} &= k\alpha A_{S1}^L && - (\mu + p_L)I_{S1,t}^L - mI_{S1,t}^L + mI_{S2,t}^L \\
\frac{dI_{S2,u}^H}{dt} &= (1-k)\alpha A_{S2}^H && - (\mu + a_H)I_{S2,u}^H - mI_{S2,u}^H + mI_{S1,u}^H \\
\frac{dI_{S2,t}^H}{dt} &= k\alpha A_{S2}^H && - (\mu + p_H)I_{S2,t}^H - mI_{S2,t}^H + mI_{S1,t}^H \\
\frac{dI_{S2,u}^L}{dt} &= (1-k)\alpha A_{S2}^L && - (\mu + a_L)I_{S2,u}^L - mI_{S2,u}^L + mI_{S1,u}^L \\
\frac{dI_{S2,t}^L}{dt} &= k\alpha A_{S2}^L && - (\mu + p_L)I_{S2,t}^L - mI_{S2,t}^L + mI_{S1,t}^L \\
\frac{dT}{dt} &= p_H(I_{S1,t}^H + I_{S2,t}^H) + p_L(I_{S1,t}^L + I_{S2,t}^L) && - \mu T
\end{aligned}
\tag{C.5}
$$

The R_0 values for this model are calculated as follows (in the absence of ART, and

using the approximation $m = 0$ as before):

$$R_0^{S1} = \frac{\gamma\beta_H}{\mu + a_H + \alpha} + \frac{\alpha}{\mu + a_H + \alpha}\frac{\beta_H}{\mu + a_H}$$
$$R_0^{S2} = \frac{\gamma\beta_L}{\mu + a_L + \alpha} + \frac{\alpha}{\mu + a_L + \alpha}\frac{\beta_L}{\mu + a_L}$$

To examine how changing the transmission profile alters the relative importance of low CD4 transmissions we switch to using the PDE form of the model. The partial differential equations for the infected populations are no different to in the original PDE model (equations 4, main text), except that λ_i changes. Let acute infection last for A years. In the simple $m = 0$ case we are now interested in when the following inequality holds:

$$\frac{\int_{T_H}^{\infty} y_{S1}^H \mathrm{d}\tau}{\int_{T_H}^{\infty} y_{S1}^H \mathrm{d}\tau + \int_{T_L}^{\infty} y_{S2}^L \mathrm{d}\tau} > \frac{\gamma \int_0^A y_{S1}^H \mathrm{d}\tau + \int_A^{\infty} y_{S1}^H \mathrm{d}\tau}{\gamma \int_0^A y_{S1}^H + y_{S2}^L \mathrm{d}\tau + \int_A^{\infty} y_{S1}^H + y_{S2}^L \mathrm{d}\tau} \tag{C.6}$$

where, as before (with $m = 0$)

$$\begin{aligned} y_{S1}^H &= \lambda_{S1} S e^{-\mu\tau} \times \begin{cases} 1 & \text{if } \tau \leq T_H \\ (1-k)e^{-d_H(\tau - T_H)} & \text{if } \tau > T_H \end{cases} \\ y_{S2}^L &= \lambda_{S2} S e^{-\mu\tau} \times \begin{cases} 1 & \text{if } \tau \leq T_L \\ (1-k)e^{-d_L(\tau - T_L)} & \text{if } \tau > T_L \end{cases} \end{aligned} \tag{C.7}$$

Note that the end of the acute period ($t = A$) is before the start of the treatment period for both high and low virulence infections ($t = T_H, T_L$). Hence

$$\int_{T_H}^{\infty} y_{S1}^H \mathrm{d}\tau = \lambda_{S1} S \frac{e^{-\mu T_H}}{\mu + d_H}$$
$$\gamma \int_0^A y_{S1}^H \mathrm{d}\tau + \int_A^{\infty} y_{S1}^H \mathrm{d}\tau = \lambda_{S1} S \left[\frac{e^{-\mu T_H}}{\mu + d_H} + \gamma \left(\frac{1}{\mu} - \frac{1}{\mu} e^{-\mu A} \right) + \frac{1}{\mu} e^{-\mu A} - \frac{1}{\mu} e^{-\mu T_H} \right]$$

Writing (C.6) in terms of the parameters of the model:

$$\left(\lambda_{S1}S\frac{e^{-\mu T_H}}{\mu+d_H}\right)\left(\lambda_{S1}S\left[\frac{e^{-\mu T_H}}{\mu+d_H}+\gamma\left(\frac{1}{\mu}-\frac{1}{\mu}e^{-\mu A}\right)+\frac{1}{\mu}e^{-\mu A}-\frac{1}{\mu}e^{-\mu T_H}\right]\right.$$
$$\left.+\,\lambda_{S2}S\left[\frac{e^{-\mu T_L}}{\mu+d_L}+\gamma\left(\frac{1}{\mu}-\frac{1}{\mu}e^{-\mu A}\right)+\frac{1}{\mu}e^{-\mu A}-\frac{1}{\mu}e^{-\mu T_L}\right]\right)>$$
$$\left(\lambda_{S1}S\frac{e^{-\mu T_H}}{\mu+d_H}\;+\lambda_{S2}S\frac{e^{-\mu T_L}}{\mu+d_L}\right)\left(\lambda_{S1}S\left[\frac{e^{-\mu T_H}}{\mu+d_H}+\gamma\left(\frac{1}{\mu}-\frac{1}{\mu}e^{-\mu A}\right)+\frac{1}{\mu}e^{-\mu A}-\frac{1}{\mu}e^{-\mu T_H}\right]\right)$$

After multiplying out, the $\lambda_{S1}\lambda_{S1}$ terms all cancel and we can then divide by $\lambda_{S1}\lambda_{S2}S^2$ to get:

$$\left(\frac{e^{-\mu T_H}}{\mu+d_H}\right)\left(\left[\gamma\left(\frac{1}{\mu}-\frac{1}{\mu}e^{-\mu A}\right)+\frac{1}{\mu}e^{-\mu A}-\frac{1}{\mu}e^{-\mu T_L}\right]\right)>$$
$$\left(\frac{e^{-\mu T_L}}{\mu+d_L}\right)\left(\left[\gamma\left(\frac{1}{\mu}-\frac{1}{\mu}e^{-\mu A}\right)+\frac{1}{\mu}e^{-\mu A}-\frac{1}{\mu}e^{-\mu T_H}\right]\right)$$
$$\Rightarrow\quad\frac{\mu+d_L}{\mu+d_H}>\frac{\left(\gamma-\gamma e^{-\mu A}+e^{-\mu A}\right)e^{\mu T_H}-1}{\left(\gamma-\gamma e^{-\mu A}+e^{-\mu A}\right)e^{\mu T_L}-1}$$

C.3.2 Results: Magnitude and direction of the ART-effect

To model a scenario in which in the absence of ART approximately 50% of all transmissions occur in acute infection, we take $\gamma = 13$ and $\alpha = 2$ (or equivalently, $A = 1/2$, so the increased transmission of acute infection lasts for 6 months). Figures C.4–C.6 show the results of this 'increased acute phase infectivity' model using these values for γ and α. Note that as we increase the proportion of transmissions that are occurring in acute infection, the importance of low CD4 transmissions to the force of infection of both strains decreases. Hence when 50% of transmissions occur in acute infection ART has a lesser effect on viral dynamics and higher coverage is needed to see effects of the same magnitude as before (see Figures C.5 and C.6 and compare with Figures 5.5 and 5.6 in the main text).

With these parameters, the condition for ART to benefit the low virulence strain is:

$$\frac{\mu+d_L}{\mu+d_H}>\frac{1.15e^{\mu T_H}-1}{1.15e^{\mu T_L}-1}$$

(whereas when we previously assumed constant probability of transmission throughout infection the RHS was $(e^{\mu T_H}-1)/(e^{\mu T_L}-1)$). Since $e^{\mu T_H}$ and $e^{\mu T_L}$ are both a little greater than 1, the fraction on the RHS is larger than previously. Hence, when we account for

increased transmission in acute infection, then d_L and d_H have to be closer in size than they did before in order to see a benefit to the low virulence strain. Or, in other words, there are fewer cases in which the effect of ART is to drive a decrease in virulence (as seen in Figure C.5 compared with Figure 5.5).

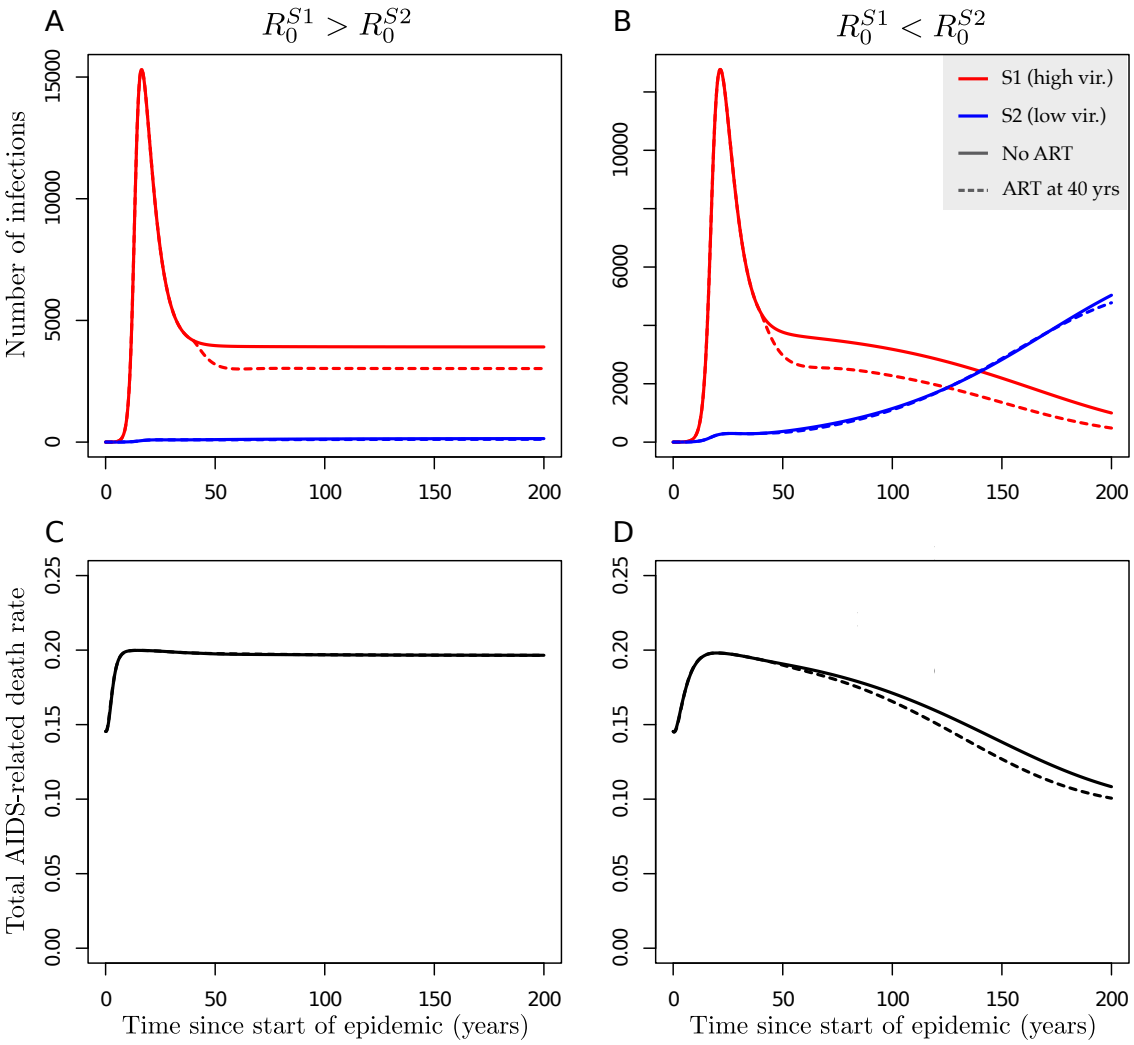


Figure C.4: Behaviour of the model with 50% of transmissions occurring in the first 6 months of infection, with and without ART. Parameters and initial conditions are as in Figure 5.3 and with $\alpha = 2, \gamma = 13$. A, C: In the absence of ART $R_0^{S1} = 2.0, R_0^{S2} = 1.8$. B, D: In the absence of ART $R_0^{S1} = 1.8, R_0^{S2} = 2.0$. Solid lines show the output of the model without ART while dotted lines plot trajectories for the model when ART is introduced at 30% coverage 40 years into the epidemic. A, B: The number of strain S1 infections through time is shown in red and the number of strain S2 infections in blue. With increased transmission earlier in infection the peak of the epidemic occurs earlier, even given lower R_0 values used in this figure compared to Figure 5.3. C, D: In this model equilibrium is reached earlier and so the decrease of virulence in (D) occurs faster. The effect of ART on virulence is of smaller magnitude compared to the original model with constant transmission profile.

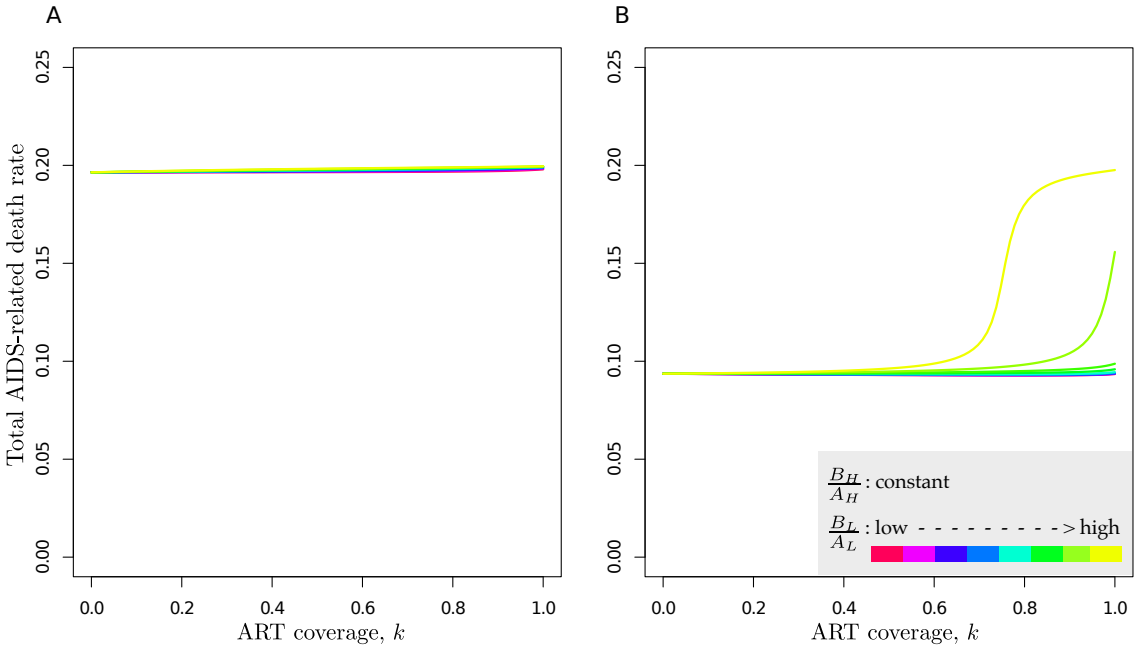


Figure C.5: The relationship between ART coverage and virulence at equilibrium, in the model with 50% of transmissions occurring in the first 6 months of infection. Parameters and colours as in Figure 5.5 plus $\alpha = 2, \gamma = 13$. Recall $\frac{B_H}{A_H}$ is kept constant while $\frac{B_L}{A_L}$ is varied from low (red line) to high (yellow line). A: $R_0^{S1} = 2.0, R_0^{S2} = 1.8$. B: $R_0^{S1} = 1.8, R_0^{S2} = 2.0$. Total number of AIDS-related deaths per untreated infected person per year is plotted on the y axis. Since transmissions late in infection are now of lesser relative importance to both strains, ART very rarely has a large effect on virulence. There are fewer cases in which the effect of ART is to drive a decrease in virulence.

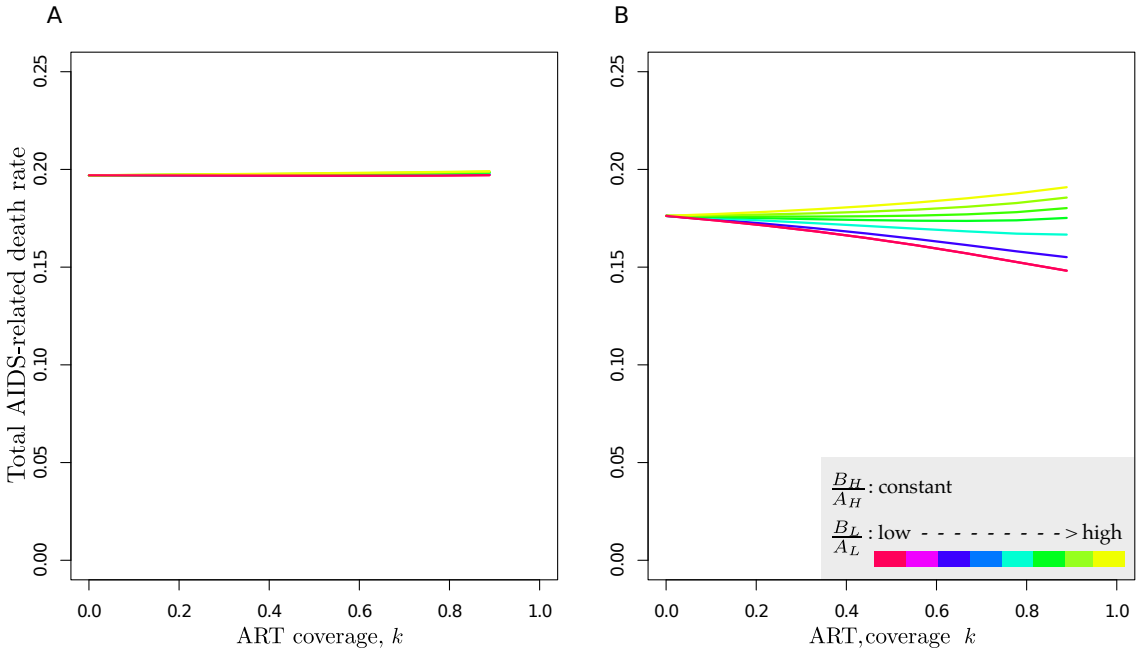


Figure C.6: The effect of ART on virulence in the short term, 50 years after the introduction of ART, in the model with 50% of transmissions occurring in the first 6 months of infection. The results of model simulations in which ART is introduced 40 years into the epidemic are shown. Parameters and colours are as in Figure 5.5 plus $\alpha = 2, \gamma = 13$. Recall $\frac{B_H}{A_H}$ is kept constant while $\frac{B_L}{A_L}$ is varied from low (red line) to high (yellow line). Initial conditions are as given in Figure 5.3. A: $R_0^{S1} = 2.0, R_0^{S2} = 1.8$. B: $R_0^{S1} = 1.8, R_0^{S2} = 2.0$. Total number of AIDS-related deaths per untreated infected person per year is plotted on the y axis. As seen in the equilibrium calculations, the effect of ART on virulence in this model is smaller in magnitude compared to the model with constant transmission profile (Figure 5.6) and there are fewer cases in which the effect of ART is to drive a decrease in virulence.

C.4 Modelling increased transmission amongst a subsection of the population

C.4.1 Methods

For this extension of the model, we split the population into a 'core' and 'periphery', where there will be much higher contact between individuals in the core and the core will be much smaller than the periphery. We assume no movement between the core and periphery compartments. So the basic structure of the model is:

$$\begin{aligned} \text{Core}: \quad & S_c \xrightarrow{\lambda_c} I_c \\ \text{Periphery}: \quad & S_p \xrightarrow{\lambda_p} I_p \end{aligned}$$

where, now specifying the viral strain, i,

$$\begin{aligned} \lambda_{i,c} &= \beta_H c_c \frac{I^H_{i,c}}{S_c + I_c} + \beta_L c_c \frac{I^L_{i,c}}{S_c + I_c} + \beta_H c_b \frac{I^H_{i,p}}{S_p + I_p} + \beta_L c_b \frac{I^L_{i,p}}{S_p + I_p} \\ \lambda_{i,p} &= \beta_H c_p \frac{I^H_{i,p}}{S_p + I_p} + \beta_L c_p \frac{I^L_{i,p}}{S_p + I_p} + \beta_H c_b \frac{I^H_{i,c}}{S_c + I_c} + \beta_L c_b \frac{I^L_{i,c}}{S_c + I_c} \end{aligned}$$

and we now have three contact rates: c_c is the contact rate within the core, c_p is the contact rate within the periphery, and c_b is the contact rate *between* the core and the periphery. Hence $c_c > c_p, c_b$. The spread of the infection within each compartment is described by the equations in (1), with λ_i replaced by $\lambda_{i,c}$ or $\lambda_{i,p}$ as appropriate. We introduce ART to the core only.

Let $c_b = c_p$, so it is only within the core that there are higher contact rates. We wish to use this model to simulate the dynamics of generalised and concentrated epidemics and compare the two. For the generalised epidemic we let $c_p = \frac{1}{2}c_c$ and then for the concentrated epidemic $c_p = \frac{1}{100}c_c$.

C.4.2 Comparison of generalised and concentrated epidemics

The results in Figure C.7 show that in the generalised epidemic the dynamics of the core and the periphery are almost identical. This situation is not much different from our original model. Therefore it is not surprising that virulence change over time is very similar to in Figure 5.3, both in the absence and presence of ART.

In contrast, in Figure C.8 we see that in the concentrated epidemic the dynamics of the periphery lag behind those of the core and the fraction of individuals infected in the periphery is more than 10 times smaller than in the core. Note that in the concentrated model the forces of infection are dominated by the following terms:

$$\lambda_{i,c} \approx \beta_H c_c \frac{I^H_{i,c}}{S_c + I_c} + \beta_L c_c \frac{I^L_{i,c}}{S_c + I_c}$$
$$\lambda_{i,p} \approx \beta_H c_b \frac{I^H_{i,c}}{S_c + I_c} + \beta_L c_b \frac{I^L_{i,c}}{S_c + I_c}$$

Hence the spread of infection in the core is influenced very little by the periphery, whereas in the periphery the incidence of infection is almost entirely determined by the prevalence of infection in the core and the force of infection is low. These observations explain the strain dynamics seen in Figure C.8.

Despite the differences in dynamics between the core and periphery, we see in Figure C.8 that patterns of virulence change in the first 200 years of the epidemic are very similar to in the generalised epidemic, both in the absence and presence of ART. We wish to gain an understanding of what we would expect the ART-effect in the long term (at equilibrium) to be in the concentrated model. First note that in general we would expect the magnitude of the effect to be slightly greater because we are targeting therapy at the individuals who contribute most to onward transmission (the core). We would expect the direction of the ART effect to be similar to that in the original model (since the relative importance of 'low CD4' transmissions to each strain hasn't changed). so long as the ratio of high:low SPVL infections in the core (where ART is applied) is similar to that in the periphery. We can use the approximated forces of infection above to do a straightforward calculation of the equilibrium position of the model (in the absence of ART):

$$\begin{aligned}
\frac{\mathrm{d}I^H_{S1,c}}{dt} = 0 \quad &\Rightarrow \quad \beta_H c_c \frac{I^H_{S1,c}}{N_c} S_c + \beta_L c_c \frac{I^L_{S1,c}}{N_c} S_c - (\mu + a_H + m) I^H_{S1,c} + m I^H_{S2,c} = 0 \\
&\Rightarrow \quad \frac{\beta_H c_c I^H_{S1,c} + \beta_L c_c I^L_{S1,c}}{(\mu + a_H + m) I^H_{S1,c} - m I^H_{S2,c}} = \frac{N_c}{S_c} \\
\frac{\mathrm{d}I^L_{S1,c}}{dt} = 0 \quad &\Rightarrow \quad -(\mu + a_H + m) I^L_{S1,c} + m I^L_{S2,c} = 0 \\
&\Rightarrow \quad \frac{m}{\mu + a_H + m} I^H_{S1,c} = I^H_{S2,c} \\
&\Rightarrow \quad \frac{\beta_H c_c I^H_{S1,c} + \beta_L c_c I^L_{S1,c}}{(\mu + a_H + m) I^H_{S1,c} - \frac{m^2}{\mu + a_H + m} I^H_{S1,c}} = \frac{N_c}{S_c}
\end{aligned}$$

Similar calculations for S2 in the core and S1 and S2 in the periphery yield

$$\begin{aligned}
\frac{\beta_H c_c I^H_{S2,c} + \beta_L c_c I^L_{S2,c}}{(\mu + a_L + m) I^L_{S2,c} - \frac{m^2}{\mu + a_L + m} I^L_{S2,c}} &= \frac{N_c}{S_c} \\
\frac{\beta_H c_b I^H_{S1,c} + \beta_L c_b I^L_{S1,c}}{(\mu + a_H + m) I^H_{S1,p} - \frac{m^2}{\mu + a_H + m} I^H_{S1,p}} &= \frac{N_c}{S_p} \\
\frac{\beta_H c_b I^H_{S2,c} + \beta_L c_b I^L_{S2,c}}{(\mu + a_L + m) I^L_{S2,p} - \frac{m^2}{\mu + a_L + m} I^L_{S2,p}} &= \frac{N_c}{S_p}.
\end{aligned}$$

Combining the core and periphery pairs of equations and rearranging gives

$$\frac{(\mu + a_H + m) I^H_{S1,c} - \frac{m^2}{\mu + a_H + m} I^H_{S1,c}}{(\mu + a_L + m) I^L_{S2,c} - \frac{m^2}{\mu + a_L + m} I^L_{S2,c}} = \frac{(\mu + a_H + m) I^H_{S1,p} - \frac{m^2}{\mu + a_H + m} I^H_{S1,p}}{(\mu + a_L + m) I^L_{S2,p} - \frac{m^2}{\mu + a_L + m} I^L_{S2,p}}.$$

When $m << 1$, as in the original model, this approximates to $I^H_c / I^H_p = I^L_c / I^L_p$. In other words the ratio of high:low SPVL infections is approximately the same in the core as in the population as a whole. Hence we would expect the direction of the ART-effect on virulence at equilibrium to be similar to that in the original model.

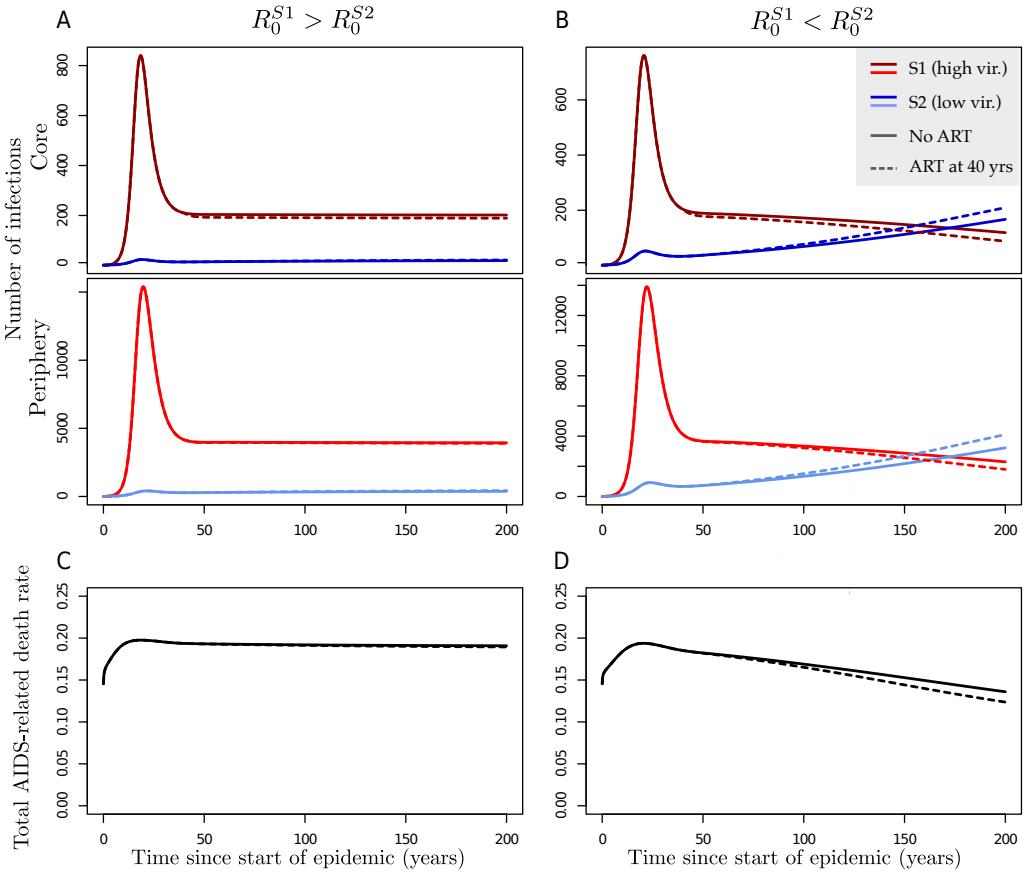


Figure C.7: Behaviour of the core-periphery model under the assumptions of a generalised epidemic, with and without ART. Parameters are as in Table 5.1 but with the differing contact rates $c_c = 1, c_p = c_b = 0.5$. The core is 20 times smaller than the periphery, so $S_c(0) = 2000, S_p(0) = 40000$. Initially there are no infections in the periphery, but in the core $I^H_{S1,u}(0) = I^L_{S2,u}(0) = 1$ and all other infected populations are 0 initially. A, C: In the absence of ART, the R_0s of the core (where $c = 1$) are set at $R_0^{S1} = 2.4, R_0^{S2} = 2.2$. In other words, we choose β_H, β_L such that $2.4 = \beta_H/(\mu + a_H)$, $2.2 = \beta_L/(\mu + a_L)$. B, D: In the absence of ART, the R_0s of the core ($c = 1$) are set at $R_0^{S1} = 2.2, R_0^{S2} = 2.4$. Solid lines show the output of the model without ART while dotted lines plot trajectories for the model when ART is introduced 40 years into the epidemic. Only the core is treated (at coverage of 30%). A, B: The number of strain S1 infections through time is shown in red and the number of strain S2 infections in blue. In this simulation of a generalised epidemic, though the dynamics are driven by transmission in the core, the dynamics in the periphery closely match those in the core. C, D: Patterns of virulence change over time are qualitatively similar to the original model, though the peak is smaller and the magnitude of the ART-effect is lesser since only the core is treated.

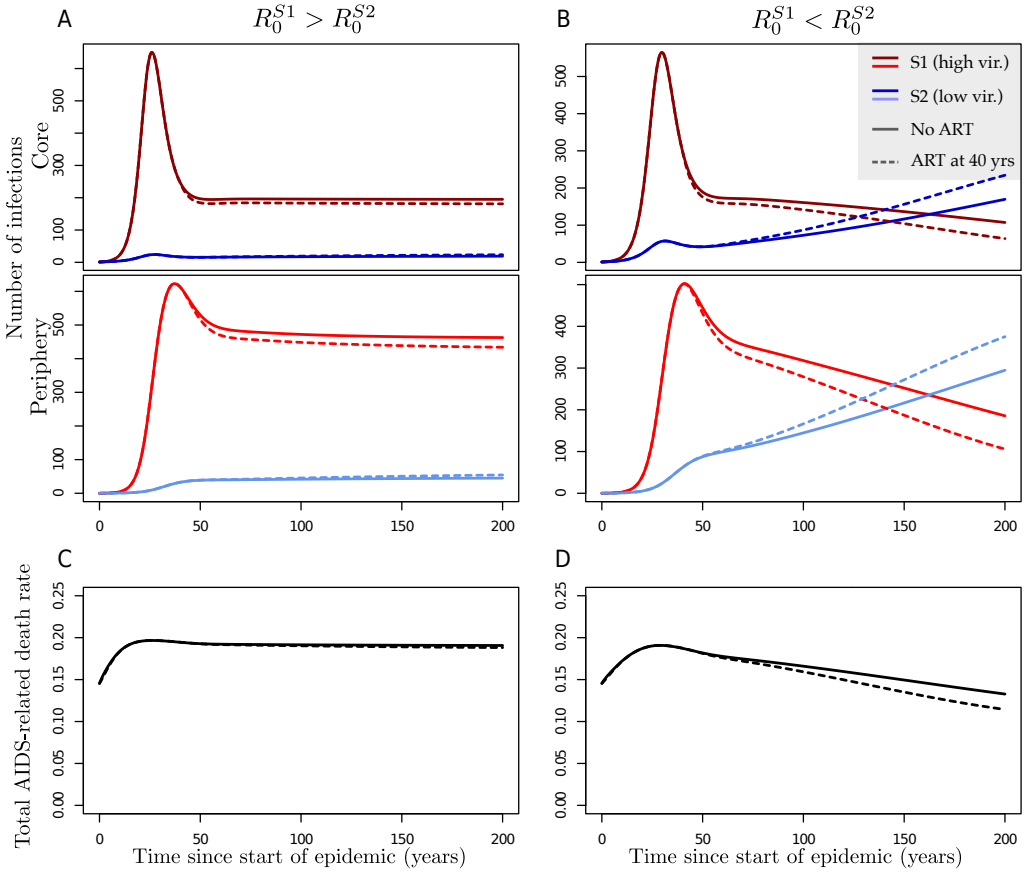


Figure C.8: Behaviour of the core-periphery model under the assumptions of a concentrated epidemic, with and without ART. Parameters are as in Table 5.1 but with the differing contact rates $c_c = 1, c_p = c_b = 0.01$. The core is 20 times smaller than the periphery, so $S_c(0) = 2000, S_p(0) = 40000$ and also $B_c = 50$ and $B_p = 1000$. Initially there are no infections in the periphery, but in the core $I^H_{S1,u}(0) = I^L_{S2,u}(0) = 1$ and all other infected populations are 0 initially. A, C: In the absence of ART, the R_0s of the core ($c = 1$) are set at $R_0^{S1} = 2.4, R_0^{S2} = 2.2$. B, D: In the absence of ART, the R_0s of the core ($c = 1$) are set at $R_0^{S1} = 2.2, R_0^{S2} = 2.4$. Solid lines show the output of the model without ART while dotted lines plot trajectories for the model when ART is introduced 40 years into the epidemic. Only the core is treated (at coverage of 30%). A, B: The number of strain S1 infections through time is shown in red and the number of strain S2 infections in blue. Compared to the generalised epidemic the peak of infections is later due to reduced transmission in the periphery, and the number of infections is much lower in the periphery. The force of infection in the periphery is very dependent on the proportion of infected individuals in the core and the shape of the epidemic peak reflects this. C, D: Patterns of virulence change are still very similar to those seen in the original model, except that the low virulence strain (S2) starts to dominate earlier in (D) than in Figure 5.3D.

C.5 Modelling an ART treatment protocol where all patients are treated as soon as possible

C.5.1 Methods

To model a set of treatment guidelines where all individuals are treated as soon as possible (i.e. as soon as they are identified as HIV-positive) we use the original ODE model with ART, as given in equations 2, main text, and set $p_H = p_L$. In other words, identification of infection and resulting treatment is independent of disease course. In the figures that follow (Figures C.9 and C.10) we vary the average time from infection to identification of infection between 6 months and 4 years and look at the resulting ART-effect at equilibrium (Figure C.9) and in the short-term (Figure C.10).

C.5.2 Results

Under this treatment protocol, the low virulence strain is always affected most when ART is introduced because a greater proportion of its onward transmissions are effectively removed (compared to the onward transmissions of the high virulence strain). Therefore in the long term (at equilibrium), ART always drives an increase in virulence, whatever the value of the parameter p_j. The magnitude of the effect is smaller when p_j is large, i.e. when patients are treated particularly early in infection, because in that case both strains are (more equally) heavily affected by ART.

In the short term, the effect of ART is either to benefit the high virulence strain (S1), in which case the magnitude is small because S1 dominates in the absence of ART anyway, or to benefit the low virulence strain. However, the benefit to the low virulence strain occurs in the (unrealistic) cases where ART is causing the eventual extinction of both strains – since the turnover of the S2-infected population is lower it decays at a slower rate and so the average virulence of an infection rises in these cases.

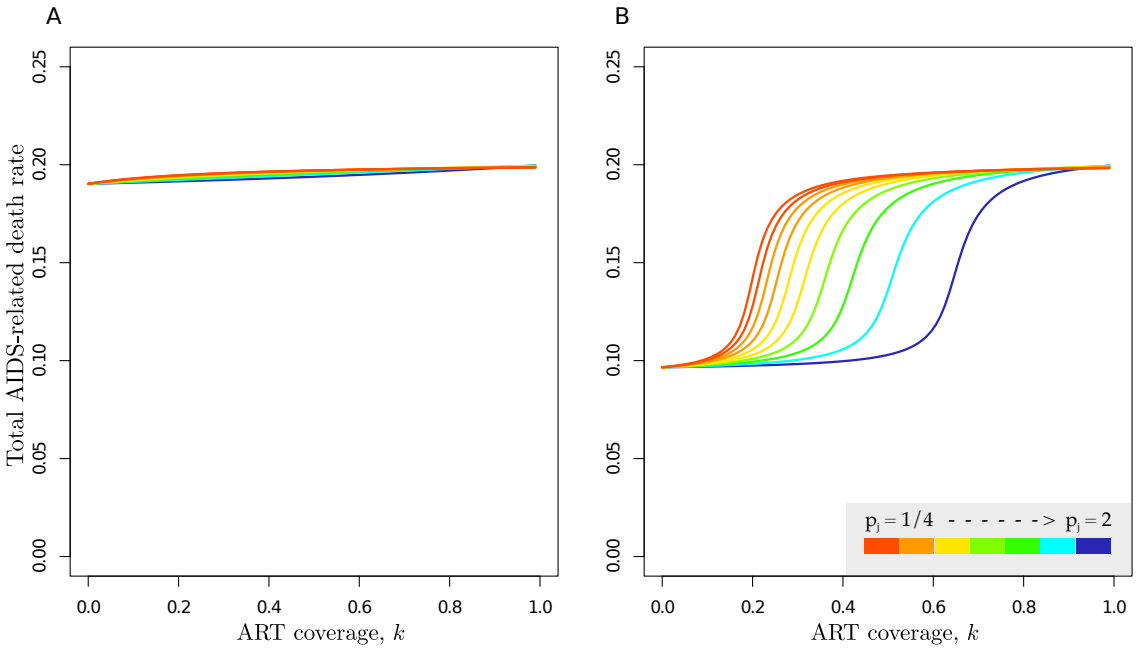


Figure C.9: The relationship between ART coverage and virulence at equilibrium when patients are treated as soon as possible after infection, regardless of disease progression. A: $R_0^{S1} = 2.4, R_0^{S2} = 2.2$. B: $R_0^{S1} = 2.2, R_0^{S2} = 2.4$. Total number of AIDS-related deaths per untreated infected person per year is plotted on the y axis. Treating independent of disease progression translates to setting $p_L = p_H$ in the ODE model. Different coloured lines here represent different rates at which individuals in the 'treated' class are treated, from $p_j = 2$ i.e. an average of 6 months of infection before initiating ART (blue) to $p_j = 1/4$ i.e. an average of 4 years of infection before initiating ART (red). The remaining parameters are the same as in Table 5.1. Note that when everyone is treated almost immediately, there is a high impact on onward transmission for both strains, whereas when individuals are treated after four years there is a higher impact on the low virulence strain, S2, hence overall virulence is higher the lower p_j is.

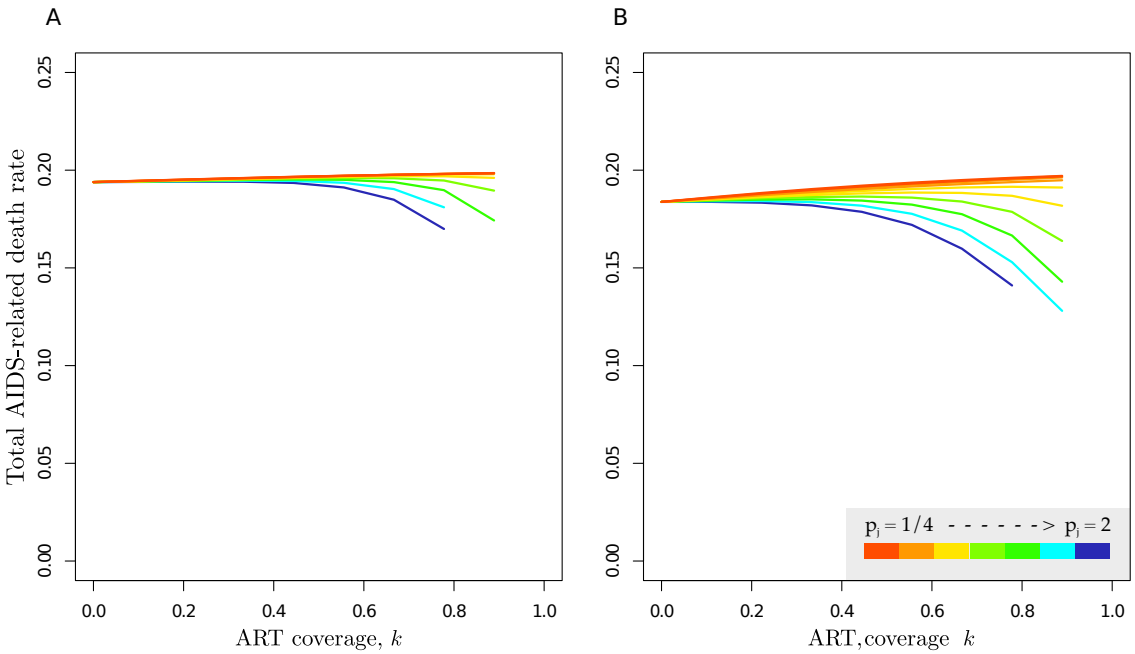


Figure C.10: The short term effect of ART on virulence, in the model where patients are treated as soon as possible after infection, regardless of disease progression. The results of model simulations at 90 years (where ART is introduced 40 years into the epidemic) are shown, with total number of AIDS-related deaths per untreated infected person per year once again used as a proxy for virulence A: $R_0^{S1} = 2.4, R_0^{S2} = 2.2$. B: $R_0^{S1} = 2.2, R_0^{S2} = 2.4$. As in Figure C.9, different coloured lines represent different rates at which individuals in the 'treated' class are treated, from $p_j = 2$ i.e. an average of 6 months of infection before initiating ART (blue) to $p_j = 1/4$ i.e. an average of 4 years of infection before initiating ART (red). The remaining parameters and initial conditions are the same as in Figure 5.3 and Table 5.1. When p_j is low then even at this stage in the epidemic the effect of ART is to benefit the high virulence strain (S1). For higher values of p_j and ART coverage, k, ART results in the eventual extinction of both strains. Since the death rate of the S2-infected population is lower than that of the S1-infected population this can lead to a rise in the proportion of S2 compared to S1 -infected individuals in the period leading to extinction, and hence a decrease in virulence by this measure. The points representing parameter sets where this extinction has already occurred at 90 years ($I_{S1}(90) + I_{S2}(90) < 1$) are not plotted.

C.6 Additional sensitivity analyses

In this section we conduct sensitivity analyses in which we vary the R_0 values (Figures C.11–C.13), the timing of ART initiation relative to the peak of the epidemic (Figures C.14 & C.15) and the initial conditions (Figure C.16). These sensitivity analyses are based on the original model as presented in the main text. Table 5.1 summarises the results of all these sensitivity analyses and the analyses in sections 2–4 in terms of the effect of the various modifications on the key results regarding virulence evolution and the ART-effect.

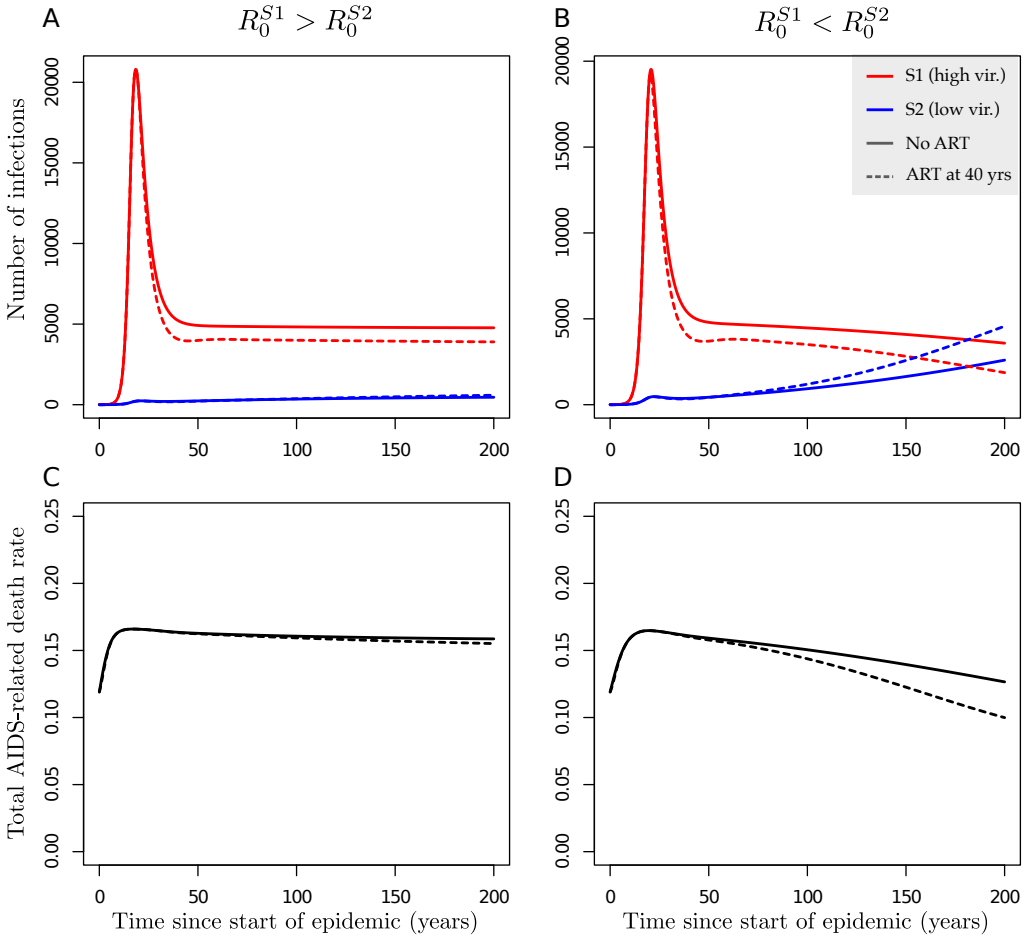


Figure C.11: Behaviour of the model where both strains have particularly high R_0s, with and without ART. Parameters and initial conditions are as in Table 5.1 and Figure 5.3, except for mortality and progression rates of infected individuals which are in general lower in this simulation ($a_H = 1/6, a_L = 1/14, p_H = 1/4, p_L = 1/12$). A, C: In the absence of ART, the R_0s are set at $R_0^{S1} = 4.4, R_0^{S2} = 4.0$. B, D: In the absence of ART, the R_0s are set at $R_0^{S1} = 4.0, R_0^{S2} = 4.4$. Solid lines show the output of the model without ART while dotted lines plot trajectories for the model when ART is introduced at 30% coverage 25 years into the epidemic. A, B: The number of strain S1 infections through time is shown in red and the number of strain S2 infections in blue. The peak of the epidemic now occurs between 20 and 25 years after the start and is slightly more severe than in the original model. Otherwise the dynamics are similar. C, D: Patterns of change in virulence are qualitatively similar to the original model and occur on the same order-of-magnitude timescales.

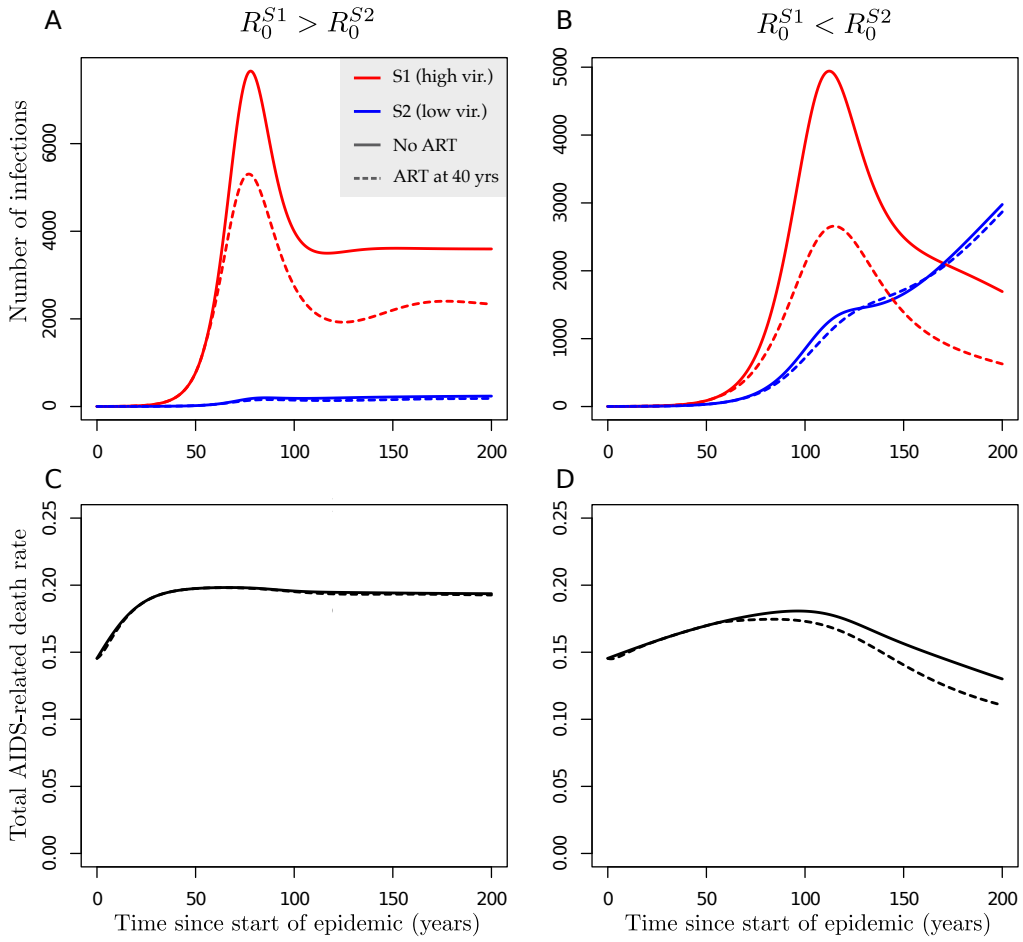


Figure C.12: Behaviour of the model where both strains have particularly low R_0s, with and without ART. Parameters and initial conditions are as in Table 5.1 and Figure 5.3. A, C: In the absence of ART, the R_0s are set at $R_0^{S1} = 1.6, R_0^{S2} = 1.4$. B, D: In the absence of ART, the R_0s are set at $R_0^{S1} = 1.4, R_0^{S2} = 1.6$. Solid lines show the output of the model without ART while dotted lines plot trajectories for the model when ART is introduced at 30% coverage 55 years into the epidemic. The number of strain S1 infections through time is shown in red and the number of strain S2 infections in blue. A, B: The peak of the epidemic now occurs much later and the progress of the epidemic is in general much slower. In the case where $R_0^{S1} < R_0^{S2}$, the high virulence strain is unable to spread through the population as quickly (B) and its domination in the early stages is significantly reduced compared to in simulations with higher R_0s. C, D: Despite this, patterns of virulence change are still quantitatively similar - a first-phase rise in virulence is followed by a second phase decline (though this is modest in (C)), and the third phase is determined by the balance of the R_0s.

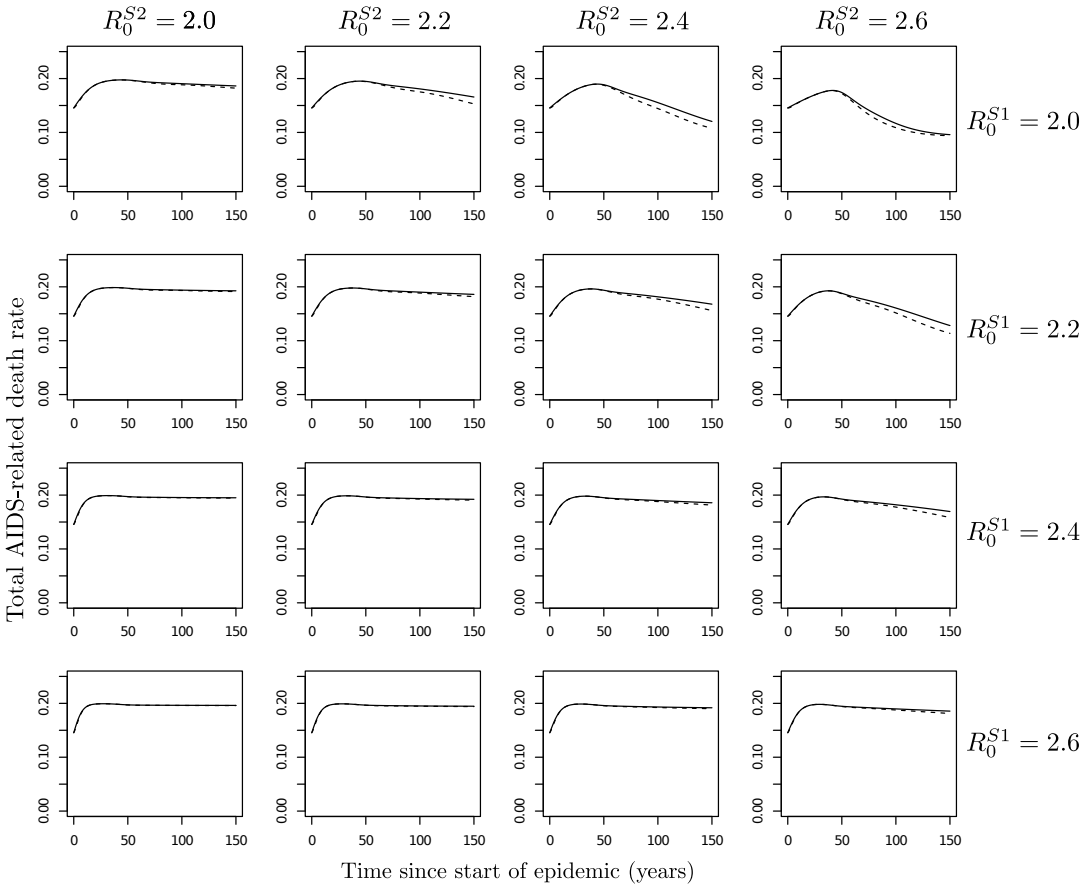


Figure C.13: Patterns of virulence change in the first 150 years of the epidemic for a range of combinations of R_0 values for the two strains. Total number of AIDS-related deaths per untreated infected person per year is plotted on the y axis. Parameters and initial conditions are as given in Table 5.1 and Figure 5.3, except for the R_0 values which are varied from 2 to 2.6. Changes in virulence are quantitatively different for different R_0 combinations but the patterns of change through time are consistent. There is a decrease in virulence in the second half-century of the epidemic in all cases, this is most severe when R_0^{S2} is much greater than R_0^{S1} and very slight when R_0^{S1} is greater than R_0^{S2}. ART always results in a decrease in virulence (compared to the model with no ART) and this ART effect is largest when R_0^{S2} is a little larger than R_0^{S1}.

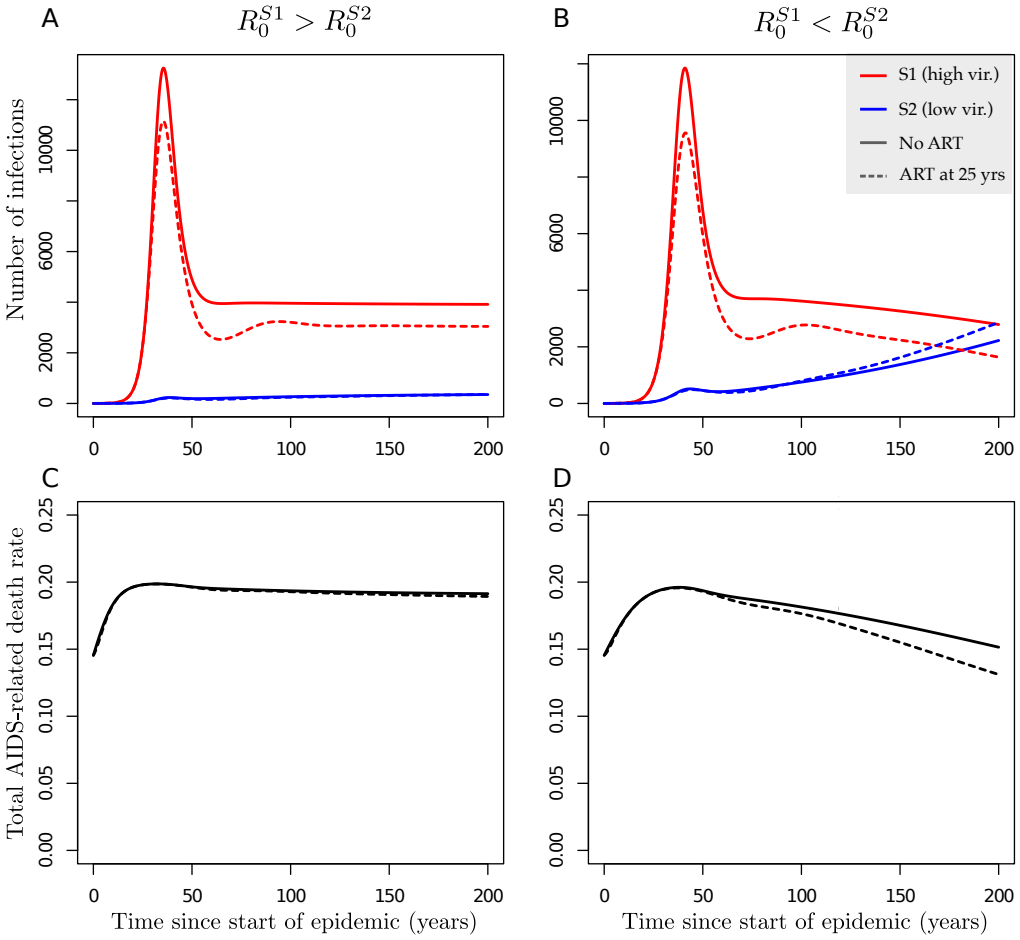


Figure C.14: Behaviour of the model without ART compared to the model where ART is introduced before the epidemic peak. Parameters and initial conditions are as in Table 5.1 and Figure 5.3, including R_0 values. Solid lines show the output of the model without ART while dotted lines plot trajectories for the model when ART is introduced at 30% coverage 25 years into the epidemic. The number of strain S1 infections through time is shown in red and the number of strain S2 infections in blue. Despite ART being introduced 15 years earlier, patterns of virulence change in this simulation, measured as total AIDS-related deaths per untreated infected person per year, are almost identical to those in Figure 5.3.

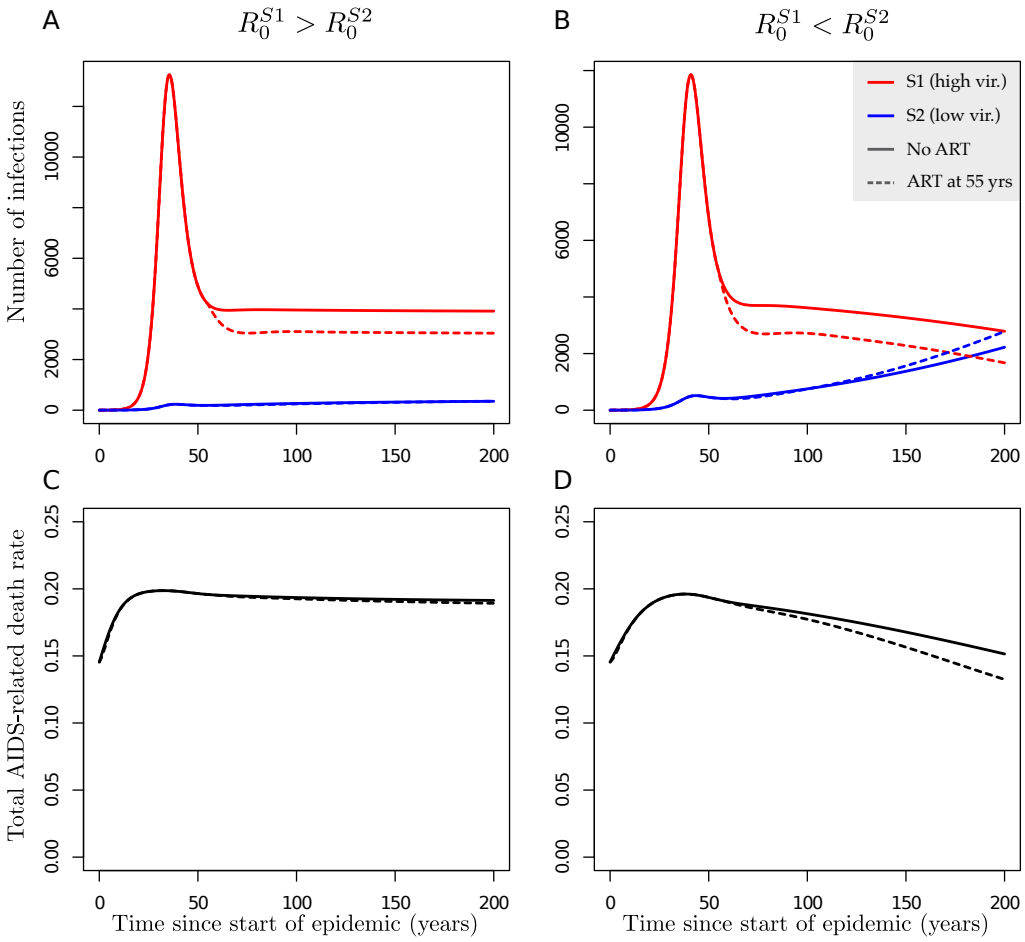


Figure C.15: Behaviour of the model without ART compared to the model where ART is introduced after the epidemic peak. Parameters and initial conditions are as in Table 5.1 and Figure 5.3, including R_0 values. Solid lines show the output of the model without ART while dotted lines plot trajectories for the model when ART is introduced at 30% coverage 55 years into the epidemic. The number of strain S1 infections through time is shown in red and the number of strain S2 infections in blue. Despite ART being introduced 15 years later, patterns of virulence change in this simulation, measured as total AIDS-related deaths per untreated infected person per year, are almost identical to those in Figure 5.3.

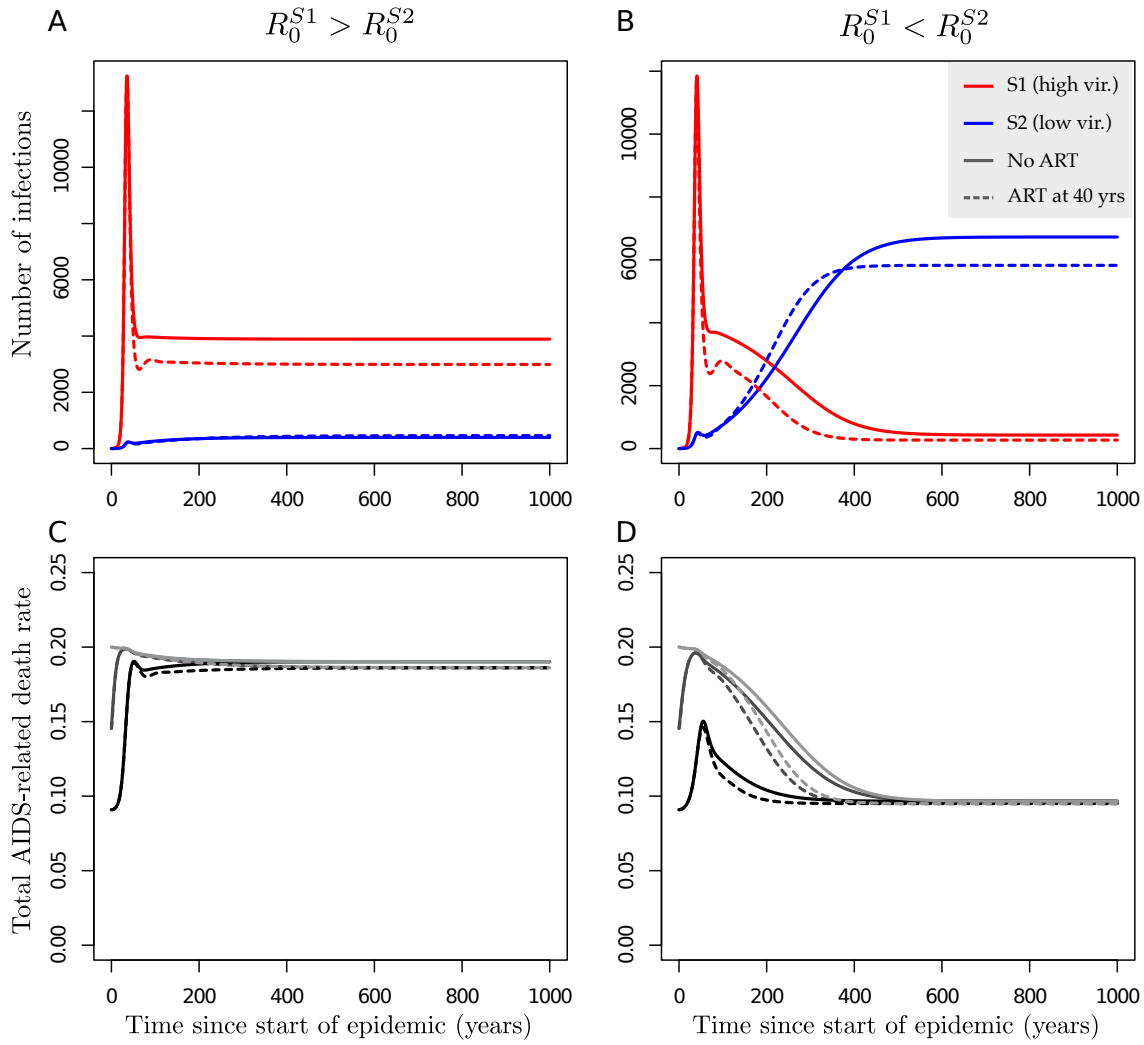


Figure C.16: Behaviour of the two strain model with and without ART and with differing initial conditions. Parameters are the same as in Figure 5.3 but the model is run for 1000 years in order to show the epidemic approaching equilibrium. A, B: The number of strain S1 infections through time is shown in red and the number of strain S2 infections in blue. The initial conditions are $S(0) = 40000, I^H_{S1,u}(0) = 1, I^L_{S2,u}(0) = 1$, all other populations equal to zero. C, D: The effect of three different sets of initial conditions on the average death rate of untreated individuals is shown (i) $I^H_{S1,u}(0) = 0, I^L_{S2,u}(0) = 2$ (black), (ii) $I^H_{S1,u}(0) = 1, I^L_{S2,u}(0) = 1$ (dark grey), (iii) $I^H_{S1,u}(0) = 2, I^L_{S2,u}(0) = 0$ (light grey). The initial conditions do not change the equilibrium position of the model. For (ii) and (iii) the model behaviour is close to identical after the peak of the epidemic, approximately 50 years in. For (i), when all infections are initially of the low virulence strain (S2) the model reaches equilibrium faster but the same 'second phase' patterns of decreasing virulence after the peak are still seen in both (C) and (D).

Table C.1: A table of the various amendments and modifications to the original model and their effect on the main results.

	Effect of amended model on... (figure in main text for comparison)		
Amendment (supplementary figures)	Patterns of virulence change in absence of ART (Fig 5.3, solid lines)	Magnitude and direction of 'early' ART-effect (Fig 5.6)	Magnitude and direction of 'late' ART-effect (Fig 5.5)
50% of transmissions occur in acute infection (C.1-3)	Similar patterns seen but twice as fast (epidemic peaks earlier).	Magnitude smaller. ART more often benefits high virulence strain.	Large effects rarer. Fewer cases of decrease in virulence in particular.
Low heritability (C.4-6)	Clearer decrease in virulence after peak. Smaller magnitude of changes in virulence in general.	Magnitude smaller. Direction largely unchanged.	Magnitude smaller. Direction unchanged.
Core-periphery model, generalised epidemic (C.7)	Very similar patterns, peak slightly earlier, progressing to equilibrium slightly faster.	Slightly larger magnitude since treatment concentrated on core. Direction still negative.	Magnitude slightly larger for lower coverages. Direction unchanged.
Core-periphery model, concentrated epidemic (C.8)	Virulence changes less pronounced.	Larger magnitude since treatment concentrated on core. Direction still negative.	Magnitude larger for lower coverages. Direction similar.
ART initiated as soon as possible (C.9-10)	n/a - unchanged.	Magnitude similar in range for this range of parameters. Direction: Sometimes an increase in virulence when ART initiation is later.	Larger magnitude possible at low coverage. Direction: Always an increase in virulence.
High R_0s (C.11)	Similar patterns seen but twice as fast.	Magnitude slightly larger. Direction still negative.	Magnitude and direction largely unchanged (still determined by equation 8, main text).
Low R_0s (C.12)	Similar patterns but epidemic progresses much slower.	Magnitude and direction seem similar.	Magnitude and direction unchanged.
ART introduced 15 years before peak (C.14)	n/a - unchanged.	Negligible change in magnitude and direction.	n/a - unchanged.
ART introduced 15 years after peak (C.15)	n/a - unchanged.	Negligible change in magnitude and direction.	n/a - unchanged.
Varying initial conditions (C.16)	First phase (before peak) varies depending on initial conditions. Second phase decrease sometimes shorter in duration.	Magnitude can be smaller. Direction unchanged.	n/a - unchanged.